Adrenergic Neuromodulation of Transmitter Release in Rat Neocortex

A dissertation for the degree of
Doctor of Philosophy

Submitted for examination in September 2011 to
The John Curtin School of Medical Research
of
The Australian National University

Presented by
Julian Min Chiang Choy

Bachelor of Science (1st Class honours) U.M.S 2006
Born August 24th, 1983, Penang, Malaysia
Citizen of Malaysia

Declaration

This thesis is an account of research undertaken between October 2007 and February 2012 at the John Curtin School of Medical Research, The Australian National University, Canberra, Australia.

Except where acknowledged in the customary manner, to the best of my knowledge the material presented in this thesis is original and has not been submitted in whole or in part for any degree at any university.

Julian Min Chiang Choy
April 2012

Acknowledgements

I would like to extend my sincere thanks to my supervisor, Assoc Prof Christian Stricker for being a great mentor and advisor throughout the course of my studies. I am grateful for the opportunity to be a lab member of the Neuronal Network Laboratory. Thus, I would also like to thank past and present members of the lab, whom I have shared fantastic times together. My lunchtime with labmates 李莉 (Li Li), Ali Shamsizadeh, Elise Bertet, Ashutosh Mohan, Mary Ann Go and Lê Thúy Vân Trần will always be cherished. I would also like to thank Dr Anna Cowan for the numerous advices and help at the John Curtin School of Medical Research. Many thanks also go to my panel members Prof Bruce Walmsley and Assoc Prof John Bekkers for their constructive inputs into the project. My special thanks goes to Dr Eric Stephenson, Freda Stephenson, Marianne Pietersen and Suzanne Rogashoff for proofreading and commenting on my thesis. I am glad to be blessed with a wonderful family; who has constantly showered me with invaluable years of love, support and encouragements. To my dad, Kuan Seng Choy, my mum, Lay Bee Teoh and my two brothers, Jason and Eujin Choy, I am blessed to have all of you in my life. I appreciate the assistance I received from Garry Rodda for his marvellous effort to keep experiments going in the lab. Last but not least, I would like to thank the Malaysian ANU alumni for providing me with three and a half years of scholarship and tuition stipend to study at the John Curtin School of Medical Research, the Australian National University.

Abstract

Presynaptic Ca^{2+} stores modulate transmitter release via presynaptic metabotropic glutamate receptors (group I). I hypothesized that presynaptic α_1-adrenoreceptors (α_1-ARs) have the potential to cause Ca^{2+} mobilization from stores, as they cause PIP_2 hydrolysis and IP_3 production.

I found in individual layer II/III pyramidal neurones a mEPSC rate of 42 ± 1 Hz. Adding noradrenaline (NA; 10 µM; after 5') increased this rate by 50 ± 11% with no effect on amplitude. After blocking β- and α_2-ARs with propranolol and yohimbine, NA still increased mEPSC frequency by 62 ± 11% suggesting α_1-ARs activation. The α_1-AR agonist cirazoline increased the frequency by the same amount. Displacement experiments using both agonists and antagonists confirmed that NA bound to the α_1-AR. These findings were further supported by immunohistochemical labelling, which showed localisation of α_{1B}-ARs to these nerve terminals.

To verify the signalling cascade activated by α_1-ARs, both the phospholipase C inhibitor edelfosine and membrane permeable IP_3R blocker 2-APB caused a drop in mEPSC frequency, which subsequent NA application did not relieve. Emptying Ca^{2+} stores with cyclopiazonic acid reduced mEPSC frequency by the same amount, as did chelating intracellular Ca^{2+} with BAPTA-AM.

When two receptors signalling via G_q were activated subsequently, the mEPSC frequency did not increase. This may indicate that these presynaptic receptors may not necessarily be signalling independently of each other.

In 101 pairs of connected pyramidal neurones, an average EPSC amplitude of -31.4 ± 3.6 pA with a CV of 0.6 ± 0.1 was recorded. 60% of these EPSCs displayed long-term depression and the remainder showed a correlation between CV^{-2} and mean EPSC. As a consequence, the quantal current of the population was estimated to be 6.0 ± 0.6 pA, giving rise to a quantal content of 4.6 ± 0.6. This correlation indicates that at these synapses, the size of the EPSCs is largely governed by the number of release sites but not by release probability. Also, these EPSCs showed little paired-pulse plasticity.

In NA, the EPSC depressed by 66 ± 23%. On average, both paired-pulse plasticity and release-independence remained unchanged. The depression was caused by α_1-AR

activation as evidenced by cirazoline; it also was not caused by Ca^{2+} release from presynaptic stores indicating that the depression was caused by an early step in the signalling cascade. The depression was not correlated with presynaptic factors. After a burst of action potentials, recovery from depression was much faster, with recovery amplitudes being larger than the first EPSC in the stimulus sequence. This indicates that NA dramatically alters the synaptic dynamics. When store release was blocked, the EPSCs depressed by 33 ± 11% suggesting that store release increases each EPSC amplitude. This aspect is consistent with the expectations raised by the mEPSC data above. A potential mechanism is presented and discussed.

I found that NA is a powerful tool to differentiate spontaneous from evoked transmitter release, as it's effect on both of these modes is opposite suggesting that the molecular elements for evoked and spontaneous transmitter release are distinct.

Table of Contents

Acknowledgements **3**

Abstract **4**

Table of Contents **6**

Abbreviations **10**

1. Introduction **13**
1.1. Overview **13**
1.2. Outline of the physiology of synaptic transmission **14**
1.2.1. Historical view 14
1.2.2. Electrical *versus* chemical transmission 14
1.2.3. Chemical transmission 15
1.2.3.1. Nature of a transmitter 15
1.2.3.1.1. Iono- and metabotropic receptors 16
1.2.3.1.2. Neuromodulation 16
1.2.3.2. Modes of transmission (evoked versus spontaneous) 16
1.2.3.3. The process of transmitter release 17
1.2.3.4. Vesicular hypothesis 17
1.2.3.4.1. Morphology of the synapse 18
1.2.3.4.2. Arguments for the vesicle hypothesis 19
1.2.3.4.3. Arguments against the vesicle hypothesis 20
1.2.3.4.4. Non-vesicular release of transmitter 21
1.2.3.4.5. Synthesis of transmitter 24
1.2.3.4.6. Generation and life-time of vesicles 26
1.2.3.4.7. Loading of vesicles with transmitter 27
1.2.3.4.8. SNARE hypothesis for exocytosis 27
1.2.3.4.9. Docking and pre-fusion 29
1.2.3.4.10. Exocytosis 30
1.2.3.4.11. Transmitter diffusion and termination of release 30
1.2.3.4.11.1. Diffusion in synaptic cleft and extracellular space 32
1.2.3.4.11.2. Break-down and/or uptake of transmitter 32
1.2.3.4.11.3. Receptor unbinding 32
1.2.3.4.12. Vesicle endocytosis and recycling 32
1.2.3.4.13. Mobility of vesicles 33
1.3. Spontaneous transmitter release **34**
1.3.1. Calcium dependence 35
1.4. Evoked transmitter release **36**
1.4.1. Quantal hypothesis 36
1.4.1.1. Arguments against the quantal hypothesis 38
1.4.1.2. Arguments for the quantal hypothesis 39
1.4.2. Calcium hypothesis 40
1.4.2.1. Calcium micro- and nano-domain hypotheses 41
1.4.3. Relationship between spontaneous and evoked release 43
1.4.3.1. Spontaneous synaptic events may be caused by tissue damage 43
1.4.3.2. Spontaneous release is due to spontaneous vesicular fusion 45
1.4.3.3. The same biochemical proteins are involved in evoked and spontaneous release 45
1.5. Synaptic plasticities **47**
1.5.1. Forms of plasticities 47
1.5.2. Long-term plasticities 47
1.5.2.1. Long-term potentiation 48
1.5.2.2. Long-term depression 51

1.5.3. Short-term plasticities 52
1.5.3.1. Synaptic enhancement 53
1.5.3.2. Synaptic depression 54
1.5.3.2.1. Synaptic vesicle pools 55
1.5.3.2.2. Depletion models of short-term depression 55
1.5.3.2.3. Alternative models of STD 55
1.5.3.2.3.1. Release independent depression 56
1.5.3.2.3.2. Frequency dependent recovery 57
1.5.4. Ca^{2+} homeostasis in the nerve terminal 58
1.5.4.1. Plasma membrane Ca^{2+}-ATPase 59
1.5.4.2. Na^{+}-Ca^{2+} exchanger 59
1.5.4.3. Ca^{2+}/H^{+} antiport 60
1.5.4.4. Cytosolic buffers 60
1.5.4.4.1. EF hand proteins 61
1.5.4.4.2. Annexins 62
1.5.4.4.3. Gelsolin 62
1.5.5. Calcium stores 63
1.5.5.1. Endoplasmic reticulum 64
1.5.5.2. Golgi complex 64
1.5.5.3. Mitochondria 65
1.5.5.4. Nucleus 67
1.5.6. Calcium dynamics of calcium stores 67
1.5.6.1. SERCA pump 67
1.5.6.2. Calcium release and leaks 68
1.5.6.2.1. Ryanodine receptor 68
1.5.6.2.2. Inositol 1,4,5-trisphosphate receptor (IP_3R) 69
1.5.6.2.3. Presenilins 70
1.5.7. Metabotropic receptors coupled to IP_3 production 71
1.5.7.1. Group I mGluRs 71
1.5.7.2. Adrenergic receptors 72
1.5.7.3. Other metabotropic receptors that are coupled to IP_3 production 74
1.5.7.3.1. Histamine (H_1) receptors 74
1.5.7.3.2. Serotonin (5-HT_2) receptors 75
1.5.7.3.3. Muscarinic acetylcholine (M_1/M_3ACh) receptors 76
1.5.7.3.4. Orexin (OX_1/OX_2) receptors 76
1.5.7.3.5. Purinergic (P2Y) receptors 77
1.5.8. Role of presynaptic Ca^{2+} stores in transmitter release 78
1.6. Barrel cortex 79
1.6.1. Organisation and synaptic physiology 79
1.6.2. Cellular organisation 79
1.7. Basis of Study 81

2. Part I 82
2.1. Introduction 83
2.2. Methods 84
2.2.1. Preparation of slices of barrel cortex 84
2.2.2. The recording chamber 85
2.2.3. Whole cell recordings 86
2.2.3.1. Optics 86
2.2.3.2. Electrodes 87
2.2.4. Whole-cell voltage-clamp recordings 88
2.2.5. Data acquisition 90
2.2.5.1. Spontaneous transmitter release 90
2.2.6. Data analysis 90
2.2.6.1. Estimation of R_s and R_{in} 90
2.2.6.2. Detection of spontaneous EPSCs 91

2.2.6.2.1. Statistical analysis 93
2.2.7. Pharmacological agents and solutions 94
2.2.7.1. ACSF 94
2.2.7.2. Stock solutions and drugs 95
2.2.7.3. AMPA iontophoresis 96
2.2.7.4. Loading of BAPTA-AM 98
2.2.8. Histology 99
2.2.8.1. Biocytin labelling technique 99
2.2.8.2. Immunohistochemistry 100
2.3. Results 104
2.3.1. Spontaneous transmitter release 104
2.3.2. Basic observation 105
2.3.2.1. Action of NA 105
2.3.2.1.1. mEPSCs can be stably recorded over time 108
2.3.2.1.2. Iontophoresis of NA onto dendritic synapses 110
2.3.2.1.3. Time course of NA action 111
2.3.2.1.4. Dose response curve for NA 113
2.3.2.2. Pharmacological identify of the AR 114
2.3.2.3. No tonic activation of α_1-AR 125
2.3.2.4. Time course of α_1-AR agonist application 126
2.3.2.5. Chelation of postsynaptic calcium 128
2.3.3. Immunohistochemical evidence for α_1-ARs 130
2.3.4. Verification of signalling cascade 133
2.3.4.1. Blocking phospholipase C 134
2.3.4.2. Blocking of IP_3R on presynaptic stores 136
2.3.4.3. Emptying of Ca^{2+} stores with CPA 138
2.3.4.3.1. Control experiments for KCl depolarisation 140
2.3.4.4. Increased mEPSC frequency is caused by Ca^{2+} release 143
2.3.5. Interaction with other IP_3 producing receptors 145
2.4. Discussion 147
2.4.1. NA increases mEPSC frequency 147
2.4.2. Effective NA concentration to activate ARs 149
2.4.3. Identity of the ARs 150
2.4.3.1. Lack of contribution of α_2- and β-ARs 150
2.4.3.2. Evidence for α_1-ARs 151
2.4.3.3. Internal consistency of pharmacological experiments 152
2.4.3.4. Immunohistochemical evidence 153
2.4.4. Downstream signalling 154
2.4.5. Interactions with IP_3 producing receptors 157
2.4.6. Functional consequences 158
2.5. Conclusion 159

3. Part II 161
3.1. Introduction 162
3.2. Methods 163
3.2.1. Statistical analysis 166
3.3. Results 167
3.3.1. Characterisation of unitary EPSCs 167
3.3.1.1. Electrophysiological properties 167
3.3.1.2. Paired-pulse characteristics of EPSCs 176
3.3.1.3. The setting of these EPSCs 179
3.3.1.4. Release-independence of EPSCs 180
3.3.2. Changes of EPSCs caused by NA 183
3.3.2.1. Depression of EPSCs caused by NA 183
3.3.2.2. Paired-pulse ratio is not altered after NA exposure 185
3.3.2.3. α_1-AR activation depresses the EPSCs 188

3.3.2.4. Further characterization of EPSCs (pooled data) 190
3.3.2.5. Simultaneous block of α_2- and β-ARs 194
3.3.3. Contribution of store release to EPSC 196
3.3.3.1. NA and EPSCs when stores are blocked 198
3.3.4. Contribution of PLCβ to EPSC depression 201
3.3.4.1. Control experiment for ES 203
3.3.5. Speed-up from depression by NA 205
3.4. Discussion 207
3.4.1. Transmitter release in pyramidal cell pairs 207
3.4.2. NA depresses evoked EPSCs 209
3.4.2.1. Noradrenergic modulation of EPSCs 210
3.4.2.2. Depression is caused by α_1-ARs 211
3.4.2.3. Extent of depression and presynaptic parameters 211
3.4.2.4. Stores contribute to each EPSC 212
3.4.2.5. Depression is independent of Ca^{2+} stores 213
3.4.2.6. Depression is also independent of PLCβ 213
3.4.2.7. Recovery from depression is accelerated 214
3.4.2.8. Molecular mechanisms causing this depression 215
3.4.2.9. Functional consequences 217
3.5. Conclusion 218

4. Conclusion 220
4.1. Stores in synaptic transmission 221
4.2. α_1-AR in pathophysiology 222

5. References 224

6. Appendix 265
6.1. Detecting and analyzing mEPSC 265
6.2. Analysing EPSC 278

Abbreviations

2-APB	2-aminoethoxy borate
5-HT	5-hydroxytryptamine
ABC	avidin-biocytin conjugation
α_1-AR	α_1-adrenergic receptor
ACh	acetylcholine
ACSF	artificial cerebrospinal fluid
AMPA	α-amino-3-hydroxyl-5-methyl-4-isoxazole-propionate
AP	action potential
ATP	adenosine triphosphate
ATPase	adenosine triphosphatase
BAPTA	1,2-bis-(o-aminophenoxy)-ethane-N,N,N',N'-tetraacetic acid
BDNF	brain-derived neurotrophic factor
BK	big conductance Ca^{2+}-activated K^+
CA	*cornu ammonis*
CICR	calcium induced calcium release
CNS	central nervous system
CD	2-hydropropyl-β-cyclodextrin
CO	cirazoline
CPA	cyclopiazonic acid
CRE	cAMP response element
cPDF	cumulative probability density function
DAG	diacylglycerol
DHPG	s-3,5-dihydroxyphenylglycine
DMSO	dimethyl sulfoxide
EAAT	excitatory amino acid transporter
EC_{50}	half maximal effective concentration
EPP	end-plate potential
EPSC	excitatory postsynaptic current
EPSP	excitatory postsynaptic potential
ER	endoplasmic reticulum
ES	(7*R*)-4-hydroxy-7-methoxy-*N*,*N*,*N*-trimethyl-3,5,9-trioxa-4-phosphaheptocosaan-1-aminium-4-oxide (edelfosine)
G-protein	guanosine triphosphatase protein
GABA	γ-amino butyric acid

GAT	GABA transporter
GDP	guanosine diphosphate
GFP	green fluorescent protein
GPCR	G-protein coupled receptor
GTP	guanosine triphosphate
HEPES	4-(2-hydroxyethyl)-1-piperazineethanesulfonic acid
KCl	potassium chloride
KS	Kolmogorov-Smirnov
iGluR	ionotropic glutamate receptor
IK	intermediate conductance Ca^{2+}-activated K^+
IP_3	inositol 1,4,5-trisphosphate
IP_3R	inositol 1,4,5-trisphosphate receptor
IPSC	inhibitory postsynaptic current
IR-DIC	infrared differential interference contrast
KA	kainate
LTD	long-term depression
LTP	long-term potentiation
mAChR	muscarinic acetylcholine receptor
MeCP2	Methyl-CpG-binding protein-2
mEPP	miniature end-plate potential
mEPSC	miniature excitatory postsynaptic current
mEPSP	miniature excitatory postsynaptic potential
mGluR	metabotropic glutamate receptor
mIPSC	miniature inhibitory postsynaptic current
MW	molecular weight
NA	noradrenaline
NAAG	*N*-acetylaspartylglutamate
NADH	nicotinamide adenine dinucleotide hydride
NCX	Na^+-Ca^{2+} exchanger
NO	nitric oxide
NMDA	*N*-methyl-D-aspartatic acid
NMJ	neuromuscular junction
NSF	*N*-ethylmaleimide-sensitive fusion
OX	orexin
P2Y	purinergic
PA	prazosin
PB	phosphate buffer
PD	p-(dipropylsulfamoyl)benzoic acid

PIP_2	phosphatidylinositol-4,5-bisphosphate
PKA	protein kinase A
PKC	protein kinase C
PLC	phospholipase C
PMCA	plasma membrane Ca^{2+} ATPase
PO	propranolol
PPD	paired-pulse depression
PPF	paired-pulse facilitation
PSD	postsynaptic densities
RID	release independent depression
R_{in}	input resistance
R_s	series resistance
RyR	ryanodine receptor
SEM	standard error of the mean
SER	smooth endoplasmic reticulum
SERCA	sarco/endoplasmic reticulum calcium ATPase
SK	small conductance Ca^{2+}-activated K^+
SNAP25	synaptosomal associated protein 25
SNARE	soluble *N*-ethylmaleimide-sensitive factor attachment protein receptor
SRF	serum response element
TCF	ternary complex factor
TBS	Trizma® buffered saline
TRP	transient receptor potential
TTX	tetrodotoxin
unc	uncoordinated-18
Munc	mammalian uncoordinated
VDCC	voltage dependent Ca^{2+} channel
vGAT	vesicular GABA transporter
vGluT	vesicular glutamate transporter
YO	yohimbine

1. Introduction

1.1. Overview

Synaptic transmission is a process whereby activity of a presynaptic neurone influences activity of an anatomically adjacent postsynaptic neurone. Synaptic transmission forms the basis for most information transfer between cells within the central nervous system (CNS). It was initially investigated at the chemical synapse formed at the frog neuromuscular junction (NMJ) between the axon terminal of the motoneurone and the muscle cell (Fatt & Katz, 1950). Transmission can be classified according to two observations with or without stimulus in the axon. In the presence of a stimulus, an end-plate potential is generated which at the NMJ causes the generation of an action potential in the muscle cell. However, in the absence of a stimulus miniature end-plate potentials (mEPP) can still be observed, which are approximately 100 times smaller than evoked EPPs (Fatt & Katz, 1952). In this thesis, the term "miniature" will also be used when discussing results, which were obtained in the presence of tetrodotoxin (TTX), a voltage-dependent Na^+ channel blocker.

Transmembrane movement of calcium ions (Ca^{2+}) is central in causing evoked synaptic transmission. At central synapses, this release is caused by Ca^{2+} influx via presynaptic Ca^{2+} channels (Llinás, 1982). It has become evident that presynaptic Ca^{2+} stores may produce some non-stochastic behaviour in evoked synaptic transmission (Llano *et al.*, 2000). Given the notion that release of Ca^{2+} from presynaptic intracellular stores into the cytoplasm can drive spontaneous transmission (Simkus & Stricker, 2002a), this mechanism is important for modulation of evoked transmission. Such modulation could occur by amplification of Ca^{2+} transient from voltage-dependent calcium channels (VDCC) in the presynaptic terminal.

In this thesis, I have investigated both spontaneous and evoked transmitter release using the whole-cell recording technique applied to pyramidal neurones in layer II/III of rat barrel cortex. The primary objective of this study is to determine if the neuromodulator noradrenaline (NA), also called norepinephrine, can cause Ca^{2+} release from presynaptic calcium stores. I reasoned that as NA activates α_1-adrenergic receptors (α_1-AR), phosphatidylinositol-4,5-bisphosphate (PIP_2) is hydrolysed into diacylglycerol (DAG) and inositol 1,4,5-trisphosphate (IP_3). Activation of IP_3 receptor on presynaptic stores then causes Ca^{2+} release from these stores and thus increases

neurotransmitter release. To determine the specificity of the action of NA and verify the signalling cascade involved, I have used a number of pharmacological compounds, which interact directly or indirectly with the signalling cascade leading to Ca^{2+} release from presynaptic stores.

The following introduction will outline the history of investigations into synaptic transmission, in particular the various presynaptic receptors that could potentially promote IP_3 production and cause subsequent Ca^{2+} release from stores. In addition, I will also look at the potential crosstalk between the different receptors that are all linked to IP_3 production.

1.2. Outline of the physiology of synaptic transmission

1.2.1. Historical view

The neurone doctrine suggests that the nervous system is connected by a network of interlacing fibres, which are physically separate from each other (Waldeyer-Hartz, 1891). In the neurone doctrine, Waldeyer-Hartz coined the word "neurone" as a basic cellular unit in the network of interlacing fibres. Based on observations with light microscopy, Kölliker (1853) provided tentative evidence that neurones are discrete cells. The point of contact between two neurones was later termed "synapse" from the Greek word that is translated into English as 'clasp' by Sherrington in a physiology textbook by Foster (1897). This later led to a debate about whether transfer of information within the synapse is electrical or chemical. The invention of the electron microscope by Knoll and Ruska (1932) enabled the ultimate verification of the neurone doctrine by establishing that cells were discrete units separated by a membrane composed of a lipid bilayer.

1.2.2. Electrical *versus* chemical transmission

When neurones are stimulated and fire action potentials, synaptic transmission in the CNS occurs classically between presynaptic nerve terminals and postsynaptic elements, typically spines, which are small protuberances on dendrites of neurones. In the CNS, synaptic transmission can either be electrical (Furshpan & Potter, 1959), chemical (Brock *et al.*, 1952) or both (Martin & Pilar, 1963). At birth, electrical synapses

are more common in the neocortex of mammals than later in life (Connors *et al.*, 1983; Lee *et al.*, 2010). Whilst an electrical synapse functions usually bi-directionally due to the pore formation via the gap junctions between two connecting neurones (Furshpan & Potter, 1959), information flow at the chemical synapse is largely unidirectional, i.e. from the presynaptic terminal to the postsynaptic neurone. From here onwards, when I use the term synaptic transmission, I will mostly refer to chemical transmission.

1.2.3. Chemical transmission

Generation of an action potential near the axon initial segment upon physiological stimulation leads to propagation of the action potential down the axon to the nerve terminals where voltage dependent Ca^{2+} channels (VDCCs) are located. At the nerve terminals, depolarisation of the membrane by the action potential causes VDCCs to open. Subsequent influx of Ca^{2+} from the extracellular fluid compartment via VDCCs triggers neurotransmitter vesicles to fuse with the presynaptic membrane, and thus results in neurotransmitter release. Once released, the neurotransmitter diffuses across the synaptic cleft, the specialised 20 – 40 nm space between the two contacting neurones (Palay, 1956) and binds to the transmitter receptors on the postsynaptic membrane.

1.2.3.1. Nature of a transmitter

Dale's principle states that a neurone uses the same neurotransmitter at all its synaptic connections to other cells, regardless of the identity of the target cell (Dale, 1934). He considered the neurone to be a single biochemical unit that can release the same neurotransmitter at all of its synapses. However, his principle no longer holds true in its strictest sense. For example, Jonas *et al.* (1998) reported that, in paired recordings, at an interneurone-motoneurone synapse in spinal cord slices, inhibition was generated by both glycine and GABA.

A neurochemical can be classified as a transmitter if it meets the following criteria (Werman, 1966):

a) The precursors and/or synthesising enzymes are located in the presynaptic terminal,
b) The chemical is present in the presynaptic terminal,
c) It is available in sufficient quantity in the presynaptic neurone to affect the postsynaptic neurone,

d) There are postsynaptic receptors for the chemical to bind, and
e) A biochemical mechanism for clearance of the chemical is established so that the extracellular concentration is kept minimal and does not interfere with synaptic transmission.

1.2.3.1.1. Iono- and metabotropic receptors

Based on their functional characteristics, neurotransmitter receptors can be divided into two broad categories: ionotropic (for review see Engelman & MacDermott, 2004), and metabotropic (Eccles & McGeer, 1979; for review see Niswender & Conn, 2010). Activation of the postsynaptic receptors, in the case of ionotropic receptors, causes a ligand-gated ion channel to open and a current to flow, which then changes the local transmembrane potential of the neurone. Depending on the identity of the neurotransmitter, if it causes an increase in the firing of action potentials, then the neurotransmitter is considered excitatory, while, when reducing the firing rate, it is inhibitory. In the mammalian central nervous system, excitation is mostly glutamatergic and inhibition GABAergic or glycinergic.

1.2.3.1.2. Neuromodulation

In contrast to standard synaptic transmission, a neuromodulator is a neurochemical substance that cannot cause neuronal firing in its own right but can modulate the neurone's firing characteristic either up or down, mostly via a second messenger system. Examples of neuromodulators are dopamine, noradrenaline, serotonin and most neuropeptides. It should be stressed here that a neurochemical can be both a "standard" transmitter (mostly via ionotropic action) as well as a neuromodulator (mostly via metabotropic action). Such neurochemicals are, among others, glutamate and acetylcholine. I will discuss the activation of one such neuromodulator on their respective receptors further below (see 1.5.7 Metabotropic Receptor Coupled to IP_3 Prodution).

1.2.3.2. Modes of transmission (evoked versus spontaneous)

Synaptic transmission can be categorised into two different modes. The first is called evoked transmitter release, in which the neurotransmitter is released after activation by an action potential. Evoked transmitter release is an activity-dependent process and the amount of neurotransmitter being released is highly regulated and precisely timed

(Eccles & O'Connor, 1939). The other mode is called spontaneous release, in which release of neurotransmitter is independent of any physiological stimulus. The underlying mechanism reflects the spontaneous fusion of synaptic vesicles with the presynaptic membrane (Fatt & Katz, 1952). It may be influenced by the internal calcium concentration, phospholipid concentration, and co-action of neuromodulators.

1.2.3.3. The process of transmitter release

In the following sections, I will systematically describe the processes that occur during the lifetime of a synaptic vesicle at a terminal of an excitatory neurone. The first step is the synthesis of glutamate, followed by loading of the glutamate into synaptic vesicles in the nerve terminals. The vesicles are then translocated close to the plasma membrane, and with the help of several proteins, the vesicles ultimately undergo exocytosis. The released glutamate in turn diffuses across the synaptic cleft and eventually binds to receptors on the postsynaptic membrane, thereby generating a postsynaptic response. Following activation of the postsynaptic receptors, glutamate in the synaptic cleft is taken up and broken down mainly by astrocytes. The emptied vesicles then undergo endocytosis for refilling with transmitter. Once refilled, the synaptic vesicles will be readied for release again. The process of transmitter release can better be conceptualised by describing the central concept of synaptic physiology, namely the vesicular hypothesis.

1.2.3.4. Vesicular hypothesis

The vesicular hypothesis (Katz, 1962) has been derived mostly from studies of correlation between the release of synaptic vesicles and the measurement of spontaneous events at the neuromuscular junction of vertebrates and later confirmed for central synapses (Kuno, 1964) and subsequently been refined using recordings of membrane capacitance (Neher & Marty, 1982). The vesicular hypothesis proposes that, upon nerve stimulation, a discrete quantum of transmitter is released into the synaptic cleft by exocytosis of a number of single synaptic vesicles (Katz, 1962), producing a response, which can be measured between stimuli, corresponding to the size of the spontaneous quantum.

1.2.3.4.1. Morphology of the synapse

Morphological observations of changes in the stimulated nerve terminals and the correlation of these changes with the electrophysiological state of the terminals have provided evidence in support for the vesicle hypothesis. Using morphological criteria derived from electron microscopy, there are two types of vesicles: asymmetrical and symmetrical. The asymmetrical vesicles with dimensions of 20 – 40 by 70 – 80 nm are mostly found in inhibitory neurones (Palay, 1956). In contrast, symmetrical vesicles can be categorised into four different classes; electron lucent, small spot, dense cored and granule vesicles. The first class of vesicles is the most common and has a typically round appearance of 20 – 40 nm in diameter with clear centres (electron lucent). These are found at the NMJ (De Harven & Coërs, 1959; Wolburg *et al.*, 1990), in autonomic ganglia (Tremblay *et al.*, 1979) and throughout the CNS (Clements *et al.*, 1990). The second type contains larger vesicles of about 40 – 60 nm in diameter, which have electron-dense centres (Krasne & Stirling, 1972). These vesicles are commonly found at sites of aminergic transmission in the CNS and in the peripheral sympathetic nervous system. The third type of synaptic vesicle is characterised by its large size (80 – 100 nm diameter) and having a central dense core (Bennett, 1941; Watanabe *et al.*, 1986; Schürmann *et al.*, 1991). These dense-cored vesicles contain neuropeptides, which are synthesised in the rough endoplasmic reticulum (ER). These are then pinched off from the ER. They are the hallmark of neuroendocrine and other secretory cell types (Kim *et al.*, 2006). Unlike small synaptic vesicles, dense-cored vesicles are located at a distance from the active zone of the presynaptic nerve terminal. The release of neurotransmitters from these dense-cored vesicles occurs in response to a higher concentration of intracellular Ca^{2+} compared to that required for the release of small vesicles (Voets *et al.*, 2001). The last type consists of very large vesicles of 120 – 150 nm in diameter (Cuadras & Marti, 1992). These vesicles are characteristic of neurosecretory nerve endings such as those found in the neurohypophysis (posterior pituitary gland), which contain neuropeptides including oxytocin and vasopressin.

Synaptic vesicles are exocytosed via fusion of the synaptic vesicle with the plasma membrane at the active zone of the presynaptic terminal (Akert *et al.*, 1969). The active zone is a specialisation of the presynaptic membrane where fusion of the synaptic vesicle with the plasma membrane occurs. Fusion discharges the content of the synaptic vesicle into the synaptic cleft (exocytosis). The mechanism for synaptic vesicle exocytosis will be discussed further below (see SNARE hypothesis for vesicle exocytosis). The fused membrane is later invaginated back into the cytoplasm

(endocytosis), away from the active zone to form new synaptic vesicles (see vesicle endocytosis and recycling).

Additional evidence in support of the vesicle hypothesis is a variation to the vesicular model known as the 'kiss-and-run' model (Ceccarelli *et al.*, 1973; for review see Fesce *et al.*, 1994). The 'kiss-and-run' hypothesis states that the exocytosis of neurotransmitter avoids the intermixing of components of the synaptic vesicle membrane with those of the plasma membrane. Therefore, about 8% of the amount of neurotransmitter is released within an exocytosis duration of 0.55 ms into the synaptic cleft (Alvarez de Toledo *et al.*, 1993). After the discharge of the neurotransmitter, the intact synaptic vesicle is recycled back into the cytoplasmic domain of the synapse to refill the synaptic vesicle.

1.2.3.4.2. Arguments for the vesicle hypothesis

Given the notion that vesicle secretion will show a rise in membrane capacitance, a number of fluorescence imaging techniques have been developed to verify the endocytosis and exocytosis process. The imaging of fluorescent vesicles via confocal microscopy has provided evidence for synaptic vesicle recycling in the presynaptic terminal (Bouevitch *et al.*, 1993). A confocal microscope utilise contrast from variation in a specimen's ability to generate light from the incident light, while a conventional optical microscope utilise its contrast by detecting variations in optical density, path length, or reflective index of the specimen. The synaptic vesicles were eventually loaded with a membrane impermeable, but hydrophilic styryl dye (Betz *et al.*, 1992). An example of a styryl dye is the FM1-43. To stain synaptic vesicles, the neurone is exposed for a period of several minutes of activity to FM1-43 so that the dye attaches itself to the membrane of the vesicles. With a number of stimuli, the dye will be taken into the vesicle pool after undergoing endo- and exocytosis of the stained vesicles. With the FM loading-unloading technique, Smith and Betz (1996) showed that with a large depolarisation from -90 to 0 mV for 1s, exocytosis precedes endocytosis. However during prolonged stimulation, the rate of endocytosis equals that of exocytosis after 3 minutes, due to the two processes converging into a steady state.

In cultured rat hippocampal neurones, single boutons containing one active zone can be activated by focal perfusion of hyperosmotic solution containing high potassium. Single 5 s stimuli evoked release of a readily releasable pool of 20 quanta, replenishing later with a 10 s time constant. This corresponds to the time required for endocytosis of

the released vesicles and their re-entry into a releasable pool, as measured by FM1-43 destaining (Ryan & Smith, 1995). In another preparation by Allen and Stevens (1994), the action potentials only release one quantum per release site, vesicle release occurs only about 25% of the time, with a refractory time of 5 – 20 ms. If a quantal response is due to release of a single vesicle, this would correspond to a vesicle depletion rate of 0.25% of the total vesicle pool. This is a close estimate of the rate of vesicle depletion per action potential from FM1-43 destaining experiments (Ryan & Smith, 1995). Ultrastructural studies of presynaptic vesicles of lamprey reticulospinal axons by Wickelgren *et al.* (1985) showed that a stimulus of either a train of action potentials (20 Hz for 15 min) or a K^+ depolarisation (50 mM K^+ for 15 min) induces the release of synaptic vesicles. They also showed that the release of vesicles is dependent of Ca^{2+}.

A prediction of the vesicular hypothesis is that when synaptic vesicles fuse with the cell membrane of the nerve terminal, there will be an increase in cell membrane, which can be tracked as an increase in membrane capacitance. Although this increase is small, it is measurable. Based on this idea, Neher and Marty (1982) managed to show that this change in membrane capacitance reflects the addition of single secretory vesicles to the surface of adrenal chromaffin cells. This type of experiment has now also been applied to a large glutamatergic synapse, namely the calyx of Held, to lend further support that the change in membrane capacitance correlates with the size of the postsynaptic response (Sun & Wu, 2001). He *et al.* (2009) further showed that, at the calyx of Held, the rate of evoked synaptic vesicle release is 3 vesicles per 10 ms.

1.2.3.4.3. Arguments against the vesicle hypothesis

With all the evidence for quantal transmission, there are, however, some experimental observations, which are not necessarily explained by the vesicle hypothesis. For example, an observation at the frog NMJ showed that a change in mEPP size is not always correlated with a corresponding change in vesicle size (Florey & Kriebel, 1988). In another instance, the distribution of the mini amplitudes can rapidly change its shape in the absence of any stimulation (Kriebel *et al.*, 1976). Both of these observations may lead to the question if the quantum is the content of a vesicle. To account for these changes, it was suggested by Vautrin *et al.* (1992) that vesicles are formed immediately before release from newly synthesized neurotransmitters. The formation of new vesicles at a later stage could account for incomplete filling and cause a smaller vesicle size. This idea suggests that the change in quantal size is at the expense of the

neurotransmitter concentration (presynaptic), and not the number of postsynaptic receptors.

Multivesicular release can occur during evoked release. Based on the size of the vesicle and the release response, the coefficient of variation of quantal amplitude is small, less than 0.2 (Boyd & Martin, 1956). Kuffler and Yoshikami (1975) reported that the time course of excitatory postsynaptic potentials caused by acetylcholine (ACh) released iontophoretically, closely matched the physiological synaptic potentials. Later, they reported that the release of a quantum of transmitter consists of less than 10'000 molecules of ACh.

Another controversial aspect to the vesicle hypothesis relates to the time requirements of the many protein interactions proposed to bring about vesicle fusion. At the frog NMJ, the response of the muscle cell to nerve stimulation has a latency of 1 ms (Katz & Miledi, 1965). This delay is about 200 µs at the squid giant synapse (Llinás *et al.*, 1981) and less than 1 ms at the mouse NMJ (Mallart & Brigant, 1982). Almers (1990) indicates that a latency of 500 µs would only allow for a single enzymatic reaction. This itself is a conundrum as the life cycle of a quantum consists of a series of steps. In addition, vesicle fusion to the lipid bilayer would require a substantial amount of energy.

To show that the single vesicle is the structural basis for the vesicle hypothesis, Heuser and Reese (1981) used a quick-freezing technique to show that the coalescence of the vesicle with the membrane can be morphologically distinguished by their apparent proximity to the presynaptic active zone. The quick freezing technique enables them to examine both the beginning and aftermath of vesicle exocytosis, from the beginning of quantal release until recycling of vesicles. The latency of the priming of vesicles allowed them to conclude that the vesicles are primed for release via an interaction with a set of specialised proteins in the presynaptic terminal.

1.2.3.4.4. Non-vesicular release of transmitter

There have been controversies regarding non-vesicular release of transmitter, a notion first described by Douglas and Paton (1954). They observed a marked depolarisation (< 10 mV) of the end-plate, not caused by twitching of the cat *gracilis* muscle after injection of tetraethylpyrophosphate, an anticholinesterase, into the circulation. Katz and Miledi (1977), together with Vyskočil and Illés (1977) provided electrophysiological

evidence for the non-vesicular release of transmitter at the same time. Katz and Miledi (1977) reported a local hyperpolarisation of 41 ± 6.7 μV originating from a continuous leakage resulting in a measurable concentration of 10 nM ACh in the extracellular space. This hyperpolarisation was observed after applying iontophoretic doses of curare, a blocker of the nicotinic ACh receptor. Vyskočil and Illés (1977) reported a hyperpolarisation of 1.82 ± 0.43 mV at the postjunctional membrane of the mouse diaphragm fibres after local application of curare and anticholinesterase. Vyskočil (1985) later showed that this form of release is caused by the vesicular ACh transporter residing in the plasma membrane after vesicle fusion. He showed that when using vesamicol, an inhibitor of the vesicular ACh transporter, to block loading of ACh into synaptic vesicles, a hyperpolarisation of 1.8 ± 0.6 mV in the mouse diaphragm fibre without a change in amplitude could be observed. Katz and Miledi (1977) estimated that this leakage of transmitter could be two orders of magnitude larger than that caused by spontaneous transmitter release.

Freeze fracture replicas of the *Torpedo* electroplaque showed that transmission of an impulse was accompanied by the momentary appearance (2 – 3 ms) of a population of large intramembrane particles > 10 nm in diameter in both the protoplasmic and external leaflets of the presynaptic plasma membrane (Muller *et al.*, 1987). This might lead to the assumption that the receptors are activated before the occurrence of vesicle fusion. However, consistent with synaptic transmission, stimulation of the electroplaque at a low extracellular concentration of Ca^{2+} (0.16 mM) did not produce any intramembrane particle. Using a chemiluminescent technique, Israël and Lesbats (1981) showed that newly synthesised ACh are released upon stimulation, while vesicular ACh remains unchanged for several minutes in the *Torpedo* electric organ. This indicates that there is little or no exchange between cytoplasmic and vesicular ACh.

The mediatophore first isolated from cholinergic nerve endings of the electric eel, *Torpedo* marmorata (Birman *et al.*, 1986), is a presynaptic membrane protein involved in exocytosis of ACh at the active zone in a Ca^{2+} dependent manner (Brochier *et al.*, 1993). It has an oligomeric structure of 8 nm in diameter, with a molecular mass of approximately 200 kDa (Israël *et al.*, 1986). Israël *et al.* (1987) reported that the mediatophore has a binding affinity for Ca^{2+} with a K_d of 25 μM. The mediatophore displays similar properties to the synaptosomes, with a reduction in ACh release induced by > 10 mM Ca^{2+}.

It has been suggested that non-vesicular release of ACh at the rat NMJ can be modulated by glutamate via activation of NMDA receptors (Malomouzh *et al.*, 2003), which have been found in the muscle membrane at the rat end-plate (Hamberger & Nyström, 1984). Using a peptidase assay, Malomouzh *et al.* (2005) demonstrated that carboxy peptidase II, a membrane-bound peptidase at the perisynaptic Schwann cells surrounding the rat NMJ, produces glutamate and *N*-acetylaspartate from hydrolysis of *N*-acetylaspartylglutamate (NAAG), which is secreted at the nerve terminal of the motoneurone. The newly synthesised glutamate in turn activates the postsynaptic NMDA receptors expressed on the muscle membrane at the rat end-plate. The consequent Ca^{2+} entry increases the activity of a Ca^{2+}-dependent synthase coupled to the NMDA receptors, thereby promoting production of NO in the sarcoplasm of the muscle fibres. The NO that is produced subsequently diffuses from the muscle fibres to the presynaptic terminal of the motoneurone to attenuate the non-quantal secretion of ACh through a cGMP-dependent mechanism. In addition, it has been shown that the non-quantal release of ACh also has a negative feedback mechanism that involves activation of VDCCs in the muscle membrane and the synthesis of NO in the sarcoplasm (Urazaev *et al.*, 1997).

Non-vesicular release of glutamate can occur via glutamate transporters (see below). Szatkowski *et al.* (1990) reported that raising the K^+ concentration around glial cells evoked an outward current that resulted from the reversed glutamate transport. The current is activated by intracellular glutamate and Na^+, but inhibited by extracellular glutamate and Na^+. By knocking out the *Drosophila* xCT gene, which codes for a subunit of the cystine/glutamate transporter, Augustin *et al.* (2007) showed that the transporter functions to maintain ambient extracellular glutamate. The constitutive desensitisation of iontotropic glutamate receptors suppresses the clustering ability of the cystine/glutamate transporter.

Unlike glutamatergic synapses, the majority of GABA that is released is transported back into the presynaptic GABAergic nerve ending while a smaller fraction is taken up by astrocytes surrounding the GABAergic synapse (for review see Schousboe *et al.*, 2004). Using immunocytochemistry, Chaudhry *et al.* (1998) showed that the vesicular GABA transporters (vGATs) are localised at both the GABAergic and glycinergic nerve terminals in the CNS of the rat. Cammack (1994) reported that GABA transporter-1 (GAT-1) couples to two Na^+ and one Cl^-, so that GABA can be translocated at a rapid rate. Deken *et al.* (2000) demonstrated that the cytoplasmic N-terminal domain of the GABA transporter interacts directly with syntaxin 1A, a component of the SNARE complex. This interaction results in a decrease in transport rate. Using pairs of

connected hippocampal neurones in culture, Wu *et al.* (2007) showed that GAT-1 regulates tonic inhibition by clamping ambient GABA level at a concentration high enough (> 0.1 μM) to activate $GABA_A$ receptors.

1.2.3.4.5. Synthesis of transmitter

There are two categories of neurotransmitters, small molecule neurotransmitters and neuropeptides. Small molecule neurotransmitters such as ACh are synthesised locally within the axon terminal. Some of the precursors necessary for the synthesis of these molecules are taken up by selective transporters on the terminal membrane while others may be readily available within the nerve terminal. The enzymes necessary to the reaction from precursor to transmitter are typically produced in the cell body and transported to the terminal by slow axonal transport. The synthesis of neuropeptides first requires gene transcription, which takes place perisomatically. Similar to protein expression, the mRNA undergoes translation in the rough endoplasmic reticulum. The resulting transmitter is then packed in the Golgi complex into secretory vesicles, which are transported to the nerve terminal.

In the case of glutamate, the main precursor is glutamine. Glutamine is synthesised by the glial-specific enzyme glutamine synthase from the precursor glutamate and ammonia in astrocytes (Norenberg & Martinez-Hernandez, 1979) or glial cells (Cammer, 1990). The concentration of glutamate and glutamine in extracellular fluid of the rabbit hippocampus is 4 ± 1.4 and 250 ± 47 μM, respectively (Hamberger & Nyström, 1984). Using gel filtration of rat cortex on Sepharose 4B column, Riveros *et al.* (1986) estimated 3640 glutamate molecules in a single glutamatergic vesicle, with an intravesicular glutamate concentration of 210 mM. Burger *et al.* (1989) reported an intravesicular glutamate concentration of 60 mM in the rat cortex using immunoisolation of synaptic vesicles. In contrast, immunocytochemical studies in the rat hippocampus revealed that a glutamatergic neurone contains approximately 5 – 10 mM cytoplasmic glutamate (Ottersen *et al.*, 1990; Ottersen *et al.*, 1992). Clements *et al.* (1992) estimated from the degree of displacement of known concentrations of D-aminoadipate, a rapidly dissociating and competitive NMDA receptor antagonist, by glutamate using EPSC recordings that glutamate concentration at the synaptic cleft in cultures of rat hippocampal neurones is 1.1 mM. Glutamine is typically metabolised by glial cells into glutamate by phosphate-activated glutaminase (Martinez-Hernandez *et al.*, 1977) or released via the amino acid transport system SN1 (Chaudhry *et al.*, 1999) to be taken up into the presynaptic terminal of the neurone. In the presynaptic terminal,

glutamine then undergoes a transamination catalysed by the mitochondrial isoform of aspartate aminotransferase. The resulting α-ketoglutarate is translocated out of the mitochondria and then transaminated in the cytoplasm by the cytoplasmic isoform of aspartate aminotransferase.

Glutamate in the extracellular space can be transported into neurones and glial cells by two classes of glutamate transporters: the excitatory amino acid transporters (EAATs) and the vesicular glutamate transporters (vGluTs). The transport activity of both of these transporters is dependent on the electrochemical gradient of Na^+. There are five subtypes of EAATs. EAAT1 and EAAT2 are predominantly expressed in glial cells (Storck *et al.*, 1992), while EAAT3 and EAAT4 are found typically in neurones (Kanai & Hediger, 1992; Fairman *et al.*, 1995) and EAAT5 is located at retinal ganglion cells (Arriza *et al.*, 1997). Most EAATs are present in astrocytes (Liang *et al.*, 2008). Zerangue and Kavanaugh (1996) used voltage-clamping with a pH sensitive fluorescent dye to measure the reuptake of glutamate by EAAT3 and found that three sodium ions and one proton are co-transported with each glutamate molecule taken up into the cell. Classically, after uptake, astrocytes convert the glutamate into glutamine and release the glutamine back into the extracellular space (Palmada & Centelles, 1998). The glutamine will be taken up by neurones to be converted back into glutamate. However, EAATs have also been reported at axon terminals and dendritic spines (He *et al.*, 2000). The EAATs clear the free glutamate from the synaptic cleft at a time constant of 100 μs (Tong & Jahr, 1994).

There are three isoforms of vGluTs, vGluT1 (Bellocchio *et al.*, 2000; Fujiyama *et al.*, 2001), vGluT2 (Takamori *et al.*, 2001) and vGluT3 (Gras *et al.*, 2002). The vGluTs, which have a strong binding affinity for L-glutamate over the D-isoform, mediate the uptake of glutamate with co-transport of inorganic phosphate and Na^+ across the plasma membrane (Moriyama & Yamamoto, 1995). Immunohistochemical and immunogold electron microscopy of the rat cortex have revealed that both the vGluT1 and vGluT2 are largely complementarily located at the presynaptic nerve terminals, with limited overlap (Fremeau *et al.*, 2001). Schenck *et al.* (2009) showed that vGluT1 acts as a glutamate/chloride exchanger. As chloride exits from the vesicle and glutamate enters, the charge and osmotic balance are maintained. vGluT1 is present at synapses known to exhibit low release probability and long-term potentiation while vGluT2 is present at synapses known to exhibit high release probability and long-term depression (Fremeau *et al.*, 2001). However, vGluT3 has been reported to be co-localised with serotonergic, cholinergic and GABAnergic neurones (Fremeau *et al.*, 2002).

Glutamate can also be produced from glucose by transamination of α-oxogluratarate, an intermediate in the citric acid cycle (Hamberger *et al.*, 1979). In another pathway, glucose can be metabolised into α-ketoglutarate to undergo transamination with alanine in the cytosol to produce glutamate (Peng *et al.*, 1991). Glutamate synthesised in the presynaptic terminal is loaded into synaptic vesicles by the vGluTs.

1.2.3.4.6. Generation and life-time of vesicles

The production of vesicles for transmitter release can result from the following pathways: firstly, and most commonly, from endosome budding; secondly, the budding from the trans-Golgi network; thirdly, from the transport of secretory vesicles along the axon, and finally the endocytic pathway.

Synaptic vesicles generated from the above pathways can be mediated by a clathrin coat-mediated budding. This budding occurs as a consequence of the invagination of the clathrin-coated plasma membrane (Roth & Porter, 1964) or from internal vacuoles with the constriction of dynamin mediated by GTP hydrolysis (Takei *et al.*, 1995). Vesicles that are generated at the soma are transported to the nerve terminals via fast axonal transport at a rate of about 0.8 – 3.5 μm/s (Levin, 1977; Grafstein & Forman, 1980; Allen *et al.*, 1982). Vesicles are moved either along microtubule tracks by ATP-driven motor proteins of the kinesin and dynein families (Goldstein & Yang, 2000) or along actin filaments of the myosin family (Schliwa & Woehlke, 2003).

Neuropeptides synthesised in the rough endoplasmic reticulum are directed to the Golgi apparatus for glycosylation. Janetzko *et al.* (1989), showed that by combining a monoclonal antibody and immunochemistry method, the synaptic vesicles in the electromotoneurone of the *Torpedo marmorata* originate directly from the trans-Golgi network. Besides being transported by secretory vesicles, neuropeptides may also be translocated to the axon by means of the endoplasmic reticulum. Using a combined technique of electron microscopy and zinc iodide-osmium tetroxide, Stelzner (1971) showed that synaptic vesicles can be produced in the Golgi apparatus and also in the smooth ER.

Synaptic vesicles can also be generated via recycling of exocytosed vesicles (Ceccarelli & Hurlbut, 1980; Torri-Tarelli *et al.*, 1987). By attaching a pH-sensitive green fluorescent protein to the luminal domain of the synaptic vesicle protein-

associated membrane protein (VAMP), the change in fluorescence caused by the alkalisation and reacidification of the vesicle provides a tool for tracking the kinetics of exocytosis and endocytosis (Sankaranarayanan & Ryan, 2000). The rate of vesicle internalisation in hippocampal neurones appears to be up to 1 vesicle per second, and the duration of recycling of the exocytosed vesicle is about 5 seconds. The mechanism of endocytosis will be discussed further below.

1.2.3.4.7. Loading of vesicles with transmitter

The transport of the L-glutamate by the vGluTs was first described by Disbrow *et al.* (1982) as an ATP-dependent, proton conductive protein in the rat brain. vGluTs prefer the membrane potential difference to the pH difference as the driving force for glutamate uptake (Maycox *et al.*, 1988). Tabb *et al.* (1992) later reported that the uptake of L-glutamate into the synaptic vesicle requires a large $\Delta\psi$ and a small ΔpH. The vGluTs use the electrochemical gradient ($\Delta\psi$) generated by the vacuolar ATPase (v-type H^+-ATPase) to transport the L-glutamate anion into the interior of the synaptic vesicles. The electrochemical gradient is created by hydrolysing ATP with v-type H^+-ATPase. The flow of H^+ into the interior of the synaptic vesicle also generates a pH gradient (ΔpH) across the vesicle membrane. The interior pH of cholinergic synaptic vesicles has been estimated to be 5.5 ± 0.3 (Fuldner & Stadler, 1982). Using a pH sensitive yellow fluorescence protein, Zhang *et al.* (2010) showed that the v-type H^+-ATPase continues to extrude cytosolic H^+ even after being incorporated into the plasma membrane (full fusion), causing an alkalinisation of the intraterminal milieu. The resulting cytosolic alkalinisation may facilitate the endocytosis of synaptic vesicles. A low concentration of chloride (1 – 5 mM) ensures best vGluT efficiency by increasing the affinity for ATP and resulting in an increased proton pump activity (Naito & Ueda, 1985). Schenck *et al.* (2009) showed that the luminal Cl^- concentration enhances the loading of glutamate by facilitation of membrane potential driven uptake. The vGluTs show strict substrate recognition for L-glutamate over the D-isoform, and also for both isoforms of aspartate (Moriyama & Yamamoto, 1995). Di Giovanni *et al.* (2010) showed that the c-subunit of the v-ATPase membrane domain interacts with the synaptobrevin, an element of the SNARE complex (see below) to undergo exocytosis.

1.2.3.4.8. SNARE hypothesis for exocytosis

Datyner and Gage (1980) observed at the mouse neuromuscular junction that, following a stimulus, there was a brief delay, followed by a sigmoidal increase in

secretion, which then decayed exponentially. The fusion of the synaptic vesicle to the plasma membrane is a process that does not occur easily. The reason is that the inner leaflet of the bi-layered membrane of the synaptic vesicle has to be fused with the outer leaflet of the plasma membrane during exocytosis while the outer leaflet of the synaptic vesicle has to be fused with the cytosolic leaflet of the plasma membrane. Khanin *et al.* (1994) showed that diffusion alone cannot account for the fast release of neurotransmitters.

To explain this conceptually, the soluble *N*-ethylmaleimide-sensitive factor attachment protein receptor (SNARE) hypothesis of a universal 'docking and fusion particle' was proposed by Rothman and Warren (1994). It identifies three key components for exocytosis. These are the v-SNARE (synaptobrevin), and the t-SNAREs (syntaxin) and the cytosolic adaptor protein (SNAP-25), which is an *N*-ethylmaleimide-sensitive fusion protein (NSF). The v-SNARE is a vesicle membrane protein and one of the t-SNAREs, syntaxin, is a target membrane protein whilst SNAP-25 is a cytosolic co-factor. The assembly of the v- and t-SNAREs into a receptor complex together with SNAP-25 forms the SNARE complex. Using quick-freeze/deep-etch electron microscopy, Hanson *et al.* (1997) showed that the SNARE motifs of syntaxin-1 and synaptobrevin bind in a parallel fashion, suggesting that the SNARE complex assembly may provide the energy for membrane fusion.

At rest, syntaxin and SNAP-25 are predominantly localised to the presynaptic plasma membrane, whereas synaptobrevin is predominantly localised to the synaptic vesicle. During vesicle docking, these SNAREs assemble into complexes in the *trans*-configuration in such a way that the synaptobrevin on the outer leaflet of the vesicular membrane and syntaxin together with SNAP-25 on the inner plasma membrane leaflet become adjacent to each other. The idea is that the SNARE assembly is sufficient to overcome the energy barrier separating the membranes and thus to initiate membrane fusion (Jahn *et al.*, 2003). However, without additional protein partners, this process can be quite slow.

Depolarisation at the nerve terminal raises the intracellular Ca^{2+} via VDCCs. This increase is detected by the Ca^{2+} sensor synaptotagmin (Littleton *et al.*, 1993). From the FRET analysis by Choi *et al.* (2010), Ca^{2+} binds to both C2 domains of synaptotagmin to initiate the binding of synaptobrevin to syntaxin-1-SNAP-25 (for review see Rizo & Rosenmund, 2008). After vesicle fusion, the SNARE complex is in the *cis*-configuration. The complex has to be reconfigured and relocalised for a subsequent round of exocytosis. This happens during endocytosis and re-priming.

Brown *et al.* (2010) showed that approximately half of the cases of glutamate release utilise the proton gradient between the vesicle and synaptic cleft of rat *cornu ammonis* 1 (CA1) pyramidal neurones. Recently, using a liposome fusion technique Van den Bogaart *et al.* (2010) showed that one SNARE complex may be sufficient for membrane fusion. However, using more sophisticated techniques, Mohrmann *et al.* (2010) estimated that at least three SNARE complexes are required for fast vesicle fusion *in vivo*.

1.2.3.4.9. Docking and pre-fusion

Docking is a process during which the vesicle and presynaptic membrane line up at the active zone via the rab3 G-proteins (Couteaux & Pécot-Dechavassine, 1970). On the vesicles, rab3 is present in the GTP-bound state and complexes with rabphilin-3, a putative effector protein (Shirataki *et al.*, 1993). Stimulation at the nerve terminal leads to hydrolysis of GTP-rab3 to GDP-rab3, with subsequent dissociation of rab3 from rabphillin-3 (Fischer von Mollard *et al.*, 1994). The free GDP reassociates with free synaptic vesicles to undergo GDP-GTP exchange. In the hippocampal synapse, Schikorski and Stevens (2001) showed that there are about 5 – 10 docked vesicles at the active zone using a combination of photoconversion of FM1-43 and electron microscopy. Using caged calcium compound DM-nitrophen, Neher and Zucker (1993) showed that the docking of vesicles in bovine chromafin cells is Ca^{2+}-dependent.

Following docking, the vesicles are primed to gain fusion competence. Vesicles that are primed at the active zones are able to fuse to create a small opening, which grows larger until the vesicle membrane collapses into the presynaptic membrane for exocytosis to occur. Vesicle docking and priming require a number of proteins, which speed up the process of exocytosis. Among the proteins involved are complexins (McMahon *et al.*, 1995), unc-13 in the nematodes and munc-13 in the mammalia (Varoqueaux *et al.*, 2002), munc-18 (Togneri *et al.*, 2006), syntaxins, synaptotagmins and the SNARE complex. Varoqueaux *et al.* (2002) found that the munc-13 is essential for vesicle docking as synaptic transmission was totally abolished by mun-13 knockout. The munc-13 protein family binds to syntaxins to regulate its machinery (Betz *et al.*, 1997). Complexins are 15 kDa proteins, which bind with high affinity to the assembled SNARE complex to prevent fusion and are removed upon the activation of synaptotagmin-1 by Ca^{2+} (Pabst *et al.*, 2002; Schaub *et al.*, 2006). Using real-time visualisation, An *et al.* (2010) showed that complexin is recruited during a late step in

exocytosis. Syntaxins also bind to synaptotagmin in a Ca^{2+}-dependent manner and interact with voltage-dependent Ca^{2+} and K^+ channels (Betz *et al.*, 1997). After the vesicles are primed, exocytosis of the vesicle can be triggered within ≤ 0.2 ms of Ca^{2+} influx that results from the arrival of an action potential in the nerve terminal (Llinás *et al.*, 1981; Schneggenburger & Neher, 2000).

1.2.3.4.10. Exocytosis

Given the notion that a Ca^{2+} sensing protein is required for vesicle release, it was proposed that synaptotagmin-1 could function as a Ca^{2+} sensor for a number of reasons. Firstly, synaptotagmin-1 is required for fast Ca^{2+}-triggered synaptic vesicle exocytosis but not for slower Ca^{2+}-independent spontaneous release (Geppert *et al.*, 1994). Secondly, synaptotagmin-1 has two prominent Ca^{2+}-dependent binding domains (C2A and C2B), each of which facilitates the binding of phospholipids to the plasma membrane in the presence of Ca^{2+} (Earles *et al.*, 2001). Thirdly, the binding of synaptotagmin to phospholipids is fast, i.e. in ≤ 500 µs (Bai *et al.*, 2000).

Using green fluorescent protein (GFP) to label SNAP-25, Knowles *et al.* (2010) reported more than ten-fold excess of SNAP-25 over syntaxin. The excess of SNAP25 can facilitate the formation of SNARE complex and cause spontaneous transmitter release. Kupchik *et al.* (2011) showed that, in addition to Ca^{2+} influx, the charge movement of the M_2-muscarinic receptor, a G protein-coupled receptor in the presynaptic membrane may be necessary for neurotransmitter release. The Ca^{2+}/H^+ antiport (see below) can also facilitate exocytosis. Cordeiro *et al.* (2010) demonstrated that the vesicular Ca^{2+}/H^+ antiport functions to shorten "phasic" transmitter release, allowing the synapse to transfer brief impulses, and also to exocytose vesicles at higher frequencies.

1.2.3.4.11. Transmitter diffusion and termination of release

When the synaptic vesicle fuses with the plasma membrane, its content is spilled into the synaptic cleft. The synaptic cleft is about 20 nm wide. Synapses are asymmetric cell junctions. They are formed from a presynaptic neurone, which releases the neurotransmitter, and a postsynaptic neurone, which receives and transduces the signal. However, in the CNS, any particular neurone would form synapses with multiple other neurones. During the release of glutamate, glutamate concentration in the

synaptic cleft is thought to reach several millimolar, depending on the shape of the synaptic cleft and density of nearby glutamate transporters (Clements *et al.*, 1992).

Once secreted into the synaptic cleft, glutamate can diffuse, bind to, and interact with a nearby target. The closest target is the postsynaptic cell membrane. The postsynaptic cell membrane contains a large amount of membrane-associated protein, known as the postsynaptic densities (PSD), 250 – 500 nm in diameter and 25 – 50 nm in thickness (Gray, 1959). The PSD contains different kinds of receptors. The released glutamate binds to the glutamate receptor proteins, which sit on the PSD, and triggers changes in the postsynaptic neurone.

There are two general types of glutamate receptors: ionotropic receptors (iGluR) and metabotropic receptors (mGluR). iGluRs are multimeric glutamate-gated ion channels. When glutamate binds to the extracellular domain of certain iGluR subunits, the entire protein changes conformation to allow cation flow through the plasma membrane. Mammalian iGluRs can be divided into three subtypes: AMPA (α-amino-3-hydroxyl-5-methyl-4-isoxazole-propionate) receptors, NMDA (*N*-methyl-D-aspartatic acid) receptors and KA (kainate) receptors.

mGluRs are a group of seven-transmembrane membrane proteins, which couple to different intracellular heterotrimeric G-proteins. Binding of glutamate to mGluRs triggers the activation of G-protein-dependent intracellular signalling cascades. There are three subtypes of mammalian mGluR, called type I, II and III. Type I mGluRs (mGluyR1 and mGluR5) transduce via activation of phospholipase C, while type II (mGluR2, mGluR3) and III (mGluR4, mGluR6, mGluR7, mGluR8) are coupled to the cAMP pathway.

In the case of the NMDA receptor, the two glutamate molecules that bind to the postsynaptic receptor (Benveniste & Mayer, 1991) must be removed to allow for the postsynaptic membrane to continue relaying subsequent excitatory postsynaptic potentials (EPSP) or inhibitory postsynaptic potentials (IPSP). This removal can happen through at least three processes. First, the neurotransmitter diffuses away from the synaptic cleft into the extracellular fluid compartment where it could activate other receptors ("spill-over"). Second, different EAATs actively pump the neurotransmitter back into the presynaptic axon terminal for subsequent release. These EAATs also allow uptake into glial cells. The average reuptake time constant for the glutamate transporters are 8.7 ± 1.7 ms (Tao *et al.*, 2010). Third, in the case of ACh and NA, specific enzymes within the subsynaptic membrane space can metabolise some of the

neurotransmitters directly; for example, about 50% of ACh is broken down by ACh-esterase even before it activates the postsynaptic receptors (Molenaar *et al.*, 1987). In the case of NA, there are two pathways for break-down (see below).

1.2.3.4.11.1. Diffusion in synaptic cleft and extracellular space

Glutamate is capable of continuously interacting with receptors until it diffuses away (Magleby & Terrar, 1975) or is removed from the extracellular fluid by the EAATs of glial cells (Storck *et al.*, 1992) or astrocytes (Liang *et al.*, 2008). Based on the diffusion of glutamine at room temperature, Longsworth (1953) estimated that the diffusion of glutamate in the extracellular space is around 0.75 μm^2/ ms.

1.2.3.4.11.2. Break-down and/or uptake of transmitter

In the case of ACh and NA, these transmitters are broken down after reaching the post-synaptic cell to prevent constant excitatory signal transduction. For example, NA can be broken down by catechol-O-methyltransferase (COMT) (Wilson *et al.*, 1988; Trendelenburg, 1989) or monoamine oxidase (MAO) (Hasegawa *et al.*, 1999).

1.2.3.4.11.3. Receptor unbinding

For synaptic transmission to occur repeatedly at high frequency, allowing rapid information transfer across the synapse, the glutamate receptors need to have a high unbinding rate. In fact, glutamate has a high unbinding rate constant for the AMPA receptors at 2000 s^{-1} compared to the NMDA receptors of 5 s^{-1} at room temperature (Attwell & Gibb, 2005).

1.2.3.4.12. Vesicle endocytosis and recycling

Vesicle endocytosis usually follows release of synaptic vesicles. In nerve terminals, two mechanisms are involved. The first mechanism is a rapid, clathrin-independent form of endocytosis. An example is the invagination of synaptic vesicles via dynamin. Dynamin belongs to the dynamin superfamily of GTPase, which forms a spiral around the neck to the invaginating vesicles. GTP hydrolysis expands and tightens the coil around the neck causing the vesicles to be pinched from the parent membrane (Takei *et al.*, 1995). The second mechanism is via clathrin-coated vesicles. As with dynamin-mediated endocytosis, clathrin mediated endocytosis also generates single synaptic

vesicles. However, the latter process is dominant during mild stimulation (Granseth *et al.*, 2006; Zhu *et al.*, 2009). Formation of clathrin-coated pits follows shortly after Ca^{2+} influx (Miller & Heuser, 1984). Sun *et al.* (2010) reported that the Ca^{2+} influx during evoked release activates calmodulin/calcineurin, which initiates the clathrin-mediated endocytosis. The vesicles in the reserve pool are replenished by the clathrin-independent endocytosis while the ready releasable pool is replenished by the clathrin-mediated endocytosis (Cheung *et al.*, 2010).

1.2.3.4.13. Mobility of vesicles

The movement of synaptic vesicles can be governed by the cytoskeleton, Ca^{2+} sensor or vesicle "super-pool". Using fluorescence and electron microscopy techniques, Richards *et al.* (2004) demonstrated that disruption of the actin filaments with latrunculin A reduced synaptic vesicle mobilisation and thus exocytosis. Sun *et al.* (2007) reported that, at the calyx of Held, different Ca^{2+} dynamics could influence the synchronous or asynchronous release of synaptic vesicles. Using photolysis of caged Ca^{2+}, they showed that synaptotagmin acts as a Ca^{2+} sensor for synchronous release. At low cytosolic Ca^{2+} concentration, the calyx terminal exhibits asynchronous release while synchronous release occurs when the intracellular Ca^{2+} concentration is high. Both the synchronous and asynchronous release acts on the same vesicle pool. However, Fredj and Burrone (2009) reported that, in hippocampal cultures, the recycling pool is involved in evoked release while the resting pool contributes to spontaneous vesicle release. The size of the spontaneous vesicle pool is half the size of the recycling pool. Recently, Staras *et al.* (2010) reported that in hippocampal slices, the recycling pool of vesicles form part of a larger vesicle "super-pool". The vesicles within the "super-pool" were highly mobile between different terminals of a neurone, with the total pool having a turnover rate of 4%. A local TrkB receptor dependent mechanism was suggested to regulate this pool.

1.3. Spontaneous transmitter release

Spontaneous synaptic events, which are independent of changes in membrane potential, were first observed in recordings of EPPs at the NMJ of the frog (Fatt & Katz, 1950). In these recordings, the end-plate was not stimulated. The recorded spontaneous synaptic events were around 100 times smaller in amplitude (1 mV) than evoked responses; peaked within 1 – 2 ms, and had a decay time of 3 – 4 ms.

Miniature excitatory postsynaptic currents (mEPSCs) are spontaneous events persisting when Na^+ electrogenesis is blocked (Fatt & Katz, 1951). As mentioned before, in this thesis, the term 'miniature' will only be used when discussing results that were obtained in the presence of tetrodotoxin (TTX), a blocker of voltage-dependent Na^+ channels (Narahashi *et al.*, 1964).

The functional role of spontaneous transmitter release is not well understood. McKinney *et al.* (1999) showed that spontaneous glutamate release helps maintain dendritic spines via AMPA receptor activation in organotypic slice cultures of hippocampal CA1 pyramidal neurones. Blocking evoked transmitter release by TTX did not affect spine density, but blocking AMPA receptors resulted in a decrease in both spine density and length. Using FM 4-64 and membrane targeted GFP assay, Richards *et al.* (2005) corroborated that the mEPSC can direct dendritic spine motility of the mouse CA1 pyramidal neurone. Tyler and Pozzo-Miller (2003) reported that the brain-derived neurotrophic factor (BDNF) could affect dendritic spine formation in rat hippocampal CA1 pyramidal neurone and that BDNF expression is regulated in part by mEPSC frequency.

In the cerebellum, the rate of spontaneous release was found to regulate firing of stellate cells. Whist large principal cells were unaffected by spontaneous release; individual inhibitory quanta terminated stellate cell firing while small numbers of coinciding excitatory quanta triggered firing (Carter & Regehr, 2002).

Spontaneous transmitter release is also shown to regulate protein synthesis and influence the expression of postsynaptic receptors. It was found that spontaneous glutamate release suppresses local mRNA translation in dendrites of hippocampal cell culture. The enhancement and inhibition of spontaneous glutamate release resulted in a decrease and increase of mRNA content, respectively (Sutton *et al.*, 2004).

Last but not least, short-term potentiation of mEPSCs, which is dissociated from changes in evoked transmitter release but dependent on postsynaptic AMPA receptors, regulates excitability of postsynaptic supraoptic neurones in the hypothalamus (Kombian *et al.*, 2000).

The miniature inhibitory postsynaptic current (mIPSC) is the functional opposite of the mEPSC (Dudel, 1977).

1.3.1. Calcium dependence

Katz and Miledi (1967b) provided evidence that spontaneous transmitter release is Ca^{2+} dependent. Using TTX to eliminates evoked responses without interfering with transmitter release, they monitored changes in membrane potential with and without the presence of extracellular Ca^{2+}. They recorded miniature potentials in the presence of extracellular Ca^{2+} but found that these miniature potentials were lost when Ca^{2+} was removed from the bath.

In another experiment, Katz and Miledi (1967a) used a frog sartorius muscle equilibrated in a Na^{+}-free Ringer solution containing 83 mM $CaCl_2$ and 2 mM KCl. They observed that the miniature end-plate potentials were similar to the experiments done in the presence of TTX. This finding emphasises the importance of Ca^{2+} but not Na^{+} in neurotransmitter release.

1.4. Evoked transmitter release

Eccles and O'Connor (1939) were the first to show that an action potential can evoke an end-plate potential (EPP). They showed that the generation of an action potential is followed by its propagation down the muscle fibre. Fatt and Katz (1951) later showed that ACh depolarises the muscle fibre, a response known as the EPP. Accordingly, the authors concluded that ACh is a neurotransmitter acting at the NMJ. However, it was later shown that glutamate might also function as a neurotransmitter in the spinal cord (Curtis *et al.*, 1959).

Del Castillo and Katz (1954) questioned whether the evoked EPP was the result of neurotransmitter release. Under normal conditions, every stimulation of the end-plate produces an action potential in the muscle cells. Therefore, the authors increased the concentration of Mg^{2+} in the bathing solution (> 5 mM) to render the amplitude of the end-plate response sub-threshold for action potential generation. By doing so, they observed that the EPP amplitudes resulting from nerve stimulation were either the same or integer multiples of the spontaneous EPP recorded at the same junction. As a result, Del Castillo and Katz (1954) concluded that the evoked EPPs were the consequences of multiple packages of neurotransmitters, which they termed 'quanta'. A single quantum, therefore, constituted the release of ACh from a spontaneously fusing vesicle. Thus, the early basis of quantal theory of neurotransmission was formed, with the quantum being the basic unit of transmission and representing an individual spontaneous event.

1.4.1. Quantal hypothesis

The quantal hypothesis proposed by Del Castillo and Katz (1954) states that neurotransmitters are released in discrete quanta in a probabilistic manner. Transmitters are released in units called quanta, stochastically such that upon every trial, only a certain chance exists to release the vesicle. The release of a quantum can arise even in the absence of action potential. The transient action potential only increases the probability that quanta of transmitters will be released. The exact number of quanta being released can only be described in statistical terms based on the amplitude distributions of the postsynaptic potentials or currents. It requires a statistical model of how quanta can be released and typically is based on a few assumptions, which are that when one quantum is released; subsequent quanta are not affected (independence in time) nor are nearby quanta affected (independence in space). Based on these assumptions, there are a few classical statistical processes that may

be able to describe transmitter release. The study of such amplitude fluctuations is called quantal analysis, which can serve to determine the efficacy of synapses. This involves determining the number of release sites (*n*), probability of transmitter release (*p*) and quantal size (*q*) (Redman, 1990). Practically, some forms of quantal analysis rest on the "peakiness" of the amplitude distributions to determine the equidistance between the modal peaks.

In general, the release of a single quantum at the NMJ generates an end-plate potential amplitude of about 0.5 mV, which is equivalent to the amplitude size of the mEPP (Del Castillo & Katz, 1954). Del Castillo and Katz realised that, in order to prevent the muscle fibre from firing an action potential and twitching, they needed to lower the release probability significantly. This was achieved by increasing Mg^{2+} (> 5 mM) and decreasing Ca^{2+} (< 2 mM) in the superfusate. Under these conditions, *p* is very low and many sites exist at the NMJ from which transmitters can be released. Under these conditions, the simplest statistical model that can account for transmitter release is a Poisson process, which is governed by a single parameter λ. This parameter is typically referred to as quantal content and represents the average quanta released on a single trial. When these authors fitted their amplitude distributions, they were indeed able to get good fits using a Poisson process. However, the situation is different if *p* is much larger, and if *n* is small; conditions that typically prevail for central synapses. Under these conditions, the release process can be better described with a binomial model determined by two parameters, *p* and *n*. Evidence for this type of statistical process was first found at the NMJ (Boyd & Martin, 1955) and much later at CNS synapses (Korn & Faber, 1991).

Del Castillo and Katz (1954) observed that the unitary mEPP amplitude changed very little from trial to trial. In fact, the coefficient of variation is typically smaller than 0.2. The effect of variability of the quantum can be seen in amplitude distributions as a loss of "peakiness" for higher order quanta. This is because the variability in the unitary amplitude adds to each quantum, and in doing so, starts to smear out the modal peaks. The small variability of the unitary EPP raises the question of what quantises the response. There are several possibilities. The content of the vesicle is constant, therefore each vesicle releases the same amount of transmitter and causes constant amplitude. An alternative view is that if the receptors are saturated by the amount of transmitters released, then the number of postsynaptic receptors determines the size of the quantum. Even more differently, if the postsynaptic response is boosted by some electrogenesis along the postsynaptic structure, the quantisation could be due to active membrane processes.

Roughly at the same time as evidence for the quantal hypothesis was published, early electron micrographs of synapses showed vesicles assembled at the nerve terminals (Palay, 1956). Given these ultrastructural features and the fact that transmission at synapses is quantised, a notion arose that the synaptic vesicle may be the morphological correlate of a quantum. However, the direct proof of this hypothesis is still outstanding. Nevertheless, there is a large body of literature in support of this notion, which also received criticisms right from its early formulation. Below, I will summarise the arguments for and against the quantal hypothesis.

1.4.1.1. Arguments against the quantal hypothesis

For a long time, there was no direct evidence for quantisation in the CNS. Kuno (1964) measured EPSCs arriving at the motoneurone of the cat spinal cord. As no "peaky" distributions were observed in the data, the author concluded that transmission at this junction might not be quantised. Likewise, when Redman and co-workers (1973) first did measurements in the same preparation, they found that the evidence for quantisation was scant. In hindsight, this finding may not be that surprising as the size of the quantum turned out to be about 100 µV which is right at the resolution of the amplifiers used in those days. In addition, the electrotonic structure of the dendritic tree of a neurone imposes differential filtering such that a quantum generated on a distal site is smaller than one generated closer to the soma. These factors can conspire to "smear out" the peaky distributions, which are required for verification of the quantal hypothesis.

In cultured rat hippocampal neurones, Bekkers and Stevens (1990) also observed a large variability in the size of synaptic quanta. One possibility is that the quantity of transmitters released varies in proportion to the vesicle volume, in particular to the cube of the vesicle diameter. As vesicle sizes in their preparation had a diameter of 34 ± 3.8 nm, the overall variability in vesicle content of transmitter is of the order of 30%, which should "smear out" any peaks beyond the first quantum. Therefore, when multiple vesicles are released simultaneously upon stimulation, the observation of quantisation is very unlikely.

Clements (1991) argued that the generation of synaptic amplitude histograms from a poorly resolved process could arise from finite sampling. Quantal behaviour is derived from equidistant peaks based on deconvolution using a maximum likelihood estimator.

This technique assumes that the process generating baseline noise is independent of that generating the synaptic amplitude fluctuation. Larkman *et al.* (1991) indeed found that a significant component of the baseline noise was due to spontaneous release of quanta generating spontaneous EPSPs.

1.4.1.2. Arguments for the quantal hypothesis

The first study in support of quantisation of evoked potentials at central synapses was done by Jack *et al.* (1981) at the synapse between the group Ia afferent fibres and the motoneurone in the spinal cord of the cat *in vivo*. They showed that these synapses behave in an all-or-none manner with respect to postsynaptic effect. The average EPSP amplitude generated by a quantum at the soma was 91.6 ± 11.7 μV. In their study, they found no correlation between the rise-time and half-width with the quantum. This points to the fact that there may be dendritic scaling.

In the rat CA1 pyramidal neurones, Stricker *et al.* (1996b) measured EPSCs obtained by minimal stimulation of Schaffer collaterals. When the recorded EPSC amplitudes were subjected to a stringent statistical test to eliminate ambiguous distributions that may arise from either large quantal variance or a non-quantal process, quantisation was observed in a subset of about 40% of all EPSCs. The quantum was in the range of about -5 pA with small quantal variance (< 0.2). The peak quantal conductance was estimated to range from 0.5 to 6.8 nS. This conductance could correspond to the opening of at least 60 – 160 AMPA channels. The authors also provided indirect evidence that the quantum was scaled for electrotonic distance on the dendrite such that a quantum of about -5 pA was always seen at the soma irrespective of where it was generated on the dendritic tree.

The evidence that somatic EPSP amplitude is independent of synapse location was later provided by Magee and Cook (2000). These authors found that, at hippocampal CA1 pyramidal neurones, the amplitude of the local dendritic EPSP, recorded at the site of input, increases nearly four-fold with distance of the synapse from the soma (0.25 – 0.8 mV with a distance from 50 – 325 μm). The dendritic EPSP may counterbalance the filtering effect of the dendrites and reduce the location dependence of somatic EPSP amplitude. However, Williams and Stuart (2002) did not find synaptic scaling at the neocortical layer V pyramid neurones. They suggest that the decrease in dendritic EPSPs results from a progressive decrease in input capacitance at more distal dendritic sites.

With regards to the evoked EPSP, the quantal hypothesis states that it is the sum of several unitary EPSPs equivalent in size to a miniature event; and results from the synchronous release of several presynaptic vesicles, most likely from several release sites. Therefore, the amplitude of the postsynaptic response is the result of a number of synaptic vesicles, which are released in response to a single action potential. An alternative interpretation suggested by Edwards *et al.* (1990), was that the size of the postsynaptic receptor cluster might determine IPSC amplitude. In their experiments in rat dentate granule cells, the unitary IPSC amplitudes were very similar to the mIPSC amplitudes, which is consistent with quantal transmission. The similarity between evoked and spontaneous events could be explained by assuming that one quantum was sufficient to saturate all postsynaptic receptors. However, more recent studies suggest that receptor saturation does not occur with a single quantum of transmitter (McAllister & Stevens, 2000; Ishikawa *et al.*, 2002).

1.4.2. Calcium hypothesis

The Ca^{2+} hypothesis of neurotransmitter release proposed by Katz and Miledi (1968) states that, during the depolarisation of the nerve terminal by an action potential, the influx of Ca^{2+} triggers the fusion of synaptic vesicles and results in subsequent release of neurotransmitters. In this process, Ca^{2+} is involved in the reaction between v- and t-SNARE complex.

Mg^{2+} was known to block transmission at the NMJ (Del Castillo & Engbaek, 1954), an effect that could be counteracted by increasing the Ca^{2+} concentration in the extracellular space. Jenkinson (1957) tried to fit the interaction of Ca^{2+} and Mg^{2+} ions with the Michaelis-Menten equation, but found that there was a significant deviation in the lower Ca^{2+} concentration range (< 2 mM). The observed curve has a sigmoidal shape, rather than the expected linear relationship. This gave rise to the notion that more than one Ca^{2+} ion may be involved in triggering release. This idea was later investigated at the frog NMJ where it was shown that, indeed, the cooperative action of about four Ca^{2+} ions is responsible for the release of a quantum of ACh (Dodge & Rahamimoff, 1967). Using a photolabile Ca^{2+} chelator DM-nitrophen, Landò and Zucker (1994) also obtained a similar result at the crayfish NMJ. However, in the CNS, the cooperative action of Ca^{2+} varies from 2 to 6 ions (Mulkey & Zucker, 1993; Bollmann *et al.*, 2000; Schneggenburger & Neher, 2000).

Katz and Miledi (1968) left open the question of whether Ca^{2+} was the only factor required for transmitter release or if membrane depolarisation by an action potential was also required. Dudel *et al.* (1983) found evidence at the crayfish NMJ that both presynaptic depolarisation and Ca^{2+} influx were required. However, Landò and Zucker (1994) did not find evidence of a voltage contribution at the crayfish NMJ. Similarly, by measuring Ca^{2+} currents at the nerve terminal of the squid giant synapse, Augustine *et al.* (1985) found no support for the voltage hypothesis. Further work by Blackmer *et al.* (2001), however, has shown that the putative voltage-sensor may be an inhibitory G-protein βγ subunit in the nerve terminal such that depolarisation at the nerve terminal results in the opening of Ca^{2+} channels and activation of the G-protein. Charge build-up in turn causes the detachment of the G-protein from it's membrane bound receptors, subsequently initiating the release of neurotransmitter (for review see Parnas & Parnas, 2007).

1.4.2.1. Calcium micro- and nano-domain hypotheses

The next question to ponder is how high the Ca^{2+} concentration has to rise in order to cause transmitter release. As transmitter release is fast, the requirement is that the site of calcium binding(s) must have low affinity for Ca^{2+}; otherwise, receptor unbinding would be prolonged and transmitter release would be lasting. Given this consideration, the next objective of experimental investigation was to determine how high the Ca^{2+} concentration has to rise at the release site. Early on, it was realised that high Ca^{2+} concentration can only be reached close to Ca^{2+} channels.

The microdomain hypothesis, first theoretically derived at the squid giant synapse (Simon & Llinás, 1985), suggests that the voltage-activated entry of Ca^{2+} into the presynaptic terminal produces a very high Ca^{2+} concentration (300 μM) in small 'microdomains' in the proximal area surrounding the Ca^{2+} channels. The delay of about 100 μs between the opening of the Ca^{2+} channel and the subsequent release of transmitter indicates that the Ca^{2+} channels are located within tens of nanometres of the Ca^{2+} binding site on the active zone. Roberts *et al.* (1990) reported that the active zone of the presynaptic terminal of the squid giant synapse contains about 1800 Ca^{2+} channels and 700 Ca^{2+} activated K^+ channels.

Llinás *et al.* (1992) later provided the experimental evidence for the microdomain hypothesis using aequorin, a photo-protein, which emits light upon binding free Ca^{2+} at the squid giant synapse. They found that a high Ca^{2+} concentration (100 – 400 μM) is

needed to initiate vesicle release because the Ca^{2+} sensor at the plasma membrane has a low binding affinity for Ca^{2+} (Llinás, 1982; Heidelberger *et al.*, 1994). The reason why they postulated a microdomain arrangement was because only around the Ca^{2+} channel mouths would the concentration of Ca^{2+} be high enough to activate the Ca^{2+} sensor for transmitter release. A few nanometers away from these channel mouths, the Ca^{2+} concentrations are much lower due to lateral diffusion and buffering by fixed and mobile buffers. In the case of the squid giant synapse, there are around 100 Ca^{2+} channels involved in generating the microdomain (Sugimori *et al.*, 1994). These authors also reported a refractory time during which subsequent Ca^{2+} influx could not induce another round of vesicle release ("refractoriness" of the release machinery). This may be because the new vesicles have to move to fill the vacated space and be close to the Ca^{2+} channels to initiate release.

The Ca^{2+} nanodomain hypothesis is a further extension of the Ca^{2+} microdomain hypothesis. It applies to typical synapses in the CNS, which have a size of about 1 µm in diameter. As a consequence of their size, much fewer Ca^{2+} channels are likely to be involved in transmitter release (Bucurenciu *et al.*, 2008). For instance, Jarsky *et al.* (2010) reported that, at the ribbon synapse of the rod bipolar cell, the opening of at least two Ca^{2+} channels is required for exocytosis to occur at the active zone. The idea of a nanodomain in boutons of axons arose from experiments by Rozov *et al.* (2001), in which they showed that the distance between presynaptic Ca^{2+} channels and the Ca^{2+} sensor(s) for exocytosis is a key factor in determining the efficacy and timing of release. By using Ca^{2+} chelators of different affinities, they found that the diffusional distance between the Ca^{2+} source and Ca^{2+} sensor is about 10 – 20 nm (Neher, 1998).

Catterall (1999) provided biochemical evidence for the Ca^{2+} nanodomain hypothesis by showing that the N and P/Q type Ca^{2+} channels are in close proximity to the SNARE complex. The t-SNARE binds to a motif on the Ca^{2+} channel and creates a macromolecular assembly of the SNARE and the Ca^{2+} channel (Lopez *et al.*, 2007).

Chelating the endogenous Ca^{2+} buffers is another way to investigate the proximity of the VDCC to the Ca^{2+} sensor located at the active zone of the nerve terminal. This is because the endogenous Ca^{2+} buffers have the ability to affect the size and time course of the Ca^{2+} transient, which in turns may mobilise the synaptic vesicles. The use of Ca^{2+} chelators to remove the Ca^{2+} transients in the terminal and from there it is possible to separate these vesicles into different categories (Naraghi & Neher, 1997). Two common Ca^{2+} chelators that are employed are ethylene glycol-bis(2-aminoethylether)-*N*,*N*,*N*′,*N*′-tetraacetic acid (EGTA) and 1,2-bis(o-

aminophenoxy)ethane-*N*,*N*,*N*',*N*'-tetraacetic acid (BAPTA). Both of these chelators have similar a affinity for Ca^{2+}. However, the binding rate of EGTA is approximately 100 – 160 times slower than that of BAPTA (Tsien, 1980; Adler *et al.*, 1991). A membrane permeable variant of the BAPTA, the 1,2-bis(2-aminophenoxy)ethane-*N*,*N*,*N*,*N*'-tetraacetic acid(acetoxymethyl ester) (BAPTA-AM) can be used to chelate intracellular Ca^{2+} without disrupting the membrane of the neurone (Tsien, 1981). The K_d of BAPTA-AM is 440 ± 20 nM (Wang & Thompson, 1995).

Using a combination of these two Ca^{2+} chelators, Mennerick and Matthews (1996) found at least two different pools of vesicles in the terminals of goldfish retinal bipolar neurones. In layer II/III of the rat barrel cortex, Rozov *et al.* (2001) reported that increasing the concentration of EGTA reduces the release of vesicles upon subsequent stimulation. The authors also suggested that several of the Ca^{2+} microdomains at the terminal would have to overlap in order to trigger transmitter release as the distance between the VDCCs and the Ca^{2+} sensor was relatively large. However, evoked transmitter release partially persisted in high concentrations of BAPTA. This suggests that a population of VDCCs is closely coupled to the Ca^{2+} sensor.

1.4.3. Relationship between spontaneous and evoked release

The quantal hypothesis states that, since the quantum is the basic unit of transmission as reflected in the miniature event, evoked release is comprised of multiple miniature events (Del Castillo & Katz, 1954). However, below I will summarise some historical notions, which may indicate that these two forms of transmission may not be directly related.

1.4.3.1. Spontaneous synaptic events may be caused by tissue damage

Although Katz was the first to discover the spontaneous transmitter release at the NMJ, he dismissed it as an artefact attributed to cutting (as reported in Katz, 1996). For fibre isolation, Katz cut the motor nerve fibre relatively close to the motor end-plate, which was not required for his experiments. As he observed sEPPs in these muscle fibres, he thought that the sEPPs were not the result of synaptic transmission, but caused by damage to the motor nerve endings. Using a more careful dissection procedure (Fatt &

Katz, 1952), Katz later rejected his early view after working with Fatt on the miniature potential.

At the frog NMJ, Fatt and Katz (1952) reported that the mean frequency of the spontaneous events was around 4.5 Hz. Other investigators have reported higher rates of spontaneous events using *in vivo* preparations. Burke *et al.* (1970) reported that the mean frequency of the spontaneous events was around 12 Hz at the cat *triceps surae* muscle. The spontaneous frequency can be as low as 0.2 Hz, which was found in embryonic rat motoneurones (Nishimaru *et al.*, 1996). However, not all slices necessarily display spontaneous events. Blight and Precht (1982b) reported an absence of spontaneous events from *in vivo* recordings from the frog spinal cord. They later compared data of spontaneous events from *in vivo* and *in vitro* studies of the frog spinal cord, in which there were no spontaneous events in the *in vivo* recordings, however, the *in vitro* recordings displayed a broad range of spontaneous event frequencies from as low as 0.1 Hz to 100 Hz. They reasoned that these spontaneous events might result from trauma caused by slicing and inadequate Ca^{2+} buffering at the terminal (Blight & Precht, 1982a).

While it seems likely that spontaneous events are the results of tissue damage, there is also some evidence against it. Nissen *et al.* (1995) reported spontaneous firing of 7 Hz in the rat supraoptic vasopressin neurones *in vivo*. However, *in vitro* recordings of the same cells yielded a lower frequency of spontaneous events. The reduced rate of spontaneous events in vitro suggests that spontaneous events may not be caused by tissue damage.

Fujiwara *et al.* (1987) reported in hippocampal slices *in vitro*, that when the neurones were exposed to hypoxic conditions (a critically low concentration of oxygen), there was a hyperpolarisation of 5 – 15 mV for 4 – 12 min, followed by a depolarisation of 25.1 ± 3.8 mV above pre-hypoxic resting membrane potential (-60 mV). The depolarisation caused an increase in the frequency of spontaneous EPSP. Application of EGTA did not alter the hyperpolarisation, which means that intracellular Ca^{2+} was not involved in the hypoxia-induced hyperpolarisation. However, anoxia-induced (total decrease of oxygen) hyperpolarisation was found to be Ca^{2+} dependent (Belousov *et al.*, 1995), and resulted from mobilisation of Ca^{2+} from intracellular stores (Katchman & Hershkowitz, 1993).

1.4.3.2. Spontaneous release is due to spontaneous vesicular fusion

Many have asked whether the spontaneous release really is spontaneous. As evoked release is caused by action potential, the blocking of the generation of action potentials would separate the two types of transmitter release. To do this, Fatt and Katz (1952) tried lowering the extracellular Na^+ concentration, but this failed to have a significant effect on the frequency of spontaneous release at the NMJ of the frog. The replication of the experiment using TTX, a pharmacological agent, which blocks voltage-dependent Na^+ channels (Turner & Fuhrman, 1947), confirmed that these events were indeed spontaneous (Bloedel *et al.*, 1966). Fredj and Burrone (2009) recently showed that spontaneous release utilises a different pool of vesicles than evoked release. The spontaneous release utilises a resting pool of vesicles while the evoked release utilises the vesicles from the ready releasable pool (see below).

1.4.3.3. The same biochemical proteins are involved in evoked and spontaneous release

Whilst Fatt and Katz (1950) noticed that both the evoked and spontaneous release is Ca^{2+} dependent, they were limited by the resolution of the experimental technology at that time. Later experiments highlighted a few Ca^{2+}-sensing proteins that facilitate vesicle release. One of them is synaptotagmin, which binds to phospholipids with high Ca^{2+} affinity (5 – 10 μM) at the C_2A domain (Davletov & Südhof, 1993) and to other release proteins such as syntaxin with a lower Ca^{2+} affinity (> 100 μM) at the C_2B domain (Li *et al.*, 1995a; Sugita *et al.*, 1996). Using an *in vitro* binding assay, Kee and Scheller (1996) showed that synaptotagmin binds to the H3 domain of syntaxin. An increase of > 20 μM Ca^{2+} drives fusion of synaptotagmin onto the base of the SNARE complex, near the transmembrane anchor of syntaxin (Davis *et al.*, 1999). Synaptotagmin forms direct contacts with t-SNAREs, syntaxin, and SNAP-25 of the SNARE complex, but does not bind to the v-SNAREs (Bai *et al.*, 2004). Bhalla *et al.* (2006) used a reconstituted fusion assay to show that the cytoplasmic domain of synaptotagmin must directly engage with the SNARE proteins to drive vesicle fusion. They reported that, in the presence of Ca^{2+}, the cytoplasmic domain of synaptotagmin drove efficient folding of SNAP-25 onto membrane-embedded syntaxin, and resulted in the recruitment of v-SNARE and t-SNARE.

Given the notion that synaptotagmin facilitates the release of neurotransmitters, the deletion of the synaptotagmin gene would eliminate spontaneous release. However,

Littleton *et al.* (1993) together with DiAntonio and Schwarz (1994) showed that this is not the case, at least in Drosophila. They reported that a mutation of synaptotagmin caused an increase in spontaneous transmitter release, but evoked transmission was much reduced. This observation can be explained with synaptotagmin having a dual role. First, synaptotagmin functions as a clamp to prevent docking and subsequent vesicle release to the presynaptic membrane. Second, it retains docked vesicles in the absence of Ca^{2+}, but releases the vesicles during increased Ca^{2+} concentration. Given this explanation, spontaneous and evoked release share the same release machinery, i.e. the same proteins control release in both cases.

1.5. Synaptic plasticities

Synaptic plasticity generally refers to the capacity of the synapse to undergo change given particular stimulation histories. The term encompasses changes in synapse size, shape, structure, and function, and may include loss of synapses or the establishment of new ones.

1.5.1. Forms of plasticities

The forms of plasticity exhibited by different synapses reflect the variety of functions that synapses serve in extracting different features of presynaptic activity. Given the previous history, synapses can either increase or decrease their efficacy, i.e. enhancement or depression is exhibited (Zucker & Regehr, 2002; Xu-Friedman & Regehr, 2004).

The change in efficacy can be of short (ms – s) or long duration (h – d); i.e. short-term and long-term changes. While short-term changes are in response to a continually changing environment, long-term changes in synaptic efficacy are thought to be the substrate for memory formation (Schulz, 2006).

Based on the quantal hypothesis, the efficacy between two neurones can be described in terms of three variables: n, the number of release sites, p, the probability of release at each site and q, the quantal size. In order to quantify the extent of plasticity at synapses, quantal analysis can be used to track these changes (presynaptic, typically n and p; postsynaptic, typically q). As synaptic efficacy changes with previous activity, a number of separate forms of use-dependent changes of synaptic plasticity have been described and characterised in different preparations.

1.5.2. Long-term plasticities

Long-term changes typically last for hours to months (Bliss & Lømo, 1973) and may well be the physiological substrate for memory formation. Memory formation is a rapid process and involves reorganisation of neural networks in the brain. Long-term plasticity is a useful phenomenon for studying the basic neurobiology of memory formation.

To track the changes in synaptic efficacy, it is helpful to distinguish three phases of long-term plasticity: induction, expression, and maintenance. Induction can be defined as the pattern of electrical activity and intracellular signalling pathways responsible for triggering the plasticity. Expression is the mechanism directly responsible for the increase in synaptic efficacy. Maintenance is the mechanism responsible for maintaining the effect in the absence of ongoing induction signals. I include these forms only for completeness and will concentrate predominantly on short-term plasticity further down in this thesis.

1.5.2.1. Long-term potentiation

Donald Hebb (1949), proposed that "when an axon of cell A is near enough to excite cell B and repeatedly or persistently takes part in firing it, some process or metabolic changes take place in one or both cells such that A's efficiency as one of the cells firing B, is increased". In other words, the coincidence of synaptic activity causes strengthening of synapses, i.e. "cells that fire together, wire together". The features of Long-term potentiation (LTP) include cooperativity, associativity, and input specificity among the co-active neurones, which is consistent with Hebb's postulate. McNaughton *et al.* (1978) observed from recordings of the perforant path synapses in the hippocampus that the cooperativity threshold caused by postsynaptic depolarisation relates to the number of inputs that are required to be simultaneously active for LTP induction. Associativity highlights the importance of postsynaptic co-activity. Barrioneuvo and Brown (1983) reported from field recordings in the rat hippocampus, that coincident activation of a weak sub-threshold input, together with a strong input, induced associative LTP of the weak input. Input specificity highlights the additional importance of presynaptic activity with the postsynaptic activity, and shows that the change is at the synaptic level rather than cell-wide (Bliss & Collingridge, 1993).

Lynch *et al.* (1983) showed that Ca^{2+} is important for LTP induction by chelating Ca^{2+} in rat hippocampal neurones with EGTA. Using a caged Ca^{2+} compound, nitr-5, Neveu and Zucker (1996) reported in CA1 pyramidal neurones that postsynaptic mechanisms involved in LTP induction are Ca^{2+} dependent. By recording EPSCs of CA1 pyramidal neurones evoked at synapses formed by the Schaffer collaterals/commissural (CA3) axons, Stricker *et al.* (1996a) demonstrated that LTP induction causes an increase in both the quantal content and quantal size at the CA1 synapse. The induction is caused by NMDA receptor activation and subsequent Ca^{2+} influx, which enhances AMPA

currents. However, Harris and Cotman (1986) found that the induction of LTP at guinea pig mossy fiber is independent of NMDA receptor activation.

Synapses and spines show remarkable plasticity in structure and function. Using a high-resolution imaging technique and Ca^{2+} dyes, Yuste and Denk (1995) showed that the dendritic spines compartmentalise and regulate Ca^{2+} independent of their parent dendrite. However, Cowan *et al.* (1998) reported that LTP at excitatory synapses onto CA1 aspinous interneurones lacks synaptic specificity. In these interneurones when two independent inputs were stimulated input specificity after the induction of LTP could not be retained. A similar finding was obtained in cultured excitatory hippocampal cells where LTP could spread to nearby spines if these were closer than 70 μm apart (Engert & Bonhoeffer, 1997).

Abraham and Huggett (1997) showed that, in the rat hippocampus, LTP is not an all-or-none phenomenon; i.e. the extent of LTP may be graded. They reported that LTP increased with the number of conditioning stimuli but excessive stimulation (> 24 repeating stimuli consisting of 10 trains of 5 pulses at 100 Hz, delivered at 200 ms interval, with a 30 s inter-train interval) caused a reduction. There are three forms of LTP reported in the hippocampus that persisted with different stimulus durations; LTP1 has a rapid decaying time course, LTP2 has an intermediate decaying time course, while LTP3 has a longer lasting decaying time course (Raymond *et al.*, 2000). LTP1 is induced by spine Ca^{2+} signalling via ryanodine receptors. LTP2 requires dendritic Ca^{2+} signals via IP_3 receptors while LTP3 is dependent on L-type VDCCs (Raymond & Redman, 2002).

Magee and Johnston (1997) used CA1 pyramidal neurones in the hippocampus to show that the subthreshold EPSPs, when paired with back-propagating action potentials, are necessary for LTP induction. However, by applying TTX to block sodium channels at the distal dendrites of the hippocampal CA1 pyramidal neurones, Golding *et al.* (2002) found that the distal dendrites require cooperative synaptic inputs, but not axonal action potential firing and backpropagation, for induction of LTP. Raymond (2008) later showed from recordings in hippocampal neurones, that only induction of LTP1 does not require the firing of postsynaptic action potential.

The associativity feature after the induction of LTP, was demonstrated by Levy and Steward (1983), in which they examined the relative timing of pre- and post-synaptic action potential of the ipsilateral projections from the entorhinal cortex to the dentate gyrus. They observed that activation of the ipsilateral system that precedes activation

of the crossed system depresses the response evoked by the crossed system. Using connected pairs of layer V pyramidal neurones in the neocortex, Markram *et al.* (1997) observed that postsynaptic action potential firing together with presynaptic stimulation is necessary for LTP induction. Later, Bi and Poo (1998) showed that activation of NMDA receptors causes spike timing dependent plasticity in the hippocampus.

Expression of LTP can be caused by both presynaptic and postsynaptic changes. Evidence for presynaptic changes comes from studies using different forms of quantal analysis (Bekkers & Stevens, 1990; Malinow & Tsien, 1990), paired-pulse facilitation (Sokolov *et al.*, 1998) and visualisation of exocytosis (Bayazitov *et al.*, 2007). The first whole-cell recording using hippocampal slices were done by Malinow and Tsien (1990). They reasoned that the induction of LTP is presynaptic based on the observed changes in synaptic variability and a decrease in the proportion of synaptic failures during LTP. Bekkers and Stevens (1990) measured EPSCs before and after LTP induction in connected pairs of hippocampal neurones and found that the conductance was increased by a factor of 2.1. This was caused by an increase in the probability of transmitter release. Sokolov *et al.* (1998) measured paired-pulse facilitation in rat hippocampal pyramidal neurone and found that the ratio persistently decreased in the majority of the neurones following LTP induction, suggesting a presynaptic mechanism in the maintenance of both early and late phases of LTP. Bayazitov *et al.* (2007) used neurones of mouse transfected with synaptopHluorin, a vesicle protein used for pH imaging, which is bound to GFP and fluoresces in response to exocytosis at the synapse between CA3 and CA1 pyramidal neurones. They reported that LTP consists of two components, a slow presynaptic component in which protein kinase A (PKA) plays a major role together with the activation of L-type VDCCs, and a fast postsynaptic component signalled via NMDA receptors.

Evidence for postsynaptic change also comes from iontophoretic AMPA agonist application at rat CA1 pyramidal neurones (Davies *et al.*, 1989), redistribution of AMPA receptors at the dendritic spines (Shi *et al.*, 1999), and insertion of AMPA receptors at silent synapses (Isaac *et al.*, 1995). From the changes in quantal parameters of EPSCs in CA1 hippocampal neurones, Stricker *et al.* (1996a) proposed that LTP expression could be both pre- and post-synaptic. They observed an increase in quantal currents, a variable EPSC time course, and a decrease in response failures in rat CA1 neurones after the induction of LTP.

Using an inhibitor of mRNA synthesis, actinomycin D, Otani *et al.* (1989) showed that the maintenance of LTP requires protein synthesis. Protein kinase Mζ (PKMζ) is an

isoform of protein kinase C (PKC). Serrano *et al.* (2005) reported that PKMζ is involved in the late phase of LTP, at least at 30 min after LTP induction.

The different observations obtained in the hippocampus may be due to the experimental age of the animals. Sans *et al.* (2000) reported a developmental change in expression of NMDA receptor subunits and their anchoring proteins at the rat hippocampal synapse. At birth, the synapse-associated protein-90 (SAP-102) located at the postsynaptic density is highly expressed while expression of postsynaptic density-93 (PSD-93) and postsynaptic density-95 (PSD-95) is low. Young rats show a high expression level of SAP-102 till the age of 6 months. After that, the PSD-93 and PSD-95 are abundantly expressed in adult rats. The authors further showed that there is a preference for complexes of NR2A/PSD-93/95 and NR2B/SAP-102.

1.5.2.2. Long-term depression

Similar to LTP, long-term deprssion (LTD) also affects learning and memory in the hippocampus. Zeng *et al.* (2001), reported that gene knockout of calcineurin at the Schaffer collateral-CA1 synapses results in an impairment in working and episodic memory of the mice. Calcineurin induces LTD via the reduction of the NMDA receptor open time, which leads to the reduced Ca^{2+} influx through the NMDA receptor (Shi *et al.*, 2000). In the cortex, LTD is a response to deprivation of sensory inputs. Cheetham *et al.* (2007) observed that whisker deprivation of the rat decreases the probability of synaptic connections between L2/3 pyramidal cells. Glazewski and Fox (1996) also showed that whisker deprivation after P7 depresses the synaptic inputs from L4 to L2/3. The L4 to L2/3 depression is likely caused by presynaptic NMDA receptors as indicated by an increase in paired-pulse ratio and slowing of NMDA currents when the NMDA receptor blocker, MK801, was applied (Bender *et al.*, 2006).

In the hippocampus, LTD induction is dependent on the presynaptic stimulus frequency. Dudek and Bear (1992) gave a low frequency stimulation (LFS) of 900 pulses at 1 – 3 Hz to the CA1 hippocampal neurones; this frequency is below the threshold for inducing LTP. The authors found a depression lasting for more than an hour. They observed LTD could be prevented by application of an NMDA antagonist. Fitzjohn *et al.* (2001) found that LTD in the hippocampus can be induced by activation of the presynaptic group I mGluR. They reported that intracellular application of the Ca^{2+} chelator BAPTA, or depletion of intracellular Ca^{2+} stores with thapsigargin, did not abolish the dihydroxyphenylglycine (DHPG) induced LTD. However, the LTD was

blocked by perfusion of a Ca^{2+} free medium, suggesting that the LTD expression could be caused by a Ca^{2+} dependent presynaptic mechanism. Goda and Stevens (1998) showed that the induction of LTD in hippocampal cultures causes a decrease in the size of the ready releasable pool, indicating a presynaptic mechanism of expression.

However, LTD expression in hippocampal slices induced by LFS is dependent on postsynaptic AMPA and NMDA receptors, and includes the dephosphorylation of the AMPA receptor GluR1 subunit at Ser 845 (Lee *et al.*, 2000a). Using a phosphatase inhibitor, Moult *et al.* (2006) showed that the group I mGluR also induces LTD in the rat CA1 hippocampal synapse via protein tyrosine phosphatase. Activation of the NMDA or mGluR receptors could trigger Ca^{2+} release from intracellular stores to cause LTD (for review see Collingridge *et al.*, 2010).

Maccaferri *et al.* (1994) reported that cesium prevents the maintenance of LTD in hippocampal CA1 neurones. By applying anisomycin, a peptidyl transferase inhibitor, Sajikumar and Frey (2003) showed that the long-term depression in rat hippocampal slices is dependent on protein synthesis. The maintenance of hippocampal LTD is established using existing mRNA (Manahan-Vaughan *et al.*, 2000). Ho *et al.* (2000) observed that mice lacking the Ca^{2+}/calmodulin-dependent protein kinase IV are deficient in the maintenance of cerebellar LTD.

Long-term depression (LTD) at the synapse enables a dynamic range of synaptic function. Functionally, it may prevent saturation of synaptic responses and subsequent loss of plasticity due to ceiling.

1.5.3. Short-term plasticities

Long-term plasticities are built upon the process of the short-term plasticity to span the gap between synaptic plasticity and permanent structural changes involved in long-term memory. Short-term plasticity causes behavioural and habitual changes as a consequence of adaptation. Short-term plasticity was first studied by Castellucci and Kandel (1976) in the marine mollusk *Aplysia*, which displays modulation of behaviour in a relatively short time scale. Using weak or moderate stimulation of the siphon, the authors observed a brisk withdrawal of the gill. A stimulation of ≤0.3 Hz to the siphon sensory neurone depresses EPSPs generated in the monosynaptically connected motoneurone, which directs the gill, and thus results in a short-term habituation of the reflex response. This short-term habituation, which ranges from several minutes to

hours, is a consequence of a reduction in neurotransmitter released from the presynaptic sensory neurone.

Unlike long-term plasticity, the maintenance of short-term plasticity is typically over within a second and therefore of little mechanistic importance. The naming convention of some forms of short-term plasticity is dependent on historical grounds and the experimental preparation under study. A similar form of short-term plasticity may have two different names in two different preparations. For example, Castellucci and Kandel (1976) used the term "facilitation" in the abdominal ganglion of *Aplysia* while Delaney *et al.* (1989) used the term "potentiation" at the crayfish NMJ.

1.5.3.1. Synaptic enhancement

Three types of short-term enhancement have been identified: facilitation, augmentation, and post-tetanic potentiation. Synaptic facilitation is a phenomenon displayed as an increase in the postsynaptic response after repetitive stimulation at stimulus rates > 10 Hz. It was first described at the NMJ between the muscle nerve and the sartorius muscle of the frog (Eccles *et al.*, 1941).

Synaptic facilitation lasts for hundreds of milliseconds. It can be seen after a pair of stimuli, when the second postsynaptic potential can be up to five times the amplitude of the first. Facilitation often builds up during repetitive stimulation and, after stimulus cessation, decays with a time course that can be approximated by an exponential decay function having a time constant of ~100 ms. Using a paired-pulse paradigm and a Ca^{2+} free Ringer solution, Katz and Miledi (1968) showed that induction of facilitation, evoked by repetitive pulses of depolarisation causes Ca^{2+} influx and subsequently changes in the intracellular Ca^{2+} concentration at the frog NMJ. This change in cytosolic Ca^{2+} is rapid and high, but only occurs at or near the site of vesicle exocytosis. In addition, the authors demonstrated that external Ca^{2+} could influence the amplitude of facilitation produced by a nerve impulse. Consistently, Tucker and Fettiplace (1995), by using a low affinity fluorescence indicator, Calcium Green™-5N, showed that facilitation at the turtle hair cells is caused by Ca^{2+} influx resulting in a concentration of < 1 μM at the release sites. However, an increase in intracellular Ca^{2+} causes a non-linear dependence of transmitter release (Hochner *et al.*, 1991).

Augmentation, on the other hand, grows and decays with a time constant of ~5 – 10 s, while post-tetanic potentiation lasts for 30 s to several minutes (Zucker & Regehr,

2002). Both, augmentation and post-tetanic potentiation are induced as a consequence of activating a much lower affinity Ca^{2+} binding site within the nerve terminal. Using a photolabile Ca^{2+} chelator to reduce residual Ca^{2+} at the crayfish NMJ, Kamiya and Zucker (1994) showed that augmentation and post-tetanic potentiation arise from Ca^{2+} acting at a separate site from that involved in facilitation. Mulkey and Zucker (1992) reported that during post-tetanic potentiation, they observed an accumulation of Na^{+} in the nerve terminal, which caused an increase in intracellular Ca^{2+} concentration via the Na^{+}-Ca^{2+} exchanger. In addition, Tang and Zucker (1997) used several mitochondrial Ca^{2+} uptake inhibitors and showed that post-tetanic potentiation, but not augmentation, depends upon increases in mitochondrial Ca^{2+} during stimulation.

1.5.3.2. Synaptic depression

Curtis and Eccles (1960) reported that, when repetitive stimulation is applied to a single synapse in the spinal cord, two processes occur. One is a brief period of enhanced action (see above) lasting for 200 ms, while the other is usually a depression, which last for several seconds. However, there are some synapses that show no depression. These include the NMJ at the crayfish opener muscle (Wang & Zucker, 1998) and the calyceal synapse in the chick ciliary ganglion (Martin & Pilar, 1964).

The causes of short term-depression (STD) have been found to be a vast variety of mechanisms; for example, a reduction in spike amplitude (Hatt & Smith, 1976), failure of spike propagation along the axon (Parnas, 1972; Brody & Yue, 2000), depletion of ready-releasable pool (Magleby & Pallotta, 1981), release of neuromodulatory substances from activated presynaptic terminals or postsynaptic cells (Mennerick & Zorumski, 1995), desensitisation of postsynaptic receptors (Magleby & Pallotta, 1981), relief of polyamine block (Koh *et al.*, 1995), and reduced calcium channel activity (Thies, 1965); all of which ultimately result in a reduced postsynaptic response.

Synaptic depression is induced by a decrease in intracellular Ca^{2+}. Xu and Wu (2005) reported that STD at the calyx of Held results from a decrease in Ca^{2+} current at the presynaptic terminal. However, Lovinger and Choi (1995) reported that activation of adenosine A1 receptors, which increases the intracellular Ca^{2+} concentration, initiates STD in rat striatum. From now on, I will be only looking at short-term changes.

1.5.3.2.1. Synaptic vesicle pools

The identification of different vesicle pools arose from functional studies in which the time course of vesicle depletion required more than a single exponential for fitting the reduced amplitudes. In general, three pools of synaptic vesicles have been identified: the ready releasable pool, the recycling pool, and the reserve pool (for review see Rizzoli & Betz, 2005). The ready releasable pool refers to a group of vesicles (around 1% of vesicles at the terminal) that is the closest to the active zone of plasma membrane ("docked") and can release its content on any given stimulus. Typically, there are only a few vesicles in this state. The recycling pool (around 10 – 15% of vesicles at the terminal) is a group of vesicles further away from the active zone; these vesicles have been endocytosed after release. The size of this pool varies for different synapses but could be as large as some 10 – 20 vesicles after repetitive stimulation and can release its vesicle content on moderate stimulation. The reserve pool (around 80 – 90%) comprises the largest pool of vesicles and is the furthest away from the active zones. These vesicles will only be released under intense stimulation.

1.5.3.2.2. Depletion models of short-term depression

The depletion model of short-term depression (STD) is based on the idea of depletion of the ready releasable pool (Liley & North, 1953; Betz, 1970). In this model, the store is transiently depleted of synaptic vesicles by an action potential. However, Sullivan (2007) did not observe any changes in the ready releasable pool in cultured hippocampal neurones, questioning the appropriateness of depletion models to account for depression.

1.5.3.2.3. Alternative models of STD

STD can result from presynaptic or postsynaptic mechanisms. Short-term depression that results from postsynaptic mechanism includes receptor desensitisation and receptor saturation. STD that results from presynaptic mechanism includes changes in presynaptic release probability and release independent depression (RID).

Postsynaptic receptor desensitisation depends on the kinetics of transmitter level in the synaptic cleft and on the ionotropic receptor kinetics. AMPA receptors desensitise after a 1-10 ms of glutamate exposure (Mosbacher *et al.*, 1994), whereas NMDA receptors desensitise on the time scale of 100 – 200 ms (Krupp *et al.*, 1998). Synaptic depression can also result from receptor saturation. Receptor saturation may occur if

the number of glutamate molecules released from a synaptic vesicle is much larger than the number of postsynaptic glutamate receptors. However, there are a few reports that a single packet of glutamate does not saturate the postsynaptic receptors. McAllister and Stevens (2000) reported the non-saturation of postsynaptic AMPA and NMDA receptors at the hippocampal pyramidal synapse. Yamashita *et al.* (2003) also reported that at the calyx of Held, postsynaptic AMPA receptors saturation does not occur.

The synaptic depression that results from a change in presynaptic release probability was first described by Bellingham and Walmsley (1999). The depression is observed in both AMPA and NMDA components of the EPSC, and can be abolished by the application of cyclothiazide (CTZ). CTZ is used to prevent AMPA receptor desensitisation (Yamada & Tang, 1993). The release probability can be influenced by influx of Ca^{2+} via presynaptic calcium channels (Dodge & Rahamimoff, 1967), the kinetics of Ca^{2+} buffering (Adler *et al.*, 1991; Lee *et al.*, 2000b; Rozov *et al.*, 2001), the distance between the Ca^{2+} channels and the Ca^{2+} sensor that triggers fusion (Matthews, 1996), and the identities of the proteins that make up the calcium sensor and release machinery (Finley *et al.*, 2002).

1.5.3.2.3.1. Release independent depression

Release independent depression is observed if a decrease in the release probability of neurotransmitter occurs even if the second synaptic response is preceded by a failure to release. RID is voltage-dependent (Fuhrmann *et al.*, 2004), has a high temperature sensitivity ($Q_{10} \approx 4$), lasts for ≥350 ms and is calcium-sensitive. There are several reasons why RID is presynaptic. Firstly, postsynaptic desensitisation cannot account for it. Secondly, the inverse of the normalised coefficient of variation squared (CV^{-2}) versus normalised mean EPSC amplitude showed that the most likely cause for RID is a change in the probability of transmitter release. Thirdly, there was no underlying facilitation, because increased vesicle release at the presynaptic terminal showed no significant involvement of postsynaptic Na^+ currents.

There are three possibilities for how RID could occur. The first possibility is the activation of a Ca^{2+}-activated K^+ conductance (SK-, IK- or BK-channels) in the nerve terminals. Based on immunohistochemistry and pharmacological techniques, SK- (Roncarati *et al.*, 2001), IK- (Sailer *et al.*, 2002; Obermair *et al.*, 2003) and BK-channels (Misonou *et al.*, 2006) were found at nerve terminals. The activation of these channels

would hyperpolarise the terminals, and thereby, limit the Ca^{2+} influx upon subsequent action potentials. As both SK- and IK-channels don't show much voltage-dependence, BK-channels might be a more likely candidate for RID.

The second possibility is a negative feedback mechanism on the VDCCs themselves (for review see Petersen, 2007). However, this may be unlikely to occur as the reported recovery from inactivation is in the order of minutes (Forsythe *et al.*, 1998) rather than the ~600 ms observed by Fuhrmann *et al.* (2004).

The third possibility could be an alteration of the release machinery itself, such as the voltage-dependent inactivation of release (Kraushaar & Jonas, 2000). Protein kinases or phosphatases might be involved in inactivation of the release machinery, thus causing RID. This hypothesis could be tested by relevant inhibitors, for example, tautomycin and microcystin, which inhibit protein phosphatases.

1.5.3.2.3.2. Frequency dependent recovery

Synaptic depression is relieved via one or more recovery process(es). The recovery time for the vesicle pool to be refilled varies from hundreds of milliseconds to tens of seconds (Xu-Friedman & Regehr, 2004). Recovery from depression was classically determined by vesicle becoming available at a constant rate (Betz, 1970). However, at some synapses, the rate of recovery from depression is activity-dependent as reported for invertebrate (Parker, 1995) and vertebrate synapses, notably at the calyx of Held (Wang & Kaczmarek, 1998; Sakaba & Neher, 2001) and cerebellum (Dittman & Regehr, 1998)

Fuhrmann *et al.* (2004) reported that, at stimulus frequencies < 10 – 20 Hz, the recovery time constant was close to 1 s whereas at > 20 Hz it was closer to 0.5 s. This was termed FDR. This recovery was sensitive to Ca^{2+} chelation and independent of augmentation, indicating that it was not an underlying facilitation that caused frequency dependent recovery (FDR).

There are a number of potential mechanisms that might explain FDR. At the level of vesicles, there are at least two pools found in nerve terminals: the readily releasable pool and the reserve pool (Koenig & Ikeda, 1996). The readily releasable vesicles are release-competent and highly sensitive to Ca^{2+} influx. The vesicles of the reserve pool are kinetically slower and require priming before becoming release-competent (Sakaba

& Neher, 2001). It could be that this priming of the reserve pool may become faster by the increased intracellular Ca^{2+} concentration.

Another possibility is that a decreased vesicle binding to the cytoskeleton causes FDR. Vesicle priming proteins may bind directly to the cytoskeleton. As components of second messenger systems interact with elements of the cytoskeleton, the cytoskeleton may play a regulatory role by altering the availability of the releasable pool. α-actinin is a cytoskeletal and adhesion protein, which connects the actin filaments to integrin adhesion proteins. It was found that α-actinin also binds to lipid layers containing DAG and palmitic acid (Meyer *et al.*, 1982). IP_3 binding (IC_{50} = 5 μM) to α-actinin at the calponin homology (CH) domain disrupts bundling and interaction with the integrin adhesion receptors (Full *et al.*, 2007). Drugs such as cytochalasins could be used to disrupt the cytoskeleton and thereby limit the availability of vesicles during repeated activity.

1.5.4. Ca^{2+} homeostasis in the nerve terminal

Ca^{2+} plays an important role in a number of cellular activities (Rizzuto & Pozzan, 2006; Clapham, 2007). Ca^{2+} is maintained at a 10,000-fold gradient by cells between their intracellular (~100 nM free) and extracellular (~2 mM) concentration of which only about 50% is in the free form. Ca^{2+} is kept low in the cytosol because of a number of reasons; firstly, it binds water much less tightly and would precipitate phosphate. Secondly, it functions as a second messenger. Thus, to exert control over Ca^{2+}, cells must chelate, compartmentalise, or extrude Ca^{2+} effectively and efficiently (Clapham, 2007).

At the synapse, as Ca^{2+} ions enter the nerve terminal and cause transmitter release, they have, due to their high signalling potency and ability to maintain release, to be either bound to fixed or mobile buffers or extruded/sequestered from the presynaptic compartment at a fast rate. This is achieved by a list of Ca^{2+} buffers and several energy-consuming mechanisms, which transport Ca^{2+} against its concentration gradient out of the cytosol. The activity of the plasma membrane Ca^{2+}-ATPases, Na^+/Ca^{2+} exchangers, and Ca^{2+}/H^+ antiports lower cytosolic Ca^{2+} levels. In addition, there are intracellular organelles, which are crucial in maintaining Ca^{2+} homeostasis. These are Ca^{2+} stores, buffers (EF hand proteins, annexins and gelsolin), smooth endoplasmic reticulum, mitochondria, nucleus and Golgi complex, which can take Ca^{2+} ions up efficiently.

1.5.4.1. Plasma membrane Ca^{2+}-ATPase

The plasma membrane Ca^{2+} ATPase (PMCA) was discovered by Dunham and Glynn (1961) in erythrocytes. The K_d of the PMCA for Ca^{2+} in the resting state is about 10 – 20 µM (Niggli & Carafoli, 1981), which decreases to < 200 nM via the modulation by calmodulin or acidic phospholipids (Enyedi *et al.*, 1987; Strehler & Treiman, 2004). The PMCA has a higher affinity for Ca^{2+} than the Na^{+}-Ca^{2+} exchanger but it also has a lower capacity. In addition, the removal of Ca^{2+} by PMCA is not as fast as by the Na^{+}-Ca^{2+} exchanger. Cloning work by Shull and Greeb (1988) revealed that the PMCA is very similar to the SERCA pump (see below), except for its long C-terminal tail. This tail is believed to regulate the function of the PMCA. Four gene sequences have been identified, generating four isoforms, PMCA1, PMCA2, PMCA3 and PMCA4. Using antibodies raised against the N-terminal sequence of the PMCA, Stauffer *et al.* (1995) reported all four isoforms of PMCA in the cortex. Alternative splicing of each of the isoforms further diversifies the PMCA pump (for review see Brini & Carafoli, 2009).

The PMCA is a 10 transmembrane protein that actively transports Ca^{2+} to the external milieu at the expense of ATP hydrolysis via one of its three main domains. The first domain is comprised of about 40 amino acids and has a strong preference for basic residues. The second domain contains the active site and a site that binds ATP. The hydrolysis of each ATP causes the removal of one Ca^{2+} from the cytoplasm. The third domain contains a calmodulin-binding site (James *et al.*, 1988). The PMCA exists as a homodimer in the membrane (Minocherhomjee *et al.*, 1983).

5,6-succinyl-imidyl-carboxyeosin is a potent inhibitor of the PMCA, with an IC_{50} of 20 nM (Gatto & Milanick, 1993). (IC_{50} is the half maximal inhibitory concentration and corresponds to the concentration of the compound required for 50% inhibition of the target). Other inhibitors are cyclopiazonic acid and thapsigargin with $IC_{50}$of 0.3 and 3 µM respectively (Fuente *et al.*, 1995).

1.5.4.2. Na^{+}-Ca^{2+} exchanger

The Na^{+}-Ca^{2+} exchanger (NCX) was first discovered by Reuter and Seitz (1968) in the heart. The NCX is a 150 kDa protein with nine transmembrane domains. The first 20 amino acids contain a calmodulin-binding site. There is an intracellular Ca^{2+} binding site between domain 5 and 6. Compared with the PMCA, the NCX has a lower affinity of 0.23 ± 0.03 mM (Fontana *et al.*, 1995) but a much higher capacity for Ca^{2+}, with a

turnover rate between 2500 and 5000 s^{-1} (Hilgemann *et al.*, 1991). Under normal resting membrane potential, it extrudes one Ca^{2+} for the uptake of three Na^{+} ions via an electrochemical gradient (Kang & Hilgemann, 2004). This causes an inward current leading to a depolarisation at rest. The direction of ion exchange (either inward or outward), however, depends on the membrane potential and the ionic gradients. During a large depolarisation, the NCX can work in the opposite direction; i.e. Na^{+} leaves and Ca^{2+} enters the cell causing a hyperpolarisation at the expense of a Ca^{2+} load. These properties displayed by the NCX may limit or accentuate excitotoxicity of the cell, which typically goes along with a significant depolarisation of the resting membrane potential. Three isoforms of the NCX has been identified: NCX1, NCX2 and NCX3. All three isoforms of the NCX can be found in the neocortex and hippocampus (Minelli *et al.*, 2007). 2-[2-[4-(4-nitrobenzyloxy)phenyl]ethyl]isothiourea methanesulfonate is a dose-dependent selective blocker of NCX with an IC_{50} of 1.2 – 2.4 µM (Iwamoto *et al.*, 1996).

1.5.4.3. Ca^{2+}/H^{+} antiport

The Ca^{2+}/H^{+} antiport is a 42 kDa (Ueoka-Nakanishi *et al.*, 2000), 11 transmembrane (Hirschi *et al.*, 1996) low-affinity Ca^{2+} pump with a K_d of 217 µM (Gonçalves *et al.*, 2000). It is activated in the presence of > 100 µM Ca^{2+} concentration (Gonçalves *et al.*, 1998). The Ca^{2+}/H^{+} antiport is dependent on the proton electrochemical gradient and works optimally at pH 8.5 (Tsuchiya & Rosen, 1976; Gonçalves *et al.*, 1999). When activated by ATP hydrolysis, the Ca^{2+}/H^{+} antiport displays a stoichiometry of 1 Ca^{2+}/ 2 H^{+} (Ohsumi & Anraku, 1983). Carbonyl cyanide *m*-chlorophenylhydrazone (CCCP) is an inhibitor of the Ca^{2+}/H^{+} antiport with a K_d of 270 nM (Bona *et al.*, 1993).

1.5.4.4. Cytosolic buffers

Most proteins in the cytoplasm can act as fast Ca^{2+} buffers, which can temporarily capture Ca^{2+} in exchange for protons within a few microseconds of entry through presynaptic Ca^{2+} channels. This capture typically reduces the Ca^{2+} concentration locally. However, as the Ca^{2+} concentration drops after the closure of Ca^{2+} channels, unbinding of the captured Ca^{2+} inevitably occurs. This can lead to a slightly elevated Ca^{2+} concentration. Electrophysiological recordings with rapid two-photon fluorescence imaging in connected cell pairs in rat neocortical layer II/III slices by Koester and Johnston (2005) demonstrated that the mode of presynaptic Ca^{2+} buffering could be specific to the type of synaptic connection. Using confocal fluorescence imaging,

Jackson and Redman (2003) reported that the endogenous Ca^{2+} buffer in the axon of the dentate gyrus is 130 ± 28 μM with a dissociation constant of 490 ± 220 nM. Important in the discussion below is the fact that there are a number of specific proteins expressed in the terminal with large Ca^{2+} buffering capacity, called Ca^{2+} binding proteins. Three main groups of Ca^{2+} binding proteins are known. These comprise the EF hand proteins, annexins and gelsolin, which could be involved in synaptic transmission.

1.5.4.4.1. EF hand proteins

The EF hand proteins derive their name from the crystal structure of parvalbumin (Kretsinger & Nockolds, 1973). This name was later expanded to cover the family of proteins, which have the EF hand Ca^{2+} binding motives (for review see Lewit-Bentley & Réty, 2000). Most of the EF hand proteins have two or more such motives. The molecular structure of this motif consists of two perpendicular 10 – 12 amino acid residues α-helixes with a 12-residue loop region in between, forming a single Ca^{2+}-binding pocket, where a single Ca^{2+} is associated with seven oxygen ligands nearby (Coffee & Bradshaw, 1973; Hendrickson & Karle, 1973). In most EF hand proteins, the residue at position 12 is glutamate (Nelson *et al.*, 2002). Examples of the EF hand proteins that are localised at the nerve terminals are calbindin-D28K, calmodulin, calsequestrin, calexcitin, calpain and parvalbumin (for review see Persechini *et al.*, 1989; Schwaller *et al.*, 2002). Calbindin-D28K is a 28-kDa calcium buffer with six EF hands, among which only four are functional and can hold up to four Ca^{2+} ions (Sun *et al.*, 2002). Calmodulin can bind up to four Ca^{2+} ions to regulate different protein targets. Calsequestrin holds Ca^{2+} in the cisterna of the sarcoplasmic reticulum (Binah *et al.*, 2007) and can hold up to 50 Ca^{2+} per molecule (Wang *et al.*, 1998). Calexcitin is a GTP binding protein that binds to two Ca^{2+} to regulate K^+ channels (Nelson *et al.*, 1996). Calpain has five EF-hand motifs in the C-terminal but only three of them can bind Ca^{2+} (Blanchard *et al.*, 1997). The crystal structure of parvalbumin (Revett *et al.*, 1997) revealed three EF-hand motifs but only two of them can bind to two Ca^{2+} (Haiech *et al.*, 1979). While most of the EF hand proteins are localised in the cytoplasm, there are some that are not. An example is the calnuc (nucleobindin), which is localised to the Golgi complex.

1.5.4.4.2. Annexins

Annexins were first characterised and reported by Creutz *et al.* (1978) while finding a Ca^{2+} dependent protein that was responsible for the aggregation of isolated granules in the cytosol and plasma membrane. They initially named the protein 'synexins' from a Greek word meaning 'meeting'. Later, Geisow *et al.* (1987) coined the word 'annexins' to represent a class of similar proteins for which a lot of different names had previously been used, including synexins, calpactins and lipocortins. These proteins have a conserved structural element of 70 amino acid residues called the annexin repeats. All annexins share a common organisational theme that involves two distinct regions; a 310 amino acid annexin core and a highly variable N-terminus. The annexin core is comprised of four annexin repeats, with each containing a Ca^{2+} binding site. The N-terminus of annexins serves as a binding site for cytoplasmic proteins.

An example of one annexin is annexin A6, which increases the mean open time and opening frequency of the ryanodine-sensitive Ca^{2+} channel in the sarcoplasmic reticulum (Diaz-Munoz *et al.*, 1990). In general, annexins bind to negatively charged phospholipids in the presence of micromolar Ca^{2+} concentrations. Annexins have been proposed to be involved in a number of membrane trafficking activities such as promotion of vesicle aggregation and fusion, inhibition of phopholipase A_2, anticoagulation, and ion channel activities (Gerke & Moss, 2002).

1.5.4.4.3. Gelsolin

Gelsolin, first isolated and named by Yin and Stossel (1979), is a 82 kDa actin binding protein that is regulated in a Ca^{2+} dependent manner. There are two forms of gelsolin: intracellular gelsolin (in the cytosol) and extracellular gelsolin (in blood plasma). Both gelsolins have six homologous subdomains, referred to as S1-S6. Each subdomain is composed of a five-stranded β-sheet, flanked by two α-helices, one of which is longer and positioned parallel while the other is perpendicular to the β strands. The N-terminal, which comprises of 3 domains (S1-3), forms an extended β-sheet, as does the C-terminal with the other 3 domains (S4-6) (Kiselar *et al.*, 2003). A high affinity Ca^{2+} binding site is located at the S6 domain. Upon Ca^{2+} binding, a conformation change allows the N-terminal to severe actin filaments (Lin *et al.*, 2000).

Gelsolin is usually inactive at rest. A rise of intracellular Ca^{2+} concentration of up to a few micromolars triggers gelsolin to polymerise actin monomers or sever the actin

filament, ultimately resulting in a capped actin filament. The action of gelsolin can be inhibited by local rise of phosphoinositides, which prevent gelsolin from binding to and severing actin (Janmey *et al.*, 1987). As a regulator of actin function, the intracellular gelsolin concentration plays a role in cell motility such as cytokinesis, ion channel modulation and even apoptosis (Kwiatkowski, 1999).

1.5.5. Calcium stores

Intracellular Ca^{2+} release has a pivotal role in synaptic transmission, where Ca^{2+} release from stores can trigger the opening of Ca^{2+} activated channels or the activation of other secondary messenger systems. It was reported in the Purkinje neurones that Ca^{2+} release from stores upon IP_3R activation causes the induction of LTD (Khodakhah & Armstrong, 1997).

Ca^{2+} stores may also play a role in modelling the cytoskeleton. Upon depletion of the stores, GTP binding proteins of the Ras superfamily are translocated into the plasma membrane. Interaction of the GTP binding proteins with Ras promotes actin polymerisation (Hajnóczky *et al.*, 1994).

Ca^{2+} stores also play an important role in gene regulation and expression, as the proteins involved in gene transcription and translation are dependent on Ca^{2+}. Three different regions of the DNA have been reported to respond to Ca^{2+} with initiation of gene transcription. They are the cAMP response element (CRE) binding site, the serum response element (SRF) binding site, and the ternary complex factor (TCF) binding site (Bading *et al.*, 1997).

To maintain the intracellular Ca^{2+} concentration at low levels, a number of organelles have been found to store Ca^{2+}. Most of these stores are single membrane-bound compartments that can store and release Ca^{2+}. These structures are the endoplasmic reticulum, endosomes, Golgi vesicles, acrosomes, lysosomes, secretory granules, and melanosomes (Clapham, 2007). The exceptions to the statement about single membrane-bound Ca^{2+} store constitute the mitochondria and the nucleus, which are double membrane-bound organelles.

1.5.5.1. Endoplasmic reticulum

There are three varieties of endoplasmic reticulum (ER), the rough endoplasmic reticulum (RER), the smooth endoplasmic reticulum (SER), and the equivalent in muscle, the sarcoplamic reticulum (SR). The ER is part of the endomembrane system, first seen by Porter *et al.* (1945) using electron microscopy. The ER is 100 – 150 nm in diameter, with an internal concentration of 500 μM free Ca^{2+} (Yu & Hinkle, 2000).

The surface of the RER is studded with ribosomes and therefore is the site where many reactions associated with the biosynthesis of membrane and secretory proteins occur. The membrane of the RER is continuous with the outer layer of the nuclear and mitochondrial envelope.

SER, is found in all eukaryotic cell types, where it appears as lace-like membranes (Porter *et al.*, 1945). It extends from the soma to the membrane of the nuclear envelope (Cataldo & Broadwell, 1984). In neurones, the SER extends into dendrites (Harris & Stevens, 1988), dendritic spines, and also axons (Terasaki *et al.*, 1994; Metuzals *et al.*, 1997; Aihara *et al.*, 2001; González *et al.*, 2011). Consisting of interconnecting tubules, the SER in the axon runs parallel with the axonal membrane and extends into synaptic terminals where it can be associated with mitochondria and intermingled with presynaptic vesicles (Cataldo & Broadwell, 1984). Using the transmission electron microscope, Westrum and Gray (1986) provided evidence that the SER is situated close to the synaptic vesicles in the rat cortex. Hartter *et al.* (1987) also provided ultra-structural evidence of the SER in the bullfrog olfactory axon terminal.

Given its structure, it has been suggested that the SER might play a role in Ca^{2+} homeostasis (for review see Görlach *et al.*, 2006). Ca^{2+} is taken into the SER via the sarco/endoplasmic Ca^{2+}-ATPase (SERCA) pump while Ca^{2+} is released from the SER via ryanodine and inositol-tris-phosphate (IP_3)-sensitive Ca^{2+} channels (discussed further below). The compartmentalisation of the Ca^{2+} stores at different loci can help distribution of the Ca^{2+} in the neurone.

1.5.5.2. Golgi complex

The Golgi complex was named after Camillo Golgi, who discovered the novel intracellular structure in 1898 using a chromoargentic impregnation of the spinal ganglia (for review see Bentivoglio, 1998). In the neurones of *Patella vulgata*, the

Golgi complex is 30 – 100 nm in diameter, with an adjacent space of 5 – 20 nm between the complexes (Lacy, 1957). The role of the Golgi complex in Ca^{2+} buffering was not understood until Alonso *et al.* (1971) reported a Ca^{2+}-ATPase like complex in smooth microsome fractions of rat submaxillary gland. Although ATP increases the uptake of Ca^{2+} into these microsomes, the authors found that ATP is not essential as the complex can perform its function without ATP. However, in the presence of ATP, this complex requires Mg^{2+} as a cofactor to take up Ca^{2+}. The role of the Golgi complex in Ca^{2+} buffering was later corroborated by Clemente and Meldolesi in 1975 using acinar cells in the pancreas of the guinea pig. They precipitated the Ca^{2+} in the Golgi complex with potassium pyroantimonate to produce an insoluble Ca^{2+} pyroantimonate. This precipitation demonstrated a high amount of Ca^{2+} associated with the membrane of the Golgi complex. In another set of experiments, an EF-hand Ca^{2+} binding protein, known as calnunc (see above), was reported to be located at the Golgi lumen where it binds to the heterotrimeric G protein $G\alpha_{i3}$, to buffer cytosolic Ca^{2+} (Lin *et al.*, 1998). Lin *et al.* also reported the presence of calnunc in the cytoplasm.

Given the notion that the Golgi complex can accumulate Ca^{2+}, it is likely that it is involved in Ca^{2+} homeostasis. The Golgi complex shares some similarities in terms of membrane bound proteins with the SER. Therefore, this leads to the juxtaposition of the Golgi complex with the SER in sharing similar function. Using electron microscopy with immunoblots, Taylor *et al.* (1997) reported that the Ca^{2+}-ATPase of the Golgi complex is a SERCA isoform.

1.5.5.3. Mitochondria

Besides being a main energy producing organelle, the mitochondria also participate in the buffering of free intracellular Ca^{2+} (Blaustein *et al.*, 1978). At rest, the Ca^{2+} concentration in the mitochondria is similar to the cytosolic Ca^{2+}, which is about 100 – 200 nM (Babcock *et al.*, 1997). However, the mitochondria will take up Ca^{2+} if the cytosolic Ca^{2+} concentration reaches about 500 nM (Pivovarova *et al.*, 1999). In rat sensory neurones, the mitochondria filter intracellular Ca^{2+} transients (Thayer & Miller, 1990).

The uptake of cytosolic Ca^{2+} into the mitochondria is not easy, as the mitochondria has two membranes. Cytosolic Ca^{2+} is taken up into mitochondria via two saturable mechanisms. The first is via an electrophoretic uniporter, first discovered by Haworth and Hunter in 1979. It is located at the inner mitochondrial membrane and maintains

the membrane potential of the intracellular compartment of mitochondria in the range of -150 and -180 mV (Kamo *et al.*, 1979). Disruption of the mitochondrial membrane potential with carbonyl-cyanide-4-(trifluoromethoxy)phenyl-hydrazone (FCCP) prolongs Ca^{2+} reuptake into the mitochondria (Werth & Thayer, 1994). If Ca^{2+} overloads (see below), the uniporter can initiate apoptosis by releasing mitochondrial Ca^{2+}. The second mechanism is called the rapid mode Ca^{2+} uptake (RaM) first described by Sparagna *et al.* (1995). The RaM allows the mitochondria to sequester < 400 nM Ca^{2+} in short pulses of 1 Hz. Although the mechanism of RaM is not fully understood, Buntinas *et al.* (2001) suggest that RaM creates a brief, high free Ca^{2+} concentration inside the mitochondria, which may activate intramitochondrial metabolic reactions with relatively small amounts of Ca^{2+} uptake. While the uptake of Ca^{2+} by the uniporter is slow, the uptake by RaM is fast. However, RaM is inhibited following its activation (Gunter & Gunter, 2001).

The low affinity for Ca^{2+} of the mitochondrial transporters makes them good candidates to prevent Ca^{2+} overload. If the mitochondria overloads with accumulation of > 0.3 µM Ca^{2+} (Nicholls & Scott, 1980), hydroxylapatite microcrystals form in the mitochondria. This formation has been reported in ankylosing spondylitis and Reiter syndrome (Delbarre *et al.*, 1981). The release of Ca^{2+} can be inhibited by ruthenium red or disruption of the mitochondrial membrane potential (Duchen, 1992). The Ca^{2+} concentration within the mitochondria recovers later via a mitochondria Na^{+}/Ca^{2+} exchanger (NXC_{mito}) into the cytoplasm (Carafoli *et al.*, 1974). The NXC_{mito} has an EC_{50} of 8 mM for Na^{+} (Crompton *et al.*, 1976) and releases Ca^{2+} at a rate of 8.5 nmol/mg min (Crompton *et al.*, 1978).

In 1978, Lehninger *et al.* proposed a mechanism for Ca^{2+} homeostasis by mitochondria. They found that oxidative phosphorylation generated by the production of energy, which causes oxidation of nicotinamide adenine dinucleotide hydride (NADH) in mitochondria, induces Ca^{2+} release from mitochondria into the cytosol whilst production of NADH from NAD+ induces its reuptake. This idea links the normal metabolic state of a neurone with its intracellular Ca^{2+} concentration and, in case of insufficient energy production typically followed by membrane depolarisation, Ca^{2+} influx with its uptake into the mitochondria.

1.5.5.4. Nucleus

Although the dual layer of the nuclear envelope separates the nucleus from the cytoplasm, it is connected to the ER. It was reported that the Ca^{2+} pump of the nucleus displays similar characteristics as the one on the ER (Lanini *et al.*, 1992). IP_3 and cyclic ADP-ribose have been reported to cause release of Ca^{2+} from the nuclear envelope into the cytoplasm (Nicotera *et al.*, 1990; Santella & Kyozuka, 1997). The regulation of Ca^{2+} in the nucleus is important because Ca^{2+} can activate enzymes that regulate transcription (Lanini *et al.*, 1992).

1.5.6. Calcium dynamics of calcium stores

The dynamics of the Ca^{2+} in the cytoplasm can be seen by the uptake of Ca^{2+} into stores through different channels, and the release of Ca^{2+} into the cytoplasm. In general, the cytoplasmic Ca^{2+} is taken up into the stores via the SERCA pump, while the ryanodine and IP_3 receptors release the Ca^{2+} back into the cytoplasmic compartment.

1.5.6.1. SERCA pump

The SERCA pump is a 110 kDa protein which consists of ten asymmetrical transmembrane spanning regions connected to a bulky cytosolic head via a stalk domain (Toyoshima *et al.*, 2000). The cytosolic head constitutes about half the mass of the SERCA and contains the phosphorylation and nucleotide binding domains that form the active site for ATP hydrolysis. Of the three paralogs of the SERCA, only SERCA 2b and SERCA 3 are found in the brain (Herbette *et al.*, 1985). The SERCA pumps transport Ca^{2+} into the ER in a series of partial reactions: two cytosolic Ca^{2+} ions have to first bind to the cytoplasmic domain of the pump, which are then internalised via active transport by ATP hydrolysis and subsequent phosphorylation. Phosphorylation of an aspartic residue causes the Ca^{2+} to be occluded within the phosphoenzyme before being released into the lumen of the ER (Inesi *et al.*, 1992). Inside the lumen, the Ca^{2+} binds to Ca^{2+} binding proteins calsequestrin and calreticulins (Lytton & Nigam, 1992) to prevent Ca^{2+}/phosphate precipitation.

All SERCA pumps have a relatively high affinity for cytosolic Ca^{2+} (0.1 – 0.4 µM). The active transport rate and the cytosolic Ca^{2+} have a sigmoidal relationship. SERCA accumulates Ca^{2+} in the lumen of the SER at 2.6 – 10 mM (Volpe & Simon, 1991) and

together with PMCA maintain the cytosolic Ca^{2+} concentration at 50 – 250 nM (Wanaverbecq *et al.*, 2003).

There are a few antagonists of SERCA pumps. Examples are thapsigargin and cyclopiazonic acid. Thapsigargin, a tumour-promoting sesquiterpene lactone, was first isolated from *Thapsia garganica*. It binds in a 1:1 stoichiometry to all SERCA pumps (Patkar *et al.*, 1979; Lytton *et al.*, 1991). Thapsigargin causes an irreversible block of pump activity by blocking the enzyme in the ER lumen with an IC_{50} of 1 nM. It does not interfere with either the Ca^{2+} or Na^+/K^+-ATPases on the plasmalemma (Ishii *et al.*, 1994). Cyclopiazonic acid (CPA) is an indole-tetramic acid metabolite first isolated from *Penicillium cyclopium* (Holzapfel, 1968). It has an IC_{50} of 9 µM and is normally used at a concentration much higher than thapsigargin (Zholos *et al.*, 2000). The blockage of the SERCA pump with thapsigargin (1 – 3 µM) or CPA (20 – 30 µM) prevents the store from replenishing the Ca^{2+} in the SER after prolonged stimulation and prevents Ca^{2+} release from stores upon subsequent stimulation (Garaschuk *et al.*, 1997).

1.5.6.2. Calcium release and leaks

Ca^{2+} release and leaks from the lumen of the SER, is balanced by the SERCA pump activity. Solovyova *et al.* (2002) reported a leak of 1.48 ± 0.17 µM/s Ca^{2+} from the lumen of the SER in rat dorsal root ganglion cells. Ca^{2+} can be either released by receptor-operated channels (ryanodine and IP_3 receptors) or by an unspecific Ca^{2+} leak.

1.5.6.2.1. Ryanodine receptor

The ryanodine receptor (RyR) is a large tetrameric complex with a molecular mass between 350 and 450 kDa (Campbell *et al.*, 1987). Under physiological conditions, > 100 µM Ca^{2+} (Meissner *et al.*, 1986) causes the RyR to open. Pharmacologically, with a binding affinity of 9 nM for ryanodine, the RyR mediates the release of Ca^{2+} from the SER (Imagawa *et al.*, 1987). The RyR displays a large conductance but low ion selectivity, which is in contrast to the Ca^{2+} channels in the plasma membrane. Ryanodine, an alkaloid from the plant *Ryania speciosa,* affects the conductance and gating properties of the ryanodine-sensitive Ca^{2+} release channels (Rousseau *et al.*, 1987). It locks the RyRs into a half-open state at nanomolar concentrations but fully closes them at micromolar concentrations (Smith *et al.*, 1988). It preferentially binds to the open form of the receptor (Chu *et al.*, 1990). Up to four ryanodine molecules can

bind to the RyR. There are three different isoforms of RyR; RyR1 is mostly expressed in skeletal muscles, RyR2 in myocardium and RyR3 in neurones (Zucchi & Ronca-Testoni, 1997) but all three isoforms are also present in neurones. Caffeine in millimolar concentrations is used to trigger Ca^{2+} release from ryanodine sensitive stores (Weber & Herz, 1968).

Ryanodine-sensitive Ca^{2+} release channels generate Ca^{2+} signals, which can, for example, cause spontaneous transmitter release. The spontaneous opening of RyRs generates Ca^{2+} sparks, first observed at the heart muscle (Cheng *et al.*, 1993). Typically, these channels have the potential to amplify action potential-driven Ca^{2+} signals in the presynaptic terminals and consequently may enhance the efficacy of transmitter release.

The cytoplasmic N-terminal domain of the RyR, which gates the channel pore located in the C terminus, can be modulated by a few proteins such as calmodulin and calstabin. In skeletal muscle, the binding of Ca^{2+} free calmodulin activates the RyR1 but the Ca^{2+} activated calmodulin inhibits the RyR1 (Samsó & Wagenknecht, 2002). Both the Ca^{2+} free and Ca^{2+} activated calmodulin bind to the RyR1 at position 3614-3643 with nanomolar affinity (Rodney *et al.*, 2001). Calstabin increases the channel open probability of RyR by stabilising the closed state of the channel (Brillantes *et al.*, 1994). Two isoforms of the calstabin, calstabin 1 and calstabin 2, bind with nanomolar affinity to RyR1 and RyR2, respectively (Samso *et al.*, 2006; Sharma *et al.*, 2006).

1.5.6.2.2. Inositol 1,4,5-trisphosphate receptor (IP_3R)

The inositol 1,4,5-trisphosphate receptor (IP_3R), with a binding affinity of 40 nM for IP_3 (Snyder & Supattapone, 1989), consists of a group of ligand-gated ion channels, which produce Ca^{2+} currents in response to stimulation by IP_3 (Bosanac *et al.*, 2002). Like the RyRs, IP_3Rs have 3 isoforms; IP_3R1, IP_3R2 and IP_3R3 which are present in all tissue types (Newton *et al.*, 1994). Using microsomal vesicles from rat brain synaptosomes, Finch *et al.* (1991) reported that Ca^{2+} is a coagonist of IP_3 induced Ca^{2+} release with a K_d of 240 ± 60 nM. Activation of the IP_3R is sensitised by < 300 nM Ca^{2+} (Iino, 1990), above which IP_3-induced Ca^{2+} release is suppressed (Chueh & Gill, 1986). IP_3R activation causes Ca^{2+} puffs and typically, there is a hierarchy of events such that Ca^{2+} release from IP_3R is amplified via RyRs (Imanishi *et al.*, 1996; Carlson *et al.*, 1997). Measurement of Ca^{2+} channel conductance in canine cerebellum (Watras *et al.*, 1991) illustrated that the Ca^{2+} release via RyRs produces approximately 1:2 amplifying ratio

compared to that via IP_3Rs. This ratio was further supported by the measurement of mEPSC frequency in the rat barrel cortex (Simkus & Stricker, 2002a).

Similar to the RyR, the IP_3R can also be modulated by Ca^{2+} binding proteins. Calmodulin binds to the IP_3R, in the presence of Ca^{2+} with a K_d of 117 ± 6 nM (Patel *et al.*, 1997). Calmodulin causes a reversible, concentration dependent inhibition of IP_3 binding by decreasing the affinity of the IP_3R for IP_3.

The IP_3R can be blocked with either xestospongin C or the membrane permeable 2-aminoethoxydiphenyl borate (2-APB). Xestospongin C, a selective membrane permeable blocker of IP_3Rs, isolated from the Australian sea sponge *Xestospongia exigua*, has an IC_{50} of 358 nM (Gafni *et al.*, 1997) with a very slow on-rate of several tens of minutes, while 2-APB has a higher IC_{50} of 42 µM but a reasonable on-rate (Maruyama *et al.*, 1997). However, the specificity of 2-APB of blocking IP_3Rs has been questioned as at 200 µM, it also blocks the SERCA pump. In addition, 2-APB has been known to inhibit certain transient receptor potential cannonical (TRPC) and transient receptor potential melastatin (TRPM) channels (Togashi *et al.*, 2008) while activating the transient receptor potential vaniloid (TRPV) channels (Hu *et al.*, 2004). However, in the layer II/III of the rat barrel cortex, Simkus and Stricker (2002a) reasoned that the TRP channels are not involved in Ca^{2+} release from stores, as the mEPSC frequency is independent of extracellular Ca^{2+}. They further did a dose response curve of 2-APB and found that 14 µM 2-APB is sufficient to block IP_3Rs in the nerve terminal.

1.5.6.2.3. Presenilins

The genes coding for presenilin were first identified by Li *et al.* (1995b). Presenilins represent a 50 kDa, nine-transmembrane protein family (Spasic *et al.*, 2006) localised on the ER membrane. Presenilins can be exported to the cytoplasm by endoproteolytic cleavage of both the N-and C-termini (Podlisny *et al.*, 1997). At the plasma membrane, presenilin assembles with nicastrins, Pen-2 and Aph-1, to form the γ-secretase (LaVoie *et al.*, 2003). The active γ-secretase cleaves the amyloid precursor protein (APP) in membrane after either the α- or β-secretase has cleaved it. Only if the APP is cleaved by β-secretase, amyloid β-peptide (Aβ) is formed. Aβ is found as insoluble fibrils in plaques predominantly in the brains of Alzheimer's disease patients (De Strooper *et al.*, 1999).

Presenilins can modulate transmitter release as it plays many roles in the ER. Tu *et al.* (2006) reported that presenilins function as Ca^{2+} leak channels in the SER. Presenilins have also been shown to upregulate the IP_3R (Cheung *et al.*, 2008), SERCA (Green *et al.*, 2008) and RyR (Zhang *et al.*, 2009).

1.5.7. Metabotropic receptors coupled to IP_3 production

Metabotropic receptors that are linked via $G_{q/11}$ to IP_3 production and are located at the presynaptic terminal have the potential to modulate Ca^{2+} release from stores. When activated, the $G_{q/11}$ protein stimulates the membrane bound phospholipase C (PLC) to cleave the other membrane bound phosphatidylinositol-4,5-bisphosphate (PIP_2) (Berridge, 1983). This hydrolysis releases diacylglycerol (DAG) and IP_3 into the cytoplasm. PLC can be inhibited by edelfosine, which has an IC_{50} of 9.6 ± 1.2 μM (Powis *et al.*, 1992). Binding of IP_3 to the IP_3R at the ER allows the release of Ca^{2+} from the ER to increase intracellular [Ca^{2+}] from ~100 nM to ~1 μM (Clapham, 2007). I will be discussing only a few of these metabotropic receptors that can potentially activate Ca^{2+} release from stores, namely the metabotropic glutamate receptors and the adrenergic receptors. However, there are others that may also be relevant including the histamine, serotonin, muscarinic, orexin and purinergic receptors (Jones *et al.*, 1979).

1.5.7.1. Group I mGluRs

The mGluRs are G-protein-coupled glutamate receptors. There are eight subtypes of mGluRs (mGluR1 – mGluR8). These subtypes of mGluRs can be sub-classified into three groups according to their sequence similarities, pharmacological properties and signalling cascades. Group I consists of mGluR1 and mGluR5, which are positively coupled to phospholipase C and lead to IP_3 production (Abdul-Ghani *et al.*, 1996). Members of group II are mGluR2 and mGluR3, which are negatively coupled to adenylyl cyclase. mGluR4, mGluR6 – mGluR8 belong to group III, which are also negatively coupled to adenylyl cyclase but are selectively activated by L-aminophosphonobutyrate (L-AP4).

Simkus and Stricker (2002a) found experimental evidence for the presence of presynaptic group I metabotropic glutamate receptors and that the activation of these receptors could significantly increase transmitter release. This is in contrast to

previously held views that the group I mGluRs are found at postsynaptic locations only while the group II and III mGluRs are generally located presynaptically (Conn & Pin, 1997; Cartmell & Schoepp, 2000). In the case of the reported spontaneous transmitter release, it is likely that activation of mGluR5 produces IP_3 and DAG in the presynaptic terminal since mGluR1 is only found on postsynaptic structures (Lujan *et al.*, 1997). In contrast, group II and III mGluRs in general act as autoreceptors by reducing transmitter release as a consequence of adenylyl cyclase inhibition.

1.5.7.2. Adrenergic receptors

The adrenergic receptors (also called adrenoreceptors or adrenoceptors) belong to a class of G protein-coupled receptors that are targets of catecholamines, especially noradrenaline (also called norepinephrine in the US) and adrenaline (epinephrine). Adrenergic receptors can be found in many regions of the cortex (Cash *et al.*, 1986; Scanziani *et al.*, 1993), and are present on a substantial percentage of axon terminals (Mobley & Greengard, 1985). The agonist of the adrenergic receptor, NA, does not cross the blood brain barrier (Axelrod *et al.*, 1959; Whirby *et al.*, 1961). In the brain, noradrenaline (NA) is synthesised in adrenergic neurones from dopamine by the enzyme dopamine β-hydroxylase. These neurones project diffusely from the *locus coeruleus* located in the rostral brain stem. The fibres of these noradrenergic neurones have been shown to innervate the barrel cortex in rodents (Simpson *et al.*, 2006), which is the area I have been studying.

There are two groups of adrenergic receptors, namely α and β receptors. The α receptors are further pharmacologically subdivided into α_1 and α_2 with α_2-AR having the highest affinity for NA followed by the α_1-AR and β-AR (Ramos & Arnsten, 2007). Only the α_1-AR couples to the $G_{p/q}$ protein (Goodhardt *et al.*, 1982) to cause Ca^{2+} release from intracellular stores via IP_3 production, while both the α_2 and the β-ARs are coupled to G_i/G_s, respectively, to modulate intracellular cAMP concentration (Han *et al.*, 1987; Tognarini & Moulds, 1997; Horinouchi *et al.*, 2007). Based on pharmacological and genetic profiles, α_1-AR can be further characterised into three subtypes, the α_{1A}-, α_{1B}- and α_{1D}-AR (Bylund *et al.*, 1994). All three α_1-AR receptor subtypes differ in their subcellular distribution. The α_{1A}-AR is present at both the plasma membrane and in the intracellular pool while the α_{1B}-AR is localised to the plasma membrane (Hirasawa *et al.*, 1997; Chalothorn *et al.*, 2002). The α_{1D}-AR is mainly expressed in the cytosolic component (McCune *et al.*, 2000). In addition, there is a putative α_{1L}-AR, which has similar characteristic to the α_{1A}- and α_{1D}-AR but displays low affinity for prazosin (Ford

et al., 1994). However, no gene has been identified to encode the α_{1L}-AR and the α_{1L}-AR was proposed to represent a functional isoform of the α_{1A}-AR (Martí *et al.*, 2005).

Jones *et al.* (1985) characterised the distribution of α_1-AR using *in vitro* autoradiography and found high signal in the frontoparietal cortex, olfactory bulb, central amygdaloid nucleus, thalamus and inferior olive. Using *in situ* hybridisation histochemistry, McCune *et al.* (1993) further examined the localisation of the mRNA encoding the α_{1A}-, α_{1B}-, α_{2A}-, α_{2C}-AR in the rat cortex. They found that α_{1A}- was highly expressed in the olfactory bulb, intermediate layers of the cortex, the hippocampus, and the reticular nucleus of the thalamus, while the α_{1B}-AR is highly expressed in the intermediate and deep layers of the cortex, thalamus, hippocampus, dorsal raphe, and cerebellum.

Like all G protein coupled receptors, the structure of the α_1-AR consists of a seven transmembrane region, with a conserved cysteine residue at the C-terminus. The cysteine residue helps keep the conformation of the α_1-AR by formation of disulfide bonds. The α_1-AR exists as a dimer with a mass of 160 kDa at the plasma membrane. Half of the receptor protrudes out from the lipid bilayer to form a helical structure for binding by catecholamines (Venter *et al.*, 1984).

A series of pharmacological α_1-AR agonists and antagonists are available to determine the activation properties of the receptor. Cirazoline, a selective α_1-AR agonist, with an IC_{50} of 1 μM (Le Rouzic *et al.*, 1995) can be used to activate the presynaptic AR. Prazosin, a selective α_1-AR antagonist has an IC_{50} of 1 nM (Mathe *et al.*, 1996).

There is evidence of crosstalk between the α_1-AR with the other ARs and also with other signalling systems. In ventricular myocytes of the rat, α_1-AR activation suppresses the Ca^{2+} current caused by activation of the β-AR (Boutjdir *et al.*, 1992). More, the crosstalk between α_{1A}- and α_{1B}-ARs, has been shown to downregulate the β-AR-mediated cardiac inotropy (Rorabaugh *et al.*, 2005). In the hearts of young rats, the α_{1A}-AR potentiates the action of angiotensin receptors, which are also coupled via G_q to IP_3 production (Li & Shi, 2009).

The systemic function of NA is to regulate alertness and the wake-sleep cycle, maintenance of attention, and is involved in memory and learning, synaptic plasticity and neuroprotection (Jouvet *et al.*, 1991). Activation of α_2-AR by NA causes inhibition of cholinergic neurones, which are sleep-promoting neurones in the rat basal forebrain (Modirrousta *et al.*, 2004). Puumala *et al.* (1998) observed that α_1-AR activation

facilitates learning in rats. Troadec *et al.* (2001) found that NA can provide long-term protection to dopaminergic neurones by reducing oxidative stress. NA also affects cerebral metabolism (Harik *et al.*, 1979), with NA depletion causing a slower recovery of the redox ratio of cytochromes a and a_3.

At the cellular level, NA was found to either facilitate or suppress the glutamate-evoked transmitter release in the rat somatosensory cortex (Waterhouse & Woodward, 1980; Waterhouse *et al.*, 1982). Facilitation was associated with the activation of α_1-AR while suppression was mediated through the β-AR. Pastor *et al.* (1996) found that NA acts on presynaptic autoreceptors in cortical and hippocampal synaptosomes to enhance its own release via receptors with the pharmacological profile of α_1-AR. It would be interesting to know if activation of α_1-AR could result in increased transmitter release via activation of intracellular Ca^{2+} stores.

There are numerous controversies in the literature about pre- *versus* postsynaptic α_1-AR activation. Scanziani *et al.* (1993) reported that presynaptic α_1-AR activation decreased EPSP amplitude in slice cultures of hippocampal CA3 pyramidal neurones. Marek and Aghajanian (1996) observed that activation of α_{1B}-ARs increases the excitability of layer III interneurones in the rat piriform cortex. However, Fort *et al.* (1995) demonstrated that the postsynaptic α_1-AR depolarises and excites guinea-pig cholinergic neurones. Chen *et al.* (2006) also showed that activation of presynaptic α_1-AR increases the mEPSC frequency without affecting the mEPSC amplitude of the rat hypothalamic paraventricular nucleus neurones. The conclusion here is that it is not entirely clear what α_1-AR activation does in cortex.

1.5.7.3. Other metabotropic receptors that are coupled to IP_3 production

There are a few other metabotropic receptors that are coupled to IP_3 production. Among them are some of the histamine, serotonin, muscarinic, orexin and purinergic receptors (Jones *et al.*, 1979). I will briefly include them here for completeness.

1.5.7.3.1. Histamine (H_1) receptors

Among histamine receptors, only the H_1 receptor is coupled via G_q to IP_3 production. The H_1 receptor is a 487-amino acid protein (De Backer *et al.*, 1993). It is distributed in a wide variety of tissues, including the CNS, smooth muscle, gastrointestinal tract

(Sander *et al.*, 2006), cardiovascular system (Finch & Hicks, 1977), endothelial cells (Ottosson *et al.*, 1988) and lymphocytes (Casale *et al.*, 1985). Histamine binds to the asparagine residue at the 207-position in the fifth transmembrane domain of the receptor (Leurs *et al.*, 1994). Immunohistochemical studies have shown that the tuberomamillary nucleus in the hypothalamus is the sole source of histaminergic projections in the cortex (Panula *et al.*, 1984; Watanabe *et al.*, 1984).

The increase in intracellular Ca^{2+} can activate a few processes. Weiger *et al.* (1997) reported that the H_1 receptor in C6 glial cells are coupled to small conductance Ca^{2+}-dependent K^+ (SK) channels. H_1 receptor activation causing Ca^{2+} release from stores opens SK channels and results in hyperpolarisation of the membrane. Jafri *et al.* (1997) reported that activation of the H_1 receptor inferret vagal afferent neurones causes a depolarisation of the membrane by blocking a leak K^+ current, and reduces the slow-after hyperpolarisation (AHP_{slow}). The H_1 receptor has been shown to crosstalk with other metabotropic receptors that are coupled to IP_3. Kendall and Hill (1988) showed that activation of the adenosine receptor selectively inhibits the H_1 receptor stimulated PIP_2 hydrolysis in mouse cerebral slices.

1.5.7.3.2. Serotonin (5-HT_2) receptors

5-HT_2 receptors are the only serotonergic receptors from the seven 5-HT families that can stimulate PLC activity (Julius *et al.*, 1990). Activation of 5-HT_2 has been reported to activate phospholipase C leading to hydrolysis of PIP_2 and production of IP_3 (Sanders-Bush *et al.*, 1990). 5-HT_2 receptors have been implicated in many physiological processes, including sleep, pain perception, mood and learning (Nichols & Nichols, 2008; Berger *et al.*, 2009). Mammalian cerebral cortex receives an abundant serotonergic input from the brainstem raphe nuclei (Lidov *et al.*, 1980; Törk, 1990). Immunohistochemical studies have shown that 5-HT_{2A} is localised to apical dendrites (Willins *et al.*, 1997; Hamada *et al.*, 1998) and a subset of presynaptic terminal in asymmetric synapses of pyramidal neurones (Jakab & Goldman-Rakic, 1998).

5-HT_{2A} receptors can modulate release probability by a presynaptic mechanism at some glutamatergic synapses. In the dorsolateral septal nucleus of the rat, it was found that application of the 5-$HT_{2A/2C}$ agonist α-methyl-5-HT increased mEPSP frequency by 72 ± 15% without affecting mEPSP amplitude (Hasuo *et al.*, 2002). In the same study, 5-HT increased mEPSC and EPSP amplitude in response to stimulation of the afferent

fimbrial pathway and decreased the paired-pulse facilitation ratio, consistent with an increase in presynaptic release probability.

More specifically, activation of 5-HT_{2A} receptors by the 5-HT_2 partial agonist 1-(2,5-dimethoxy-4-iodophenyl-2-aminopropane) can lead to an increase in the frequency of sEPSC in layer V neocortical pyramidal cells while co-application with the selective 5-HT_{2A} antagonist MDL 100,907 reverses the effect of the agonist (Aghajanian & Marek, 1999). A reduction in the ratio of paired-pulse facilitation together with an increase in release probability has also been demonstrated in response to 5-HT_{2A} receptor stimulation in layer II/III of the rat somatosensory cortex (Torres-Escalante *et al.*, 2004).

1.5.7.3.3. Muscarinic acetylcholine (M_1/M_3ACh) receptors

Of the five identified subtypes of muscarinic acetylcholine receptors, only the M_1, M_3 and M_5 subtypes are coupled to PLC activation (for review see Volpicelli & Levey, 2004). Immunolocalisation using subtype-specific antibodies raised against the non-conserved third intracellular loop of the muscarinic receptors showed the M_1 and M_2 subtypes are strongly expressed in the rat cortex, where lower levels of the M_3 and M_4 subtypes are present. The M_5 receptor subtype is relatively scarce (Levey *et al.*, 1991).

M_3-AChRs are localised to nerve terminals (Grillner *et al.*, 1999). The M_3 subtype has been reported to reduce neurotransmitter release, probably by increasing a Ca^{2+} dependent K^+ conductance in the synaptic terminal (Shen & Johnson, 2000).

1.5.7.3.4. Orexin (OX_1/OX_2) receptors

The neuropeptides orexin A and B (also known as hypocretin 1 and 2), two peptidergic neurotransmitters produced in some hypothalamic neurones, are crucial regulators of sleep, wakefulness, coordination of emotion, energy homeostasis, reward, drug addition and arousal (Sakurai, 2007). The neuropeptides orexin A and B mediate their effects through G-protein-coupled receptors, called OX_1 and OX_2 receptors. Orexinergic neurones activate and promote wakefulness with an increase in firing rate. In Alzheimer's disease patients, it was found that lower levels of orexin A causes increased wake fragmentation (Friedman *et al.*, 2007). It has been suggested that the orexin system may be the "master" system that may integrate several neuromodulatory systems, as seen by the anatomical projections into the rat *locus coeruleus*

noradrenergic system (Horvath *et al.*, 1999) and the ventral tegmental dopaminergic system (Fadel & Deutch, 2002).

Orexinergic nerve fibres branch diffusely from the hypothalamus throughout the CNS, with particular abundance found in the olfactory bulb, thalamus, perifornical and the lateral hypothalamic area, and all levels of the spinal cord (Cutler *et al.*, 1999). The functional role at the cellular level is less known; in some preparations, it can increase the release of either excitatory or inhibitory neurotransmitters by acting on axon terminals (De Lecea *et al.*, 1998).

Orexins accumulate in vesicles in axon terminals, suggesting a function in intercellular communications (Peyron *et al.*, 1998). Stimulation of Chinese hamster ovary cells expressing OX_1 receptors with orexin A results in an increase of intracellular Ca^{2+} (Lund *et al.*, 2000). Xia *et al.* (2009) reported that, in the deep layers of the rat prefrontal cortex, the Ca^{2+} influx is caused via the L-type Ca^{2+} channel. The intracellular Ca^{2+} increase depends on the concentration of the ligand. At low orexin concentrations, Ca^{2+} increase is primarily triggered by activation of orexin receptor-operated Ca^{2+} channels, which enhance PLC activation and lead to Ca^{2+} release from the ER. At high orexin concentrations, PLC is activated independently of orexin receptor-operated Ca^{2+} channels (Kukkonen & Åkerman, 2001).

1.5.7.3.5. Purinergic (P2Y) receptors

P2Y receptors are G protein-coupled receptors that respond to extracellular purine (ATP) and pyrimidine nucleotides (UTP). Six of the eight subtypes of the mammalian P2Y receptors currently known, are coupled to PLC activation ($P2Y_1$, $P2Y_2$, $P2Y_4$, $P2Y_6$, $P2Y_{11}$, $P2Y_{14}$; (Moore *et al.*, 2001). The Cys^{42} and Cys^{296} disulfide bridge in the extracellular loops 2 and 3 is critical for P2Y receptor activation (Hoffmann *et al.*, 1999). P2Y receptors have been shown in deep layers of the cortex using both immunohistochemistry (Moran-Jimenez & Matute, 2000) and autoradiography (Simon *et al.*, 1997). Using fura-2/AM to measure changes in Ca^{2+} concentration in rat neocortical neurones, Lalo *et al.* (1998) observed that activation of P2Y receptors increases intracellular Ca^{2+} concentration. Baryshnikov *et al.* (2003) were able to demonstrate that activation of the P2Y receptors causes IP_3 production and leads to subsequent Ca^{2+} release from stores.

1.5.8. Role of presynaptic Ca^{2+} stores in transmitter release

Metabotropic receptors that are coupled to IP_3 production could potentially cause Ca^{2+} release from intracellular stores via activation of IP_3Rs. At peptidergic terminals of hypothalamic neurones, spontaneous Ca^{2+} signals termed syntillas have been reported (De Crescenzo *et al.*, 2004). These are not triggered by activation of VDCCs and occur with equal frequency in both Ca^{2+}-free and normal solutions. Activation of RyRs by membrane depolarisation generates these syntillas.

Simkus & Stricker (2002a) described that pyramidal cells in layer II of the rat somatosensory cortex exhibited a high frequency of mEPSCs. The authors showed that these mEPSCs were caused by Ca^{2+} release from intracellular stores since blocking SERCA pumps on the ER reduced the mEPSC frequency. Further testing showed that there were both RyR and IP_3R on these stores. In addition, there was indirect evidence for Ca^{2+}-induced Ca^{2+} released (CICR) in these nerve terminals such that the response of IP_3 release may be amplified by Ca^{2+} release through RyRs. They further found evidence that IP_3 could be produced from autoreceptor activation of group I mGluRs. In addition, there is evidence in cerebellar Purkinje cells that presynaptic Ca^{2+} influx has a significant effect on spontaneous transmitter release (maxi-minis). Increasing the extracellular Ca^{2+} concentration increased spontaneous transmitter release while decreasing the extracellular Ca^{2+} concentration has the opposite effect (Llano *et al.*, 2000; Yamasaki *et al.*, 2006).

There are more reports of store release contributing to evoked transmitter release. At the NMJ, store involvement causes increased transmitter release after a burst of action potentials (Suzuki *et al.*, 2000). At central synapses, the most direct evidence was provided in pairs of basket Purkinje cells in the cerebellum (Galante & Marty, 2003), in which blockade of RyRs by ryanodine caused the evoked IPSCs to become much smaller. Stricker *et al.* (2007) found that stores contribute about 20 – 30% to the peak amplitudes of EPSCs evoked in pairs of layer V cells in rat.

1.6. Barrel cortex

1.6.1. Organisation and synaptic physiology

The barrel cortex is a specific area of the somatosensory cortex. It derives its name from a dark barrel-like structure of layer IV, which can be imaged via a tangential plane to the pial surface. This region extends from 4.7 to 6.4 mm^2 over the cortical surface (Welker & Woolsey, 1974). As this region of the barrel cortex is similar to the pattern of the vibrissae on the mystacial pad of the rat (Woolsey & Van der Loos, 1970), it was not surprising that each discrete area of the barrels is linked to a particular whisker. However, afferent inputs from the whiskers project to the contralateral barrel cortex. A minimum of three synaptic connections carries the primary afferent from the whisker follicle receptor to the barrel cortex. The sensory fibres from the mystacial pad run parallel via the trigeminal nerve to the brainstem nuclei, which then project to the contralateral thalamus and finally to layer IV of the barrel cortex. The most striking characteristic of this projection is that a single barrel, which contains around 2000 neurones (Pasternak & Woolsey, 1975), responds preferentially to stimulation of a single whisker (Welker & Woolsey, 1974).

1.6.2. Cellular organisation

There are altogether six layers of cell organisation in the barrel cortex. Layer I is the closest to the pia while layer VI the farthest. Layer IV receives thalamic inputs and projects collaterals horizontally to the border of layers V and VI. As with layer IV, layers V and VI can also receive thalamic inputs on their apical dendrites. Most cells in layer II/III receive their inputs from layer V. Pyramidal cells in layer II/III are special because they are not confined to a single barrel; this means that they can send their projections several barrels away from the cortex (Gottlieb & Keller, 1997). In this study, I will be focusing on the layer II/III pyramidal neurones of the barrel cortex. Therefore, I will describe below the morphology, electrophysiology and connectivity of these neurones.

Layer II/III pyramidal neurones are located around 286 ± 78 µm from the pia of the barrel cortex (Feldmeyer *et al.*, 2006). The pyramidal neurones within the upper half of layer II/III barrel cortex have a shorter apical dendrite, which often projects sideways towards the pial surface, while the pyramidal neurones in the lower half of this layer tend to project almost vertically towards the pia. The apical dendrites, with an average length of 79.8 ± 39.1 µm, of the upper half of layer II/III pyramidal neurones often

branch extensively within layer I of the barrel cortex, forming small apical tufts with a dendritic length of 1863 ± 628 µm and 17 ± 7 bifurcating nodes (Feldmeyer *et al.*, 2006). The axonal collaterals extend both horizontally within the same layer and into the infragranular layers of the barrel cortex. The basal dendrites of these neurones have an elaborated symmetrical field.

In contrast, the apical dendrites from pyramidal neurones in the lower half of layer II/III barrel cortex have an average length of 278 ± 89 µm, which often branch extensively within layer I of the barrel cortex, forming small apical tufts with a dendritic length of 1033 ± 552 µm and 7 ± 4 bifurcating nodes (Feldmeyer *et al.*, 2006). Unlike the upper layer II/III pyramidal neurones, these neurones have axons that ascend towards the superficial and into the deeper layers of the barrel cortex. The basal dendrites of these neurones are similar to the upper layer II/III pyramidal neurones.

The probability of obtaining a synaptically connected cell pair in layer II/III is ~10% (Feldmeyer *et al.*, 2006). Layer II/III pyramidal neurones have a mean resting membrane potential of -76 ± 4 mV. The distance between the soma of two synaptically connected pyramidal neurones is 42 ± 20 µm. From the analysis of morphologically identified synaptic contacts between pairs of layer II/III pyramidal neurones, the number of contacts is 2.8 ± 0.7 with an average distance of 91 ± 47 µm from the soma. 95% of the synaptic contacts are formed onto the basal dendrites of the postsynaptic targets.

In pairs of synaptically connected layer II/III pyramidal neurones, Koester *et al.* (2005) and Feldmeyer *et al.* (2006) reported an average unitary EPSP of 0.92 ± 1.01 (n = 34) and 1.0 ± 0.7 (n = 35) mV, respectively. The average latency of the EPSPs was 1.1 ± 0.4 (Feldmeyer *et al.*). In voltage clamp, the mean EPSC was 58 ± 35 pA (n = 7) with a rise time of 0.35 ± 0.16 ms. The release probability of the synaptically connected layer II/III pyramidal neurones was 0.46 ± 0.26 (Koester & Johnston, 2005).

Due to the higher reciprocal connectivity of Layer II/III pyramidal neurones than the other layers, these cells are thought to provide a recurrent circuit in the barrel cortex. Shimegi *et al.* (1999) reported that layer II neurones produced the largest response facilitation when a principal rat whisker was first stimulated, followed by the adjacent whisker in the same row. Celikel *et al.* (2004) lend further support to the associational activity of layer II neurones. They found that acute whisker deprivation reverses the firing order of layer IV to layer II/III neurones. Kampa *et al.* (2006) observed that layer II/III and V pyramidal neurones are reciprocally connected within the same column.

These layer II/III neurones thus can provide feed-forward and perhaps even feed-back excitation within cortex. As such, this layer may serve as the major "amplifier" within the canonical microcircuit of neocortex (Douglas & Martin, 2004).

1.7. Basis of Study

This study corroborates the signalling cascade of the α_1-adrenergic receptor in layer II/III of the rat somatosensory cortex using a slice preparation. Although the neuromodulator NA signals via the α_1-adrenergic receptor to cause Ca^{2+} release from intracellular stores (Han *et al.*, 1987), this has not been reported in the barrel cortex. However, Simpson *et al.* (2006) have shown that neurones from the *locus coeruleus*, which are the main source for NA, send their projections to the barrel cortex.

Therefore, I investigated whether NA causes Ca^{2+} release from intracellular stores by applying various pharmacological compounds to identify the underlying signalling cascade leading to store release. I restricted myself to pyramidal neurones only as there are too many classes of inhibitory neurones in the barrel cortex.

2. Part I

Noradrenergic modulation of spontaneous transmitter release

2.1. Introduction

I attempted to find if the neuromodulator noradrenaline (NA) can cause presynaptic Ca^{2+} release from stores. NA was chosen, as it may have the potential via the α_1-adrenergic receptor (α_1-AR) to produce inositol-1,4,5-trisphosphate (IP_3) and subsequent store release.

First, I tested if NA has any effect on spontaneous transmitter release. Later, I tested which receptor NA was acting on, by using both agonist and antagonist. Using a specific antagonist for that receptor, I provided evidence that the antagonist could reverse the effect of the agonist. I also answered the question whether the α_1-ARs were tonically activated by NA, as there were a background concentration of glutamate and GABA. In addition, I used immunohistochemistry to verify the presence of the AR that NA acted on, by labelling the α_1-AR subtype at the nerve terminal. Finally, I did some control experiments that arose from my experiment.

In a later part, I verified the presynaptic signalling cascade of the α_1-AR using specific blockers. I checked each step in the signalling cascade starting from α_1-AR activation, the generation of IP_3 via phospholipase Cβ, activation of IP_3 receptors on presynaptic calcium stores and finally the release of calcium from these stores that drives fusion of vesicles causing some of the mEPSCs. I also checked if there was receptor interaction between the α_1-AR with other IP_3 producing receptors.

2.2. Methods

2.2.1. Preparation of slices of barrel cortex

15 – 19 day old male Wistar rats were decapitated with a guillotine. The brain was rapidly removed and placed into ice cold (2 – 4 °C) artificial cerebrospinal fluid (ACSF) containing (mM): NaCl, 125; KCl, 2.5; $NaHCO_3$, 25; NaH_2PO_4, 1.25; $CaCl_2$, 2; $MgCl_2$, 1; glucose, 10; gassed with 95% O_2 and 5% CO_2 (Carbogen™, BOC Gases Australia Limited, North Ryde, Australia) to obtain a final pH of 7.4. The osmolarity was typically 315 $mOsmL^{-1}$. All chemicals used in the ACSF were purchased from Sigma-Aldrich (California, USA). The brain was then hemisected along the midline and the cut surfaces were glued with cyanoacrylic glue (Loctite® 406; Loctite Australia Pty. Ltd, Caringbah, NSW, Australia) onto a stainless steel stage angled forward by 15°. To provide optimal access to the posterial medial barrel cortex, the stage was mounted such that the cortex faced the cutting blade within the cutting chamber of a vibrating microtome (Leica VT 1200S, Leica Biosystems Nussloch GmbH, Nussloch, Germany), which was filled with ice-cold, gassed ACSF. Parasagittal slices were cut to a thickness of 300 µm with a double-edge stainless steel, teflon-coated 0.004' thick razor blade (Personna, Electron Microscopy Sciences, Fort Washington, PA, USA) angled at 15° to the horizontal plane, a forward sectioning speed of 0.07 mm/s and blade amplitude of 1.5 mm.

The slices, which displayed the most extensive dendritic arborisations in the plane of the cut surface, also contained the fewest necrotic cells, presumably due to the minimised damage to the main dendrites. Two initial cuts were then made to remove the lateral poles of each hemisphere and allow access to the posterior lateral barrel subfield; i.e. an initial cut of 3.5 mm, followed by a single slice of 0.3 mm thickness, which are discarded. The best slices were in general the third or fourth slice.

Following the separation of the cortex from the rest of the brain tissue using gentle pressure along the bent shaft of a fine-tipped syringe (0.6 mm diameter), the slices consisting of neocortex and hippocampus were placed in a holding chamber containing gassed ACSF. The holding chamber was then partly submerged in a heated water bath (Grant Instruments Ltd, Shepreth, Cambridgeshire, UK) for at least 30 min at 34 °C, and later maintained at room temperature until usage in an experiment. The holding chamber contained a platform made of nylon gauze, which was mounted halfway up a

250 ml beaker. A perforated tube delivered the oxycarbon® into a small cylinder positioned at the side of the platform. This arrangement allowed sufficient circulation of oxygenated ACSF such that the gentle downward "draft" from the circulating ACSF holds the slices in position.

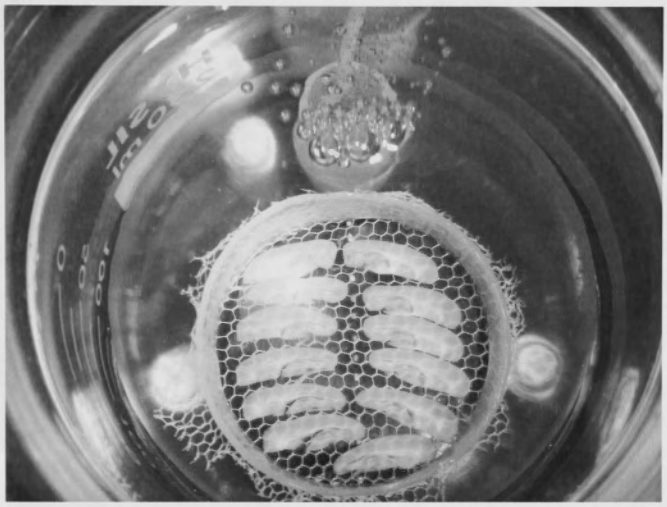

Figure 2.2.1. Photograph of the holding chamber, in which 6 slices from both hemispheres are arranged on the gauze in cutting sequence, from top to bottom. The tube entering the chamber (top), causing the formation of bubbles supplies the Oxycarbon® for buffering and establishes some circulation of the ACSF.

2.2.2. The recording chamber

The recording chamber represents a modification of a similar design by Nicoll and Alger (1981). The chamber was cut into a slab of Perspex™, which was glued with Sylastic glue onto a Mediglass coverslip (24 x 50 mm). It formed the base of the recording chamber. The temperature for all experimental recordings in the recording chamber was set at 36 ± 1 °C unless otherwise stated. The ACSF for superfusion was heated before entering the recording chamber by a water jacket around the inflow tube, which was connected to an external water pump and heater (Grant Instruments Ltd, Shepreth, Cambridgeshire, UK). The flow rate of the ACSF was controlled by placing an adjustable clamp on the inflow tube, which allowed a drip rate of 0.5–1 Hz, producing an average flow rate of 2–4 ml/min. To minimize the mechanical disturbance introduced by the ACSF dripping from the inflow tube, a mesh of nylon gauze was used to trap small bubbles entering the recording chamber. The solute then enters the main recording compartment and is sucked off in an outflow compartment with angled

surfaces using a fine-tipped, fire-polished glass pipette, which was attached to a waste reservoir and a vacuum pump. The recording slice was prevented from being dragged away by the flow of the solution by placing a harp over the slice. The harp was consisted of a tempered platinum frame, across which silk threads were glued into place.

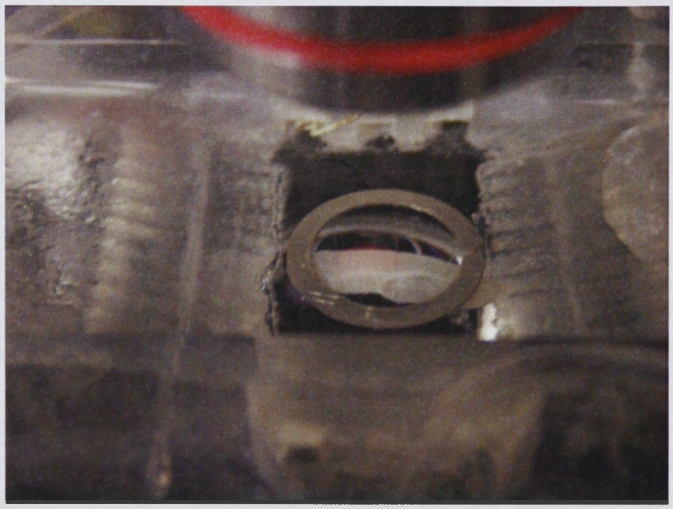

Figure 2.2.2. The slice in a main recording compartment of the slice chamber. A platinum harp is placed onto the slice to prevent movements cause by the flow of the solution. Note the dorsolateral area of somatosensory cortex in the centre of the red circle caused by the infrared light in relationship to thalamus on the left and hippocampus on the bottom right.

2.2.3. Whole cell recordings

2.2.3.1. Optics

Target neurones in layer II of rat somatosensory cortex were imaged using differential contrast optics under infra-red illumination (IR-DIC;) with an Olympus BX52WI microscope optimised for IR transmission (Olympus, Shibuya-ku, Tokyo, Japan), using a 40x long-working distance lens (3.3 mm; NA 0.8). The IR filter used had a bandwidth for optimal transmission in the range between 760 – 790 nm (Omega optical, Brattleboro, VT, USA). A camera (model VX45 by Optronics GmbH, Kehl, Germany) with some sensitivity in the IR range was used to visualise the infra-red picture on a high resolution black-and-white video monitor (PVM-145E, Sony, Tokyo, Japan) with the controller parameters, gain and offset, set to approximately 85 and 50, respectively. The DIC phase slider on the microscope was set fully to one direction such that the neurones were displayed with positive phase; i.e. the shape of the somata appeared as convex bodies. The condenser of the microscope was optimised to follow Köhler illumination.

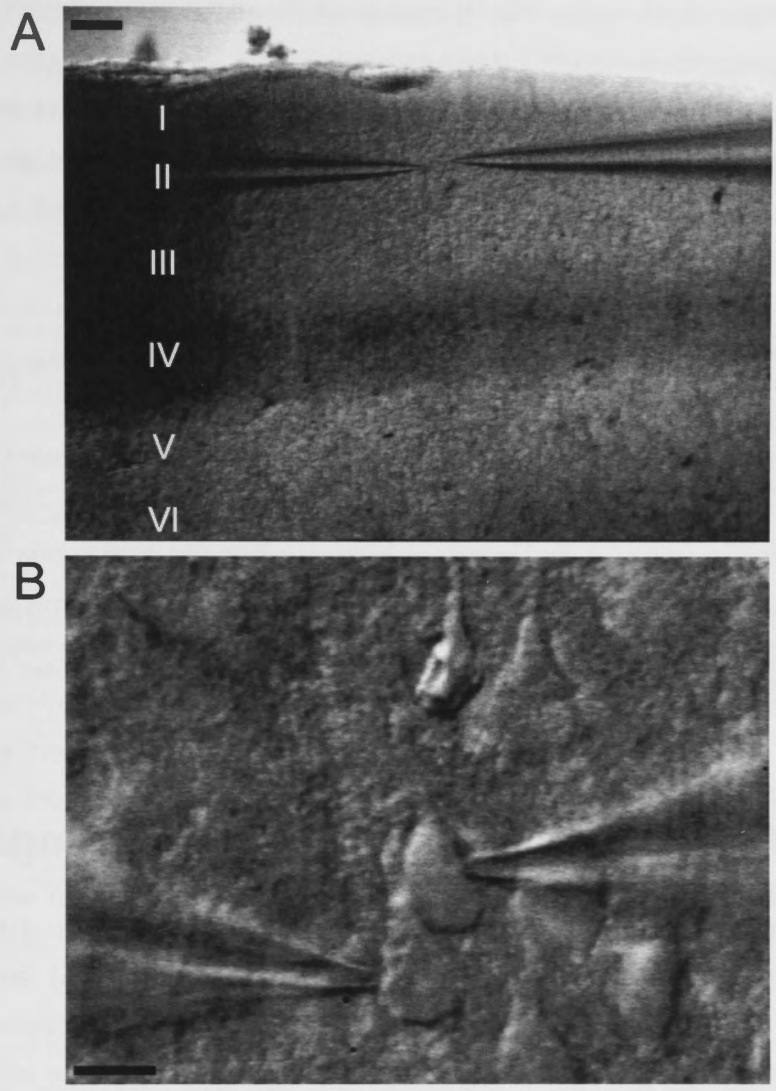

Figure 2.2.3. A) IR-DIC image showing a portion of a slice (scale bar 100 μM). Two electrodes are positioned in layer II with the posterior-lateral barrel subfield below (darker layer with hints of barrels). B) IR-DIC image showing a close-up view of two neurones recorded from (scale bar 10 μM).

2.2.3.2. Electrodes

Whole-cell recordings were made from cortical neurones in layer II/III of rat somatosensory cortex using patch electrodes (tip resistance 3–5 MΩ), pulled from borosilicate glass (outer diameter 2 mm, inner diameter 1 mm, length 75 mm; Hilgenberg, Malsfeld, Germany, Art-No. 1807502) using a five stage pull on a P-97 type Brown-Flaming type horizontal puller (Model P-97; Sutter Instruments Co. Novato, Ca, USA) using a 3 mm box filament. The puller settings are given in Table 2.2.1, below.

The tip of the electrodes was filled with the following intracellular solution unless slight modifications are given in the text. It contained (in mM) K-gluconate, 115; KCl, 20; HEPES 10; phosphocreatine, 10; Mg-ATP, 4; Na-GTP, 0.3 and biocytin, 0.25%. The pH of the intracellular solution was titrated with 1M KOH to a final pH of 7.3 and the osmolarity adjusted to 305 $mOsmL^{-1}$ with water or sucrose. All chemicals used in the intracellular solutions were purchased from Sigma-Aldrich (California, USA).

Whole cell electrode program (Ramp value: 671)			
Heat	**Pull**	**Velocity**	**Time**
Ramp + 10	20	30	180
Ramp + 81	15	20	200
Ramp + 91	15	20	200
Ramp + 97	15	20	200
Ramp + 113	10	25	200

Table 2.2.1. Values in arbitrary units (set by Sutter) used to pull electrodes for whole-cell recordings, using a Brown-Flaming type electrode puller with a 3.0 mm box filament. The air pressure was set to 500 units and the air duration at the beginning and end were set at 500. Electrodes were pulled at intervals of 9 minutes to allow the filament and chamber to cool down to ambient conditions.

2.2.4. Whole-cell voltage-clamp recordings

Whole-cell voltage-clamp recordings were done using a Multiclamp 700A amplifier (Axon Instruments, now Molecular Devices, Sunnyvale, CA, USA) and using the Multiclamp 700A Commander (version 1.3.0.5) software on the Macintosh computer. The manipulators on which the headstages were mounted at an angle of 27° from the horizontal plane were MP-225 (Sutter Instruments, Novato, CA, USA), which were driven on a 0 step length size for coarse positioning, but once close to the slice, a step length of 5 was chosen.

For obtaining a recording, the following approach was taken. Firstly, after the electrode was placed in the ACSF, the pipette offset potential was compensated to provide a holding current of zero at 0 mV holding potential. A brief 5 mV command potential was then applied to the electrode to gauge electrode tip resistance and current flow. While advancing the pipette, positive pressure (3.5 kPa) from a 25 ml syringe and monitored on a manometer (DM20, Sentinel Systems, Colorado, USA) was applied to the pipette. This causes a stream of intracellular solution to emanate from the tip of the electrode and prevents the accumulation of debris and soiling of the electrode tip. The electrode was lowered about 40 µm lateral to the cell and down to about the plane in which the cell was in the slice. At this stage, for a last time, the electrode offset was compensated

and a negative pressure of about 1.8 kPa chosen, using the syringe before a pressure valve (Type 74.001, Kuhnke, Malente, Germany). In a last step, the electrode was quickly horizontally advanced towards the neurone until close to the cell surface a "halo" appeared between the electrode tip and the cell surface membrane. At this point, the negative pressure was released from the syringe via quickly flipping the valve dial, which caused the cell membrane to seal to the electrode tip immediately. The sealing was further facilitated by the application of at least -70 mV hyperpolarisation of the electrode. Seal formation was monitored via the holding inward current amplitude slowly decaying to ≤ -40 pA.

When the series resistance (R_s) was in the 1–2 GΩ range, brief pulses of suction (approximately -10 kPa) were applied by mouth to rupture the membrane within the electrode tip and provide electrical access to the cytoplasm of the neurone. R_s and whole-cell capacitance (C_m) were not compensated, as R_s was well under 10% of the input resistance (R_{in}) of the pyramidal neurones recorded from in this study (50–200 MΩ). On a number of occasions, I switched to current-clamp and noted a value of -76 ± 2 mV for the membrane potential, which was slightly above the holding potential. In addition, the measured membrane potential (V_m) was not corrected for the liquid junction potential of the electrode. I measured the Vm less than a minute after break-in. This was done to avoid dilution of the internal solution of the patch pipette with the intracellular fluid.

Using the liquid junction potential calculator, JPCalc by Barry (1994), I obtained a value of 12.5 mV at 25 °C. After converting the liquid junction potential value to the recording temperature of 36 °C, which is the temperature that all my experiments were done, I acquired a value of 13.0 mV. I expected this value to be higher than the simplified Goldman-Hodgkin-Katz equation due to a larger sample of ions taken into consideration.

A negative current represents an inward current, which in current-clamp would depolarise the cell. A reported shift in mean amplitude will therefore be represented as a shift in the magnitude of the amplitude.

2.2.5. Data acquisition

2.2.5.1. Spontaneous transmitter release

Miniature excitatory postsynaptic currents (mEPSC) were measured in continuous voltage-clamp recordings of individual cells. The recordings were further amplified (typically 200 times) using a sample-and-hold unit that also contains a built-in 8-pole Bessel filter (custom made at JCSMR - ANU, Canberra, Australia). In recordings, from which R_s was estimated, the data was filtered at 10 kHz whereas for continuous or episodic recordings of EPSCs, 1 kHz was chosen. The recordings were then converted into a digital representation using an ITC-18 analogue-to digital converter board (Instrutech Corporation, Port Washington, NY, USA), which was operated at a sampling rate of 5 kHz. Data was recorded using custom-made software (Anna Cowan and Christian Stricker) developed for IGOR Pro 6.2 (Wavemetrics, Lake Oswego, OR, USA) and then stored on the hard drive of a Macintosh PowerMac G5 computer (Apple Inc, Cupertino, CA, USA). The timing of the acquisitions and repetition intervals of EPSCs was done using a Master-8 timer (A.M.P.I., Jerusalem, Israel), which also controlled the sample-and-hold unit as well as an oscilloscope.

2.2.6. Data analysis

Data stored previously were analysed using a set criteria. Below, I will go through the analysis of my recordings of how I estimated R_s, detection of mEPSC and the statistical comparison of the mEPSC.

2.2.6.1. Estimation of R_s and R_{in}

To check for stationarity of recording conditions, R_s and R_{in} were monitored between the start and the end of each recording period by applying a brief (40 ms) depolarising voltage step (V_s = 0.5 mV) and measuring the subsequent current response. Changes in either value can easily be picked up by comparing the average response between the two trials. To estimate R_s, it can be approximated from the peak amplitude of the capacitive current transient (I_c) at the onset and turn-off of the voltage step (t = 0) when all current is largely flowing into the capacitance and is limited only by R_s; at that point $R_s = V_s / I_c$ provided there is little stray capacitance of the electrode. R_{in} was estimated as the difference between R_s and the total resistance (R_{tot}) calculated from the steady

state current evoked by the test potential (R_{in} = R_{tot} - R_s). A cell was immediately discarded, if R_s was greater then 20 MΩ or if both values changed by more than 20%.

2.2.6.2. Detection of spontaneous EPSCs

Initial recordings of miniature events from the NMJ used visual inspection and manual measurement to analyse the data (Fatt & Katz, 1952). This was only possible due to the relatively small numbers of events (< 1000) recorded. In the present study, some cells displayed a rate of mEPSCs of > 100 Hz, from which I often made 5 minute recordings in order to check for the stationarity of the recording conditions. The task of detecting and measuring such a large number of events would be impossible if a visual inspection technique were used.

Automated detection of mEPSCs is a challenge in itself for a number of reasons. The detection algorithm was implemented in the following way. A template algorithm was used as described in Clements and Bekkers (1997) and implemented in Axograph X (Axograph, Sydney, Australia). In short, the template is slid along the recording and is optimally scaled and offset to fit the data sequence during each consecutive time window. The scaling factor and offset are calculated such as to minimise the sum of squared errors between the template and the data points. A detection criterion is determined from the template scaling factor and the goodness-of-fit between the scaled template and the data. A miniature event is considered detected when this detection criterion is above a user selected threshold level, reaches a peak when offset by a number of points and then drops below the level in the opposite direction, while the template is moved along further.

However, I noticed that if the template algorithm were used without moderation, it provided a large number of potentially false positive outcomes, particularly of small mEPSCs indistinguishable from recording noise which may have very small amplitudes or fast rise and decay times (or even negative values). I therefore considered the output of Axograph X as raw data, which had to be "filtered" for our purposes. This data was loaded into IGOR and a few custom-made routines served to eliminate mEPSCs with amplitudes < 2.5 times the standard deviation of the measured recording noise or that had too fast or even negative kinetic parameters (see also Appendix 1). The routines also adjusted instantaneous frequencies and latencies and automatically marked detected events for visual inspection.

At the heart of the analysis performed is the realisation that to achieve accuracy, the detected mEPSCs need to be re-checked by visual inspection; i.e. an mEPSC is only considered detected if visual inspection in a section of the recording confirms it. That meant that an optimisation between the values detected by eye and what we obtained by the template-matching algorithm is performed. For each recording, the parameters needed to be interactively adjusted to minimise the number of detection errors (either falsely positive or negative events) based on the events detected by eye during the first 2 seconds of every recording, which typically contained around 50 to over 100 events. Figure 2.2.4 shows a typical example of the first 2 seconds of a recording, in which the use of a truncated mEPSC resulted in the automated recovery of 27 out of a set of 29 events detected by eye.

Using the steps stated above, I was able to recover > 95% of events detected by eye from most recordings. The event detection algorithm returned the latency, amplitude, instantaneous frequency, and rise time and half width of each mEPSC. A step-by step set of instructions for using this approach, including the parameters used, is presented in the Appendix.

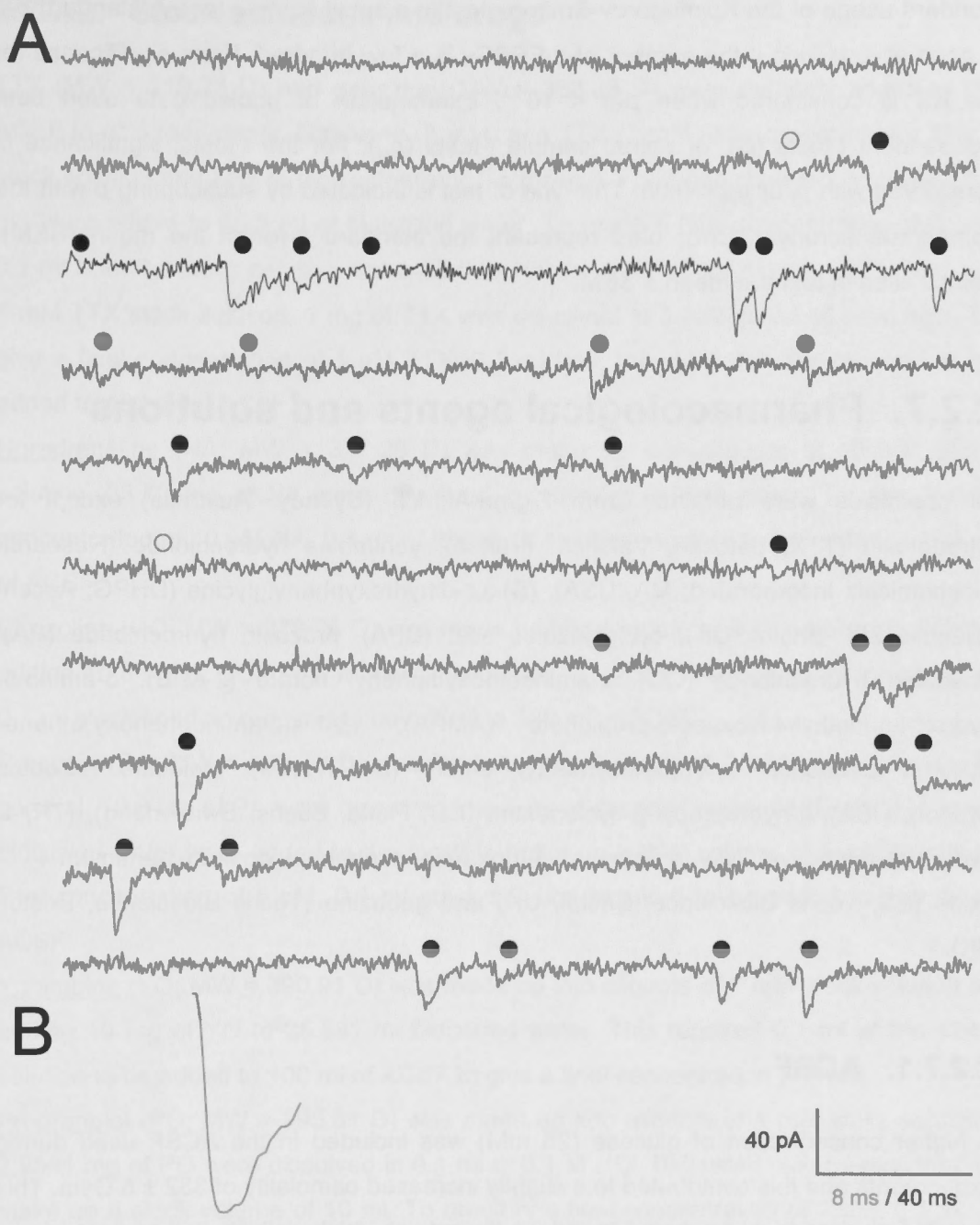

Figure 2.2.4. A) The first 2 seconds of a continuous recording broken in 200 ms periods, each vertically separated. The total number of events detected by eye was 30 (total circles filled and unfilled), of which 28 were recovered using the partial template in B. B) The partial template.

2.2.6.2.1. Statistical analysis

After the initial event detection with Axograph X and the subsequent thresholding in IGOR, comparisons between cumulative probability density functions were made using the Kolmogorov-Smirnov statistic (KS). Due to the large sample size of mEPSCs (typically > 10'000), a standard significance level of $p_{KS} < 0.05$ was insufficient as

standard usage of the Kolmogorov-Smirnov test is a small sample test. A standard p_{KS} is good at detection if the number of mEPSCs is a few hundred. From significance for the KS is considered when $p_{KS} < 10^{-21}$. Examination of pooled data used both independent *t*-tests (p_t), or paired sample *t*-tests (p_{pt}). For the *t*-tests, significance is considered with p_t or $p_{pt} < 0.05$. The type of test is indicated by subscripting *p* with the appropriate acronym. Error bars represent the standard error of the mean (SEM). Values cited in text are mean ± SEM.

2.2.7. Pharmacological agents and solutions

All chemicals were obtained from Sigma-Aldrich (Sydney, Australia) except for tetrodotoxin (TTX; Latoxan, Valence, France), yohimbine hydrochloride (Research Biochemicals Incorporated, MA, USA), (S)-3,5-dihydroxyphenylglycine (DHPG; Ascent scientific Ltd, Bristol, UK), cyclopiazonic acid (CPA), prazosin hydrochloride (PA), cirazoline hydrochloride (CO), 2-aminoethoxydiphenyl borate (2-APB), α-amino-3-hydroxyl-5-methyl-4-isoxazole-propionate (AMPA), 1,2-bis(2-aminophenoxy)ethane-*N*,*N*,*N*,*N*'-tetraacetic acid(acetoxymethyl ester) (BAPTA-AM; Molecular Probes, Oregon, USA), 2-hydropropyl-β-cyclodextrin (CD; Fluka, Buchs, Switzerland), (7*R*)-4-hydroxy-7-methoxy-*N*,*N*,*N*-trimethyl-3,5,9-trioxa-4-phosphaheptocosaan-1-aminium-4-oxide (ES; Tocris Bioscience, Bristol, UK) and gabazine (Tocris Bioscience, Bristol, UK).

2.2.7.1. ACSF

A higher concentration of glucose (25 mM) was included in the ACSF used during experiments and this contributed to a slightly increased osmolality of 332 ± 5 Osm. This elevated glucose level appeared to reduce the rate at which visibility in the slices deteriorated. We included this glucose concentration only in the solute used during the experiments whereas incubation and storage was done in a solute containing 10 mM glucose. The ACSF during an experiment in the superfusion chamber contained (mM): NaCl, 125; KCl 2.5, $NaHCO_3$, 25; NaH_2PO_4, 1.25; $CaCl_2$, 2; $MgCl_2$, 1; glucose, 25; gassed with 95% O_2 and 5% CO_2 to obtain a final pH of 7.4.

2.2.7.2. Stock solutions and drugs

TTX (MW = 319.28 D) and gabazine (MW = 368.23 D) were routinely added to the ACSF in all experiments. Gabazine (3 mM) and TTX (1 mM) was prepared in a 1000x stock solution and kept in the refrigerator. To make a 3 mM gabazine stock solution, 50 mg were added to 45.3 ml of bidistilled water. To reach a final concentration of 3 µM, 0.1 ml from the stock solution was added to 100 ml of ACSF for experiments. To make 1 mM TTX stock solution, 1 mg of TTX was dissolved in 3.132 ml 0.1 M citric acid. To give a final concentration of 1 µM TTX, 0.1 ml from the stock solution required to be added to 100 ml of ACSF.

Noradrenaline (NA; MW = 337.28 D) was made up into aliquots of 10 mM stock solution. 33.73 mg of NA were dissolved in 10 ml bidistilled water. To give a final concentration of 10 µM NA, 0.1 ml of the stock solution required to be added to 100 ml of ACSF.

Cirazoline (CO; MW = 270.76 D) was made up into aliquots of 5 mM stock solution by adding 10.8 mg of CO to 7.4 ml bidistilled water. To give a final concentration of 5 µM, 0.1 ml stock solution required to be added to 100 ml of ACSF.

Prazosin (PA; MW = 433.78 D) was made up into aliquots of 5 mM stock solution. In general, 10.8 mg of PA were dissolved into 1 ml of dimethyl sulfoxide (DMSO). 4 ml of bidistilled water were added to the stock to make up a total volume of 5 ml. To give a final concentration of 5 µM, 0.1 ml stock solution required to be added to 100 ml of ACSF.

Yohimbine (YO; MW = 390.91 D) was made up into aliquots of 1 mM stock solution by adding 10 mg of YO to 25.581 ml bidistilled water. This required 0.1 ml of the stock solution to be added to 100 ml of ACSF to give a final concentration of 5 µM.

Propranolol (PO; MW = 295.81 D) was made up into aliquots of 1 mM stock solution. 2.9581 mg of PO were dissolved in 0.1 ml of 0.1 M HCl. Bidistilled water was added to make up a stock volume of 10 ml. To result in a final concentration of 1 µM, 0.1 ml of the stock solution required to be added to 100 ml of ACSF.

2-APB (MW = 225.10 D) was made up into aliquots of 16 mM stock solution by first dissolving 50 mg of the compound in 2.22 ml of DMSO. 11.66 ml of bidistilled water were then added to the stock to make up a total volume of 13.88 ml. To give a final concentration of 16 µM, 0.1 ml of the stock solution required to be added to 100 ml of ACSF.

Cyclopiazonic acid (CPA; MW = 336.40 D) was made up into aliquots of 20 mM stock solution. To make this, 50 mg of CPA were dissolved in 1.486 ml of DMSO to which 5.944 ml of bidistilled water were added to make up a total volume of 7.43 ml. To give

a final concentration of 20 µM, 0.1 ml of the stock solution required to be added to 100 ml of ACSF.

Dihydroxyphenylglycine (DHPG; MW = 196.67 D) was made up into aliquots of 30 mM stock solution. To make this stock, 1.2 mg of DHPG were added to 0.2 ml bidistilled water. To give a final concentration of 30 µM, 0.1 ml of the stock solution required to be added to 100 ml of ACSF.

1,2-bis(2-aminophenoxy)ethane-*N,N,N,N'*-tetraacetic acid(acetoxymethyl ester) (BAPTA-AM; MW = 764.69) was made up into aliquots of 5 mM stock solution. In general, 7.7 mg of BAPTA-AM was dissolved in 0.3 ml DMSO. 1.7 ml of bidistilled water was then added to make up a stock volume of 2 ml to result in a final concentration of 50 µM.

2-hydropropyl-β-cyclodextrin (CD; MW = 1380 D) was made up into aliquots of 70 mM stock solution. To make this stock, 193.2 mg of CD were added to 2 ml of bidistilled water. To give a final concentration of 70 mM, 1 ml of the stock solution required to be added to 100 ml of ACSF.

p-(dipropylsulfamoyl)benzoic acid (PD; MW = 285.4) was made up into aliquots of 50 mM stock solution. To make this stock, 28.54 mg of PD were dissolved in 2 ml of 1 M NaOH. To give a final concentration of 0.5 mM, 1 ml of the stock solution required to be added to 100 ml of ACSF.

(*7R*)-4-hydroxy-7-methoxy-*N,N,N*-trimethyl-3,5,9-trioxa-4-phosphaheptocosaan-1-aminium-4-oxide (Edelfosine, ED; MW = 523.73) was made up into aliquots of 3 mM stock solution by dissolving 10 mg of ED in 2 ml bidistilled water. To give a final concentration of 30 µM, 1 ml of the stock solution required to be added to 100 ml of ACSF.

Where necessary, drugs were included in a second reservoir of ACSF next to the bottle containing the standard ACSF. This reservoir was connected to the main inflow pipe via a three-way valve. When two ACSF reservoirs were used, an effort was made to keep an equivalent level of solution in both bottles in order to not change the flow rate throughout the experiments.

2.2.7.3. AMPA iontophoresis

Iontophoretic experiments were required as positive controls to show that the drugs used did not change the size and kinetic of the mEPSCs. This is to check if a change in iEPSC amplitude occurs as a consequence of unspecific drug action. As has been reported for example by Savic *et al.* (1998), 30 µM ryanodine depressed $GABA_A$-

mediated IPSC amplitude in rat CA3 hippocampal pyramidal neurones. This could potentially be seen as a drop in mIPSC frequency, if a large number of mEPSCs is right at the level of detection to start with. To rule such an action out, thin-tipped microelectrodes were made from borosilicate glass (Clark Electromedical Instruments, Reading, England; outer diameter 1.2 mm, inner diameter 0.6 mm, length 100 mm; with omega-dot filament; Art-No. GC120F-10) using a single stage pull on a P-97 electrode puller (Sutter, Nova Alto, CA, USA) equipped with a box filament of 3 mm. These electrodes were backfilled with ACSF containing 10 mM AMPA. The electrodes had a resistance of about 80 MΩ when filled with 3 M KCl, and a tip size < 1 µm, which makes the visualisation of the tip in the IR range impossible.

Iontophoresis electrode program (Ramp value: 542)			
Heat	**Pull**	**Velocity**	**Time**
Ramp + 7	100	22	200

Table 2.2.2. Settings used to pull electrodes used for AMPA iontophoresis (3.0 mm box filament). The air pressure was set to 500 units and the air duration at the beginning and end were set at 500.

After a somatic whole-cell recording was obtained with a standard patch electrode, a positive holding current of between 0.4 – 2 nA was applied to the iontophoresis electrode attached to a x1 headstage connected to an Axoclamp-2B amplifier (Molecular Devices, Sunnyvale, CA, USA) in bridge mode. This was done to prevent diffusion of AMPA from the electrode, which could result in desensitisation of AMPA receptors (Colquhoun *et al.*, 1992). The leakage could be gauged by a sudden increase in holding current of the whole-cell recording, when the AMPA electrode was positioned close to a dendrite. The electrode tip was positioned using a micro-manipulator (MP-225; Sutter Instrument Company, Novato, CA, USA) at the surface of the tissue approximately 40–80 µm away from the soma on a putative piece of distal apical dendrite. The tip was then advanced until I could see the approximate tip in proximity of the apical dendrite. Iontophoresis of AMPA was triggered by short voltage pulses generated using an isolated stimulator unit model DS-2 (Digitimer Ltd, Welwyn Garden City, UK), connected to the Axoclamp-2B via the external ME1 command input. This was required as the command voltage level on the Axoclamp-2B required 100 V for the full range of current; such a large voltage is impossible to get from the D/A unit on the Instrutech ITC-18.

Negative command voltages in the range of -60 V (10 ms at 0.2 Hz) were applied to the Axoclamp 2B amplifier, which generated an iontophoretic current of -600 nA (iEPSC) at the electrode tip. When an inward current was detected in the whole-cell

recording, the command voltage was reduced in amplitude and duration and the electrode positioned in the region of the dendrite to optimally produce the fastest iEPSC possible. Figure 2.2.5 shows a typical example of a sequence of two iontophoretic responses, generated by -600 nA current pulses of 0.8 ms duration, separated by a 75 ms interval. The 10 – 90% iEPSC rise times were measured as the difference between two time windows of 1.2 ms before the time of stimulus and around the peak of the iEPSC. The half-widths of the iEPSCs were measured as the time at the half maximum of the iEPSC between the rising and the decay phase. In this case, the first and second pulse had iEPSC amplitudes of 68.5 and 61.0 pA, 10 – 90% rise times of 11.8 and 11.9 ms and a half width of 29.2 and 27.6 ms, respectively. The dashed line indicates that the iEPSC had not fully decayed back to baseline by the time the second iEPSC was evoked, which explains the difference between the two events in terms of amplitude and kinetics. After a stable iontophoretic response had been established, the drugs were then perfused.

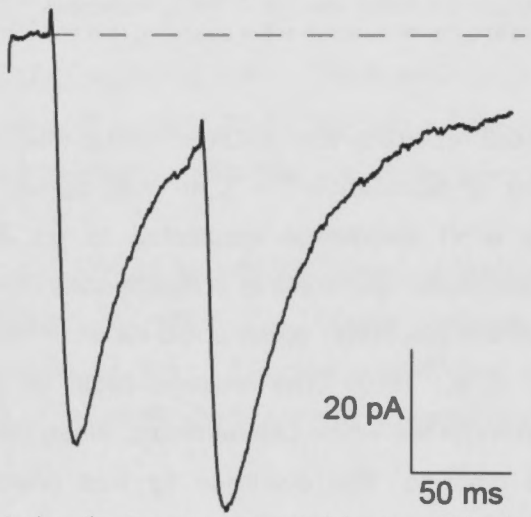

Figure 2.2.5. A pair of iontophoretic response generated by two -600 nA pulses of 0.8 ms duration separated by 75 ms, applied to a microelectrode containing 10 mM AMPA. The positive deflections are the stimulus artefacts. The dashed horizontal line represents the baseline before the initial pulse.

2.2.7.4. Loading of BAPTA-AM

The AM moiety of BAPTA-AM allows the transmembrane transfer of BAPTA-AM into the cytoplasm of the neurone, upon which the AM moiety is cleaved by the action of non-specific esterases (Ouanounou *et al.*, 1996). 0.7 mM CD and 0.5 mM PD were used to stabilize the AM moiety in the ACSF and to facilitate the accumulation of BAPTA within the cytoplasm of the neurone. 1 M NaOH was use to dissolve PD in the preparation of the stock solution, but after dilution from the stock solution to the perfusion, the concentration of NaOH dropped to 5 mM. This change accounts for about 3 % change of the total sodium concentration (150 mM). Thus, the concentration

of sodium in the ACSF was not adjusted. For the control experiment for CD and PD, a mEPSC recording was done with only CD and PD in the standard ACSF solution prior to the application of BAPTA-AM.

To ensure that BAPTA-AM had penetrated the cell membrane and accumulated within the cytoplasm of the neurone, I monitored the disappearance of the slow-afterhyperpolarisation (sAHP) previously described by Sah (1992). The sAHP is caused by a Ca^{2+}-dependent K^+ channel current, which can be seen after a burst of action potentials. The disappearance of sAHP after 10 min of BAPTA-AM incubation suggests that a sufficient concentration of the compound had accumulated in the cell to chelate the inflow of calcium in the stores (Simkus & Stricker, 2002a). After the block of the sAHP, I resumed my recordings of mEPSCs.

2.2.8. Histology

Histology was performed to positively identify the recorded pyramidal cell after the experiments using a biocytin labelling technique. In addition, fluorescence immunohisto-chemistry was preformed to identify the α_1-adrenergic receptor subtypes on the nerve terminals of pyramidal neurones.

2.2.8.1. Biocytin labelling technique

0.25% biocytin was routinely included in the intracellular solution. Following the recording, the slice was fixed in 0.1 M phosphate buffer solution (200 mM Na_2HPO_4 + 200 mM NaH_2PO_4 equilibrated to a pH of 7.4) containing 4% formaldehyde and stored in the refrigerator until further processing within a few days after recording. After fixation for at least 20 hours in the refrigerator, the slices were washed of fixative several times using phosphate buffer. They were then incubated overnight with avidin and biotin-conjugated horseradish peroxidase (ABC Elite kit; Vectastain, Vector Labs, Geneva, Switzerland), 10% normal swine serum (Vector labs) in 0.5% t-octylphenoxypolyethoxyethanol (triton X-100™; Sigma-Aldrich, Sydney, Australia) buffered with Trizma® (pH 7.4, Sigma-Aldrich, Sydney, Australia). Following overnight incubation at 4 °C, the slices were washed in Trizma® solution and reacted for 1 hour with 0.1% catechol, 0.05% phenylenediame (Sigma-Aldrich, Sydney, Australia), 0.4% di-ammonium-nickel-sulphate-6-hydrate and 0.6% cobalteous chloride (Sigma-Aldrich, Sydney, Australia). A small drop of peroxide was then added until the desired level of staining had been achieved. The reaction was halted by washing the slices in

phosphate buffer solution. The slices were mounted on slides (76.2 x 25.4 mm; Livingstone International Pty Ltd, NSW, Australia) and later embedded in 0.1% moviol (Sigma-Aldrich, Sydney, Australia) and covered by coverslips (24 x 24 x 0.15 mm; Knittel Gläser, Braunschweig, Germany). The slices were imaged on a Zeiss Axioshop 2 MOT (Carl Zeiss Light Microscope, Göttingen, Germany) using a microfire® true colour firewire microscope digital CCD camera 1600 x 1200P by Optronics (SciTech Pty Ltd, Victoria, Australia) mounted on the microscope. The software used was Neurolucida 9.10.2 (MBF Bioscience-MicroBrightField Inc, Vermont, USA).

Figure 2.2.6. Two layer II pyramidal neurones after histologically processing showing the main apical, basal dendrites and the axons (scale bar 20 µM). Note the two blebs at the axon endings indicative of cutting the axon.

2.2.8.2. Immunohistochemistry

The method used for immunohistochemistry is a modified version from Schneider Gasser *et al.* (2006). 0.5% biocytin was routinely included in the intracellular solution. Following the filling of the cells, the slice was fixed in a 0.1 M phosphate buffer solution containing 4% formaldehyde and stored in the refrigerator until further processing. After

fixation for at least 1 hour, the slices were taken out of the fixative, washed and put into cryoprotectant overnight (30% sucrose in 0.1 M PBS).

In order to get the maximum 20 µm slices with the intact soma and dendrites, a series of step were taken so that the cut slices were parallel to the blade of the cryostat microtome. A flattened stage was made with the solidified Tissue-Tek® O.C.T. compound (ProSciTech, Thuringowa, Australia) on an aluminium base. The stage was flattened parallel to the blade of the cryostat microtome (model CM1850 by Leica Microsystems GmbH, Nussloch, Germany). Next, the slice was mounted with the same position when the slice were filled with biocytin on an aluminium slide, which has a cross marking similar to the base of the stage. Then, a few drop of Tissue-Tek® O.C.T. compound was applied to the slice so the slice is covered with the solution. The aluminium slide containing the slice was placed into an icebox containing dry ice to solidify the Tissue-Tek® O.C.T. compound. When the Tissue-Tek® O.C.T. compound is almost solid, it is inverted and mounted on the stage, with the orientation of the slide and the stage parallel to each other. Both the stage and aluminium slide are left in the icebox for a minute, so that the Tissue-Tek® O.C.T. compound continue to solidify. After this, the aluminium slide can then be slid off. A few more drops of Tissue-Tek® O.C.T. compound is added to secure the stage and the slice. The slices that were mounted onto an aluminium stage were sliced 20 µm thick using a cryostat microtome onto silane-coated slides and air-dried. A hydrophobic ring was drawn around the section of the slices with a Pap pen (Daido Sangyo Co. Ltd, Tokyo, Japan).

For immunofluorescence staining, the slices were washed for 5 min in 0.1 M PBS, followed by 3 times washing for 5 min in a solution containing 0.1 M PBS with 0.1% triton X-100™. After that the slides were transferred to a humidified chamber, made from a large plastic lunch box with some blotting paper at the bottom soaked with bidistilled water. 1% bovine serum albumin (Sigma-Aldrich, California, USA) in 0.1 M PBS and 0.1% triton X-100™ was applied to the slices for 30 min. They were then incubated with the primary antibodies in 0.1 M PBS, 0.1% triton X-100™ and 1% bovine serum albumin. The primary antibodies consisted of rabbit polyclonal antibodies against the α_{1A}- or α_{1B} adrenergic receptors (1:100). The α_{1A}-AR antibodies was raised against a synthetic peptide (KTDKSDSEQV) and the α_{1B}-AR against the peptide sequence of KEMSNSKE corresponding to the third intracellular loop of rat, human and hamster α_{1A}- and α_{1B}-AR (Grayson *et al.*, 1998). A guinea-pig antibody was used against vGluT1 with a ratio of 1:3000 (Catalogue number 135304, Synaptic Systems GmbH, Göttingen, Germany). Revealing the biocytin marking of the cell was done

using streptavidin-conjugated alexa-750 with a ratio of 1:500 (Catalogue number SA1027; Invitrogen Corporation, California, USA). The slides were stored with the primary antibodies and the streptavidin-conjugate overnight at 4 °C in a light protected container.

The next day, the slices were washed in 0.1 M PBS for 5 min and reacted for 2 hours with the secondary antibodies at room temperature in the light protected container. The secondary antibodies consisted of a goat antibody against rabbit linked with alexa-568 (dilution 1:400; Catalogue number S-11226, Invitrogen Corporation, California, USA) and a goat antibody against guinea-pig linked with alexa-488 (dilution 1:2000; Catalogue number S-32354, Invitrogen, California, USA). The reaction was halted by washing the slices in 0.1 M PBS. The slices were left to air-dry overnight at 4 °C under light protected conditions. The slices were embedded in a buffered glycerol-mounting medium (Sigma-Aldrich) by combining 2 parts of glycerol with 1 part of sodium carbonate buffer (0.5 M Na_2CO_3 + 0.5 M $NaHCO_3$ equilibrated to a pH of 8.6). The embedded slices were covered by coverslips (24 x 24 x 0.15 mm; Knittel Gläser, Braunschweig, Germany) and stored in the dark at 4 °C

The slices were imaged on a Zeiss LSM5 Pascal, Axioskop 2 FS MOT (Carl Zeiss advance imaging microscopy, Jena, Germany) with a 63 x 1.4 NA lens, using a Hamamatsu Hisca CCD camera (Model C6790-81, SDR clinical technology, Middle Cove, Australia) mounted on the confocal laser-scanning microscope. Stacks of about 30 frames of 1024 x 1024 pixels each were acquired every 0.5 µm using a pinhole size of 200 nm. This pinhole size should give a resolution < 0.4 µm along the z-axis and much smaller in the xy plane. Image acquisition was done using the standard Zeiss software package (version 3.2, imaged at 12 bits) on Windows 2000 operating system.

To obtain images of colocalisation, the streptavidin-conjugated alexa-750 was excited using an Argon-ion laser (Lasos, Lasertechnik Gmbh, Jena, Germany) at 633 nm (red wavelength). The laser intensity was set at 10%, and fluorescence detected using a long-pass optical filter at 650 nm. The α_{1A} or α_{1B}-AR bound to a goat antibody against rabbit linked with alexa-568 was excited using a Helium-neon laser (Lasos, Lasertechnik Gmbh, Jena, Germany) at 543 nm (green wavelength). Laser intensity was set at 20% and fluorescence detected with a band-pass filter set to 560 – 615 nm. vGluT1 staining was traced using a goat antibody against guinea-pig linked with alexa-488 (blue wavelength) which was excited using a Helium-ion laser (Lasos, Lasertechnik Gmbh, Jena, Germany) at 488 nm. This laser intensity was again set to

about 20% and fluorescence intensity measured using a band-pass filter of 505 – 600 nm. Detector gain, amplifier offset and gain were adjusted and optimised individually and for each stack separately.

To determine if the fluorescent signals were colocalised, a method developed by Jaskolski *et al.* (2005) was used. An algorithm incorporated into Image J (version 1.45J) first selects the "region of interest" (ROI) in the three differently coloured images (red for biocytin labelling, blue for vGluT1 and green for either α_{1A}- or α_{1B}-AR) to separate these from background staining. It then produces a single ROI covering all three images. For each pixel and each frame within the single ROI, the algorithm calculates the deviation from the mean intensity of each image, and multiplies the mean deviation of the three images with the mean intensity to give the mean deviation product. To normalise the mean deviation product, the algorithm divides it by the product of the maximum mean deviation. This result in a normalised mean deviation product (nMDP) ranging from -1 to 1, with the negative nMDP corresponding to uncorrelated and positive to correlated pixels. The correlation index (I_{corr}) was calculated as a fraction of positive nMDP values over the total of all nMDP values.

2.3. Results

2.3.1. Spontaneous transmitter release

In order to study the action of noradrenaline on excitatory transmission independently of changes in inhibitory transmission, I examined pharmacologically isolated mEPSCs in identified pyramidal cells of layer II/III in rat barrel cortex. Inhibitory synaptic postsynaptic currents (mIPSC), which could be mistaken as mEPSCs due to the increased intracellular Cl^- in my patch-pipette solution, were blocked with the $GABA_A$ receptor antagonist gabazine (3 µM). All experiments showed that there were no significant changes in either amplitudes or frequency after superfusion of the slice with TTX and gabazine (data not shown). For most of the recordings, the average amplitudes and frequencies were determined during a 300 s recording period unless otherwise stated.

To avoid changes to the mEPSC frequency and amplitude caused by the changes in electrical resistance from the seal formation between the recording electrode and the cell membrane, all spontaneous transmitter release experiments were checked for changes in R_s before and after each sequence during an experiment. Experiments were discarded if R_s changed > 20% relative to the starting value or if the initial R_s value for the control experiment was > 20 MΩ. The mEPSC frequency and amplitude values are given as mean ± SEM.

I also analysed some basic electrophysiological parameters of these pyramidal neurones before applying the pharmacological compounds. The membrane potential, which was measured within 1 min after impalement ranged from -76 – -80 mV (n = 186), with R_s of 10 ± 1 MΩ and input resistance of 119 ± 5 MΩ (ranging from 28 to 577 MΩ). The membrane potential (V_m) was not corrected for the liquid junction potential of the electrode, but was calculated using JPCalc (Barry, 1994) to be approximately -13 mV. The average whole-cell noise, filtered at 1 kHz (without mEPSCs) during a recording was 2.64 ± 0.03 pA (standard deviation of noise ranging from 1.8 to 3.9 pA).

2.3.2. Basic observation

2.3.2.1. Action of NA

During control recordings, the instantaneous mEPSC frequency, which was calculated on the basis of the inter-event intervals, had an average of 42 ± 1 Hz (ranging from 8 to 78 Hz). The average mEPSC amplitude was -14.1 ± 0.3 pA (ranging from -27.0 to -1.7 pA), respectively. My observation supports the findings of Simkus and Stricker (2002b), where in 18 sets of experiments they observed an average instantaneous mEPSC frequency of 28 ± 24 Hz and amplitude of -10 ± 3 pA in the presence of TTX (p_{pt} values of 0.23 and 0.14 for comparison of average instantaneous mEPSC frequency and amplitude, respectively). Noradrenaline (NA) was first bath applied to check whether it had any effect on spontaneous transmitter release.

The first 2s of a five minutes recording before and after application of NA is shown in figure 2.3.1A. Taking a prominent mEPSC as template (Fig. 2.3.1C) from the same experiment, I analysed the first two seconds of all mEPSC recordings. The template is often chosen from the mEPSC recordings before the application of any pharmacological compounds. The error detection using the template from this recording had 19% false positive and 17% false negative mEPSCs. The choice of a short template baseline (≤ 0.1 ms) and only the initial half of the decay phase (~5 ms) allow the detection of closely occurring mEPSCs, as the mEPSC frequency recorded from pyramidal neurones in layer II/III of the barrel cortex can reached up to 70 Hz (Simkus & Stricker, 2002b).

I detected a total of 2'987 mEPSCs during the control period (Fig. 2.3.1E, G) and 18'070 mEPSCs in the presence of NA (Fig. 2.3.1F, H). The many dots that afar look like continuous lines in figure 2.3.1F are due to the sampling rate of 5 kHz set at the ITC-18 analogue-to digital converter board. It corresponds to a conversion time of 200 µs. The high occurrence of detected mEPSCs between 200 – 300 Hz indicate that there were many subsequent instantaneous mEPSC frequency being detected between 3 – 5 ms. Using Igor Pro 6.2, histograms of the frequencies (assigned to bins of 10 Hz) and amplitudes (assigned to bins of 0.5 pA) were generated as shown in figures 2.3.1I and 2.3.1J. In this example, both the instantaneous mEPSC frequency and amplitude histogram had a prominent peak at ~30 Hz and ~5 pA, respectively. The histograms were converted into cumulative probability density distributions (cPDF) for comparison. The cPDFs were compared using Kolmogorov statistics (p_{KS}), with the

level of significance set at $p_{KS} < 10^{-21}$ due to a large sample size (> 3'000 mEPSCs per min of recording sequence).

The application of 10 µM NA in this experiment increased the instantaneous mEPSC frequency from 41 ± 2 to 60 ± 1 Hz ($p_{KS} < 10^{-81}$; Fig. 2.3.1K); i.e. by 46 ± 2%. The mEPSC amplitude remained unchanged ($p_{KS} < 10^{-15}$; Fig. 2.3.1L). After application, most of the cumulative probability density for mEPSC frequency of this neurone was shifted to the right, demonstrating that mEPSC frequency was increased particularly in the higher frequency range. To check if there is a significant change in mEPSC kinetics, I averaged all mEPSC time courses before and after NA (Fig. 2.3.1D). These whole-sample average mEPSCs were truncated at 50% of the decay phase as many minis that straddle the decay phase are included for this averaging and therefore the tail becomes very variable. Likewise, there is not a straight baseline either, as again, minis that straddle the decay are used in forming this average. As is evident, I observed no significant change in the mEPSC kinetics, which I later verified with an iontophoresis experiment.

During control periods, an average mEPSC amplitude of -12.2 ± 0.6 pA and an instantaneous frequency of 42 ± 4 Hz were detected in pyramidal neurones (n = 33). Application of NA caused a significant increase in the mEPSC rate by 50 ± 11%, from 42 ± 4 to 63 ± 4 Hz (p_{pt} = 0.007; Fig. 2.3.2A) while the amplitude remained at -11.1 ± 0.4 pA (Fig. 2.3.2B).

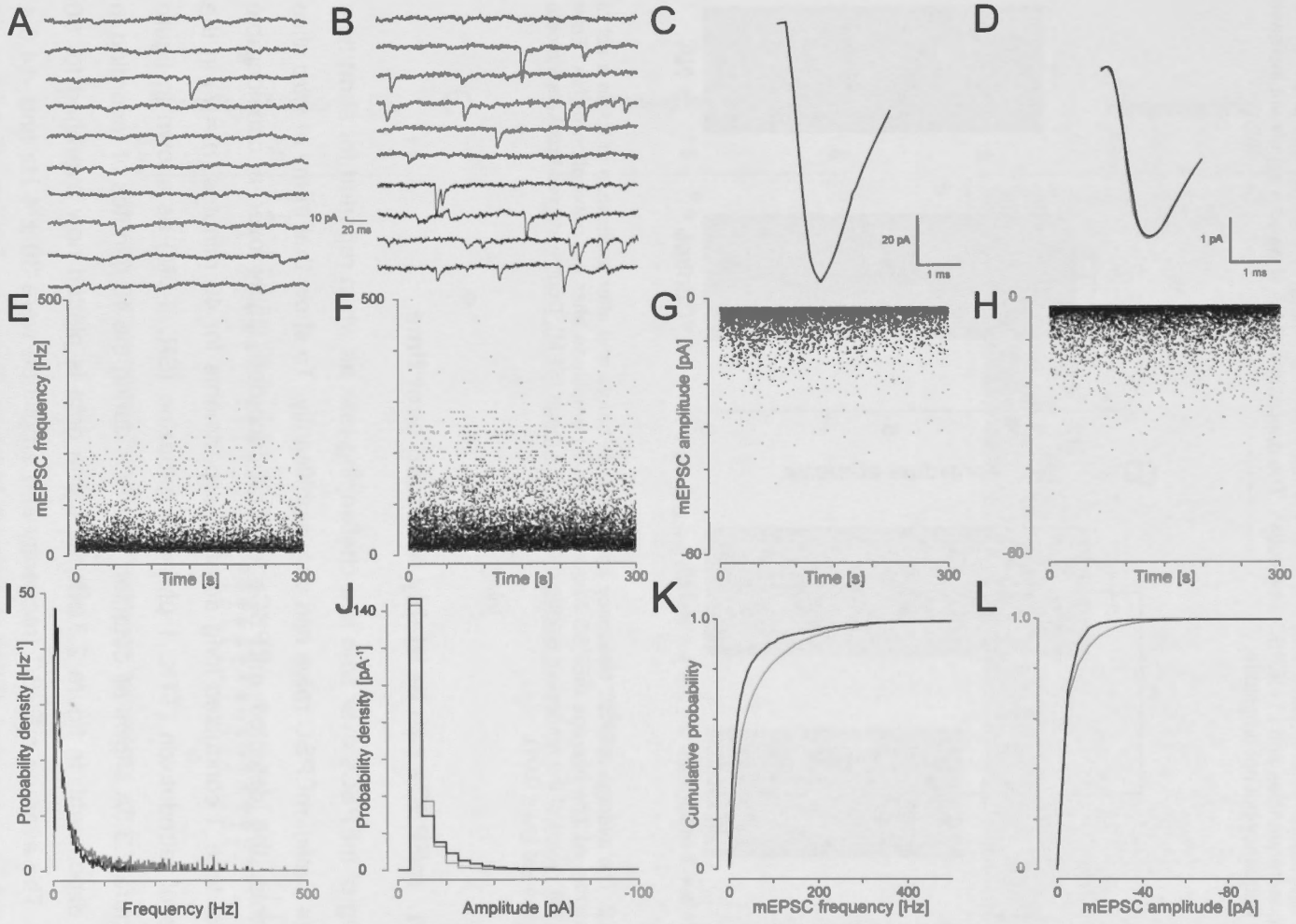
A
B
C
D
10 pA
20 ms
20 pA
1 ms
1 pA
1 ms
E
F
G
H
mEPSC frequency [Hz]
mEPSC amplitude [pA]
Time [s]
I
J
K
L
Probability density [Hz⁻¹]
Probability density [pA⁻¹]
Cumulative probability
Frequency [Hz]
Amplitude [pA]
mEPSC frequency [Hz]
mEPSC amplitude [pA]

Figure 2.3.1. The detected mEPSCs during a control period and after 5 minutes application of NA (10 µM). A) The first two seconds of recording are shown before and B) after application of NA. C) Template used to detect the mEPSC. D) The time course of the mEPSC amplitude after the application of NA (grey line) was normalised to the control condition (black line); the grey and black lines coincide due to similarity. The detected instantaneous mEPSC frequencies during the 300 s recording period are shown E) before and F) after application of NA. The detected mEPSC amplitudes during the 300 s recording period are shown G) before and H) after application of NA. I) The probability density histograms of the mEPSC frequencies and J) mEPSC amplitudes before (black line) and after the application of NA (grey line). K) The cPDF of the instantaneous frequencies and L) mEPSC amplitudes. The application of NA showed a significant increase in mEPSC frequency but not amplitude.

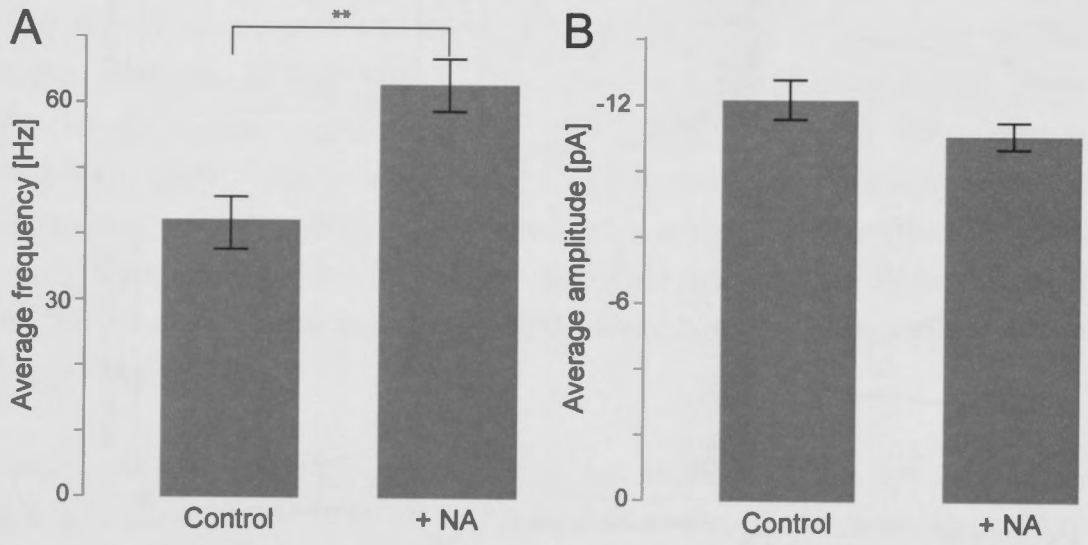

Figure 2.3.2. The average mEPSC frequency and amplitude before and after application of NA in a set of 33 experiments. A) The average mEPSC frequency and B) amplitude after the application of NA. Error bars mark the values of the respective standard error of the mean (SEM). Double starred brackets indicate significant change ($p_{pt} < 0.01$).

2.3.2.1.1. mEPSCs can be stably recorded over time

Recording of mEPSCs over time is a challenging task as when reported for short time periods (≤ 1 min), mEPSC rates can vary significantly. To show that in my *in vitro* slice experiments, the detected mEPSCs can be recorded stably over a considerable amount of time, I conducted long duration experiments for 40 minutes (n = 7) in the presence of tetrodotoxin (TTX, 1 µM) and gabazine (SR, 3 µM) as shown in figure 2.3.3. Figure 2.3.3A shows all detected mEPSCs during the 40 minutes of recording in a single experiment. In figure 2.3.3B, the same data is plotted now averaged for 60 seconds. The average mEPSC frequency and amplitude were 39 ± 4 Hz and -14.0 ± 0.8 pA. In figure 2.3.3C, the population averages of the type of data illustrated in figure 2.3.3B are illustrated. The error bars represent the variability within the population. There was no significant change in the mEPSC rates and amplitudes. Thus, mEPSCs can be stably recorded over a long period of time.

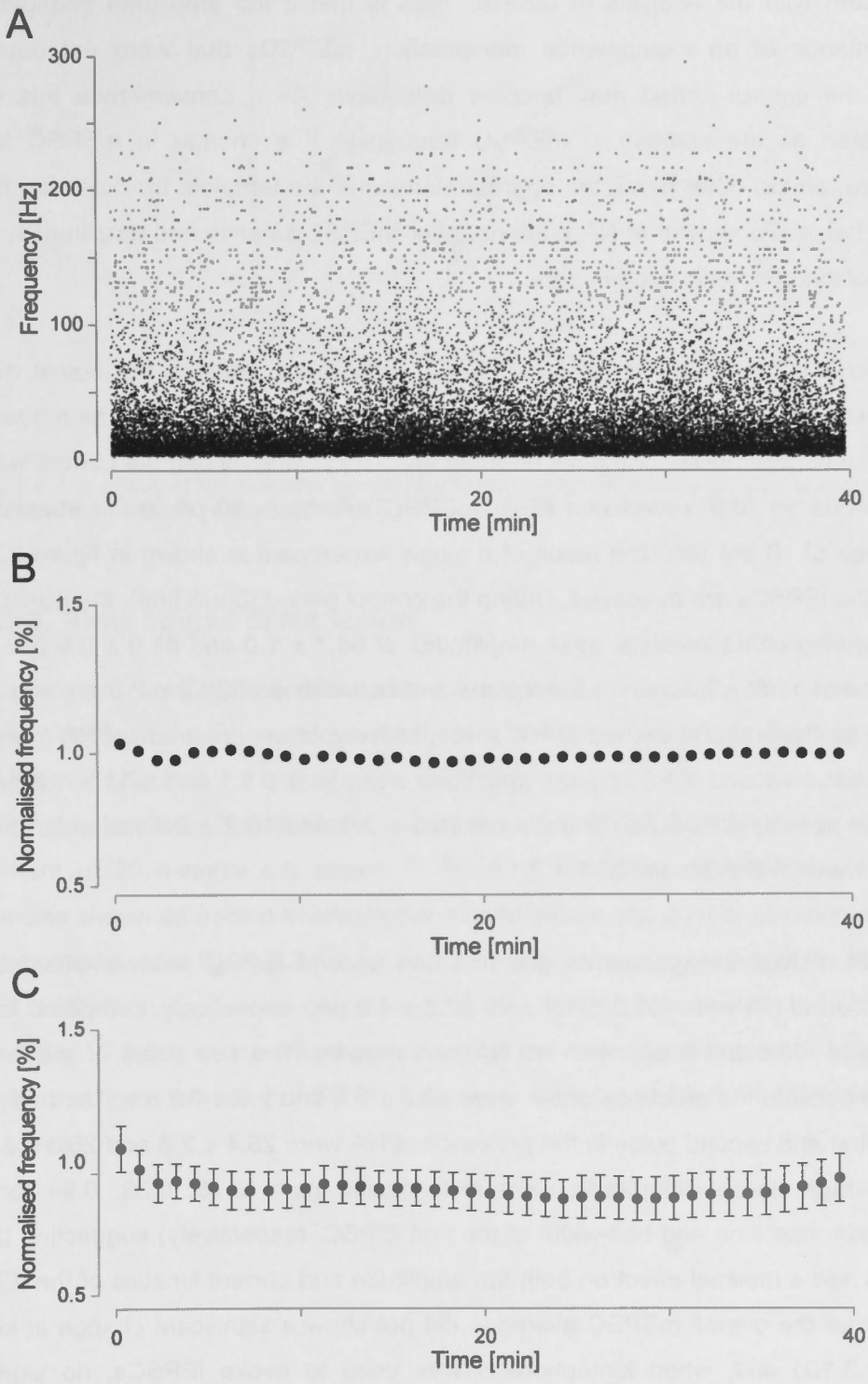

Figure 2.3.3. The mEPSC rate over 40 minutes of recording. A) mEPSC frequency as a function of time. B) TTX and gabazine co-application in a single experiment. C) Average time course of seven experiments. Error bars represent the value of the SEM of the population.

2.3.2.1.2. Iontophoresis of NA onto dendritic synapses

A concern with the analysis of mEPSC data is that if the amplitude changed as a consequence of an experimental manipulation, mEPSCs that were not detectable during the control period may become detectable. As a consequence this will be interpreted as an increase in mEPSC frequency. If a change in mEPSC kinetics occurred, on the other hand, the appropriateness of the template for detection may be questionable. To show that NA does not alter mEPSC kinetics and amplitudes, I did a series of iontophoresis experiments.

An electrode containing 10 mM AMPA was positioned close to the apical dendrite approximately 40 µm away from the soma. Iontophoresis of AMPA was triggered by two short current pulses of 0.8 ms duration and 75 ms interval and the current adjusted to generate an AMPA-mediated EPSC (iEPSC) of about -50 pA in the absence and presence of 10 µM NA. The result of a single experiment is shown in figure 2.3.4, in which the iEPSCs are overlayed. During the control period (black line), the iEPSCs had the following characteristics: peak amplitudes of 68.7 ± 1.0 and 61.0 ± 0.9 pA, with a rise time of 11.8 ± 2.3 and 11.9 ± 2.0 ms and half-widths of 29.2 ± 2.0 ms and 27.6 ± 2.1 ms for the first and second iEPSCs, respectively. In the presence of NA (grey line), the first and second iEPSCs peak amplitude were 64.9 ± 1.1 and 57.1 ± 1.2 pA. The first and second iEPSC rise times were 10.3 ± 2.0 and 10.2 ± 2.1 ms while the half-widths were 30.6 ± 2.0 and 30.6 ± 2.1.

In a set of twelve experiments, the first and second iEPSC peak amplitudes after application of NA were -55.5 ± 4.0 and -52.5 ± 4.0 pA, respectively, compared to -55.8 ± 4.7 and -50.8 ± 4.2 pA when no NA was present. The rise times of the first and second pulse in the presence of NA were 10.2 ± 0.6 and 9.9 ± 0.6 ms. The half-widths of the first and second pulse in the presence of NA were 25.4 ± 2.8 and 26.3 ± 2.6 ms. On average, these differences were insignificant (p_{pt} = 0.75, 0.33, 0.94 for peak amplitude, rise time and half-width of the first iEPSC, respectively) suggesting that 10 µM NA had a minimal effect on both the amplitude and current kinetics of the iEPSCs. Given that the overall mEPSC averages did not show a significant change in kinetics (Fig. 2.3.1D) and, when iontophoresis was used to evoke iEPSCs, no significant change was observed, I can therefore conclude that for the detection of mEPSCs the same template can be safely used both for control and after application of NA.

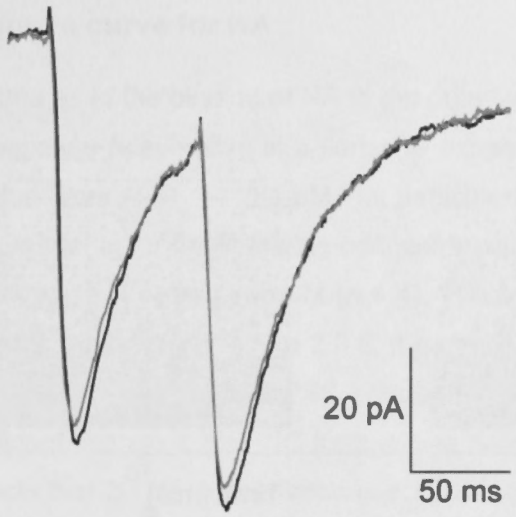

Figure 2.3.4. The effects of NA on AMPA currents evoked by two iontophoretic pulses separated by 75 ms (averages of 100 trials), after application of NA (grey line).

2.3.2.1.3. Time course of NA action

Because in my recordings the effect after NA application is typically observed only for about 5 minutes and as a consequence if there were changes afterwards I would not detect them, I checked if the change in mEPSC frequency remained elevated over a much longer duration. The detected instantaneous mEPSC frequencies in a single experiment of 20 minutes are shown in figure 2.3.5A. The instantaneous mEPSC frequencies shown as pooled averages per minute before and after application of NA in a single experiment in figure 2.3.5B, while the average of eight experiments is shown in figure 2.3.5C. Bath application of NA reached the maximal effect within the first 3 – 5 minutes (Fig. 2.3.5B) of superfusion after which the rate was maintained. I therefore conclude that the increase in mEPSC frequency lasts for at least 20 minutes in the presence of NA.

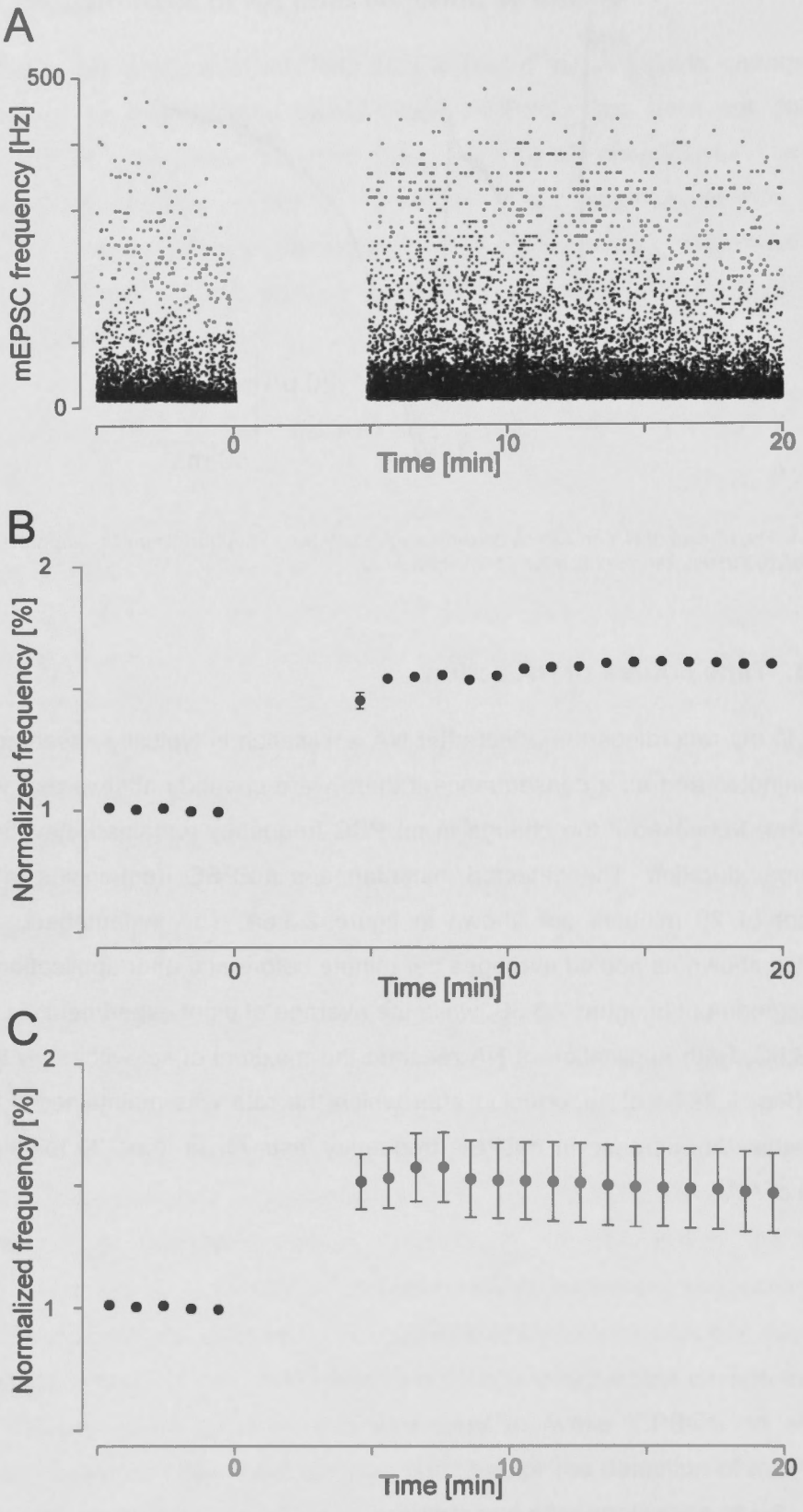

Figure 2.3.5. Time course of mEPSC frequency after NA application. A) Individual mEPSCs plotted as a function of time, both during control and after waiting of NA to wash in (5 min). B) The time course of a single experiment. C) Average of eight experiments. Error bars mark the value of the SEM. Perfusion of NA started at time zero and was maintained throughout.

2.3.2.1.4. Dose response curve for NA

To obtain quantitative data as to the binding of NA to the putative adrenergic receptor, I determined the dose response relationship in a series of experiments in which the NA concentration was varied from 0.01 – 100 µM. In particular, the set included the following number of experiments for the following concentrations: 0.01 (n = 6), 0.1 (n = 7), 0.5 (n = 7), 1 (n = 8), 10 (n = 8) and 100 µM (n = 4). The average and normalised data for each concentration are given in figure 2.3.6. It can easily be seen that for NA concentrations ≥ 1 µM, the instantaneous mEPSC frequencies were already maximal. I did not observe a significant change in mEPSC frequencies between 1 and 100 µM NA (p_{pt} = 0.18). This suggests that for NA concentrations ≥ 1 µM, equilibrium concentration of NA has been reached, causing saturation of the AR at the nerve terminal.

To this data a Hill equation of the following form was fitted (solid line in Fig. 2.3.5). Curve fitting was done using Igor Pro 6.2 using the following formula

$$\text{relative mEPSC frequency} = \frac{1}{1 + \left(\frac{EC_{50}}{[NA]}\right)^{coop}}$$

The EC_{50} was estimated to be 0.22 ± 0.13 µM (Fig. 2.3.5) with a cooperativity (*coop*) of 2.1 ± 1.4. The value from the EC_{50} suggests that 1 µM NA is sufficient to saturate the ARs at the nerve terminals.

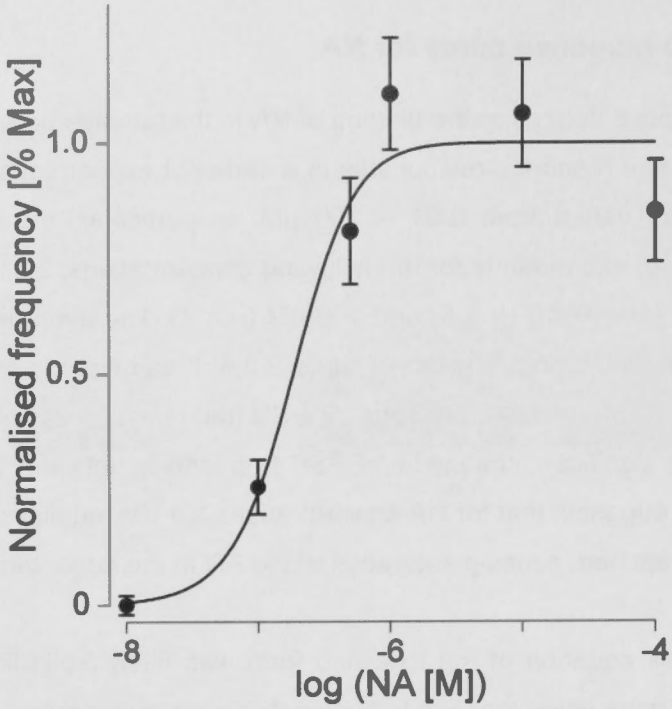

Figure 2.3.6. Normalised change in frequency plotted as a function of NA concentration. The solid line is a fit to the Hill equation, normalised to the maximum of the Hill equation.

2.3.2.2. Pharmacological identify of the AR

To identify the pharmacological and molecular identity of the adrenergic receptor(s) involved in producing the increase in mEPSC frequency, both specific agonists and antagonists were used, and in the case of antagonists, they were applied either on their own or in combination with NA.

To test if in rat somatosensory cortex, NA activates predominantly α_1-ARs, α_2- and β-ARs were blocked. Experimentally, I first blocked both the α_2- and β-ARs with yohimbine (YO, 1 µM) and propranolol (PO, 1 µM), respectively, and after 5 minutes applied NA to see if the α_1-ARs could still be activated. The results of a single experiment are shown in figures 2.3.7A–F. In this example, a control period without drug application is shown in figure 2.3.7A. As evidenced in figure 2.3.7B in the first two seconds of this recording, the simultaneous application of YO and PO did not change the instantaneous mEPSC frequency. When NA was then applied in the presence of YO and PO (Fig. 2.3.7C), the instantaneous mEPSC frequency increased by 46 ± 4% (from 37 ± 2 to 54 ± 3 Hz; $p_{KS} < 10^{-59}$; Fig. 2.3.7D). The mean frequency significantly shifted to the right after application of NA. The mEPSC amplitudes did not change in the presence of YO, PO or NA (Fig. 2.3.7E). The truncated average mEPSCs for the

three recording conditions are illustrated in figure 2.3.7F where the peak normalised mEPSCs are given before (black line), after co-application of YO and PO (grey line) and subsequent application of NA (dashed line). I observed no significant change in the mEPSC kinetics after the application of YO, PO or NA.

To rule out the possibility that YO, PO together with NA are not affecting postsynaptic AMPA receptors and subsequently, the characteristics of the mEPSC, I examined the effect of 1 µM YO, 1 µM PO and 10 µM NA on currents generated by iontophoresis of AMPA onto dendrites. The result of a single experiment is shown in figure 2.3.7G. The first and second iEPSCs in the presence of YO and PO were 51.2 ± 1.5 and 47.4 ± 1.4 pA, respectively, compared to 43.9 ± 1.7 and 43.1 ± 1.6 pA for control. Co-application of NA did not change either of the two amplitudes (52.8 ± 1.0 and 50.8 ± 0.9 pA).

In a set of six experiments, the first and second iEPSCs in the presence of both YO and PO were 45.9 ± 2.0 and 39.2 ± 2.1 pA compared 50.5 ± 4.2 and 45.6 ± 4.2 pA for control. Further application of NA did not change either of the two amplitudes (48.0 ± 3.9 and 41.4 ± 2.8 pA). The half-widths of the first and second AMPA-mediated iEPSCs in the presence of YO and PO were 24.4 ± 1.9 and 24.0 ± 2.2 ms compared to 21.2 ± 2.4 and 21.0 ± 2.4 ms. Co-application of NA also did not change either of the two amplitudes (28.4 ± 2.9 and 25.8 ± 2.3 pA). On average, these differences were not significant (p_{pt} = 0.46, 0.43, 0.13 for first peak iEPSC amplitude, rise time and half-width, respectively), suggesting that neither YO and PO nor NA at these concentrations had an appreciable effect on iEPSC kinetics, and that the detection of mEPSC is most likely not affected by these drugs.

The average frequencies in the control and in the presence of the α_2- and β-receptor blockers were 42 ± 6 and 37 ± 6 Hz, respectively (n = 8), but increased by 62 ± 11% to 60 ± 5 Hz (p_{pt} = 0.001; Fig. 2.3.7H) in the presence of NA. No significant changes were observed for the mEPSC amplitudes (Fig. 2.3.7I). The average amplitudes for control, in the presence of the blockers and NA were -16.3 ± 1.1, -14.9 ± 1.0 and -14.1 ± 1.3 pA, respectively. This observation indicates that most likely NA mostly works via α_1-ARs activation.

To further corroborate that in barrel cortex, NA signals via the α_1-AR, I used the specific α_1-AR agonist cirazoline (CO; 5 µM). It is a competitive agonist at α_1- and an antagonist at α_2-adrenergic receptors (Li *et al.*, 1988). The results of a single experiment are shown in figures 2.3.8A–D. The first two seconds of recordings before the application

of CO are shown in figure 2.3.8A and after in figure 2.3.8B. In this example, the application of CO increased the instantaneous mEPSC frequency by 47 ± 4% (from 30 ± 2 to 44 ± 2 Hz, $p_{KS} < 10^{-31}$; Fig. 2.3.8C). The mEPSC amplitude did not change in the presence of CO (Fig. 2.3.8D). The mean mEPSC frequency significantly shifted to the right after application of CO. The truncated average mEPSCs for the two recording conditions are illustrated in figure 2.3.8E where the peak normalised mEPSCs are given before (black line) and after application of CO (grey line). I observed no significant change in the mEPSC kinetics after the application of CO, which I later verified with a set of iontophoresis experiments (Fig. 2.3.9G).

In 19 experiments, the addition of CO (n = 19) significantly increased the average mEPSC frequency from 42 ± 3 Hz to 57 ± 6 Hz (p_{pt} = 0.021; Fig. 2.3.8F), i.e. by 36 ± 5%, while the amplitude did not change (-12.3 ± 0.9 and -11.6 ± 0.8 pA, respectively; Fig. 2.3.8G). I, therefore, checked if the increase in frequency observed with CO is comparable to the one with NA and found that the increase was not statistically significant (36 ± 5 *vs.* 50 ± 11%, n = 33; p_t = 0.48). This comparison then may indicate that for our experimental conditions, CO has a similar potency as NA in increasing mEPSC frequency.

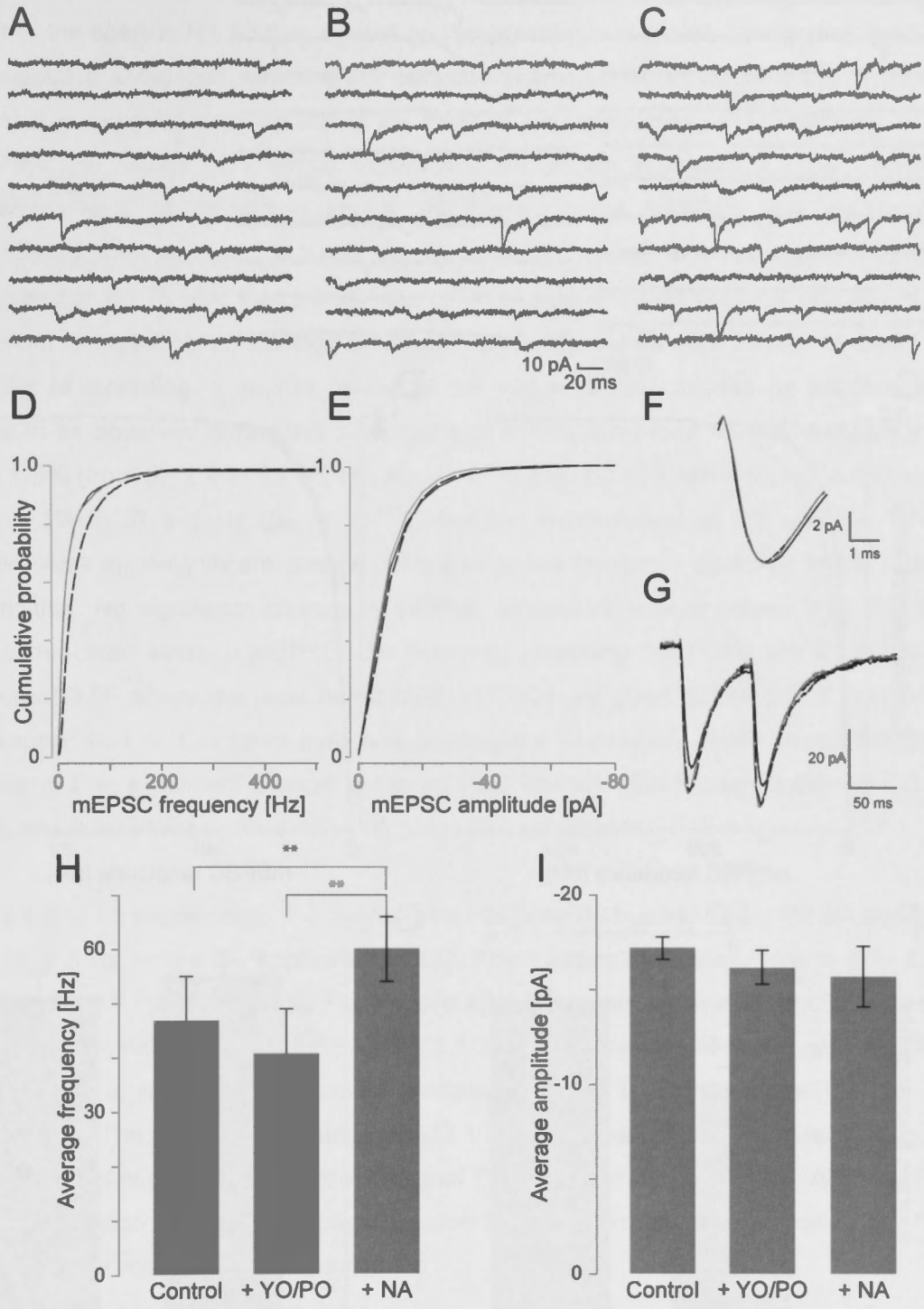

Figure 2.3.7. mEPSCs after application of YO, PO and NA. A) The first two seconds of recording is illustrated before and B) after the co-application of YO and PO and C) the subsequent application of NA. D) The cPDF of the instantaneous frequencies are shown and E) mEPSC amplitudes before (black line), after co-application of YO and PO (grey line) and subsequent application of NA (dashed line) in E), respectively. F) The normalised amplitude of the average mEPSC time course before (black line), after the co-application of YO and PO (grey line) and subsequent application of NA (dashed line). G) The effects of YO, PO and NA on AMPA-mediated currents evoked by two iontophoretic pulses separated by 75 ms (average of 100 evoked iEPSCs), both after co-application of YO and PO (grey line) and subsequent application of NA (dashed line). H) The average instantaneous frequencies and I) amplitudes before and after application of YO, PO and the subsequent co-application of NA.

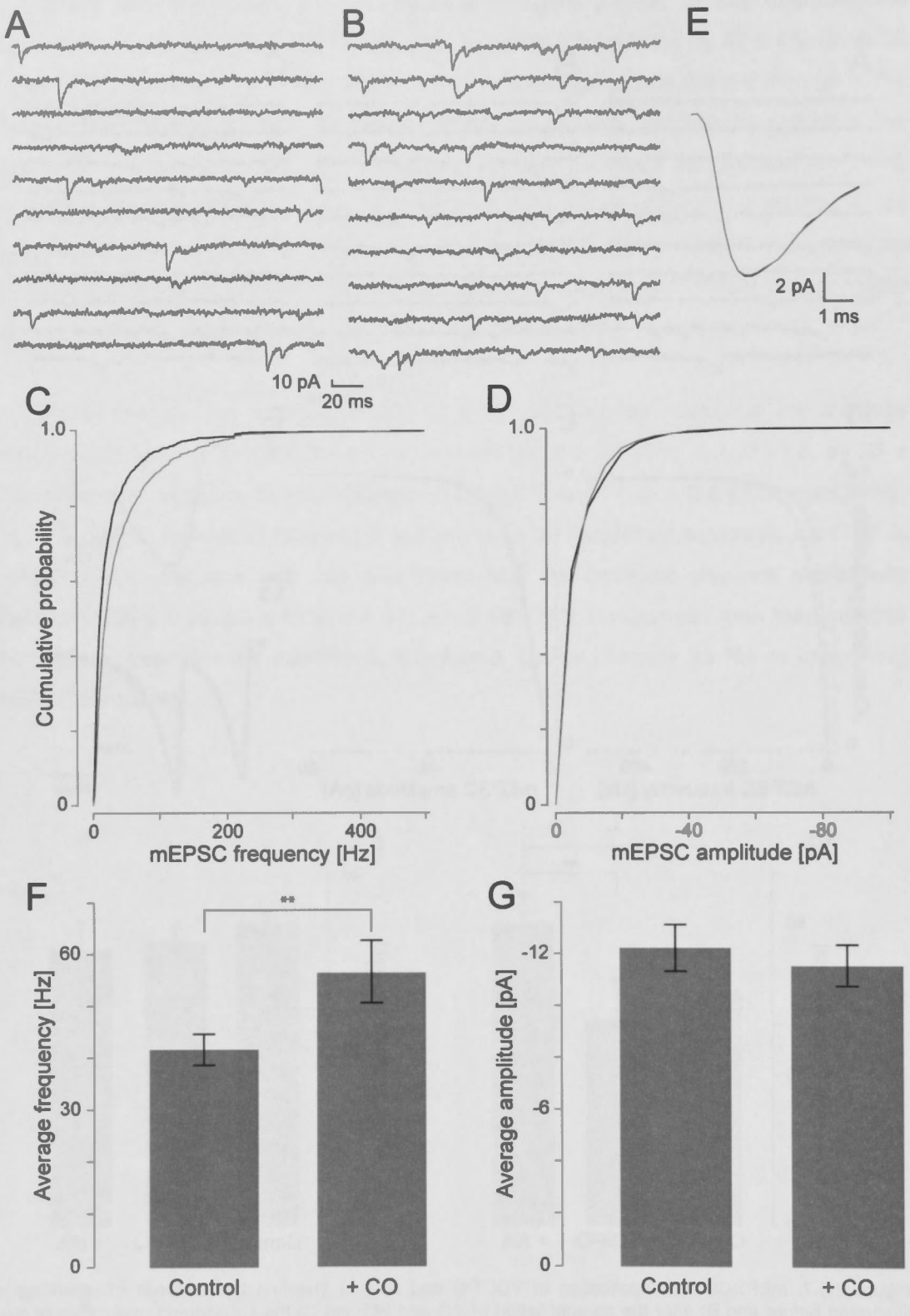

Figure 2.3.8. mEPSCs before and after application of 5 µM CO. A) Two seconds of recording are shown before and B) after application of CO. C) The cPDF of the instantaneous frequencies and D) mEPSC amplitudes before (black line) and after the application of CO (grey line). E) The normalised amplitudes of the average mEPSC time course before (black line) and after the application of CO (grey line). F) The average instantaneous mEPSC frequencies and G) amplitudes before and after application of CO.

To further corroborate the nature of the activated receptor and narrow the binding of CO to the specific NA binding pocket on the adrenergic receptor, I attempted to use a competitive antagonist, which at the concentration used would displace CO. Prazosin (PA) is a competitive antagonist at the α_1-AR (Cambridge *et al.*, 1977; Hornung *et al.*, 1979). The results of a single experiment are shown in figures 2.3.9A–F. In this example, and as described above, the frequency of mEPSCs was significantly increased after addition of CO (5 µM; Fig. 2.3.9B). In line with the hypothesis, after addition of PA (5 µM; Fig. 2.3.9C) the mEPSC frequency significantly decreased. In this set of experiments, average amplitudes and frequencies were estimated based on 120 s of recording, a shorter period as the expected drop caused by displacement should be observed during this time. CO significantly increased mEPSC frequency by 49 ± 3% (from 37 ± 2 to 55 ± 2 Hz, $p_{KS} < 10^{-181}$; Fig. 2.3.9D) with a significant drop by 33 ± 1% to 37 ± 1 Hz ($p_{KS} < 10^{-177}$) after the displacement of CO with PA, which represents an insignificant change compared to the frequency observed in the control condition. No significant change in mEPSC amplitudes was observed (Fig. 2.3.9E). The truncated average mEPSCs for the three recording conditions are illustrated in figure 2.3.9F where the peak normalised mEPSCs are given before (black line), after co-application of CO (grey line) and subsequent application of PA (dashed line). I observed no significant change in the mEPSC kinetics after the application of CO or PA, which was later verified with iontophoresis experiments.

In a set of six experiments, the average mEPSC amplitude was -12.1 ± 0.8 pA and rate of 45 ± 6 Hz before the application of CO. The average frequency increased by 49 ± 8% to 67 ± 7 Hz ($p_{pt} = 0.006$; Fig. 2.3.9H) after 5 minutes application of CO while the amplitude remained -11.7 ± 0.6 pA (Fig. 2.3.9I). After 5 minutes of superfusion with PA, there was a significant decrease in frequency ($p_{pt} = 0.007$) by 48 ± 7% but not amplitude. The average amplitude was -12.1 ± 0.5 pA and rate of 35 ± 3 Hz. This set of experiments is consistent with the idea that PA displaced CO from the α_1-AR. This line of investigation lends even stronger support to the notion that the increase in mEPSC frequency is relayed by α_1-AR activation.

To rule out the possibility that both CO and PA were affecting postsynaptic AMPA receptors and subsequently, the detection of mEPSCs, I examined the effect of 5 µM CO and 5 µM PA on currents generated by iontophoresis of AMPA onto dendrites. The result of a single experiment is shown in figure 2.3.9G. In the presence of CO, the first and second iEPSCs were 43.8 ± 1.2 and 41.7 ± 0.8 pA compared 36.1 ± 1.3 and 35.9

± 1.1 pA during control conditions. Co-application of PA also did not change either of the two amplitudes (45.1 ± 0.8 and 41.9 ± 0.8 pA, respectively).

In a set of eight iontophoretic experiments, the first and second iEPSC in the presence of CO were 51.3 ± 3.7 and 44.7 ± 3.4 pA compared 46.8 ± 3.8 and 41.9 ± 3.2 pA for control. Co-application of PA also did not change either of the two amplitudes (51.7 ± 4.3 and 45.7 ± 4.3 pA). The half-widths of the first and second iEPSC in the presence of CO were 31.4 ± 3.5 and 31.5 ± 3.2 pA compared to 30.7 ± 3.2 and 30.5 ± 1.3 pA. Co-application of PA also did not change either of the two amplitudes (33.1 ± 3.1 and 31.3 ± 2.3 pA). On average, these differences were not significant, suggesting that neither CO nor PA at this concentration had an appreciable effect on iEPSC kinetics, and that the detection of mEPSC is most likely not affected by these drugs.

As PA was dissolved in 8 µM DMSO, a set of control experiments was done to check if this concentration of DMSO could alter mEPSC characteristics. There were no significant changes after addition of DMSO (Fig. 2.3.10). In this example, the application of DMSO (Fig. 2.3.10B) or PA (fig 2.3.10C) did not change either mEPSC frequency or amplitude. The normalised amplitudes of the average mEPSC were truncated at 50% of the decay phase before (black line) and after the application of DMSO (grey line) or PA (dashed line), as shown in figure 2.3.10D. In 5 experiments, the average amplitude did not change (-12.6 ± 0.6 and -12.0 ± 0.5 pA), nor did the frequency (16 ± 5 and 14 ± 5 Hz) nor the mEPSC kinetics after the application of DMSO or PA. This indicates that DMSO at the chosen concentration has minimal effects on mEPSCs.

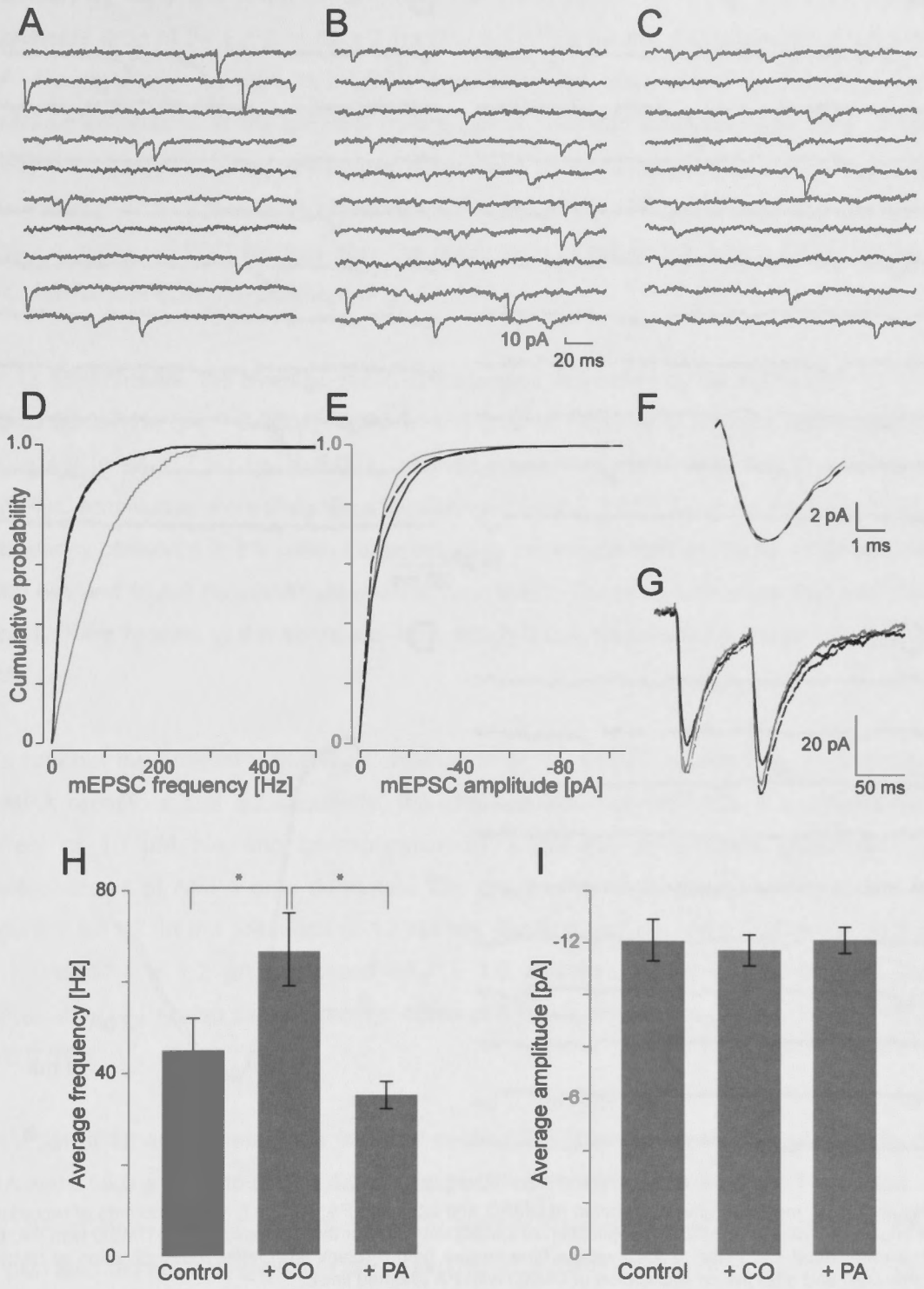

Figure 2.3.9. mEPSC after application of CO and later PA. A) Two seconds of recording taken before and B) after the application of CO and C) co-application of CO with PA. D) The cPDF of the instantaneous mEPSC frequencies and E) amplitudes before (black line) and after the addition of CO (grey line) and subsequent co-application of PA with CO (dashed line). F) The normalised amplitudes of the averaged mEPSC time courses before (black line), after the addition of CO (grey line) and after the co-application of CO with PA (dashed line). G) The effects of CO and PA on AMPA currents evoked by two iontophoretic pulses separated by 75 ms (average of 100 pairs), both after application of CO (grey line) and after co-application of PA with CO (dashed line). H) The average frequency and I) amplitude before and after application of CO and the subsequent co-application with PA. Single starred brackets indicate where significance was reached ($p_{pt} < 0.05$).

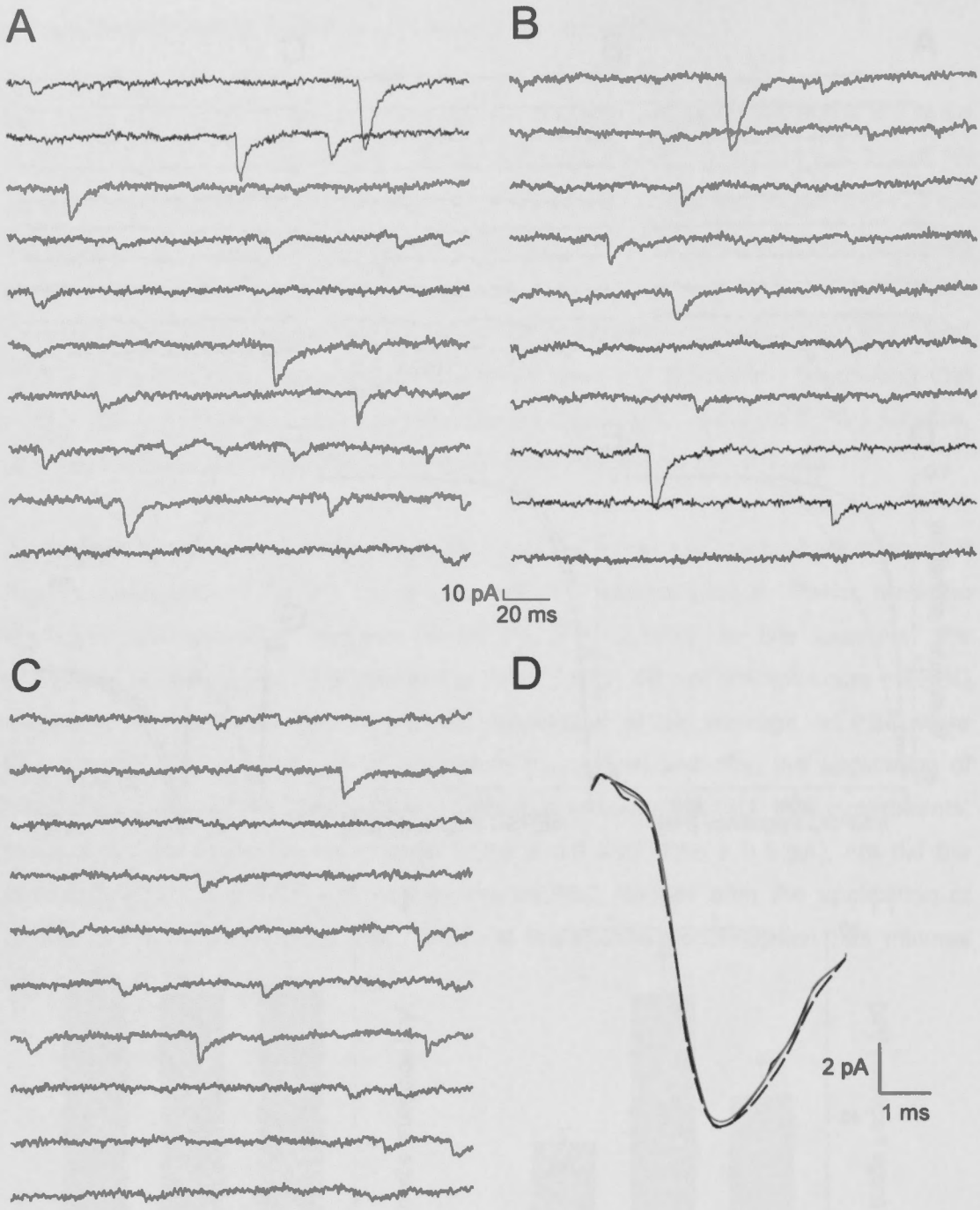

Figure 2.3.10. mEPSCs after application of DMSO and later with PA. A) The first two seconds of recording is shown before and B) after the application of DMSO and C) after the co-application of DMSO with PA. D) The normalised amplitude of the average time course before (black line), after the application of DMSO (grey line) and after the co-application of DMSO with PA (dashed line).

So far, I have been able to show that CO can be displaced using PA from the α_1-AR. However, I have not yet shown that the same displacement also holds in the case of NA. To do this, I first activated the α_1-AR with 10 μM NA, and later displaced NA binding to the α_1-AR with PA (5 μM). The results of a single experiment are shown in figures 2.3.11A–F. In this example, NA significantly increased mEPSC frequency (Fig.

2.3.11B) by 49 ± 2% (from 37 ± 1 to 55 ± 1 Hz, $p_{KS} < 10^{-63}$; Fig. 2.3.11D) with a significant drop of 24 ± 1% to 42 ± 2 Hz ($p_{KS} < 10^{-38}$) after the displacement of NA with PA. No significant change in mEPSC amplitude was observed (Fig. 2.3.11E). The average amplitudes of the mEPSC before (black line) and after the application of NA (grey line) or PA (dashed line) were normalised to the amplitude of the control and truncated at 50% of the decay phase, shown in figure 2.3.11F. I observed no significant change in the mEPSC kinetics after the application of NA or PA, which I later verified with the iontophoresis experiment (Fig. 2.3.11G).

In 12 experiments, the average mEPSC frequency increased by 34 ± 7% from 41 ± 7 Hz to 55 ± 7 Hz ($p_{pt} = 0.0004$; Fig. 2.3.11H) after application of NA and decreased by 20 ± 4% to 44 ± 7 Hz ($p_{pt} = 0.004$) after co-application of PA with NA. The average mEPSC amplitudes were insignificantly changed (Fig. 2.3.11I). I compared the mEPSC frequency observed in the control experiment to the experiment where PA is co-applied with NA and found no significant change ($p_t = 0.49$). These results show that both NA and CO are binding to the same site from which it can be displaced competitively with PA.

To rule out the possibility that the combination of NA and PA is affecting postsynaptic AMPA receptors and subsequently, the characteristics of mEPSCs, I examined the effect of 10 µM NA and co-application of 5 µM PA on currents generated by iontophoresis of AMPA onto dendrites. The result of a single experiment is shown in figure 2.3.11G. In the presence of 10 µM NA, the first and second EPSC were 64.9 ± 1.1 and 57.1 ± 1.2 pA compared 68.7 ± 1.0 and 61.0 ± 0.9 pA for control. Co-application of PA also did not change either of the two amplitudes (69.2 ± 1.1 and 62.0 ± 0.9 pA).

In a set of 12 experiments, the first and second iEPSC amplitudes after application of NA were 55.0 ± 6.3 and 52.5 ± 4.0 pA, respectively, compared to 55.8 ± 4.7 and 50.8 ± 4.2 pA when no NA was present. Co-application of the α_1-ARs antagonist prazosin (PA, 5 µM) also did not change either of the two iEPSCs (55.0 ± 6.3 and 51.2 ± 5.7 pA). The half-widths of the first and second iEPSCs in the presence of NA were 25.4 ± 2.8 and 26.3 ± 2.6 pA compared to 24.9 ± 2.1 and 27.0 ± 2.5 pA. Co-application of PA also did not change either of the two amplitudes (28.2 ± 3.0 and 27.0 ± 2.5 pA). On average, these differences were not significant, suggesting that neither NA nor PA at this concentration had appreciable effect on postsynaptic AMPA receptor kinetics, and that the detection of mEPSC is most likely not affected by these drugs.

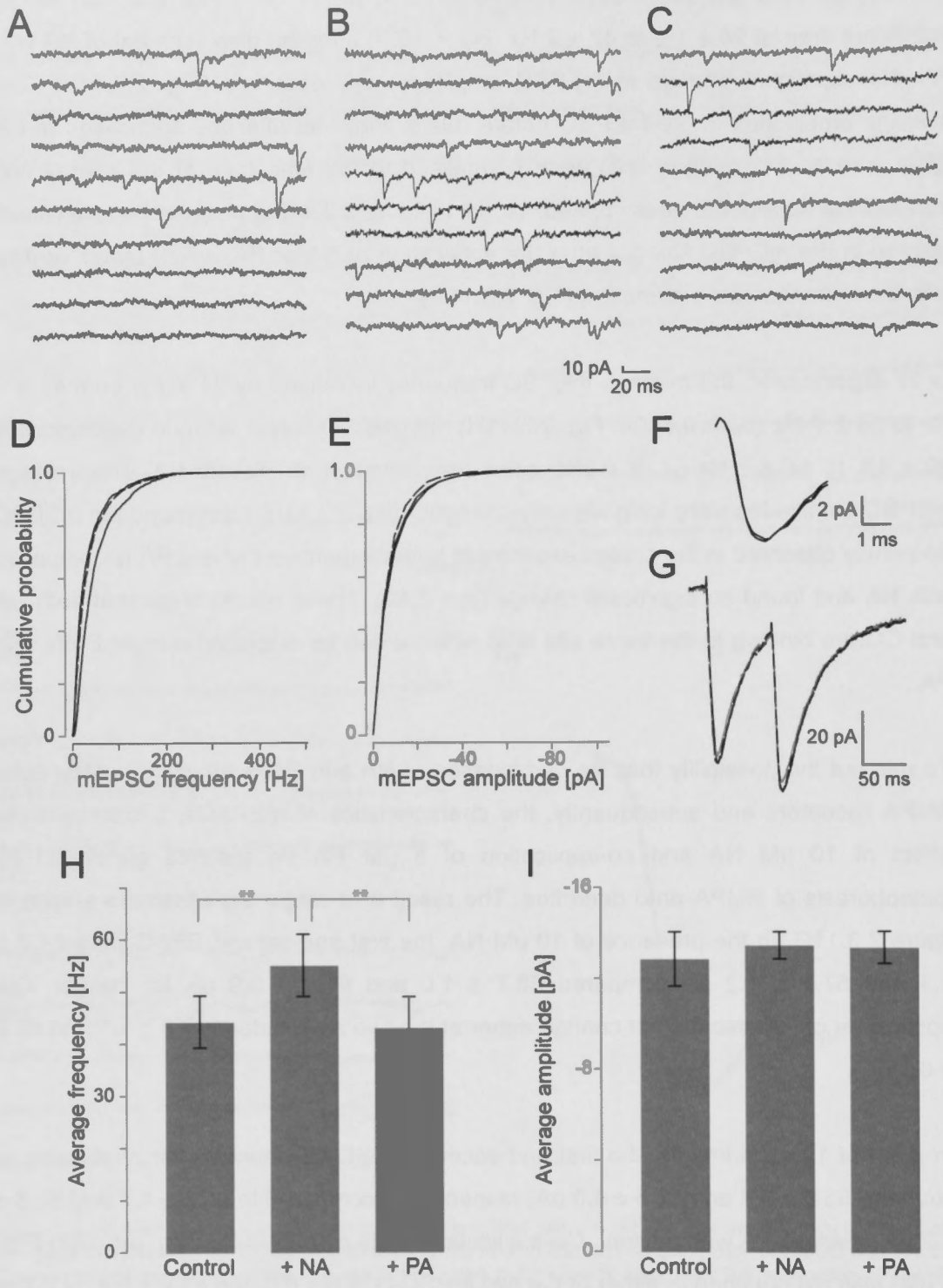

Figure 2.3.11. mEPSCs during a control period and after application of NA and PA. A) Two seconds of recording taken before, B) after the application of NA and C) co-application of NA with PA. D) The cPDFs of the instantaneous mEPSC frequencies and E) amplitudes before (black line), after the addition of NA (grey line) and subsequent co-application of PA with NA (dashed line). F) The normalised amplitude of the average mEPSC time course before (black line), after the addition of NA (grey line) and after the co-application of NA with PA (dashed line). G) The effects of NA and PA on AMPA-mediated iEPSCs evoked by two iontophoretic pulses separated by 75 ms (average of 100 pairs), both after application of NA (grey line) and after co-application of PA with NA (dashed line). H) The average mEPSC frequency and I) amplitude before and after application of NA and the subsequent co-application with PA.

2.3.2.3. No tonic activation of α_1-AR

Rutherford *et al.* (2007) and Dash *et al.* (2009) used cyclic amperometry to measure the L-glutamate concentration in cortex of awake rats and reported an extracellular concentration of 7.3 ± 0.9 and 16.6 ± 3.3 µM, respectively. If this applied equally to NA, and if there is a background NA concentration of similar magnitude, the possibility could arise that α_1-AR may be tonically activated. Even though axon collaterals are certainly cut in the slices of barrel cortex that I have used, it is possible that NA may still be spontaneously released within a few hours after slicing and thereby binds to and activate the α_1-ARs. I, therefore, tested this possibility by applying the α_1-AR blocker PA after a control condition. The results of a single experiment in which PA was administered are shown in figures 2.3.12A–E. In this example, application of PA did not change the mEPSC frequency or amplitude.

In a set of eight experiments, the addition of PA had no significant effect on either of the two parameters. The average amplitude remained unchanged (-12.7 ± 0.6 and -12.1 ± 0.6 pA, respectively), as did the rate (42 ± 5 and 37 ± 3 Hz, respectively). I conclude, therefore, that there is minimal or no tonic activation of α_1-AR.

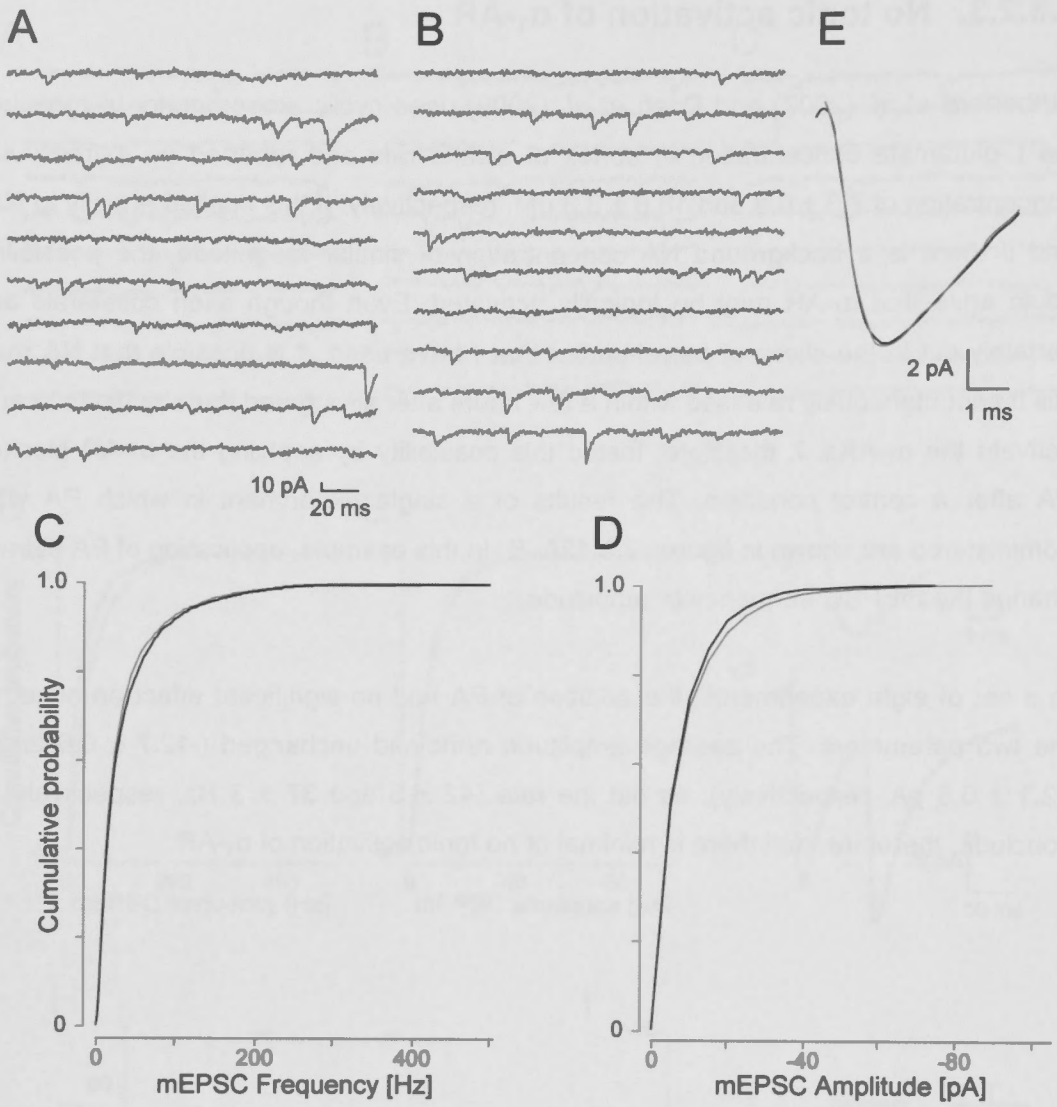

Figure 2.3.12. Tonic α_1-receptor activation. A) Two seconds of a recording taken before and B) after the application of PA. C) The cPDFs of the instantaneous mEPSC frequencies and D) amplitudes before (black line) and after the application of PA (grey line). E) The normalised amplitude of the average mEPSC time course before (black line) and after the application of PA (grey line).

2.3.2.4. Time course of α_1-AR agonist application

In some preliminary experiments, there was some evidence that the mEPSC frequency may decay over many minutes after the application of CO. I checked the time course of α_1-ARs activation by applying CO for a period of 20 minutes. The mEPSC frequency time course of CO application both in a single experiment and the average of six experiments are shown in figure 2.3.13. In most experiments, the activation of α_1-ARs exhibited a maximal effect after ~5 minutes of CO application, consistent with the experiment with NA. On average, the increase mEPSC frequency is maintained over

the whole period of 20 minutes. I therefore conclude that the increase in mEPSC frequency lasts for at least 20 minutes in the presence of CO.

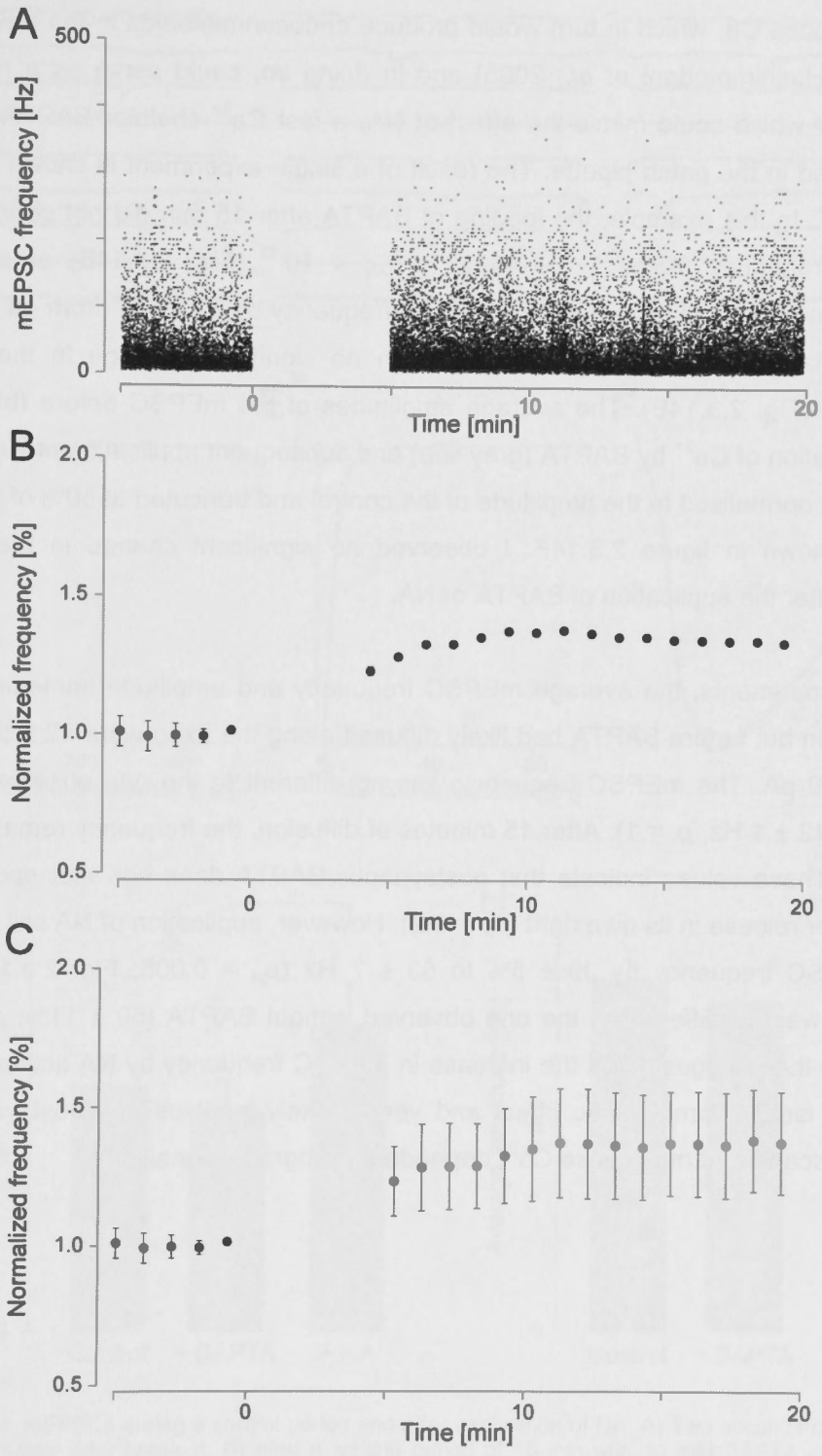

Figure 2.3.13. Time course of mEPSC frequency before and after CO application. A) mEPSC frequency as a function of time. B) The time course of a single experiment. C) Average of six experiments. Error bars mark the value of the SEM. Perfusion of CO starts at time zero and were maintained at a constant rate.

2.3.2.5. Chelation of postsynaptic calcium

To determine if postsynaptic Ca^{2+} entry or release from stores could activate phospholipase Cβ, which in turn would produce endocannabinoids in the postsynaptic dendrite (Hashimotodani *et al.*, 2005) and in doing so, could serve as a retrograde transmitter which could mimic the effect of NA, a fast Ca^{2+} chelator BAPTA (10 mM) was applied in the patch pipette. The result of a single experiment is shown in figures 2.3.14A–F. In this example, the loading of BAPTA after 15 min did not change either mEPSC frequency (48 ± 1 vs. 46 ± 1, $p_{KS} < 10^{-13}$, Fig. 2.3.14B) or amplitude. Application of NA still increased the mEPSC frequency by 33 ± 1% (from 46 ± 1 Hz to 61 ± 1 Hz; $p_{KS} < 10^{-82}$; Fig. 2.3.14.D) with no significant change in the mEPSC amplitude (Fig. 2.3.14E). The average amplitudes of the mEPSC before (black line), after chelation of Ca^{2+} by BAPTA (grey line) and subsequent application of NA (dashed line) were normalised to the amplitude of the control and truncated at 50% of the decay phase, shown in figure 2.3.14F. I observed no significant change in the mEPSC kinetics after the application of BAPTA or NA.

In five experiments, the average mEPSC frequency and amplitude immediately after breaking in but before BAPTA had likely diffused along the axon were 42 ± 5 Hz and -10.4 ± 0.9 pA. The mEPSC frequency was no different to the one observed without BAPTA (42 ± 1 Hz, $p_t = 1$). After 15 minutes of diffusion, the frequency remained at 38 ± 5 Hz. These values indicate that postsynaptic BAPTA does not alter spontaneous transmitter release in its own right ($p_{pt} = 0.2$). However, application of NA still increased the mEPSC frequency by 39 ± 5% to 53 ± 7 Hz ($p_{pt} = 0.005$; Fig. 2.3.14G). This increase was no different to the one observed without BAPTA (50 ± 11%, $p_t = 0.19$). This data then suggests that the increase in mEPSC frequency by NA activation of α_1-AR is at large a presynaptic effect and very unlikely involves any postsynaptic G_q-linked cascade that may cause Ca^{2+} dependent retrograde signalling.

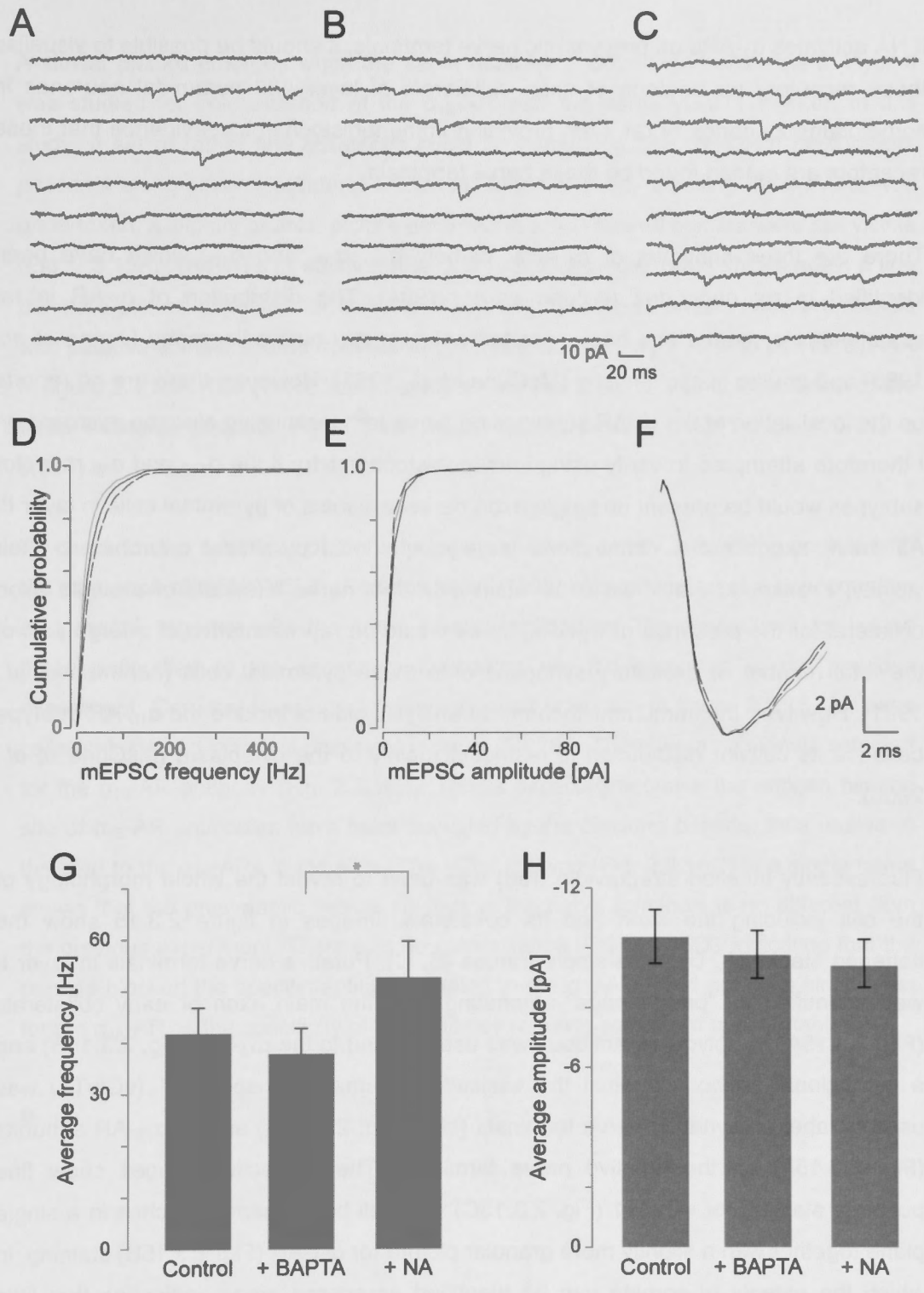

Figure 2.3.14. mEPSCs during a control period and after application of NA. A) Two seconds of recording taken immediately after break-in, B) after a waiting period of 15 min with 10 mM BAPTA in the patch pipette and C) subsequent application of NA. D) The cPDFs of the instantaneous mEPSC frequencies and E) amplitudes before (black line), after chelation of intracellular Ca^{2+} by BAPTA (grey line) and subsequent application of NA (dashed line). F) The normalised amplitude of the average mEPSC time course before (black line), after Ca^{2+} chelation by BAPTA (grey line) and after the application of NA (dashed line). G) The average mEPSC frequency and H) amplitude before and after chelation of Ca^{2+} by BAPTA and the subsequent application with NA.

2.3.3. Immunohistochemical evidence for α_1-ARs

If NA activates α_1-ARs on presynaptic nerve terminals, it should be possible to visualise these receptors on boutons of axon collaterals of layer II/III pyramidal neurones in somatosensory cortex of rat. I am providing immunohistochemical evidence that these receptors are indeed found on these nerve terminals.

There are three subtypes of α_1-ARs, namely α_{1A}, α_{1B}, and α_{1D}, which have been identified in rat neocortex (Bylund *et al.*, 1994). The distribution of α_1-AR in rat somatosensory cortex has been reported using *in situ* autoradiography (Jones *et al.*, 1985) and *in vitro* histochemistry (McCune *et al.*, 1993). However, there are no reports on the localisation of the α_1-AR subtypes on nerve terminals using electron microscopy. I therefore attempted to verify using immunohistochemistry if the α_{1A}- and α_{1B} receptor subtypes would be present on single axon nerve terminals of pyramidal cells in layer II. As these axons make connections largely onto local pyramidal neurones in their vicinity, I reasoned that if we could stain individual nerve terminals of a single axon collateral for the presence of α_1-ARs, these would be representative of a large part of the total number of excitatory synapses onto these pyramidal cells (Larkman *et al.*, 1991). However, the immunohistochemical analysis did not include the α_{1D}-AR subtype because its cellular distribution is restricted mainly to the cytoplasm (McCune *et al.*, 2000).

Fluorescently labelled streptavidin (red) was used to reveal the whole morphology of the cell including the axon and its collaterals. Images in figure 2.3.15 show the flattened stacks (A, D) or as single frames (B, C). Putative nerve terminals in layer II were identified as "pearl-strings" emanating from the main axon or early collaterals (Fig. 2.3.15A). A polyclonal antibody was used to bind to the α_{1A}-AR (Fig. 2.3.15B) and a monoclonal antibody against the vesicular glutamate transporter 1 (vGluT1) was used to label presynaptic nerve terminals (blue; Fig. 2.3.15C) and or α_{1B}-AR subunits (Fig. 2.3.15F) on the putative nerve terminals. The respective images show fine punctate staining for vGlutT1 (Fig. 2.3.15C) with cell body sparing patches in a single plane together with a slightly more granular picture for α_{1A}-AR (Fig. 2.3.15B) staining, in which the extents of somata can be identified as spared areas, indicating that little immunolabelling is restricted to the cytosolic and nuclear compartments. The colocalisation study shows that there is indeed colocalisation of the three elements labelled (Fig. 2.3.15D; I_{corr}=0.197, positive nMDP value = 0.079 ± 0.001). The distribution of the α_{1A}-ARs seems to be dominant and patchy on boutons and bouton-like structures along the axon with minimal in between.

A similar picture emerges when the same neurone and its axon collaterals in layer II was studied for colocalisation of the α_{1B}-AR with the same vGluT1 marker. In this study, a set of rather fine collaterals could be found (Fig. 2.3.15E) with *boutons-en-passants* along several collateral branches. When antibody labelling for α_{1B}-ARs was undertaken, a slightly grainier picture emerged in which spared somata were still visible (Fig. 2.3.15F). The vGluT1 staining (Fig. 2.3.15G) in a single frame shows again a fine punctate picture expected for staining presynaptic vesicle clusters in nerve terminals with putative somata spared from labelling. This picture is very similar to that for α_{1A}-AR in figure 2.3.15A. The colocalisation study shows that there is also colocalisation of the three elements labelled (Fig. 2.3.15H; I_{corr} = 0.206, positive nMDP value = 0.019 ± 0.001).

To check for the specificity of the polyclonal α_{1B}-ARs antibody, a blocking peptide with the sequence of KEMSNSKE (Grayson *et al.*, 1998) was incubated at a concentration of 1 mg/ml, together with the same primary antibodies. The procedures for linking these antibodies to the secondary antibodies are the same as in the previous experiment. Confocal imaging of this experiment is shown in figure 2.3.16. An axon collateral, stained in red, is displayed in figure 2.3.16A. There were no signals detected for the α_{1B}-AR antibody (Fig. 2.3.16B). This is expected because the antigen binding site of α_{1B}-AR antibodies have been occupied by the blocking peptide, thus unable to the bind to the α_{1B}-ARs in the slice. The vGlut staining (Fig. 2.3.16C) in a single frame shows that the presynaptic vesicle clusters in the nerve terminals is no different from the previous experiment. There was no colocalsation (Fig. 2.3.16D), indicating that the peptide blocked the specific antibody binding to the α_{1B}-AR. I did not do a similar test for the α_{1A}-AR as the specificity of this antibody remains somewhat questionable.

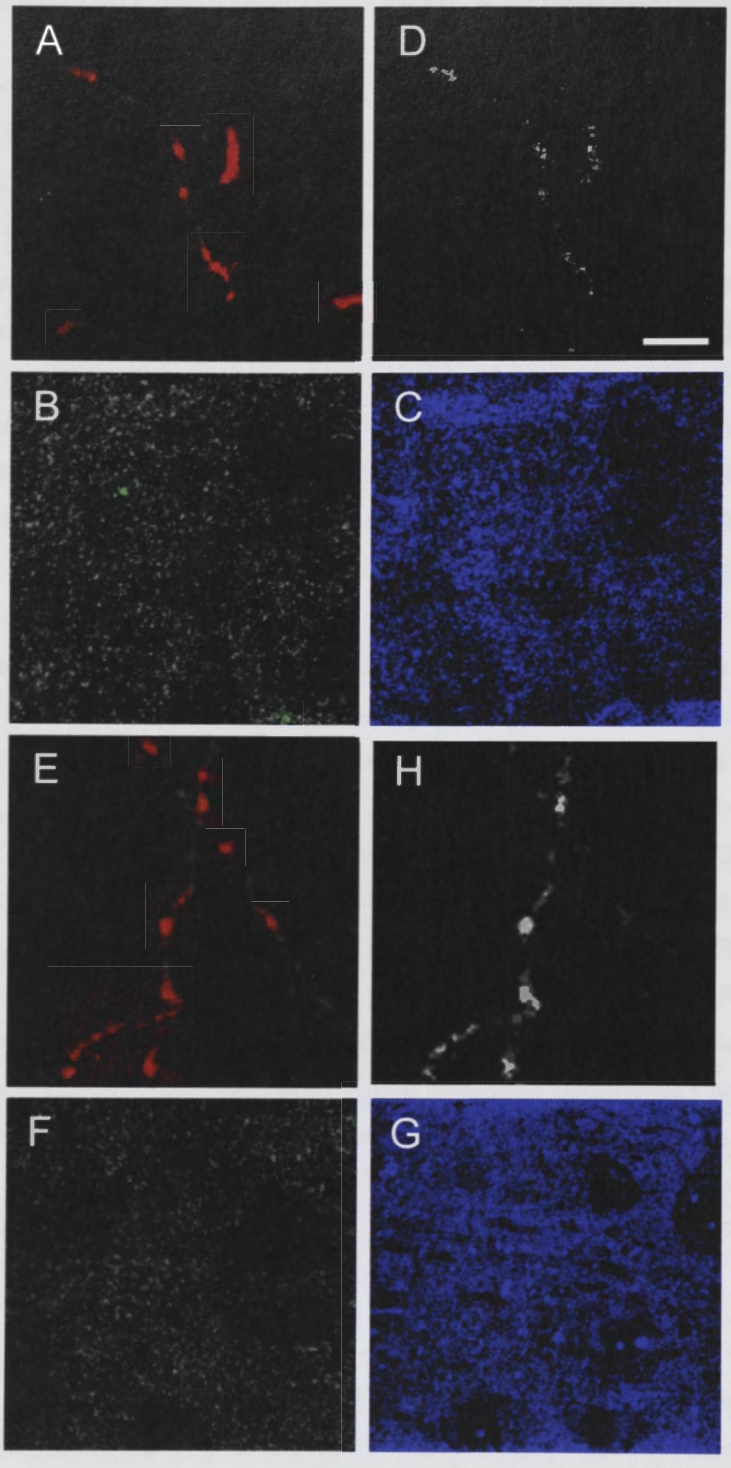

Figure 2.3.15. Immunohistochemical study of α_{1A}-AR, α_{1B}-AR and vGluT1 staining in putative nerve terminals of a stained axon. A) A flattened stack of axon terminals of pyramidal neurones. A single frame of B) α_{1A}-AR and C) vGluT1 staining. D) Co-localisation of α_{1A}-ARs with vGluT1 at putative nerve terminals of along axon collaterals of a stained pyramidal neurone. E) A flattened stack of axon terminals of pyramidal neurones. A single frame of F) α_{1B}-AR and G) vGluT1 immunohistochemical staining. H) Co-localisation of α_{1B}-ARs with vGluT1 at putative nerve terminals along pyramidal neurone axon collaterals. The scale bar represents 5 μm.

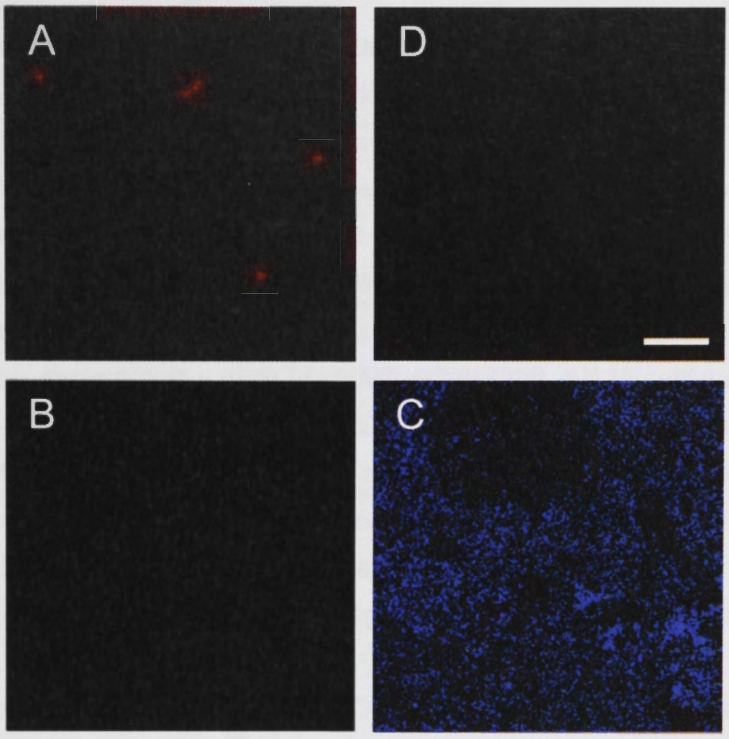

Figure 2.3.16. Specificity of the α_{1B}-AR antibody using blocking peptide. A) A flattened stack of axon terminals. A single frame of B) α_{1B}-AR exposure and C) vGluT1 staining. D) Lack of co-localisation of α_{1B}-ARs with vGluT1 at the putative nerve terminals. Scale bar represents 5 µm.

2.3.4. Verification of signalling cascade

There is evidence in the literature that α_1-ARs mediated signalling may be non-classical. For example, Bacic *et al.* (1992) reported in cell culture of human cerebromicrovascular endothelium that the α_1-ARs can couple to the G_s protein and signal via adenylyl cyclase. Stimulation of the α_1-ARs in rat ventricular myocyte activates AMP phosphodiesterase resulting in cyclic AMP degradation (Buxton & Brunton, 1985). Thus, it is important to verify that the α_1-ARs signal via G_q and ultimately produce an increase in intracellular Ca^{2+}. I, therefore, checked each step in the signalling cascade starting from α_1-AR activation, the generation of IP_3 via phospholipase Cβ, activation of IP_3 receptors on presynaptic calcium stores and finally the release of calcium from these stores that drives fusion of vesicles causing some of the mEPSCs. Iontophoresis experiments to show that the pharmacological compounds do not alter mEPSC kinetics were omitted in this section because Simkus and Stricker (2002a) have already shown that 2-APB, CPA, KCl or BAPTA-AM do not alter the mEPSC kinetics in layer II of neocortex.

2.3.4.1. Blocking phospholipase C

To test if activation of the α_1-ARs could cause production of IP_3 from the hydrolysis of PIP_2 via phospholipase Cβ, I applied the phospholipase C inhibitor edelfosine (ES, 30 μM Horowitz *et al.*, 2005). This concentration is most likely sufficient to inhibit the phospholipase Cβ as it has an IC_{50} of 9.6 ± 1.2 μM (Powis *et al.*, 1992). The results of a single experiment are shown in figures 2.3.17A–F. In this example, application of ES for 20 min significantly decreased mEPSC frequency by 19 ± 1% (from 48 ± 1 to 39 ± 1 Hz, $p_{KS} < 10^{-50}$ Fig. 2.3.17D) but not amplitude (Fig. 2.3.17E). However, upon subsequent addition of NA, the increase typically seen with NA alone was blocked as no increase in either mEPSC frequency (35 ± 1 Hz) or amplitude (1.1 ± 0.1 pA) was observed. The average mEPSC amplitudes before (black line) and after the application of ES (grey line) or NA (black line) were normalised to the control, as shown in figure 2.3.17F. With PLCβ blocked by ES and after the application of NA, I observed no significant change in the mEPSCs including their kinetics.

Overall, the average instantaneous mEPSC frequency (n = 5) decreased by 20 ± 2% from 42 ± 4 to 33 ± 3 Hz after application of ES (p_{pt} = 0.01; Fig. 2.3.17G). The amplitudes of control and ES were -13.4 ± 1.0 and -13.3 ± 1.3 pA, respectively (Fig. 2.3.17H). Subsequent NA did neither change mEPSC frequency (32 ± 1 Hz) nor amplitude (-12.4 ± 1.0 pA). This finding illustrates that there is tonic activity of PLCβ. Subsequent NA activation of the α_1-AR did not increase the instantaneous mEPSC frequency. This set of experiments is then consistent with a classical signal transduction at the α_1-AR via the adaptor protein G_q activating PLCβ.

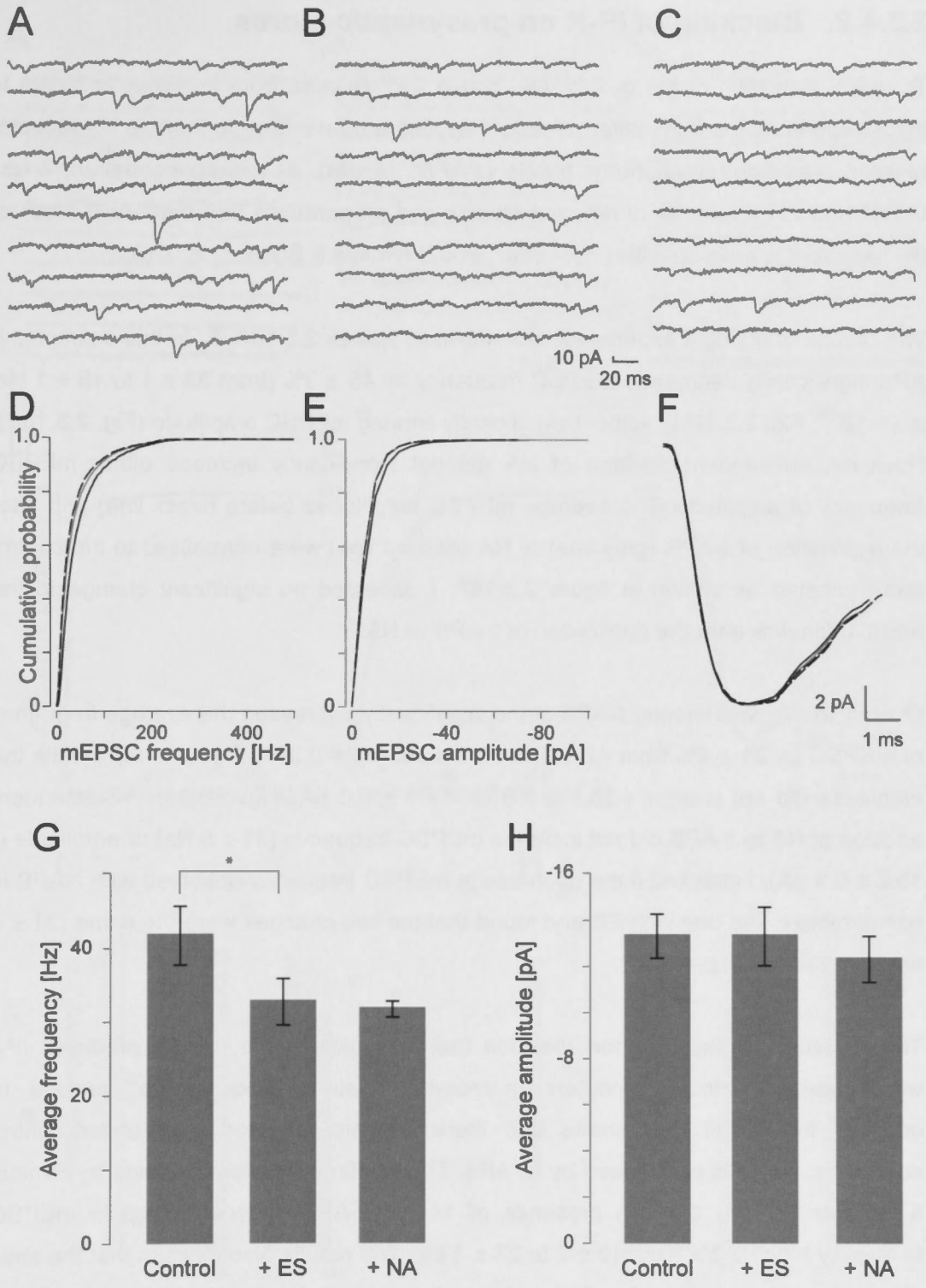

Figure 2.3.17. Block of PLC by edelfosine. A) The first two seconds of recording are taken before and B) after the addition of ES and C) co-application of NA with ES. D) The cPDF of the instantaneous mEPSC frequencies and E) amplitudes before (black line), after the addition of ES (grey line) and after the co-application of NA together with ES (dashed line). F) The normalised amplitude of the average mEPSC time course before (black line), after the addition of ES (grey line) and after the co-application of NA with ES (dashed line). G) Pooled data of the average mEPSC frequency and H) amplitude before and after application of ES and the subsequent co-application with NA.

2.3.4.2. Blocking of IP_3R on presynaptic stores

To test if activation of the α_1-ARs can cause Ca^{2+} release from presynaptic stores to trigger spontaneous transmitter release, I applied a membrane permeable IP_3 receptor blocker, 2-aminoethoxydiphenyl borate (2-APB, 16 µM). At this concentration, it has been shown in a number of different studies and preparations that the 2-APB block of IP_3 receptors is quite specific (Hirst *et al.*, 2002; Simkus & Stricker, 2002a).

The results of a single experiment are shown in figures 2.3.18A–F. In this example, 2-APB significantly decreased mEPSC frequency by 45 ± 3% (from 33 ± 1 to 18 ± 1 Hz, $p_{KS} < 10^{-94}$; Fig. 2.3.18D), without significantly altering mEPSC amplitude (Fig. 2.3.18E). However, subsequent addition of NA did not significantly increase either mEPSC frequency or amplitude. The average mEPSC amplitudes before (black line) and after the application of 2-APB (grey line) or NA (dashed line) were normalised to the control and truncated as shown in figure 2.3.18F. I observed no significant change in the mEPSC kinetics after the application of 2-APB or NA.

Overall, in 17 experiments, 2-APB alone significantly decreased the average frequency of mEPSC by 21 ± 4% from 42 ± 5 to 33 ± 4 Hz ($p_{pt} = 0.004$; Fig. 2.3.18G), while the amplitude did not change (-15.1 ± 0.9 to -12.1 ± 0.6 pA; Fig. 2.3.18H). Subsequent addition of NA to 2-APB did not increase mEPSC frequency (31 ± 5 Hz) or amplitude (-15.2 ± 0.9 pA). I checked if the decrease in mEPSC frequency observed with 2-APB is comparable to the one with ES and found that the two changes were the same (21 ± 4 *vs.* 20 ± 2%, $n = 5$; $p_t = 0.37$).

These results strongly support the idea that activation of the α_1-ARs produces IP_3, which then binds to IP_3 receptors on presynaptic stores to cause Ca^{2+} release. In addition, this result also shows that there is tonic IP_3 production under control conditions, which is not caused by α_1-ARs. This confirms previous findings by Simkus & Stricker (2002a) that the presence of 14 µM 2-APB causes a drop in mEPSC frequency by 43 ± 3% from 40 ± 2 to 23 ± 1 Hz. The results also indicate that the tonic IP_3 production is, within the limits of these experiments, caused largely by PLCβ activity.

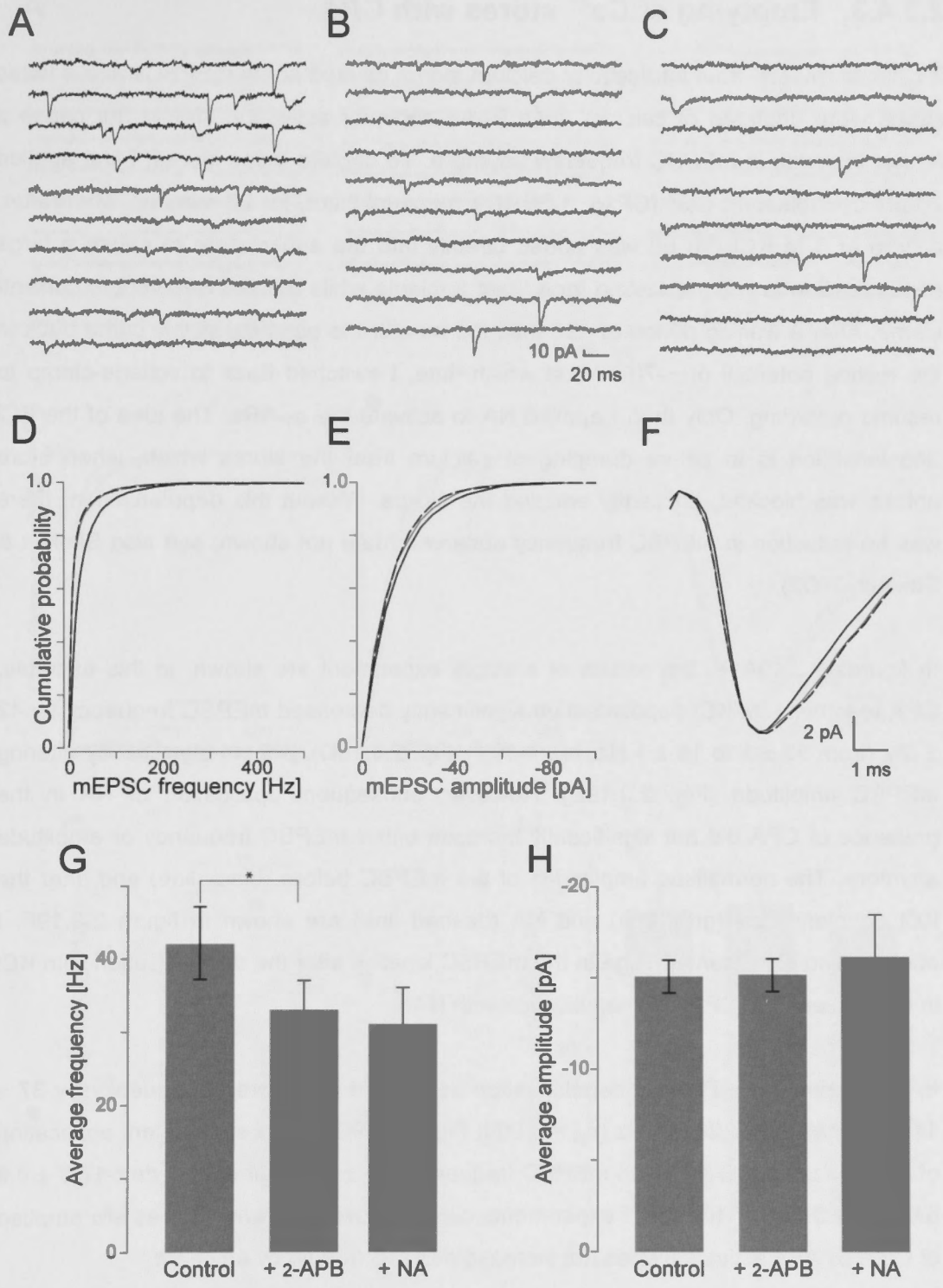

Figure 2.3.18. IP_3 receptor block using 2-APB. A) Recording taken before and B) after the addition of 2-APB and C) co-application of NA with 2-APB. D) The cPDF of the instantaneous mEPSC frequencies and E) amplitudes before (black line), after the addition of 2-APB (grey line) and after the co-application of NA together with 2-APB (dashed line). F) The normalised amplitude of the average mEPSC time course before (black line), after the addition of 2-APB (grey line) and after the co-application of NA with 2-APB (dashed line). G) The average mEPSC frequency and H) amplitude before and after application of 2-APB and the subsequent co-application with NA.

2.3.4.3. Emptying of Ca^{2+} stores with CPA

If calcium release from intracellular calcium stores caused some mEPSCs and if these stores were depleted of calcium, then α_1-AR receptor activation should not cause a further increase in mEPSC frequency anymore. To deplete these stores, I first applied 20 µM cyclopiazonic acid (CPA), a SERCA pump inhibitor, for 20 minutes. Thereafter, a drop of 3 M KCl (40 µl) was added directly into the superfusate to cause a large depolarisation to > 5 mV lasting for a least a minute while the cell was kept in current-clamp. After a waiting period of ~30 min, the membrane potential slowly came back to the resting potential of ~-70 mV, at which time, I switched back to voltage-clamp to resume recording. Only then I applied NA to activate the α_1-ARs. The idea of the KCl depolarisation is to cause dumping of calcium from the stores which, when store uptake was blocked, efficiently emptied the stores. Without this depolarisation, there was no reduction in mEPSC frequency observed (data not shown; see also Simkus & Stricker, 2002)

In figures 2.3.19A–F, the results of a single experiment are shown. In this example, CPA together with KCl depolarisation significantly decreased mEPSC frequency by 42 ± 3% (from 33 ± 1 to 19 ± 1 Hz, $p_{KS} < 10^{-36}$; Fig. 2.3.19D), without significantly altering mEPSC amplitude (Fig. 2.3.19E). However, subsequent application of NA in the presence of CPA did not significantly increase either mEPSC frequency or amplitude anymore. The normalised amplitudes of the mEPSC before (black line) and after the KCl depolarisation (grey line) and NA (dashed line) are shown in figure 2.3.19F. I observed no significant change in the mEPSC kinetics after the depolarisation with KCl in the presence of CPA or co-application with NA.

In 5 experiments, CPA with depolarisation decreased the average frequency by 37 ± 14% from 41 ± 9 to 26 ± 8 Hz ($p_{pt} = 0.003$; Fig. 2.3.19G), while subsequent application of NA was unable to increase mEPSC frequency (26 ± 9 Hz) or amplitude (-17.8 ± 0.6 pA; Fig. 2.3.19H). This set of experiments clearly shows that when stores are emptied of Ca^{2+}, α_1-ARs activation does not increase mEPSC frequency anymore.

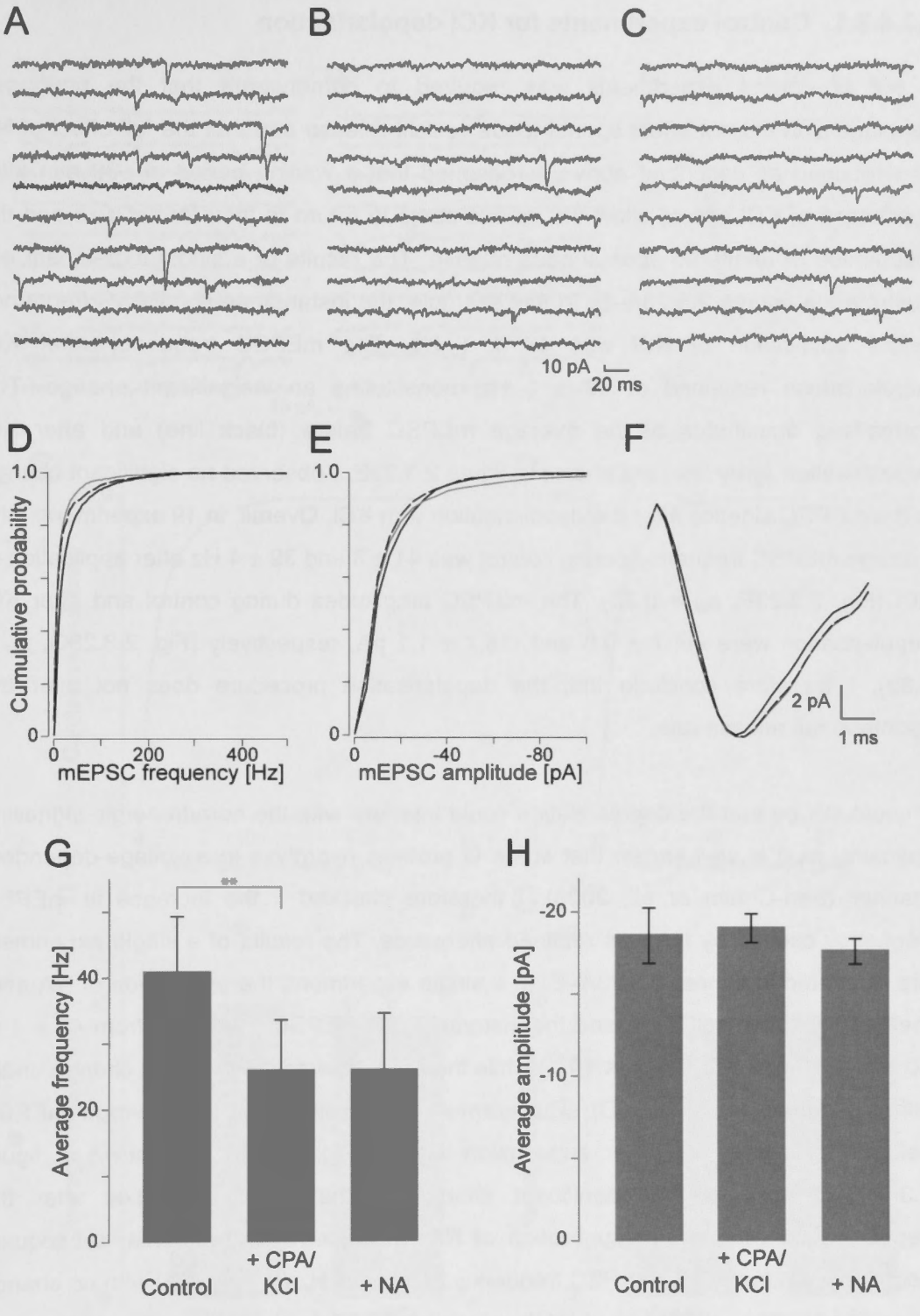

Figure 2.3.19. Store depletion causes a drop in mEPSC frequency and subsequent NA application does not increase mEPSC frequency. A) Recordings before and B) after depolarisation in the presence of CPA and C) co-application of NA. D) The cPDF of the instantaneous mEPSC frequencies and E) amplitudes before (black line), after the depolarisation (grey line) and after the co-application of NA with CPA (dashed line). F) The normalised amplitude of the average mEPSC time course before (black line), after the depolarisation (grey line) and after the co-application of NA with CPA (dashed line). G) The average mEPSC frequency and H) the average mEPSC amplitude before and after KCl depolarisation in the presence of CPA and the subsequent co-application with NA.

2.3.4.3.1. Control experiments for KCl depolarisation

A set of control experiments was required to demonstrate that the prolonged depolarisation did not affect spontaneous vesicle release and that the full effect of NA was retained as described above. I reasoned that a waiting period of ~30 min after application of KCl should allow the vesicle pools to return to their former size and the resumption of unaltered spontaneous release. The results of a single experiment are illustrated in figures 2.3.23A–E. In this example, the instantaneous mEPSC frequency before application of KCl was 48 ± 1 Hz. The mEPSC frequency after KCl depolarisation remained at 49 ± 1 Hz, constituting an insignificant change. The normalised amplitudes of the average mEPSC before (black line) and after KCl depolarisation (grey line) are shown in figure 2.3.23E. I observed no significant change in the mEPSC kinetics after the depolarisation with KCl. Overall, in 19 experiments, the average mEPSC frequency during control was 41 ± 3 and 39 ± 4 Hz after application of KCl (Fig. 2.3.23F, p_{pt} = 0.73). The mEPSC amplitudes during control and after KCl depolarisation were -14.7 ± 0.8 and -15.7 ± 1.1 pA, respectively (Fig. 2.3.23G, p_{pt} = 0.83). I therefore conclude that the depolarisation procedure does not alter the spontaneous release rate.

It could still be that the depolarisation could interfere with the noradrenergic signalling cascade, as it is well known that some G proteins hydrolyse in a voltage-dependent manner (Ben-Chaim *et al.*, 2006). I therefore checked if the increase in mEPSC frequency caused by NA was retained afterwards. The results of a single experiment are illustrated in figures 2.3.23A–E. In a single experiment, the application of NA after the depolarisation still increased the instantaneous mEPSC frequency from 49 ± 1 to 60 ± 1 Hz (Fig. 2.3.23C, $p_{KS} < 10^{-67}$) while the mEPSC amplitude did not change under either condition (Fig. 2.3.23D). The normalised amplitudes of the average mEPSC before (black line) and after superfusion with NA (grey line) are shown in figure 2.3.23E. I observed no significant change in the mEPSC kinetics after the depolarisation with KCl or application of NA. In those 19 experiments, subsequent addition of NA increased mEPSC frequency to 59 ± 11 Hz (p_{pt} = 0.025) with no change in amplitude. The application of NA increased mEPSC frequency by 51 ± 11%, which was similar to the increase with NA that was originally observed (50 ± 11%, n = 33; p_t = 0.46). Thus, the depolarisation with KCl neither affects the release of synaptic vesicles nor the signalling cascade of NA.

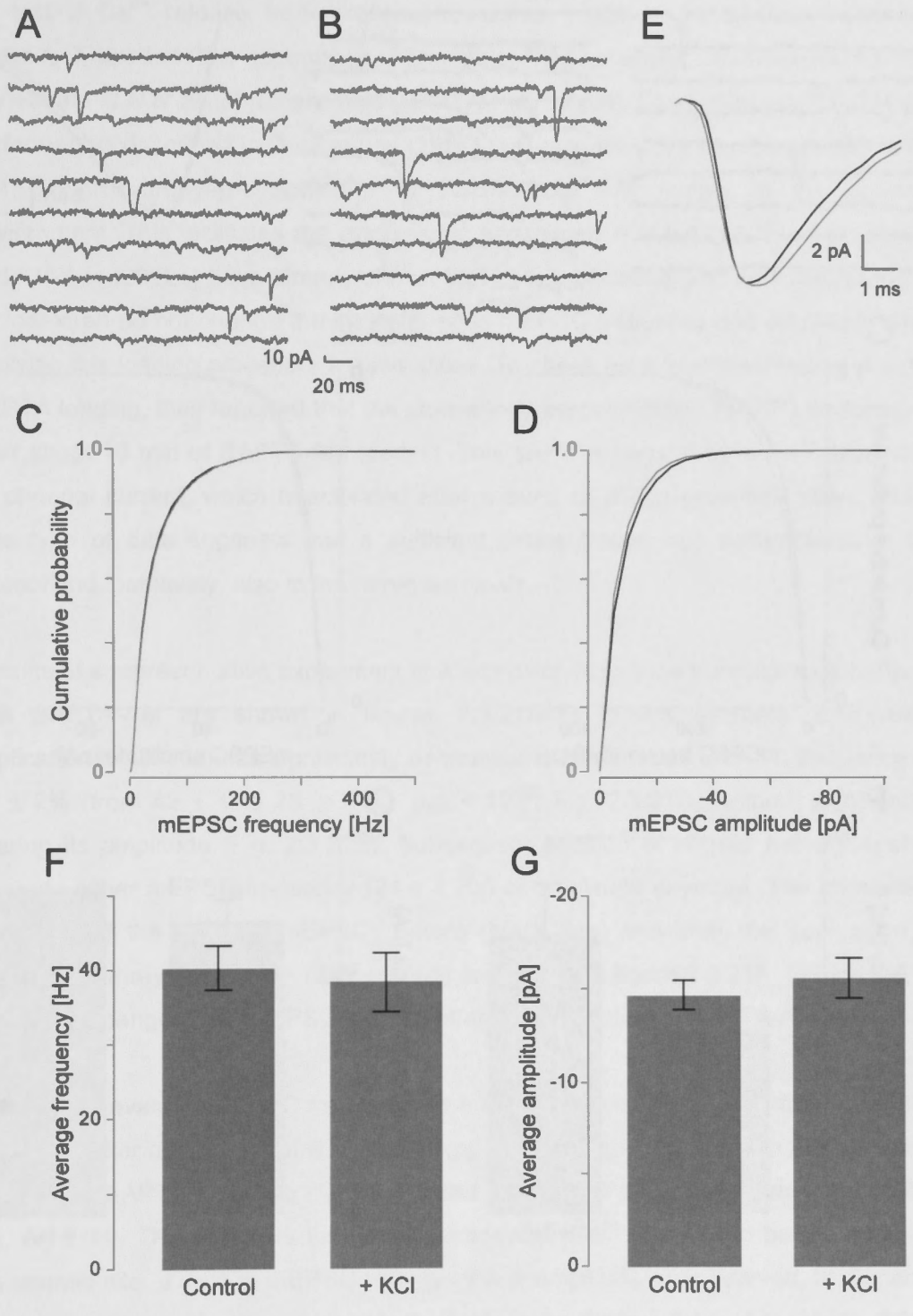

Figure 2.3.20. The KCl depolarisation does not affect mEPSC frequency and amplitude. A) Recording sequences taken before and B) after the depolarisation. C) cPDF of instantaneous mEPSC frequencies and D) amplitudes before (black line) and after depolarisation (grey line). The depolarisation neither changed instantaneous mEPSC frequency nor amplitude. E) Normalised amplitude of average mEPSC time course before (black line) and after depolarisation (grey line). F) The average instantaneous mEPSC frequencies and G) amplitudes before and after KCl depolarisation.

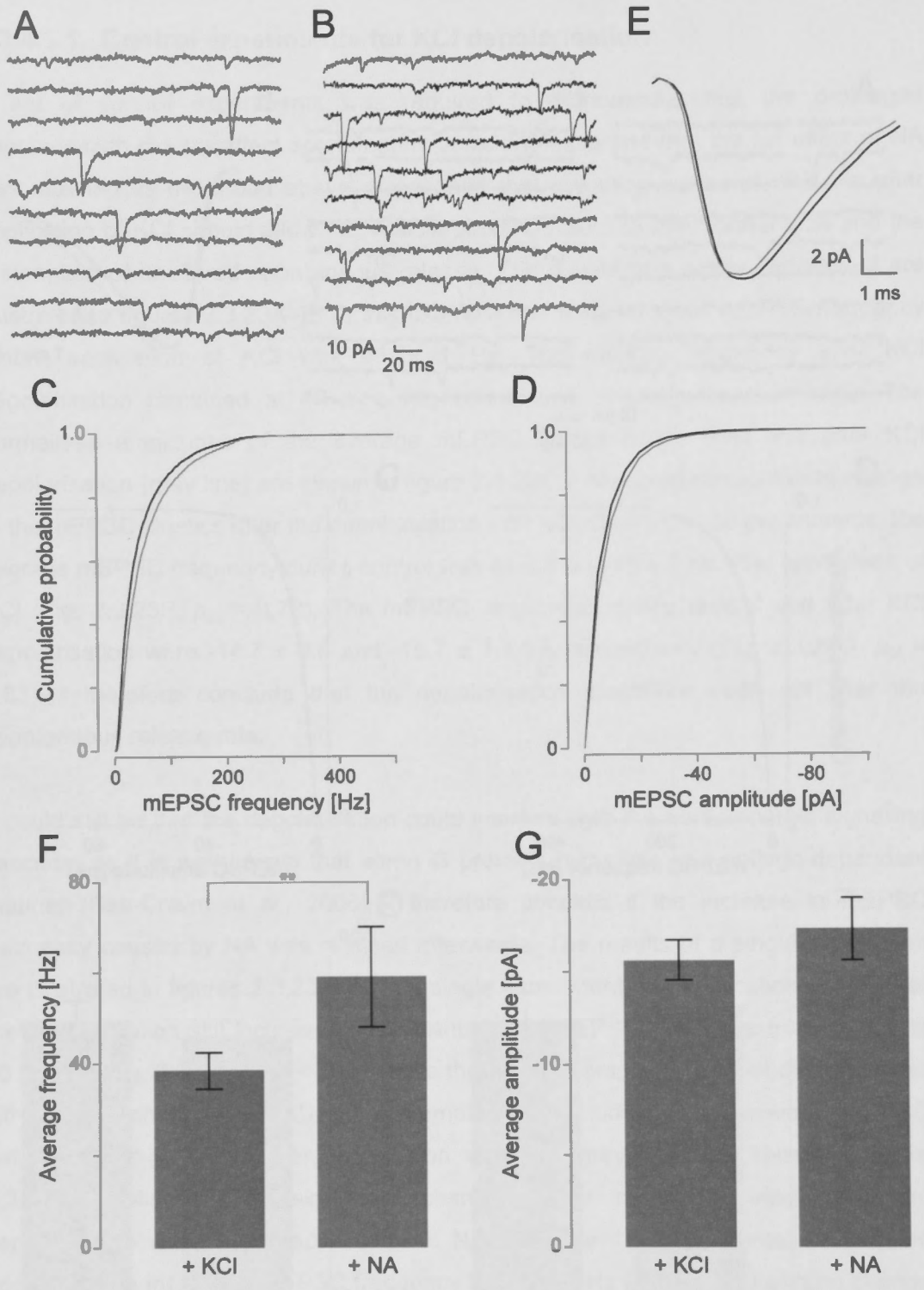

Figure 2.3.21. The KCl depolarisation fully retains NA response. A) Recording sequences taken after the depolarisation and B) the subsequent application of NA. C) cPDF of instantaneous mEPSC frequencies and D) amplitudes after depolarisation (black line) and NA application (grey line). Subsequent application of NA still showed a full sized increase in mEPSC frequency but not amplitude. E) Normalised amplitude of average mEPSC time course after depolarisation (black line) and after the application of NA (grey line). F) The average instantaneous mEPSC frequencies and G) amplitudes after KCl depolarisation and NA application.

2.3.4.4. Increased mEPSC frequency is caused by Ca^{2+} release

To test if Ca^{2+} release from presynaptic stores triggers spontaneous transmitter release, I applied the membrane permeable Ca^{2+} chelator, 1,2-bis(o-aminophen-oxy)ethane-*N*,*N*,*N'*,*N'*-tetraacetic acid (BAPTA-AM, 50 µM). Loading of BAPTA-AM was performed as described in Ouanounou (1996) that includes 0.5 mM probenecid and 0.7 mM 2-hydroxypropyl-β-cyclodextrin to stabilse the AM moiety in the aqueous environment. This facilitates the cytoplasmic accumulation of BAPTA. Further, Simkus and Stricker (2002a) have already shown that both probenecid and 2-hydroxypropyl-β-cyclodextran do not change the instantaneous mEPSC frequency and amplitude when applying this loading procedure to their slices. To check for a functional read-out of the BAPTA loading, they reported that the slow-afterhyperpolarisation (sAHP) disappeared after about 10 min of BAPTA-AM loading. This sAHP is caused by a Ca^{2+}-dependent K^+ channel current, which is activated after a burst of action potentials (Sah, 1992). This type of data suggests that a sufficient concentration has accumulated in the cytosol and, putatively, also in the nerve terminals.

Results of a representative experiment in which calcium release from stores is buffered with BAPTA-AM are shown in figures 2.3.21A–F. In this example, BAPTA-AM application for 20 minutes significantly decreased instantaneous mEPSC frequency by 32 ± 2% (from 42 ± 1 to 26 ± 1 Hz, $p_{KS} < 10^{-93}$; Fig. 2.3.21D), without significantly altering its amplitude (Fig. 2.3.21E). Subsequent addition of NA did not significantly increase either mEPSC frequency (24 ± 1 Hz) or amplitude anymore. The normalised amplitude of the average mEPSCs before (black line) and after the application of BAPTA-AM (grey line) or NA (dashed line) are shown in figure 2.3.21F. I observed no significant change in the mEPSC kinetics after the application of BAPTA-AM or NA.

Overall, the average mEPSC frequency (n = 4) decreased by 24 ± 3% from 40 ± 3 to 30 ± 3 Hz after application of BAPTA-AM (p_{pt} = 0.04; Fig. 2.3.21G). The amplitudes of control and BAPTA-AM were -12.3 ± 1.3 and -10.0 ± 0.8 pA, respectively (p_{pt} = 0.002, Fig. 2.3.21H). This suggests that when intracellular Ca^{2+} is chelated before reaching the release site, a drop in mEPSC frequency and amplitude are observed, the latter of which is small. This is consistent with the findings by Simkus & Stricker (2002). When NA is applied subsequently, neither the mEPSC frequency nor amplitude are changed. Comparison of the decreases in mEPSC frequency observed both with ES and 2-APB were all identical (p_t = 0.27 and 0.30, respectively). This data indicates that it is Ca^{2+} most likely from stores that drive a considerable part of all increase in mEPSCs

frequency caused by the activation of the α_1-AR. This data also suggests that all Ca^{2+} release from stores is largely driven either by receptor activation on the nerve terminal or tonic PLCβ activity.

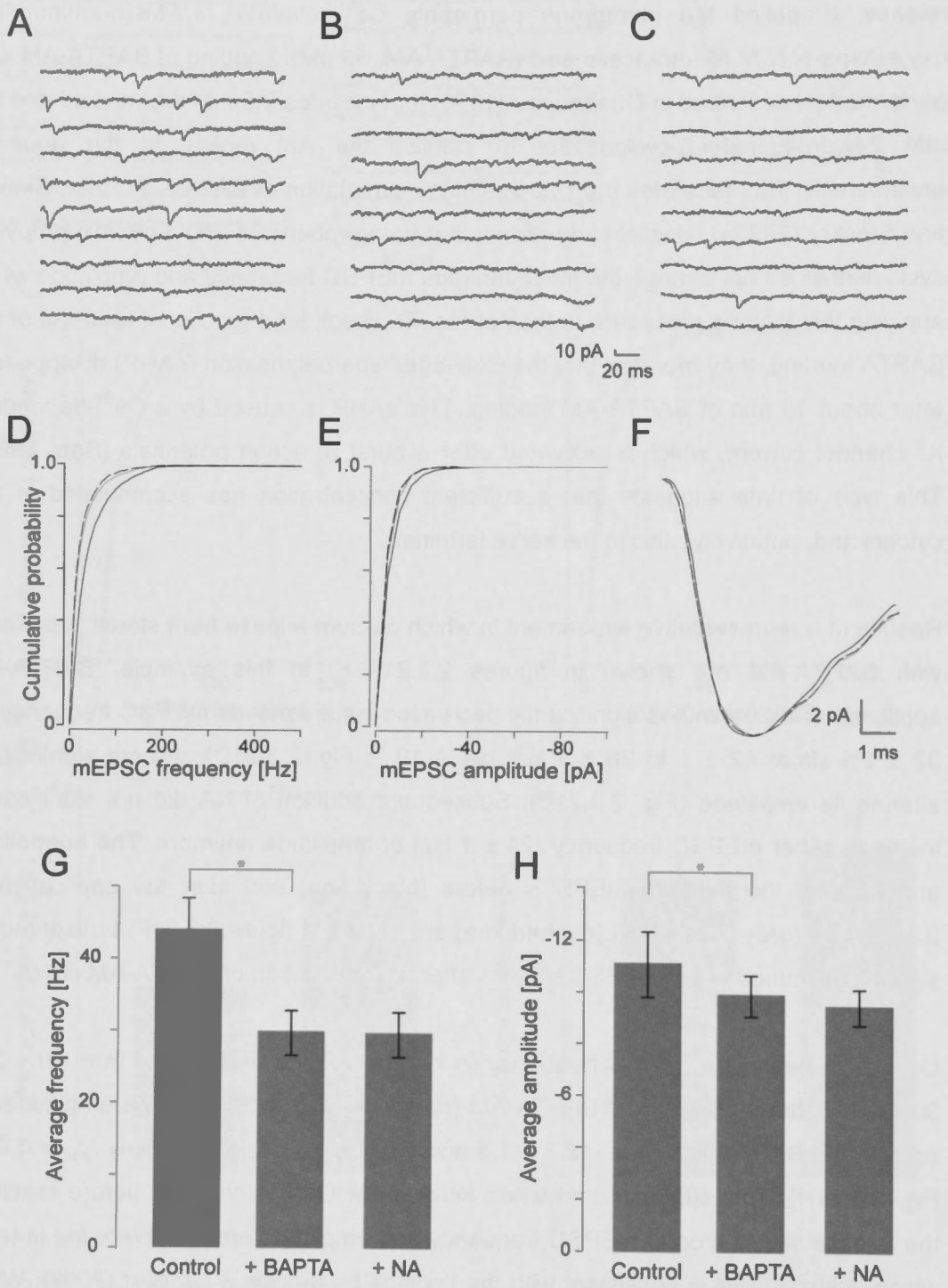

Figure 2.3.22. Chelation of intracellular calcium with BAPTA-AM. A) Two seconds of recordings taken before and B) after application of BAPTA-AM and C) the co-application of NA with BAPTA-AM. D) cPDF of the instantaneous mEPSC frequencies and E) amplitudes before (black line), after application of BAPTA-AM (grey line) and subsequent application of NA (dashed line). F) The normalised amplitude of the average mEPSC time course before (black line), after application of BAPTA-AM (grey line) and after application of NA (dashed line). G) Data summary of the average instantaneous mEPSC frequencies and H) amplitudes before and after application of BAPTA-AM and subsequent application of NA.

2.3.5. Interaction with other IP_3 producing receptors

As there are a number of neurotransmitter receptors on nerve terminals, which can signal via IP_3 production, there is the potential for crosstalk and/or occlusion between different receptors; i.e. if one receptor is activated, the activation of another receptor may be potentiated or occluded. One example of another IP_3 producing receptor is the group I metabotropic glutamate receptors (mGluR1 and 5), which have the capacity to increase presynaptic IP_3 concentration (Simkus & Stricker, 2002a).

I tested for occlusion between mGluR1/5 and α_1-ARs by first activating the mGluRs with DHPG (30 µM) followed by co-application of NA (10 µM). Results of a single experiment are illustrated in figures 2.3.22A–F. In this example, DHPG significantly increased mEPSC frequency by 53 ± 3% (from 36 ± 2 to 55 ± 1 Hz, $p_{KS} < 10^{-78}$; Fig. 2.3.22D) without significantly altering mEPSC amplitude (Fig. 2.3.22E). However, when NA was added in the presence of DHPG, no further increase of either mEPSC frequency or amplitude was detected. The normalised amplitude of the average mEPSCs before (black line) and after application of DHPG (grey line) or co-application with NA (dashed line) are shown in figure 2.3.22F. I observed no significant changes in the mEPSC kinetics after application of DHPG or co-application with NA.

In ten experiments, application of DHPG increased the mEPSC frequency by 27 ± 3% from 41 ± 3 to 52 ± 4 Hz ($p_{pt} = 0.0005$; Fig. 2.3.22G). Co-application of NA did not show any further increase in instantaneous mEPSC frequency (49 ± 4 Hz) with no significant change in amplitudes (Fig. 2.3.22H). This result provides evidence that there may be occlusion between these two signalling cascades. This observation may be explained by either a limited concentration of PIP_2 in the membrane of the nerve terminal for IP_3 production or IP_3 saturation of the respective receptors on the Ca^{2+} stores.

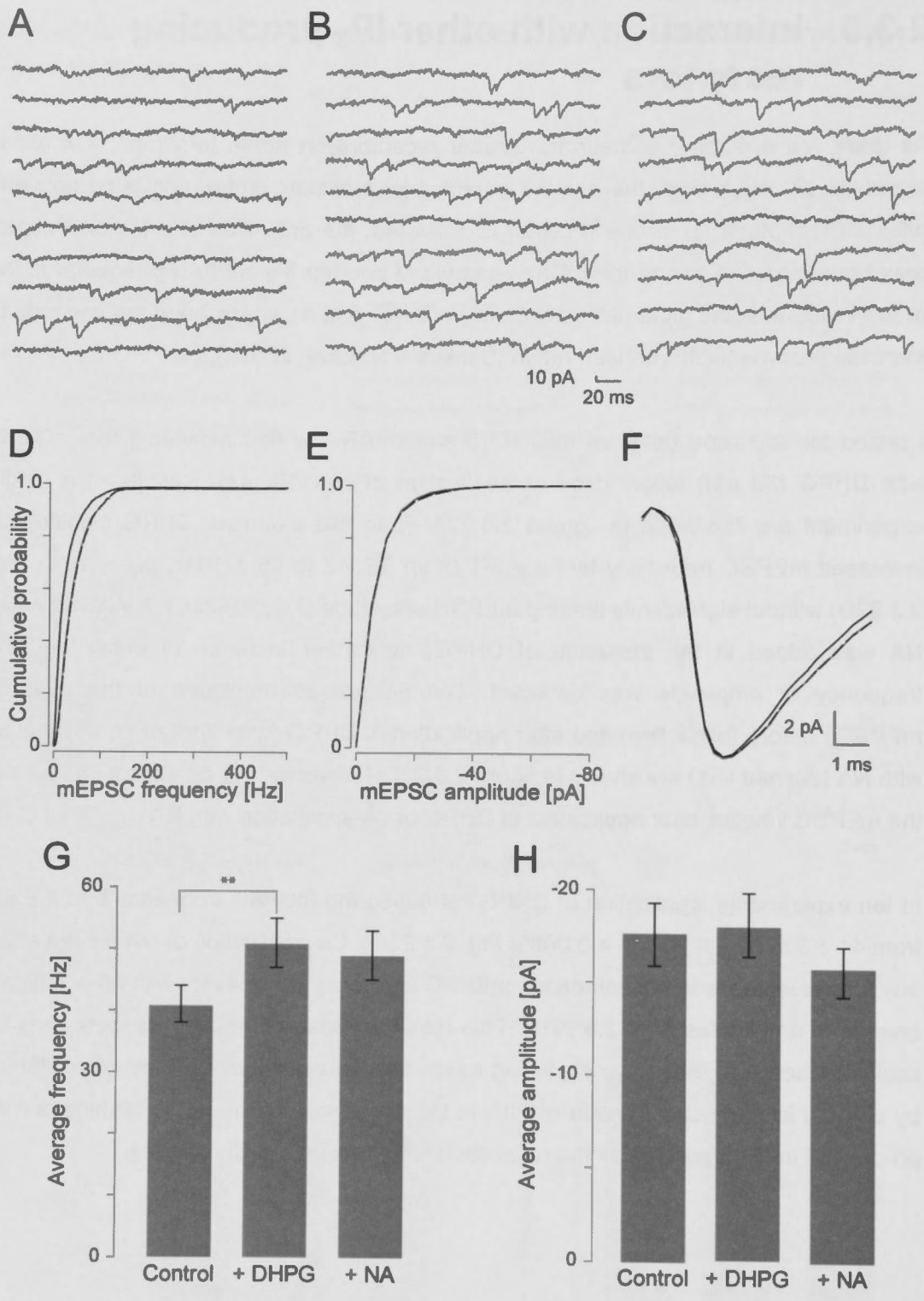

Figure 2.3.23. Occlusion of DHPG and NA. A) Two seconds of recordings taken before and B) after addition of DHPG and C) co-application of NA with DHPG. D) The cPDFs of the instantaneous mEPSC frequencies and E) amplitudes before (black line), after the application of DHPG (grey line) and after the co-application of NA with DHPG (dashed line). F) Normalised amplitudes of the average mEPSC time course before (black line), after DHPG (grey line) and after co-application of NA with DHPG (dashed line). G) Summary of the average mEPSC frequency and H) amplitude before and after application of DHPG followed by the co-application with NA.

2.4. Discussion

In this first part of my thesis, I have investigated how NA modulates spontaneous transmitter release in a homogeneous population of layer II/III pyramidal neurones of rat barrel cortex. Consistent with my initial hypothesis that NA increases instantaneous mEPSC frequency as a consequence of Ca^{2+} release from presynaptic stores, bath application of NA at a concentration of 10 µM increased the instantaneous frequency of mEPSCs by 50 ± 11% but did not alter their amplitude. The increase in mEPSC frequency reached the maximal effect about 5 minutes after NA administration to the superfusate, was saturating, and remained elevated for as long as recordings were maintained. Iontophoretically applied AMPA did not increase mEPSC amplitude or kinetics, and, therefore, suggests a presynaptic site of action. To narrow down the molecular identity of the activated receptors, I also provide evidence using both agonists and antagonists that the increase is caused by α_1-ARs. In support of this idea and based on immunohistochemistry I found that the α_{1A}- and α_{1B}-AR subtypes are most likely expressed on these presynaptic nerve terminals. I further checked the molecular signalling steps involved in the cascade after α_1-AR activation and found that after G_q protein activation, which then activates PLCβ resulting in the hydrolysis of PIP_2 to produce IP_3 and DAG. IP_3 subsequently binds to IP_3 receptors on presynaptic calcium stores to release Ca^{2+}, which then releases vesicles of transmitter. Because receptor activation of several types of neurotransmitter receptors can result in IP_3 production, I investigated if there was occlusion when two such receptor cascades produced IP_3. I chose the group I mGluR activator DHPG to pharmacologically turn the signalling cascade on and then checked if NA could further increase mEPSC frequency. I found that there was occlusion under these experimental conditions indicating that IP_3 producing neurotransmitter receptors may not signal independently of each other.

2.4.1. NA increases mEPSC frequency

From the data that I presented earlier, the effect of NA on the AR is largely presynaptic for the following reasons. Firstly, the increase in mEPSC frequency but not amplitude is a clear indicator of a presynaptic increase in the probability of vesicle fusion. Secondly, chelation of postsynaptic calcium with 10 mM BAPTA did not change mEPSC characteristics and as a consequence, rules out a postsynaptic retrograde signalling as suggested by Hashimotodani *et al.* (2005). Thirdly, the insignificant change of iEPSC

kinetics when AMPA was iontophoretically applied directly onto the dendrites in the presence of NA verified that the postsynaptic AR does not affect much either the kinetics or the peak current of AMPA mediated iEPSCs.

Noradrenergic modulation of transmitter release has been documented for many different cell types in different brain areas, including neocortical (Kawaguchi & Shindou, 1998) and hippocampal pyramidal neurones (Madison & Nicoll, 1988).

My finding of increased mEPSC frequency after application of NA is in line with the findings of Marek and Aghajanian (1999) in frontal cortex. However, my study is much more detailed as these authors did not investigate the mechanisms, which caused the increased transmitter release (i.e. mEPSC frequency and/or amplitude).

In the rat hypothalamic slice containing the presympathetic neurones, Gordon and Bains (2003) reported a 354.2 ± 34.9% (n = 24) increase in mEPSC frequency but not amplitude caused by 100 µM NA. Chen *et al.* (2006) observed that application of 50 µM α_1-ARs agonist, phenylephrine produced a 62 ± 19% increase (from 6.03 ± 1.35 to 9.77 to 2.09 Hz; n = 13) in mEPSC frequency but not amplitude in the same brain region. I compared the increase in mEPSC frequency by NA with those cited above. Unfortunately, it is not possible to quantitatively compare my data set with the one by Marek and Aghajanian (1999). However, with the remainder I saw that my data is much smaller than that for Chen et al, but similar to the latter (p_{pt} = 0.02, 0.24 respectively).

My findings are in contrast to observations by Scanziani *et al.* (1993) in organotypic hippocampal slice cultures and Delaney *et al.* (2007) in the lateral division of the rat central amygdala. They both reported that there were no or minimal changes in mEPSC frequency and amplitude after application of NA. There are two potential explanations for this. Firstly, there may not be many α_1-ARs on presynaptic nerve terminals of either hippocampal CA3 pyramidal neurones or excitatory cells in the amygdala. The other possibility is that there is either much less pronounced intracellular store involvement in hippocampus and amygdala than in neocortex or the density of presynaptic stores is much reduced.

2.4.2. Effective NA concentration to activate ARs

In neocortex, NA is the physiological agonist of the adrenergic receptors because the enzyme phenylethanolamine-*N*-methyl transferase, which can convert NA to adrenaline, is not present either in barrel cortex (Saavedra *et al.*, 1974) or *locus coeruleus*. In addition, when synthesised by the adrenal glands as a hormone, neither adrenaline nor NA can cross the blood brain barrier (Axelrod *et al.*, 1959; Weil-Malherbe *et al.*, 1959).

A large range of different NA concentrations has traditionally been used by various groups, ranging from 5 – 200 µM; namely 5, 10 and 200 µM in the hippocampus (Scanziani *et al.*, 1993), amygdala (Delaney *et al.*, 2007) and hypothalamus (Gordon & Bains, 2005), respectively. Early in this study, I decided to use a NA concentration of 10 µM because I reasoned that NA could be broken down by extracellular enzymes such as MAO (Hasegawa *et al.*, 1999) and COMT (Wilson *et al.*, 1988), which could lower the effective concentration of NA at nerve terminals below 1 µM. A higher concentration would also facilitate reaching the maximal effective concentration at these nerve terminals faster. Only much later, I measured the dose-response relationship of NA and found that the EC_{50} was 0.22 ± 0.13 µM with the maximal effect reached with a concentration of ≥ 1 µM.

I did not observe decay in the mEPSC frequency after prolonged application of NA for 20 min. This may suggest that the high concentration of NA has saturated the extracellular MAO and COMT enzyme. Choi and Kellogg (1992) reported that NA turnover rate in rat cortex is 20.9 ng/g/h by estimating the decrease in NA following inhibition of catecholamine synthesis using α-methyl-*p*-tyrosine methyl ester hydrochloride, a tyrosine hydroxylase inhibitor. The oxidation rate of NA by MAO in the cerebral cortex of the rat is 272 ± 78 pmol min^{-1} (O'Carroll *et al.*, 1986). Therefore, in my experiments, both MAO and COMT enzymes may have a little or insignificant role.

In this study, the EC_{50} was characterised as it describes the functional readout of NA binding to the adrenergic receptor including the subsequent signal transduction cascade. It is not straightforward to compare the EC_{50} obtained with published values for K_d, which result from agonist binding studies to the receptor alone. Therefore, if there are indirect consequences of direct binding of NA to the adrenergic receptor, the EC_{50} of the adrenergic receptor producing the effect will be larger than the K_d for the specific receptor (Holford, 1984); in essence, $EC_{50} > K_d$ in my case. If there is an

indirect link, then the EC_{50} will be less than the K_d. In rat cortex, NA has been found to have the highest affinity to α_2-ARs, with a K_d of 30 ± 0.2 nM, followed by that for the α_1-ARs, with a K_d of 112 ± 1.1 nM (Ruffolo *et al.*, 1982) and the lowest affinity for β-ARs with a K_d of 80 ± 3 μM (Bockaert *et al.*, 1977). The EC_{50} value that I obtained from my experiment is close to the K_d of the α_1-AR, which could indicate that NA has a direct binding to the α_1-AR. I will later give more evidence that NA activates the α_1-AR later.

2.4.3. Identity of the ARs

2.4.3.1. Lack of contribution of α_2- and β-ARs

It is very unlikely that the change in mEPSC frequency were caused by the activation of α_2- and/or β-ARs. I have excluded this possibility by co-applying the specific antagonists for β-AR propranolol (1 μM) and α_2-AR yohimbine (1 μM). Under these conditions, there was no significant change in either the mEPSC frequency or amplitude. Subsequent exposure to NA raised the average mEPSC frequency by 46 ± 4%, a change that was indistinguishable from when NA was applied alone (50 ± 11%; p_{pt} = 0.007) indicating that most if not all increase is most likely caused by α_1-AR.

α_2-ARs have been reported in various brain regions, including the neocortex and the hippocampus in the rat using autradiography (Boyajian *et al.*, 1987). In other systems, α_2-AR activation typically leads to a decrease in mEPSC frequency (Dismukes & Mulder, 1976; Pan *et al.*, 2002). Hayar and Guyenet (1999) reported that 30 μM NA reduced the mEPSC frequency by 74 ± 3% via the presynaptic α_2-AR in bulbospinal neurones of the rat rostral ventrolateral medulla. A variant to explain my experiments, however, could be that the decrease in instantaneous mEPSC frequency by α_2-AR activation may be too small to be detected by monitoring the increase in frequency of mEPSCs. However, the specific α_2-AR antagonist YO did not show an expected increase in mEPSC frequency either (see also below) indicating that this explanation is unlikely to be true.

Using autoradiography, Rainbow *et al.* (1984) found that the β_1-ARs are predominantly located in layer I and II of the cerebral cortex while the β_2-ARs are concentrated on layer IV of the cerebral cortex. I checked if presynaptic β-ARs as reported for rat frontal cortex (Mobley & Greengard, 1985) were involved in generating mEPSCs. In rat medial prefrontal cortex, activation of β-ARs causes an increase of 46.1 ± 6.8% in spontaneous and miniature EPSCs (Ji *et al.*, 2008), an effect blocked by the addition of

cadmium to the superfusate. The authors concluded this was caused by activating the β-adrenergic signalling cascade altering the phosphorylation of presynaptic calcium channels. However, when using the specific blocker of β-ARs, propranolol (1 μM), I could not detect any significant decrease in the instantaneous mEPSC frequency when ARs were activated by NA. This indicates that in barrel cortex, β-ARs are either minimally or not at all involved in modulating spontaneous transmitter release.

2.4.3.2. Evidence for α_1-ARs

With both α_2- and/or β-ARs largely excluded from modulating spontaneous transmitter release, only the family of α_1-ARs is left for consideration. In order to further support the idea that α_1-ARs on these nerve terminals modulate transmitter release, I used several different approaches. Firstly, I verified the identity of the AR using specific pharmacological agonists and antagonists. Secondly, I checked if competitive agonists and antagonists could displace NA from the binding site of the receptors. Thirdly, the interruption of the specific signalling steps downstream of receptor activation supported the transduction via a specific group of AR (see also later in this discussion). Fourthly, immunohistochemical evidence strongly supports the idea that in somatosensory cortex of rat NA activates the α_1-AR on presynaptic nerve terminals. All these lines of study unequivocally lent very strong support to the idea that the α_1-ARs are the only adrenoceptors involved in modulating transmitter release.

Previous work by Chen *et al.* (2006) has also identified the α_1-AR as the modulator for spontaneous transmitter release. When the G protein inhibitor guanosine, 5'-O-(2-thiodiphosphate) was added to the solute in the patch pipette to inhibit the action by the postsynaptic G protein coupled to the α_1-AR of rat hypothalamic paraventricular nucleus (PVN) neurones in another study, they also saw an increase in mEPSC frequency after activation of the α_1-AR. However, they concluded that activation of α_1-ARs increases the excitability of PVN neurones through augmentation of the glutamatergic "tone" and attenuation of the effect of GABAergic inputs. The molecular mechanisms behind this increase remained unexplored.

Rogawski and Aghajanian (1980) iontophorised 0.1 M NA and phenylephrine onto the lateral geniculate nucleus (LGN) of the rat and observed a two-fold increase in the spontaneous firing rate. They concluded that NA activates the α_1-AR on the LGN neurones.

2.4.3.3. Internal consistency of pharmacological experiments

Three lines of internally consistent evidence for the identity of α_1-ARs were generated. Firstly, a known partial agonist of α_1-AR, cirazoline, caused an increase in instantaneous mEPSC frequeny similar to NA (50 ± 11 *vs.* 36 ± 5%; p_t = 0.48). CO was chosen as it acts both as competitive agonist for the α_1-ARs and an antagonist for the α_2-ARs (Ruffolo & Waddell, 1982). Li *et al.* (1988) reported that CO produced a 40 – 60% submaximal response when compared with NA. My results with CO are in line with the finding by Ruffolo and Wadell (1982), but are in contrast to the report by Li *et al.* (1988) that CO is a competitive partial agonist in rat cortical slices. Ruffolo and Wadell (1982) reported that when the efficacy of CO was normalised to the efficacy of NA, the relative efficacy of CO is nearly identical to NA (0.93 ± 0.07). I, too, found that in barrel cortex, CO and NA are largely equipotent. However, the resolution of my method to track changes in instantaneous mEPSC frequency may not allow fine changes in potency to be observed. Secondly, the competitive antagonist prazosin (5 µM, K_d = 0.4 nM) was able to block the increase in instantaneous frequency that NA would cause. This finding is internally consistent with the converse experiment using CO. This set of experiments also sheds some light on the question if there is tonic activity of α_1-AR in these slices. I have not found evidence that there is tonic α_1-AR activation. However, I am not surprised either as the nerve fibres from the *locus coeruleus* that innervate this part of the cortex are cut while slicing and, most likely, the activity required for NA release is absent. Thirdly, from a set of experiments, in which the two properties of PA were employed to competitively displace CO and NA from the binding site, namely the very high affinity of PA to bind to α_1-ARs and the competitive nature of this antagonism, the increase in mEPSC frequency was abolished. This observation strengthens the argument that after agonist binding the antagonist PA competed for the same binding site on the α_1-ARs.

In this thesis, I did not investigate which of the three α_1-AR subtypes is/are responsible for signal transduction for the following two reasons. Firstly, the major aim of this project was to test the idea if presynaptic adrenoreceptors producing IP_3 could cause calcium release from presynaptic stores. Secondly, there is a very limited pharmacological tool set available to potentially distinguish between these three receptors. Only the α_{1A}-AR subtype can be distinguished by a specific agonist and antagonist. Oxymetazoline, an agonist of the α_{1A}-AR with a K_d of 6 ± 0.6 nM (Horie *et al.*, 1995), and 5-methylurapidil, a selective antagonist with a K_d of 0.89 nM, could be used of to test for α_{1A}-AR involvement (Graziadei *et al.*, 1989). There is only one known α_{1D}-AR antagonist, BMY 7978 (Goetz *et al.*, 1995) but no known specific α_{1D}-AR

agonist. In addition, BMY 7978 is also an α_{2c}-AR antagonist (Cleary *et al.*, 2005) and a partial agonist of the 5-HT_{1A} receptor (Sharp *et al.*, 1990; Zemlan *et al.*, 1990). However, there is no known specific agonist or antagonist for the α_{1B}-AR subtype.

Although there is evidence that α_{1D}-AR subtype may not be located on the cell surface, McCune and colleagues (2000) have reported that it is constitutively active and thereby causing tonic IP_3 formation. My experiments using PA, which is membrane permeant, can provide some evidence to this idea. When PA was first applied on a slice that was not stimulated with NA, no decrease in mEPSC frequency was noticeable. As a consequence, I think that this experiment suggests that α_{1D}-AR is unlikely to be present on these nerve terminals.

2.4.3.4. Immunohistochemical evidence

My study provides evidence with a triple labelling immunohistochemistry technique that α_{1B}-AR may be located at thes terminals of pyramidal neurones in the barrel cortex. There is a chance, though, that also α_{1A}-AR may be localised to these nerve terminals, but given the uncertainty about this receptor, I think that this data has to be interpreted with caution (see below). Although the α_{1D}-AR is also likely to be present at the nerve terminal, immunohistochemistry staining for the α_{1D}-AR was not done because of the localisation of α_{1D}-AR in the cytosolic fraction of the neurone (McCune *et al.*, 2000).

I did not purchase any of my α_{1A}-AR or α_{1B}-AR antibodies from known major antibody producing companies because Jensen *et al.* (2009) have recently shown that some of the α_{1A}-AR or α_{1B}-AR antibodies from commercial companies show non-specific binding when used on tissue of mice in which the specific adrenoceptor subtype had been knocked out. To provide state-of-the-art evidence of antibody specificity, the antibody subtypes require testing either on knockout animal models or transfected cell lines that do not express the receptor subtypes. Indeed, Jensen *et al.* (2009) used knockout mice for the α_{1A}-, α_{1B}- and α_{1D}-AR and found that the antibodies from Abcam and Santa Cruz Biotechnology still produced a visible band when Western blotting of membrane proteins was performed. I used a polyclonal α_{1B}-AR antibody, which was produced, characterised and published from work done at The John Curtin School of Medical Research. This antibody was raised against the 3rd intracellular loop of the α_{1B}-AR (Grayson *et al.*, 1998). I am, therefore, confident that the observed staining for α_{1B}-AR is both sensitive and specific. In addition, the α_{1A}-AR immunohistochemical staining

displayed a dimmer fluorescence than the α_{1B}-AR. Taken at face value, this could mean that the density of α_{1B}-AR may be higher than that for α_{1A}-AR.

Morphological support for my findings comes from a immunohistochemical study at both the light and electron microscopy level showing that α_1-adrenoreceptors are present both presynaptically and postsynaptically in rat visual cortex (Nakadate *et al.*, 2006). Dopamine-β-hydoxylase staining in monoaminergic projections originating from the *locus coeruleus* to the barrel cortex provides evidence that NA release can functionally occur in this part of the brain. Given that the innervations exist, it is likely that adrenergic receptors are therefore present in the barrel cortex (Simpson *et al.*, 2006). Indeed, using *in situ* hybridization histochemistry, McCune *et al.* (1993) examined the localization of the mRNA encoding the α_{1A}-, α_{1B}-, α_{2A}-, α_{2C}-AR in the rat cortex and found that the one encoding the α_{1A}-AR is localised in the upper layer of the barrel cortex.

The noradrenergic fibers that release NA in the barrel cortex originate from the caudal portion of the ipsilateral *locus coeruleus* (Simpson *et al.*, 1997). EEG measurements of the rat forebrain showed that activation of the *locus coeruleus* with the cholinergic agonist bethanechol induced a shift in EEG activity from low-frequency, high-amplitude to high-frequency low-amplitude (Berridge & Foote, 1991). The authors concluded that the rat *locus coeruleus* can cause the release of NA at a rate of 0.8 – 2.7 Hz. In another set of experiments, Florin-Lechner *et al.* (1996) reported both tonic and phasic release of NA in the rat media prefrontal cortex. The tonic release of NA with 5 and 10 Hz stimulation (700 µA, 0.2 ms pulses) increased NA release by 49 ± 3 and 66 ± 20%, respectively. The phasic release of NA with 6, 12 and 24 Hz trains (500 ms duration) increased NA release by 57 ± 9, 83 ± 7 and 70 ± 16%, respectively. These two different modes of NA release result from different activity in the *locus coeruleus* (for review see Aston-Jones & Cohen, 2005). In prefrontal cortex, phasic release follows task-related decision processes (Aston-Jones *et al.*, 1994), while tonic release is caused by the disengagement from the current task (Aston-Jones & Bloom, 1981).

2.4.4. Downstream signalling

I now focus on how the signalling cascade initiated by NA modulates presynaptic transmitter release. In rat visual cortex, Kobayashi *et al.* (2008) reported that activation of α_1-AR lead to non-classical signalling via PKC. PKC activation from DAG production could attenuate PIP_2 turnover by phosphorylation of the α_1-AR (Leeb-Lundberg *et al.*,

1987) or facilitate the fusion of vesicles by phosphorylation of SNAP-25 (Houeland *et al.*, 2007). Indeed, the α_1-AR contains various sites for phosphorylation by PKC (Lomasney *et al.*, 1991). However, this scheme is unlikely to operate in the presynaptic nerve terminals as I provide evidence that the last step in down stream signalling results in the release of Ca^{2+} from stores.

Subsequently, I will discuss each step in the α_1-AR signalling cascade. The first is the activation of PLC, most likely PLCβ (López de Jesús *et al.*, 2006), which causes the hydrolysis of membrane PIP_2 into cytosolic IP_3 and intramembrane DAG. There is early biochemical data in the literature that α_1-AR activation causes an increase in IP_3. Nalepa *et al.* (1989) found an increase of 68 – 78% in IP_3 by measuring the inositol phosphate formed in [^{3}H]*myo*-inositol-preloaded rat cerebral cortex slices when α_1-ARs were activated with NA. They also noted an increase in response with older (24 month-old) compared to younger rats (3 month-old).

PLCβ is highly expressed in cortex (Rhee *et al.*, 1991) and is activated by the α-subunit of the G_q protein at the C terminus region between Thr-903 and Gln-1030 (Wu *et al.*, 1993). To inhibit PLCβ, I used the phospholipase C inhibitor edelfosine. ES was chosen over U73122 because the latter had an unspecific effect at 10 μM of activating Ca^{2+}-activated cation channels and increasing intracellular Ca^{2+} as documented in pancreatic acinar cells (Mogami *et al.*, 1997). On the other hand, ES, an ether lipid analogue (Powis *et al.*, 1992), produces a much cleaner inhibition of PLCβ as evidenced in human embryonic cell cultures (Horowitz *et al.*, 2005). I found that when PLCβ was blocked by ES, the instantaneous mEPSC frequency decreased by 20 ± 2%.

This decrease could be due to two explanations: firstly, due to tonic receptor activation, and secondly, due to constitutive PLCβ activity, independent of receptor activation. The latter explanation seems most likely due to the finding that spontaneous release of glutamate containing vesicles has the potential to activate presynaptic group I metabotropic glutamate autoreceptors (Romano *et al.*, 1995). Under unstimulated conditions, the α-subunit of G_q, which directly activates PLCβ (Taylor *et al.*, 1991), is located in the plasma membrane and does not interact with PLCβ, which is located in the cytosolic compartment (Dowal *et al.*, 2006). This then indicates that there must be tonic PLCβ activity. This reasoning is consistent with reports of both Georgiev *et al.* (2005) and Hardie *et al.* (2004) in *Drosophila* photoreceptors, where there is constitutive activity of PLC. Hardie *et al.* (2004) compared the PLCβ activity from the

mutant *Drosophila* lacking the α subunit of the G_q protein, and found an indistinguishable basal PLCβ activity from the wild type.

The next step after IP_3 production is the binding of this molecule to IP_3 receptors on presynaptic calcium stores. When IP_3 receptors were blocked by 16 μM 2-APB, a decrease of 21 ± 4% was observed and subsequent NA application could not increase mEPSC frequency anymore. This experiment now sheds light on two important issues. Firstly, that there is tonic IP_3 production, which is blocked by 2-APB, likely caused by PLCβ activity, as subsequent α_1-AR activation does not increase the mEPSC frequency. In addition, there is no statistically significant difference when either PLCβ or IP_3 receptors are blocked. My observation is similar to Simkus and Stricker (2002a), in which they reported a 24 ± 10% (n = 10) decrease in mEPSC frequency after application of 14 μM 2-APB. Arguments about the specificity of 2-APB in this system have been documented and discussed in Simkus & Stricker (2002a). Secondly, the outcome of this experiment is inconsistent with the idea that DAG activates PKC in this instance as 2-APB blocks IP_3 receptors but does not interfere with DAG synthesis and its downstream effects. If DAG or PKC were involved, there would be an increase in mEPSC frequency after exposure to NA.

I further have been able to show that there is store involvement downstream of α_1-AR signalling by depleting Ca^{2+} stores with the SERCA pump blocker CPA for 20 minutes. With CPA alone, I did not observe any changes in mEPSC frequency. This is identical to the observation by Simkus and Stricker (2002a) that blocking alone does not result in immediately emptying the Ca^{2+} stores. Like in their report, I later augmented store depletion by a large depolarisation with a small drop of 3 M KCl. I observed a similar decrease in the mEPSC frequency as reported in Simkus and Stricker (2002a), where a 33 ± 19% (n = 5) decrease in mEPSC frequency after the depolarisation with KCl was reported. The decrease in mEPSC frequency caused by the depletion of Ca^{2+} stores is also identical with the decrease in mEPSC frequency when the membrane permeable calcium chelator, BAPTA-AM was applied. This suggests that most of the stores have been emptied by the depolarisation with KCl. When NA was subsequently applied under these conditions, no increase in mEPSC frequency was observed indicating that Ca^{2+} from stores drives the increase in frequency.

Although I have shown in this thesis that the activation of presynaptic α_1-AR causes Ca^{2+} release from presynaptic stores, I have not investigated if other Ca^{2+} stores such as mitochondria are also involved. Mitochondria start accumulating cytosolic Ca^{2+} following an increase above 500 nM Ca^{2+} concentration (Pivovarova *et al.*, 1999).

Similar to the uptake of Ca^{2+} into the mitochondria, there are two mechanisms of Ca^{2+} release from mitochondria. The first mechanism is via the reversal of the mitochondrial proton uniporter (Haworth & Hunter, 1979), while the second mechanism is via the activation of the electroneutral H^+/Ca^{2+} antiporter (Pozzan & Azzone, 1976). Mitochondria may play a regulatory role in spontaneous transmitter release by cyclic changes in Ca^{2+} sequestration, which has been suggested by Cohen *et al.* (1974) to account for the clustering of mEPP at the frog neuromuscular junction. Given that no IP_3 receptors have so far been identified on mitochondria, I think that calcium release from mitochondria is unlikely, except for the remote possibility that 2-APB may bind to and block a mitochondrial calcium release channel. However, as the block by CPA reduces the mEPSC frequency by about the same amount, I don't think this latter idea is likely to occur.

The last step in the signalling cascade is the release of Ca^{2+} from stores. To check for this release, I used 50 µM BAPTA-AM to chelate calcium in the cytosol. I observed the same effect (a decrease of 32 ± 11%, n = 6) as reported by Simkus & Stricker (2002a). The necessary control experiments were done in Simkus & Stricker (2002a). A concern when using the acetomethoxy-form of BAPTA for loading of the nerve terminals is the generation of formaldehyde when the AM moiety is cleaved. This could unspecifically cause an increase in mEPSC frequency. I argue that the matching decreases in mEPSC frequency observed in each set of experiments with ES, 2-APB, CPA and BAPTA-AM provide the internal control for settling this issue. Since the values are indistinguishable (p_t = 0.37, 0.27, 0.27, 0.27, 0.30, 0.29; ES *vs.* 2-APB, ES *vs.* CPA, ES vs. BAPTA-AM, 2-APB *vs.* CPA, 2-APB *vs.* BAPTA-AM and CPA *vs.* BAPTA-AM, respectively), it is reasonable to suggest that this hypothesised effect of formaldehyde is minimal or even absent.

From the internal consistency in all experiments verifying the down-stream actions after receptor activation, I can safely conclude that a classical α_1-AR signalling cascade is involved; this includes that after ES, 2-APB, CPA and BAPTA-AM application, subsequent NA addition could not increase the mEPSC frequency any more.

2.4.5. Interactions with IP_3 producing receptors

Given the notion that the activation of the α_1-AR follows a classical signalling cascade, other IP_3 producing receptors could also potentially increase the instantaneous mEPSC

frequency provided that the receptors signal via $G_{p/q}$ proteins. Among them are group I metabotropic glutamate (mGlu), histamine (H_1), serotonin ($5\text{-}HT_2$), muscarinic (M_1/M_3), orexin (OX_1/OX_2) and purinergic (P2Y) receptors such as the $P2Y_1$, $P2Y_2$, $P2Y_4$, $P2Y_6$, $P2Y_{11}$ and $P2Y_{14}$ (Jones *et al.*, 1979). This idea asks the question what the overall effect would be when two of these receptors were activated simultaneously.

I tested if after pharmacological activation of group I mGluRs, which increases mEPSC frequency on its own by 27 ± 3%, subsequent co-application of NA would result in a further increase or not. There was no increase in the instantaneous mEPSC frequency under these conditions; i.e. the increase expected to be caused by NA was occluded by DHPG. I have three potential explanations why this occlusion may have occurred. Firstly, IP_3 production could be limited due to restricted availability of PIP_2 in the membrane. Indeed, Falkenburger *et al.* (2010) found direct evidence for this idea from Förster resonance energy transfer (FRET) using cell cultures expressing a voltage sensitive PIP_2-5-phosphatase, the rate limiting enzyme for PIP_2 synthesis. They reported that the time constant of replenishment of PIP_2 in the membrane is about 130 s whereas hydrolysis is much faster. Secondly, if the number of IP_3 receptors on stores was small and the IP_3 concentration is saturating, a further increase in the concentration of IP_3 would not necessarily result in more calcium release from stores. Thirdly, the available Ca^{2+} for store release may be depleted quickly. This is unlikely as Simkus and Stricker (2002a) reported that the application of 10 mM caffeine was insufficient to deplete Ca^{2+} stores for more than 20 minutes.

In the experiments testing for occlusion, saturating pharmacological concentrations of both DHPG and NA were used. However, it could be that if non-saturating concentrations were used, much more subtle interactions may be detectable. In addition, under such conditions, it may even depend on the specific order in which the different receptors were activated. I envisage similar results for other presynaptic IP_3 producing receptors like the serotonin receptor, $5\text{-}HT_2R$.

2.4.6. Functional consequences

With its ability to modulate transmitter release, NA, as a neuromodulator, could potentially play an important role in learning and memory. The plasticity of dendritic spines is believed to play important role in information processing and learning (Leuner & Shors, 2004). At the single cell level, NA could be an important trophic factor in postnatal dendritic spine development. McKinney *et al.* (1999) found that spontaneous

release of glutamate is essential for the maintenance of dendritic spines on dendrites of juvenile CA1 pyramidal neurones in organotypic slice cultures. Therefore, by modulating transmitter release, NA could help the maintenance or even promote the formation of new dendritic spines. This idea is in agreement with the observation that NA shapes spine formation in the neocortex of rats (Felten *et al.*, 1982). Tyler and Pozzo-Miller (2003) also reported that the brain-derived neurotrophic factor (BDNF) could affect dendritic spine formation in rat hippocampal CA1 pyramidal neurone and that BDNF expression is regulated in part by mEPSC frequency.

Studies by Desai *et al.* (2002) have revealed that mEPSCs are involved in homeostatic plasticity in the rat visual cortex. The authors reported that the mEPSC amplitudes can be globally scaled up or down as a function of development and sensory experience. In addition, Diamond and Jahr (1995) proposed that the mEPSC can shape the AMPA receptor EPSC decay in cultured hippocampal neurones.

Given the data provided here, and aware of the quantal hypothesis which states that neurotransmitter is released in individual synaptic vesicles, I predict that for evoked transmitter release an internally consistent picture would emerge. Given that activation of the presynaptic α_1-ARs increases the rate of mEPSC, I would expect that the amplitude of the evoked transmitter release becomes larger due to a rise in Ca^{2+} in the nerve terminal, which increases the probability of release.

2.5. Conclusion

From the experiments conducted in this chapter, I can conclude that NA increases the instantaneous mEPSC frequency but not amplitude. The EC_{50} of the dose response relationship of mEPSC frequency with NA concentration is 0.23 ± 0.05 μM. In regard to the signalling mechanism of the α_1-ARs, NA activates presynaptic α_1-ARs, resulting in PIP_2 hydrolysis and IP_3 production and subsequent Ca^{2+} release from stores. I also found that presynaptic α_1-ARs are not tonically active in slices of neocortical tissue. I provide some evidence that the α_{1B}-AR is most likely present on nerve terminals of pyramidal neurones. Using occlusion experiments between α_1-ARs and group I mGluRs, different IP_3 producing receptors on nerve terminals may not operate independently of each other. The summary picture of the mechanisms investigated in this study is given in Figure 2.5.1.

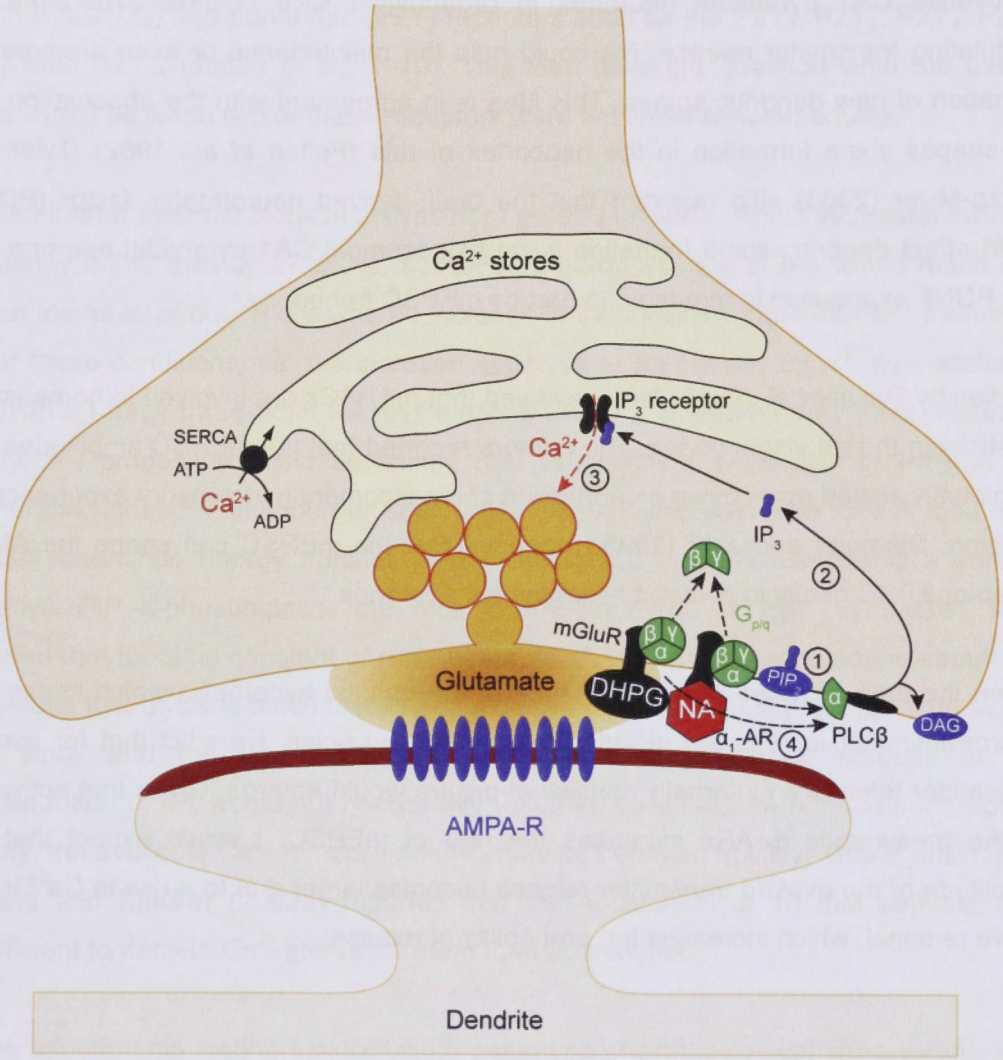

Figure 2.5.1. Summary cartoon of a presynaptic nerve terminal onto a postsynaptic spine. The results from this part of the study suggest that when activated by its physiological agonist (NA), the α_1-AR initiates the signalling cascade by activating the membrane PLCβ via the G_α subunit (①). The activated PLCβ then hydrolyses the membrane PIP_2 to IP_3 and DAG (②). Production of IP_3 causes binding to the IP_3 receptor on the Ca^{2+} stores, resulting in the release of Ca^{2+} (③). Different IP_3 producing receptor may utilise the same signalling cascade to cause Ca^{2+} release from these stores (④).

3. Part II

Noradrenergic modulation of evoked transmitter release in pairs of connected layer II neurons

3.1. Introduction

In the previous part of my thesis, I have provided strong evidence that α_1-AR plays a significant role in modulating mEPSCs. I then proceed to pairs of connected neurones, to directly see whether the increase in spontaneous transmitter release rate was mimicked as an increase in evoked transmitter release. Excitatory postsynaptic currents (EPSCs) were evoked in pairs of connected neurones to test the prediction that if the results were consistent with increased transmitter release, as seen in the increased instantaneous mEPSC frequency, evoked EPSCs in the presence of NA should become larger.

I started by characterising the electrophysiological properties of the pairs of pyramidal neurones in layer II/III of the barrel cortex. I next tested the effect of NA on evoked transmitter release. I later investigated the potential molecular mechanism of NA. Using the specific agonist and antagonist, I examined on which of the AR was NA acting. In a final set of experiment, I checked if NA could alter the synaptic dynamics.

3.2. Methods

Here, I present the methodological aspects specific to this chapter. Specifically, the strategies to obtain recordings from connected cell pairs in layer II of somatosensory cortex are described. It is important to stress that for these types of recordings, there is no difference in the slicing procedure, bathing solutions or patch electrodes and their solutes used, compared to the methods described in Part I. The approach does not differ much from that already described in Cowan & Stricker (2004) and Fuhrmann *et al.* (2004) for layer IV and V excitatory cells. The most important two aspects in obtaining cell pairs is to firstly record at physiological temperature (36 ± 1°C in this case) as the release probability drops significantly with temperature (Hardingham & Larkman, 1998) and secondly, to be able to record from the slice with the best connectivity as otherwise there is no success whatsoever. For our slicing procedure with cutting parasagittally at a 15° angle, this "best" slice is usually around the 5th slice (5'300 µm from the lateral pole) for a 15 – 19 days old Wistar rat. From experience, there are typically only 1 – 2 "best" slices. I have used the following criteria for identification of this "best" slice. First, somata of both pre- and postsynaptic neurones are to be in the same optical plane. These are typically found in "nests" of about 5 or more similar neurones. Second, the somata are usually not more than about 10 – 20 µm apart. Third, the dendrites of both neurones should be firstly parallel with each other and secondly also parallel to the cut surface of the slice.

Recordings between two connected neurones were obtained in whole-cell mode using largely the same techniques as in the preceding part of this thesis. The slices were superfused with standard ACSF to which gabazine (3 µM) was routinely added to block inhibition by $GABA_A$ receptors. The presynaptic cell was kept in current-clamp while the postsynaptic cell was in voltage-clamp. Bridge balance was automatically compensated for the presynaptic cell. Electrode capacitance was not compensated as this increased the recording noise considerably. In some cells, a continuous hyperpolarizing bias current was used to keep the cell at a membrane potential of < -70 mV. The peak amplitude of the AP in whole-cell mode was required to be > 70 mV otherwise the recording was aborted. The postsynaptic EPSC was recorded at a holding potential of -70 mV with neither R_s nor whole-cell capacitance compensated. Connectivity was assessed by evoking two action potentials in the presynaptic cell using short current pulses of 3 – 5 ms duration and ~1.5 nA amplitude at an interval of 50 ms. This paired-pulse paradigm serves to quickly assess if during repetitive stimulation the EPSC depressed or facilitated. Each episode of recording contained a

voltage step of 1 mV for 20 ms to gauge if the R_s changed throughout the recording. Recordings were aborted or not considered for analysis if the R_s was > 20 MΩ or changed by > 20% or . The rate of evoking these episodes was typically 0.2 Hz unless specified otherwise. Recordings were sampled at 5 kHz and filtered similarly to the mEPSCs at 1 kHz using the custom-built sample-and-hold unit. Timing of the episodes was generated by a Master-8™. EPSC peak amplitudes and their kinetics (rise times and half-widths) were measured off-line using custom-made Igor Pro procedures. The data of the recordings were saved on the hard disk of a computer in the ITC-18 binary format.

The recording solute contained 0.5% biocytin, which allowed cell pairs to be histologically developed and identified later using the same procedures and criteria as in the previous part. Only cell pairs between pyramidal cells in layer II/III were included for subsequent analysis. Figure 3.2.1 shows a histologically verified pair of a synaptically connected pyramidal neurone making contact with a postsynaptic pyramidal cell in layer II of barrel cortex. The presynaptic neurone is situated on the right while the postsynaptic neurone is to the left. On average, axons and their collaterals were hard to stain.

For analysis of all experiments, checks were done that for each stimulus current an action potential was evoked from the presynaptic neurone for a corresponding EPSC from the postsynaptic neurone. The amplitude of the action potential generated in the presynaptic neurone was measured as the difference of six data points during resting membrane potential and six points around the peak of the AP interpolated using a 3rd order polynomial. The half-width of the action potential was measured as the time at half maximum of the action potential between the interpolated rising and decay phases. EPSC amplitudes of the postsynaptic neurone were measured as the difference between two time windows of about 1.2 ms at the base immediately before the AP and at the peak of the EPSC. The measurement of all EPSC amplitudes was typically done manually for all EPSCs (see Appendix). The 10 – 90% rise times of the EPSCs were measured as the difference between two time windows of 1.2 ms before the time of stimulus and around the peak of the EPSC. The half-widths of the EPSCs were measured as the interpolated time at the half maximum of the EPSC between the rising and the decay phase. The EPSC latencies were estimated as the difference between the peak of the action potential and the 10% point of the rising phase of the EPSC.

Figure 3.2.1. Two synaptically connected layer II pyramidal neurones after processing histologically showing the main apical, basal dendrites, the two axons and axon collaterals (scale bar 20 μM). Note the two blebs at the axon endings indicative of cutting the axon.

Stability of the recordings over time was assessed using compound averages of the peak amplitude of the EPSCs of at least 20 trials. A recording was considered stable if based on a Student's *t*-test (p_t), the first and last averages were comparable with a significance level of $p_t < 0.05$.

To test for the synaptic dynamics, a series of action potentials was evoked. In particular, this protocol consisted of a sequence of 20 action potentials evoked at a frequency of 50 Hz, to which an additional action potential was added with a delay of 500 ms to gauge recovery from synaptic depression. The recovery from depression, R_{50} was calculated as the difference between the average first EPSC amplitude ($\bar{E}_1$) and the recovery pulse ($\bar{E}_{Rec}$) divided by the difference between the average amplitude

of the first EPSC ($\bar{E}_1$) minus the average amplitude in steady state (estimated as the average of the last four EPSCs in the train of twenty; $\bar{E}_{SS}$); i.e.

$$R_{50} = \frac{\bar{E}_1 - \bar{E}_{Rec}}{\bar{E}_1 - \bar{E}_{SS}}.$$

It can easily be seen that if $\bar{E}_{Rec}$ is larger than $\bar{E}_1$, this value becomes negative.

3.2.1. Statistical analysis

After the initial action potential or EPSC detection with IGOR, comparisons between the pooled data used both independent *t*-tests (p_t), paired sample *t*-tests (p_{pt}), Pearson's *r* (p_r) and analysis of covariance (Snedecor & Cochran, 1989). The type of test is indicated by subscripting *p* with the appropriate acronym. For the *t*-tests, significance is considered with p_t or $p_{pt} < 0.05$. For the Pearson's *r*, the two parameters are considered correlated if $p_r < 0.05$. Likewise, when testing for differences in slope, a significance of $p_{ANCOVA} < 0.05$ was required. Error bars represent the standard error of the mean (SEM). Values cited in text are mean ± SEM. In the figures, statistical significance is indicated by asterisks: * $p < 0.05$; ** $p < 0.01$.

3.3. Results

3.3.1. Characterisation of unitary EPSCs

In this section, I am reporting some basic electrophysiological characteristics from a set of 101 excitatory connections between pairs of pyramidal neurones mostly in upper layer II of rat somatosensory cortex. The rate of connectivity was found to be about 20 – 30% of the cells tested. This rate drops off sharply if recordings are attempted in slices outside the optimal range. In this set of 101 cell pairs, three were found to be bidirectional. For subsequent analysis of bidirectional connections, the pair that showed the larger unitary EPSC amplitude was included. Subsequently, because EPSCs recorded in pairs of neurones are by nature unitary, I refrain from using the word unitary.

3.3.1.1. Electrophysiological properties

Recordings for this part were considered only if the R_s and R_{in} followed the same quality criteria as in part I. Figures 3.3.1A–C show an example of a connected pair. Two simultaneous recordings were obtained from two pyramidal cells, which had resting membrane potentials of -75.1 mV (presynaptic) and a similar value of the postsynaptic (not documented in this case). When a current of 1.5 nA was injected into the presynaptic cell for 3 ms, an action potential was evoked which had a peak amplitude of 105.8 mV and a half-width of 1.3 ms (Fig. 3.3.1A upper trace). In this example, an EPSC was recorded in the postsynaptic cell, which at a latency of 1.0 ms had a peak amplitude of -45.3 ± 1.2 pA, a rise time of 1.2 ms and a half-width of 4.1 ms (Fig. 3.3.1.B lower trace). The small notch right before the rising phase of the EPSC is due to the capacitive coupling of the action potential evoking current between presynaptic stimulus and postsynaptic recording electrode. This cell pair was then stimulated once every 5 s (0.2 Hz) for 300 trials. The peak amplitudes of these trials after manual measurement are shown in Fig. 3.3.1B in which 292 events are illustrated; 8 EPSCs were required to be discarded during the measurements as a consequence of uncertainty about the measurement of the peak amplitude. The average time course of the 300 EPSCs is that displayed in figure 3.3.1A (lower trace).

The recording noise in this example was 1.5 pA (not shown). In figure 3.3.1C, averages are formed for 12 EPSCs (corresponding to 1 minute) and depicted as minute averages during the recording period together with error bars for SEM. A comparison of the first and last 20 EPSC amplitudes based on Student's *t*-test indicates no significant change (p_t = 0.42). As a consequence, the EPSCs during the 300 stimuli remained stable. The minute averages of R_s and R_{in} relating to this EPSC are shown in figures 3.3.1D and E, respectively. It shows that during the whole recording period neither R_s nor R_{in} changed. I therefore consider this example to represent a stable recording, which can be included in the subsequent analysis.

As it is important to know if NA could potentially change presynaptic characteristics, I will now describe some properties of the presynaptic neurones. The resting membrane potential in all these pyramidal neurones was -70.5 ± 1.5 mV (without adjustment for junction potential), ranging from -52.4 to -81.0 mV. The distribution of these values is given in figure 3.3.2A, where the bin width was chosen to be 2 mV. The average bridge-balance of the recording pipette was 12 ± 1 MΩ. The average R_{in} of these cells was 146 ± 15 MΩ (Fig. 3.3.2B; ranging from 32 to 449 MΩ), with a small but distinct mode of a few cells around 400 MΩ. The average amplitude of the action potential (AP) was 100.6 ± 1.0 mV (Fig. 3.3.2C; ranging from 72.5 to 122.8 mV) with a half-width of 1.5 ± 0.1 ms (Fig. 3.3.2D; ranging from 0.9 to 5.6 ms). All neurones histologically identified for this set of data had a pyramidal-shaped soma from which several basal dendrites originated and from which a slightly oblique primary apical dendrite extended towards the pial surface.

In order to measure the membrane potential of the postsynaptic neurone, I first switched to current-clamp mode after opening the membrane patch. The membrane potential of the postsynaptic neurones was not much different to that of the presynaptic cells. I then switched back to voltage-clamp mode to measure both R_s and R_{in}. From the whole data set, R_s had a value of 13 ± 1 MΩ (range 5 – 20 MΩ) and R_{in} had value of 128 ± 13 MΩ (ranging from 13 to 567 MΩ). The relevant histograms in figures 3.3.3A–H illustrate some characteristics of all postsynaptic neurones recorded from.

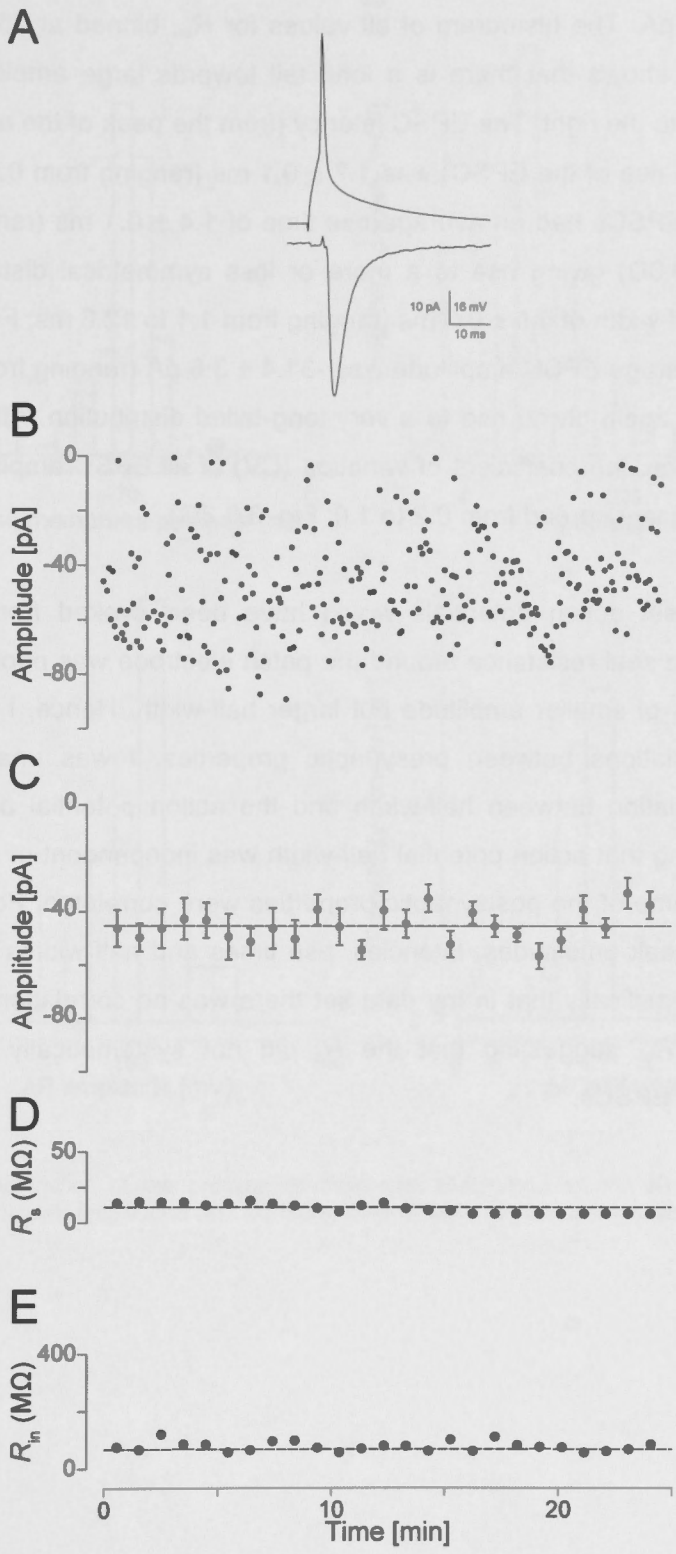

Figure 3.3.1. Unitary EPSCs observed in a single recording together with controls for stability and quality of recording. A) Average of 300 action potentials and EPSCs. B) Time course and C) minute averages of the EPSCs in a single experiment. D) R_s and E) R_{in} of the EPSC during the entire recording.

The average whole-cell noise, filtered at 1 kHz during a recording was 1.7 ± 0.1 pA (ranging from 1.1 to 2.2 pA). The relevant histogram is shown in figure 3.3.3A with a bin width of 0.2 pA. The histogram of all values for R_{in}, binned at 25 MΩ, is given in figure 3.3.3B. It shows that there is a long tail towards large amplitudes causing a significant skew to the right. The EPSC latency (from the peak of the action potential to the point of 10% rise of the EPSC) was 1.7 ± 0.1 ms (ranging from 0.5 to 4.5 ms; Fig. 3.3.3C). These EPSCs had an average rise time of 1.4 ± 0.1 ms (ranging from 0.4 to 2.6 ms; Fig. 3.3.3D) giving rise to a more or less symmetrical distribution of these values and a half-width of 4.5 ± 0.5 ms (ranging from 1.1 to 12.6 ms; Fig. 3.3.3E) with a long tail. The average EPSC amplitude was -31.4 ± 3.6 pA (ranging from -0.6 to -152.3 pA; Fig. 3.3.3F) again giving rise to a very long-tailed distribution. After correction for recording variance, the coefficient of variation (CV) of all EPSC amplitudes was 0.6 ± 0.1 (with a significant spread from 0.2 to 1.0; Fig. 3.3.3G).

If in this data set action potentials would have been evoked from a depolarised potential or if the seal resistance around the patch electrode was poor, I would expect action potentials of smaller amplitude but larger half-width. Hence, I checked if there were any correlations between presynaptic properties. I was unable to find any significant correlation between half-width and the action potential amplitude ($r_{(101)}$ = 0.054) suggesting that action potential half-width was independent of amplitude. I next determined if some of the postsynaptic properties were correlated. For this purpose, I compared the peak amplitudes, latencies, rise times and half-widths of the EPSCs. I mention here specifically that in my data set there was no correlation between EPSC amplitude and R_s, suggesting that the R_s did not systematically scale the peak amplitude of the EPSCs.

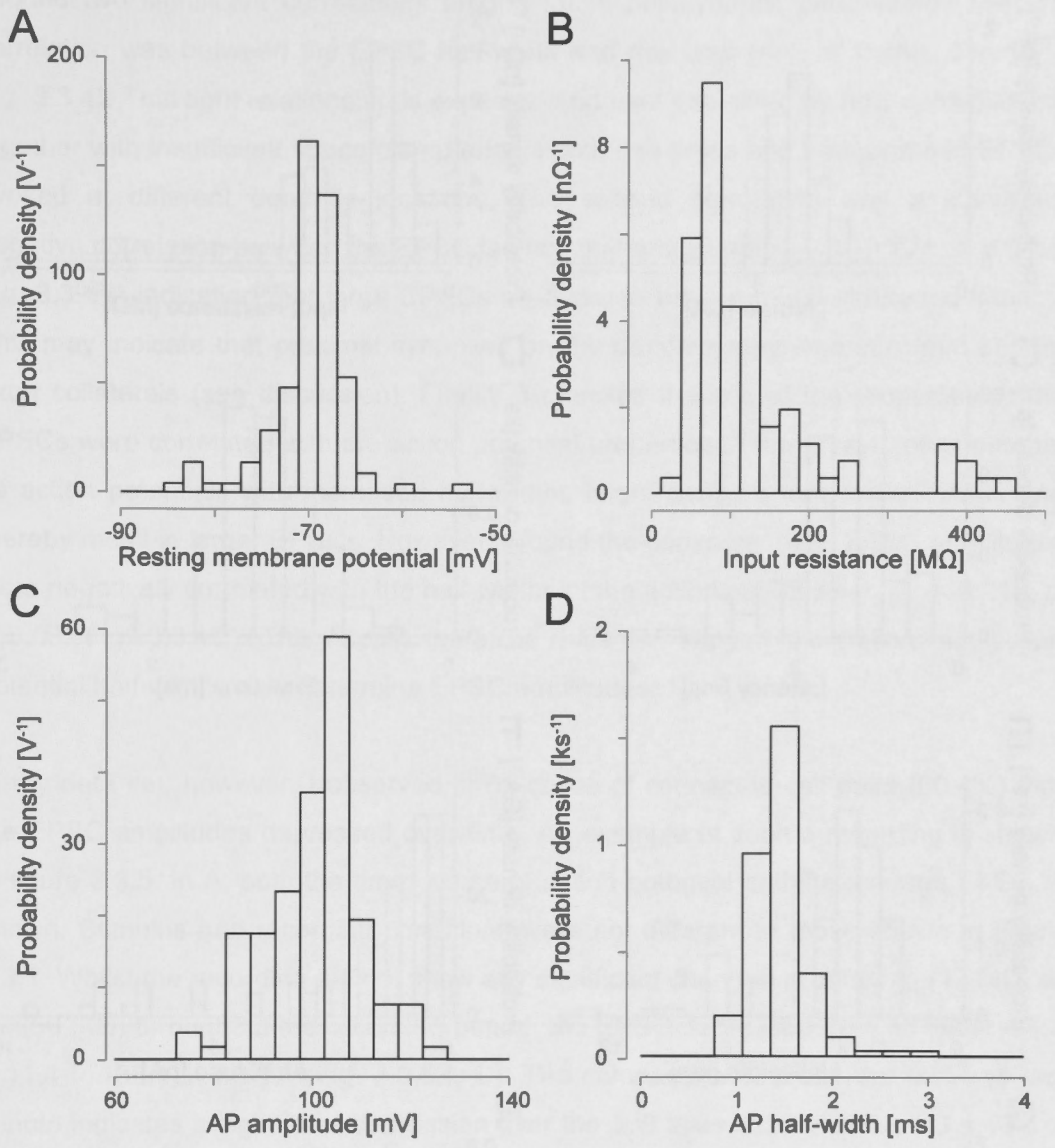

Figure 3.3.2. Characteristics of the presynaptic neurones. Histograms of the A) resting membrane potentials, B) R_{in}, C) peak amplitudes and D) half-widths of action potentials evoked in the presynaptic neurones.

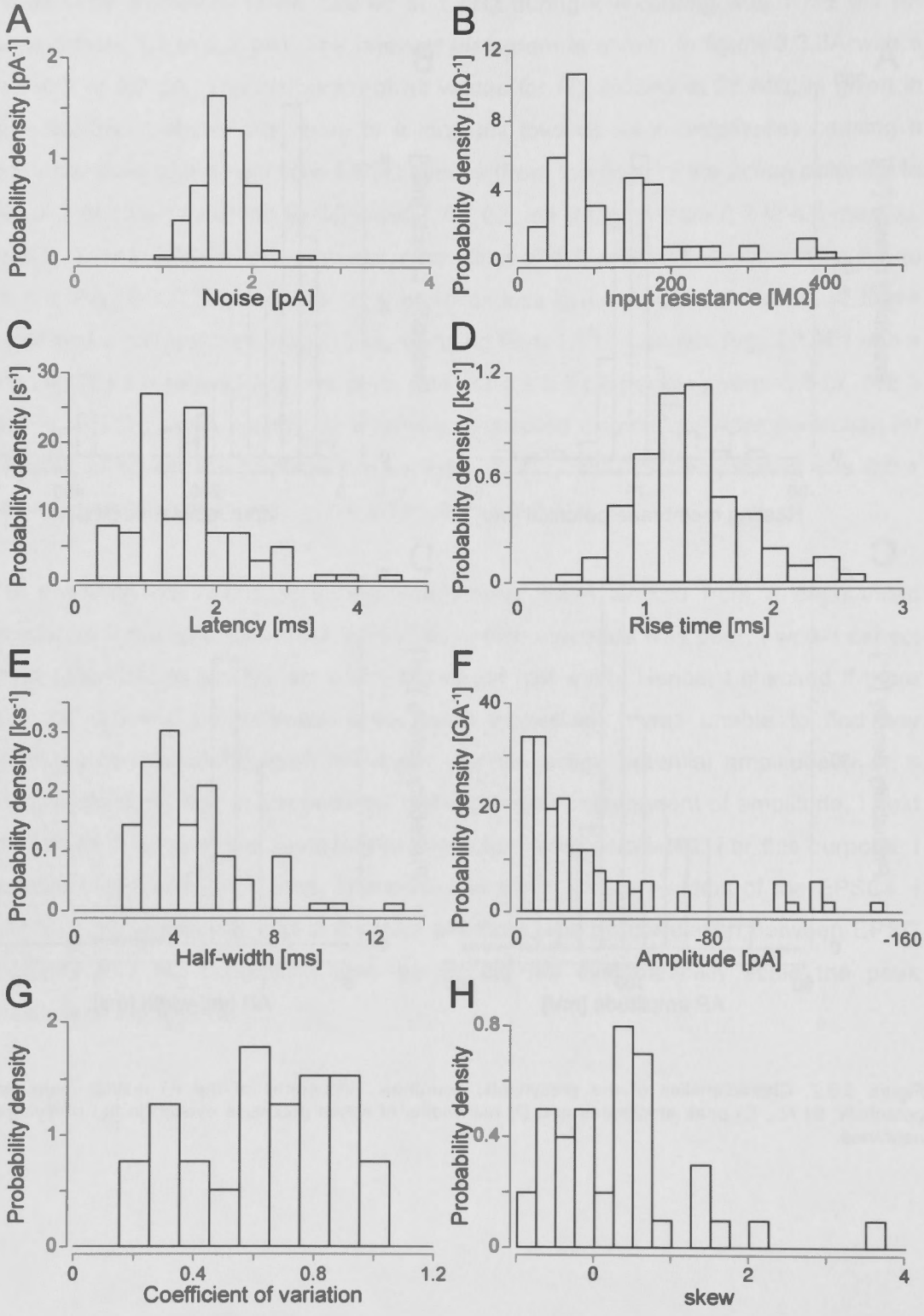

Figure 3.3.3. Characteristics of the postsynaptic pyramidal neurone and EPSCs. Histograms of A) the recording noises, B) R_{in}, C) EPSC latencies, D) EPSC rise times, E) EPSC half-widths, F) EPSC amplitudes, G) CVs and H) skews of the EPSC distributions.

I found two significant correlations among these postsynaptic parameters. The first correlation was between the EPSC half-width and rise time ($r_{(101)}$ = 0.849, $p_r = 10^{-17}$; Fig. 3.3.4). This tight relationship is expected and best explained by how cable filtering together with insufficient space clamp affects both rise times and half-widths of EPSCs evoked at different dendritic locations. The second correlation was a significant negative correlation between the EPSC latency and amplitude ($r_{(101)}$ = -0.224, p_r = 0.04; Fig. 3.3.4B) indicating that large EPSCs on average have a much shortened latency. This may indicate that proximal synapses on the dendrite may emanate from shorter axon collaterals (see discussion). Finally, I checked if some of the properties of the EPSCs were correlated with the action potential properties of the presynaptic neurone, as action potentials with increased half-widths might cause a longer Ca^{2+} influx and thereby result in larger EPSCs. However, I found the converse: peak EPSC amplitudes were negatively correlated with the half-widths of the action potentials ($r_{(101)}$ = -0.216, p_r = 0.03; Fig. 3.3.4C). This finding therefore does not support the notion that action potential half-widths may determine EPSC amplitudes.

In my data set, however, I observed in 61 cases of connected cell pairs (60.4%) that the EPSC amplitudes depressed over time. An example of such a recording is shown in figure 3.3.5. In A, both the time course of action potential and the average EPSC is shown. Stimulus and recording conditions were not different to those shown in figure 3.3.1. Whilst the recording did not show any significant changes in either R_s (17 MΩ) or R_{in} (56 MΩ) throughout the recording period, the EPSC depressed from an initial -64.3 ± 11.4 to -38.1 ± 5.6 pA (Fig. 3.3.5B, C). The comparison between the first and last minute indicates a significant depression over the 300 trials in 25 minutes (41 ± 9%; p_t = 0.003). I found that this depression is long-lasting, takes a few minutes for onset and can still be documented at stimulus frequencies < 0.03 Hz though the rate of depression is smaller at these latter frequencies. A complete description and characterisation of this form of long-term depression will be done elsewhere and considered outside the scope of this thesis. However, whilst the peak EPSC amplitude depressed, I did not see any changes in either AP or EPSC kinetics. In fact, all parameters with the exception of EPSC amplitude remained the same. From this point onwards, all recordings shown and used for analysis fulfilled the criteria of stationarity and stability.

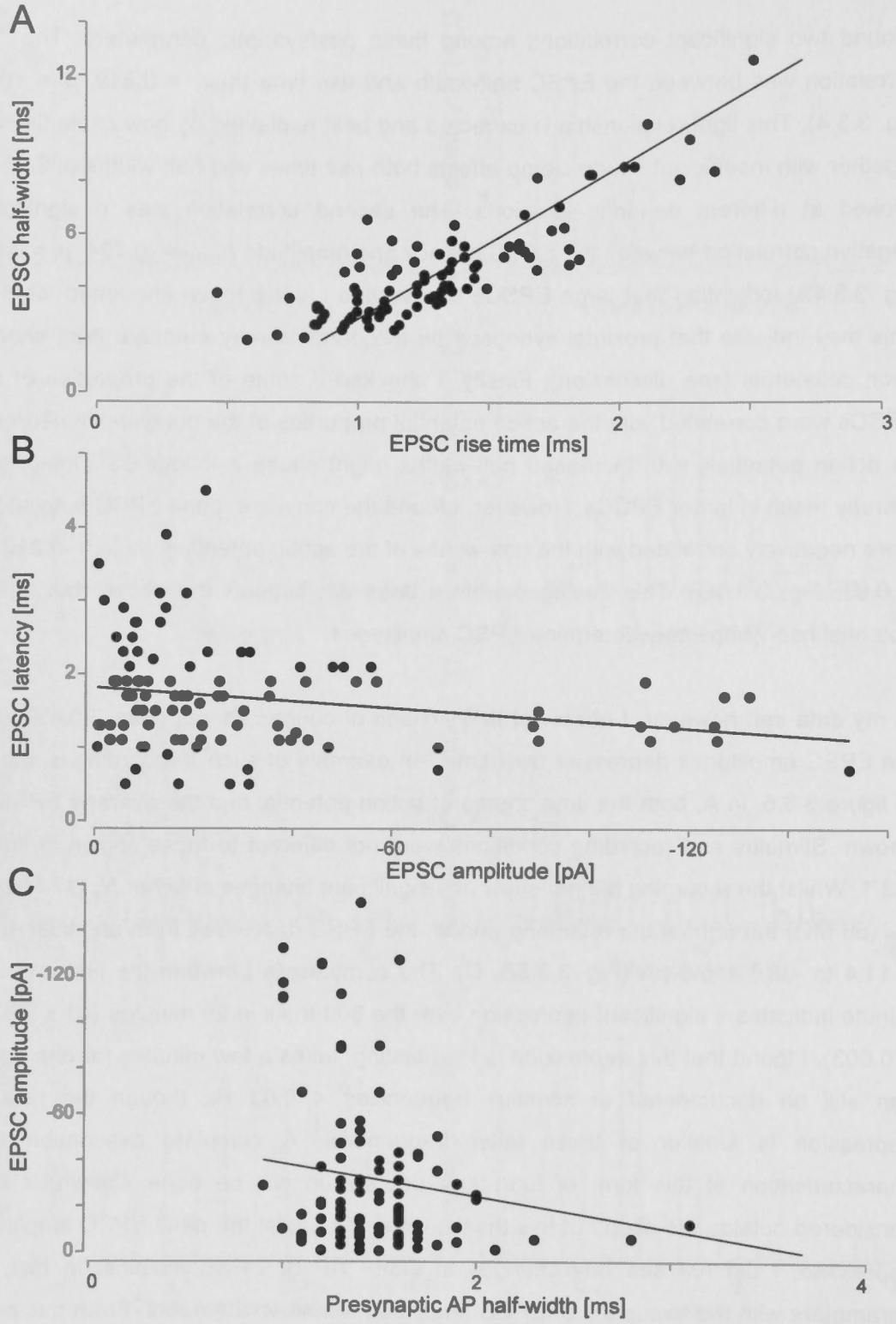

Figure 3.3.4. Significant correlations between properties of the EPSCs. A) A significant correlation between the EPSC half-width and rise time of the postsynaptic neurone was found with the line indicating the correlation. B) A negative correlation between EPSC amplitudes and latencies was found. C) Negative correlation between EPSC amplitudes and half-widths of presynaptic action potentials shown as a line.

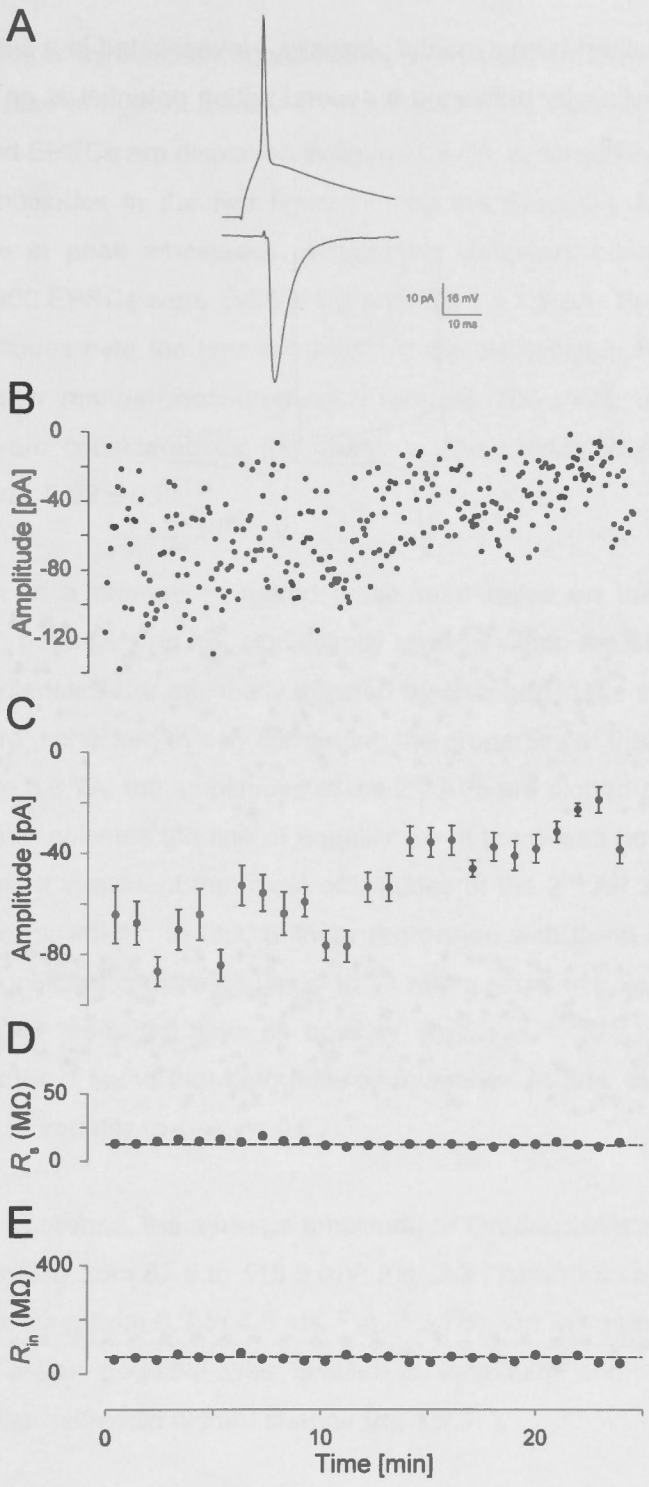

Figure 3.3.5. An example of a non-stationary EPSC over time. A) Average time courses of 300 action potentials and the corresponding EPSCs. B) Time course of depression as monitored by individual peak amplitudes of EPSCs and C) corresponding minute averages in this experiment. D) Minute averaged for series and E) R_{in} throughout the recording period.

3.3.1.2. Paired-pulse characteristics of EPSCs

To get insight into short-term synaptic plasticity, I investigated in a subset of 40 EPSCs paired-pulse behaviour by delivering a second action potential at an interval of 50 ms to the presynaptic cell.

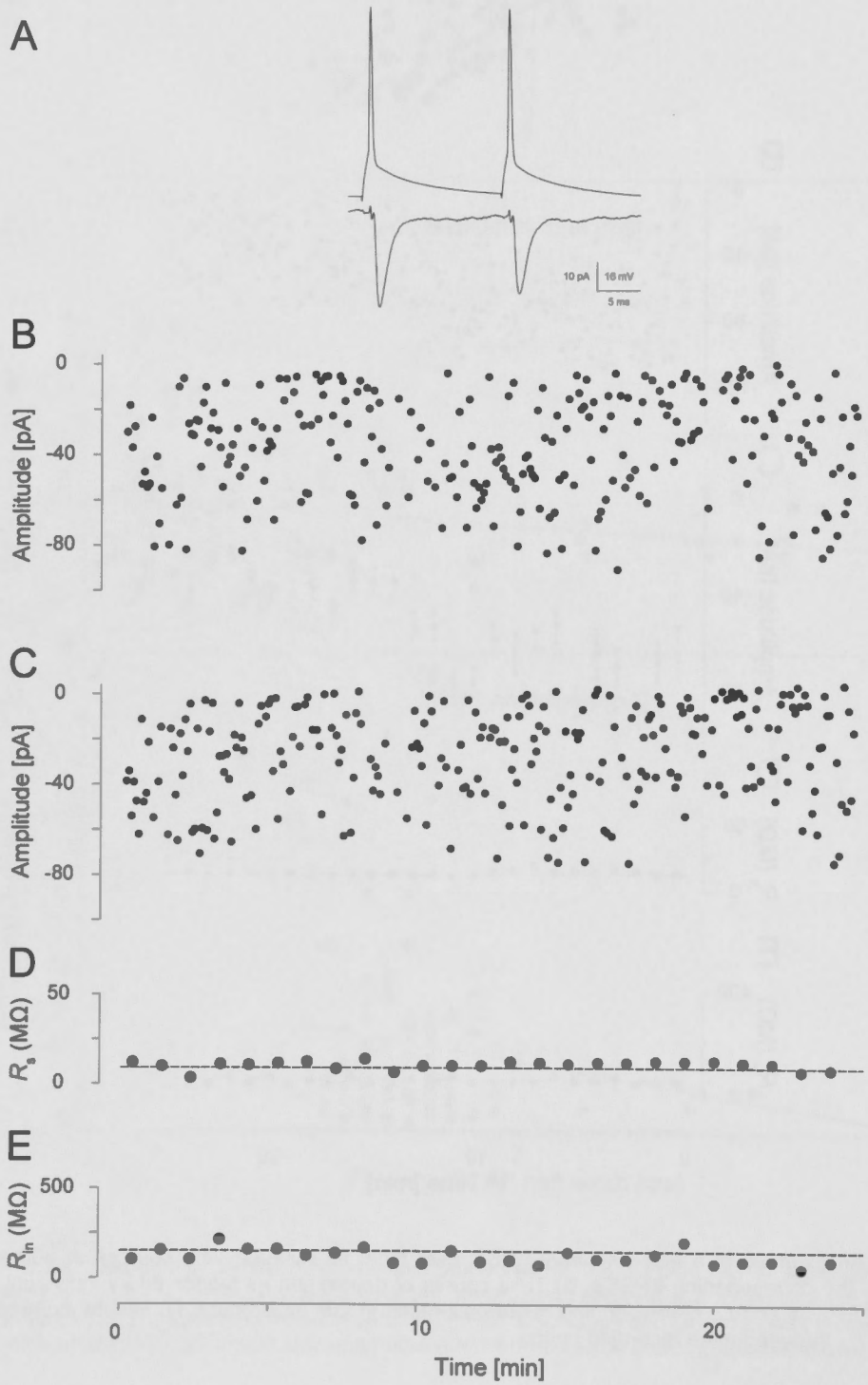

Figure 3.3.6. EPSCs evoked by paired-pulse stimuli. A) Average of 300 action potentials and EPSCs. Peak amplitudes of EPSCs plotted versus time when the stimuli were evoked of B) 1st and C) 2nd EPSC during a single experiment. In D and E minute averages are given for R_s and R_{in}.

An example of a pair of synaptically connected neurones stimulated with a paired-pulse paradigm is illustrated in figures 3.3.6A–C. In this example, the average time courses of the 300 APs and EPSCs are displayed in figure 3.3.6A. A comparison of the first and last 20 EPSC amplitudes in the two figures using the Student's *t*-test indicates no significant change in peak amplitudes, suggesting stationary conditions. The peak amplitudes of all 300 EPSCs were -34.5 ± 1.3 and -28.3 ± 1.2 pA. The first and second peak EPSC amplitudes over the time of recording are displayed in figures 3.3.6B and C, respectively, after manual measurement. From the 300 trials, only 252 first and second EPSCs were considered for the analysis. The calculated paired pulse ratio ($EPSC_2/EPSC_1$) was 0.82 ± 0.05.

The interpretation of a change in paired pulse ratio relies on the notion that the presynaptic action potentials do not significantly change within the 50 ms interval and the release characteristics are minimally affected by changes in the subsequent action potential. Therefore, I checked this by comparing the properties of the 1st and 2nd action potentials. In figure 3.3.7A, the amplitudes of the 2nd APs are plotted against that of the 1st. The dashed line indicates the line of equality; i.e. if there was no change between the two amplitudes. It is evident that most amplitudes of the 2nd AP are systematically smaller than those for the 1st. In fact, a linear regression with fixing the offset to zero provided a very significant correlation ($p_{Pr} < 10^{-40}$) with a slope of 0.94 ± 0.01. This fit is significantly different from the line of equality ($p_{ANCOVA} < 10^{-15}$). Comparing the respective half-widths, I found that both differed minimally. In fact, the line of fit is not different from that of equality ($p_{ANCOVA} = 0.78$).

Of all presynaptic neurones, the average amplitude of the second action potential was 94.6 ± 0.8 mV (ranging from 67.8 to 118.9 mV; Fig. 3.3.7A) with an average half-width of 1.5 ± 0.1 ms (ranging from 0.9 to 4.0 ms; Fig. 3.3.7B). On average ($n = 94$), I found that the second action potential was smaller in amplitude compared to the first ($p_{pt} = 10^{-21}$) while the half-width did not change ($p_{pt} = 0.47$).

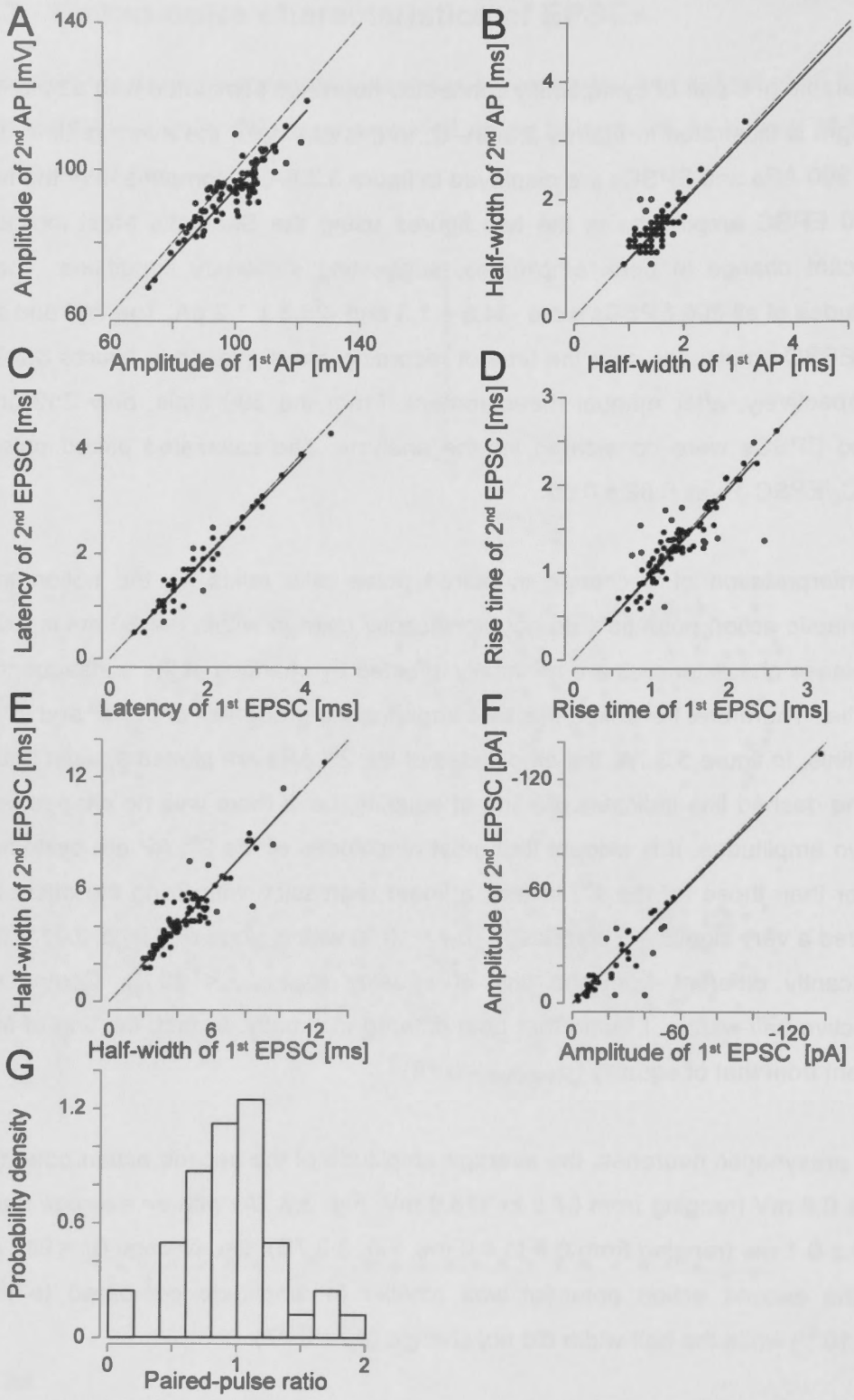

Figure 3.3.7. Comparison of the first and second action potentials and the characteristics of 1st and 2nd EPSCs. Plot of A) amplitudes second *vs.* first action potential for all experiments. The dashed line indicates identical values. The solid line is the best fit to the data. In B), half-widths of 2nd *vs.* 1st AP are given with the line of identity indicated (dash) and the best fit to the data (solid line). In each figure the dashed line indicates line of identity. Linear fits are indicated with the solid line. C) Latencies, D) rise times, E) half-widths and F) peak amplitudes of the 2nd EPSCs are plotted against the values of the 1st for all experiments. In F) only a subset is indicated which fulfilled stability criteria. G) Density of paired-pulse ratio given for all stabile recordings.

I will now describe some comparisons between the 1st and 2nd EPSCs. If the release process remained largely identical between the two stimuli, there should be minimal changes in latency between the two trials, which is illustrated in figure 3.3.7C. The fit constrained around zero is insignificantly different from the line of equality (p_{ANCOVA} = 0.22). A similar picture emerged when comparing the rise times and half-widths (Figs. 3.3.7D and E; p_{ANCOVA} = 0.56 and 0.29, respectively). From this analysis it can be concluded that, indeed, the kinetic properties of the EPSCs change minimally between the two stimulus trials.

When comparing the peak EPSC amplitudes, I observed that most 2nd EPSC amplitudes compared to the 1st ($p_{pt} = 10^{-13}$) depressed by a small amount. The average 2nd EPSC amplitude was -29.9 ± 3.5 pA compared to -31.4 ± 3.6 pA, indicating that, on average, at these synapses, there is little paired-pulse plasticity (0.95 ± 0.16; Fig 3.3.7F). When a fit to this data was done constrained to pass through zero, a highly significant fit was found ($r_{(40)}$ = 0.94; $p_{Pr} < 10^{-44}$), which was not different to the line of equality (p_{ANCOVA} = 0.73). The distribution of paired-pulse ratios is given in figure 3.3.7G showing a close to symmetrical distribution with a mean at 0.94 ± 0.06.

3.3.1.3. The setting of these EPSCs

In a previous set of papers, Fuhrmann *et al.* (2004) and Cowan & Stricker (2004) found that in layer V and IV, respectively, there were correlations between some synaptic properties and the higher moments (2nd, 3rd) of the EPSC fluctuations. To check if in layer II, the synapses share similar properties, I first tested if the paired pulse ratio were correlated with the average of the 1st EPSC amplitude, the implied hypothesis being that small EPSCs would show facilitation and large ones depression. I found no correlation between the paired-pulse ratio and the average EPSC amplitude ($r_{(40)}$ = 0.035, $p_r < 0.83$; Fig. 3.3.8A). When the CV^{-2} after adjusting for noise variance was plotted against the average peak EPSC amplitude, there was a significant correlation ($r_{(39)}$ = 0.65, $p_r < 0.0001$; Fig. 3.3.8B). For illustration purposes and assuming a binomial process, CV^{-2} equals $n * p / (1 - p)$. As the average EPSC equals $n * p * q$ and having found a linear correlation, the simplest explanation is that both the sizing of the EPSC and the CV^{-2} are dominated by n. This could indicate that the EPSC amplitudes are largely governed by the number of release sites (n). I next checked if the skew were correlated to average EPSC amplitude. I found no correlation between the skew and average peak EPSC amplitude ($r_{(40)}$ = 0.18, $p_r < 0.27$; Fig. 3.3.8C). Likewise, there

were no further significant correlations found between paired-pulse ratio and the skew ($r_{(40)}$ = -0.11, p_r < 0.5; Fig. 3.3.8D), CV^{-2} and the skew ($r_{(40)}$ = -0.22, p_r < 0.16; Fig. 3.3.8E) and CV^{-2} and the paired-pulse ratio ($r_{(40)}$ = -0.06, p_r < 0.69; Fig. 3.3.8F). This data then suggests that at these synapses, the probability of transmitter release has little influence on either the average EPSC, CV^{-2} and the skew, something very different to findings at layer V and IV synapses (Cowan & Stricker, 2004; Fuhrmann *et al.*, 2004).

3.3.1.4. Release-independence of EPSCs

At both layer IV and V synapses, evidence for release-dependence and -independence was found. The idea behind this concept is that if a vesicle is released from the vesicle pool, upon a 2nd stimulus, the pool is smaller and as a consequence, the 2nd EPSC is depressed. Therefore, one would expect an anticorrelation between the 2nd and the 1st EPSC (for more details see Fuhrmann *et al.*, 2004). I, therefore, checked in a subset of 16 recordings, in which about 300 1st and 2nd EPSCs could be successfully evoked and for which we had stationary conditions, if there was evidence for release dependence.

In figure 3.3.9, some examples are illustrated from this type of analysis. In A), from all 300 EPSCs, 217 amplitudes were recovered for which both the amplitude of the 2nd and 1st EPSCs could be measured manually. The average peak amplitudes of the 1st and 2nd EPSCs were -13.0 ± 0.7 and -11.6 ± 0.8 pA, respectively. These values are indicated by solid lines in the plot. The dashed lines indicate the value around release failures. In this case, a small depression was observed, which resulted in a paired-pulse ratio of 0.89 ± 0.12. As can be easily seen, there is no anticorrelation in this data set; in fact, the spread of points is dominated by failures of the 2nd after evoking the 1st EPSCs.

In B) a similar example is illustrated, here in the case for a facilitating synapse (283 EPSCs). The 1st and 2nd peak amplitudes of the EPSCs were -46.8 ± 1.2 and -49.5 ± 1.2 pA, respectively, giving rise to a paired-pulse ratio of 1.06 ± 0.05. Again, the value of the average EPSCs are given as solid lines and the dashes indicate failures. In this case, both 1st and 2nd EPSC are largely the same with a good spread around the two average values. Again, no anticorrelation could be identified.

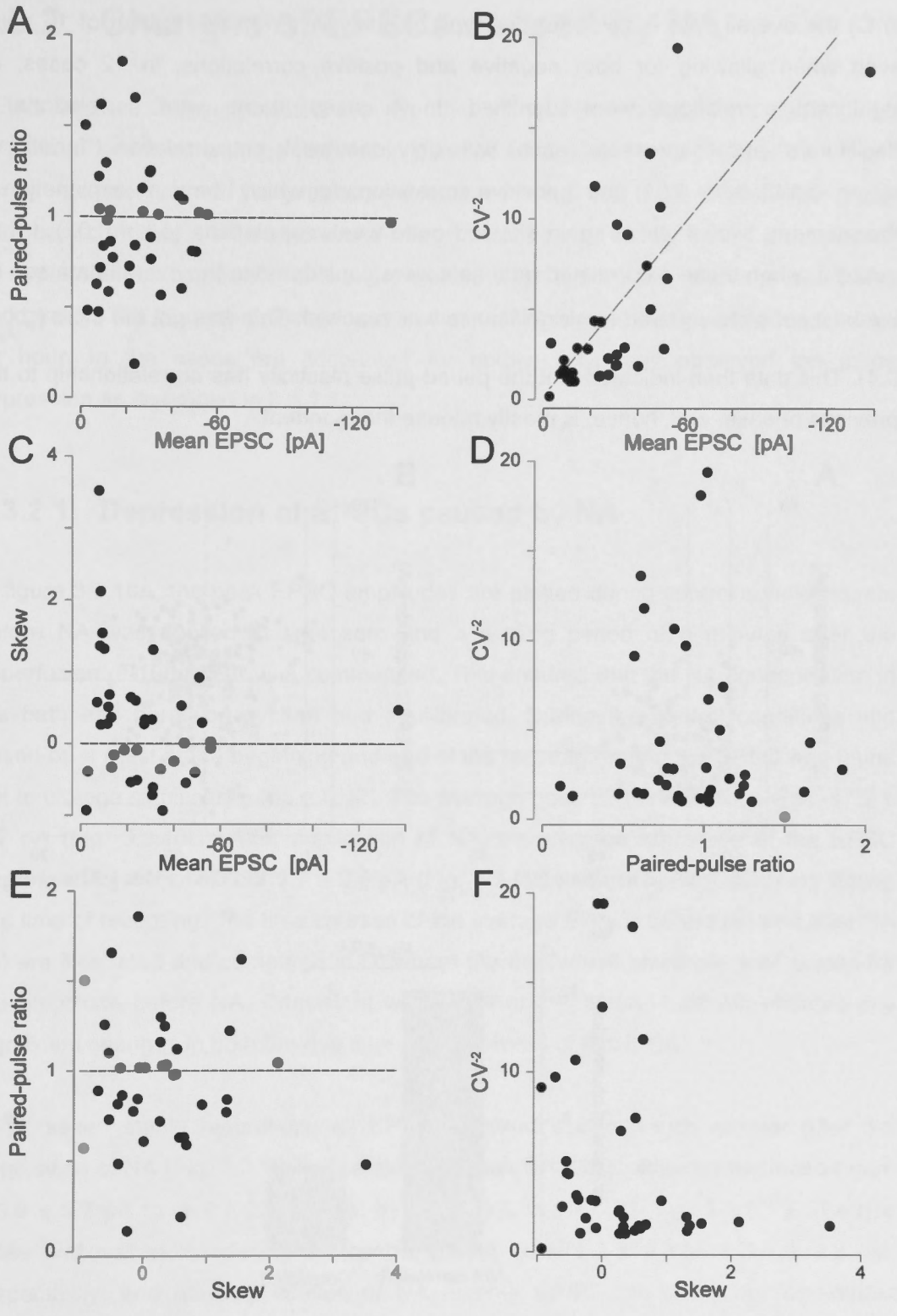

Figure 3.3.8. Characteristics of variability of EPSCs. In A) the paired pulse ratio is plotted against the average peak EPSC amplitude with the dashed line indicating no paired-pulse plasticity. B) Similar plot as in A) but with CV^{-2} against average peak EPSC amplitude. The solid line indicates a statistically significant positive correlation. In C – F, other moments of the variability are plotted against average amplitude, skew and paired-pulse ratio. No significant correlations were found. The dashed line in C indicates a skew of 0, suggesting a symmetrical distribution of EPSCs.

In C) the overall data is given for this type of analysis. From this subset of 16 pairs, even when allowing for both negative and positive correlations, in 12 cases, no significant correlations were identified. In 4 cases, there were correlations (2 "facilitators" and "depressors" each) with only one weak anticorrelation ("facilitator"; $r_{(283)} = -0.148$; $p_{Pr} = 0.01$) and 3 positive correlations for which I have no explanation at the moment, two of which again showed quite weak correlations ($p_{Pr} = 0.02$). I then asked if, when these 4 correlated data sets were considered in the overall data set, on the basis of a chi-squared test significance was reached. This was not the case ($p_{\chi^2_{16}} =$ 0.4). This data then indicates that the paired-pulse plasticity has no relationship to the previous release, and, hence, is mostly release-independent.

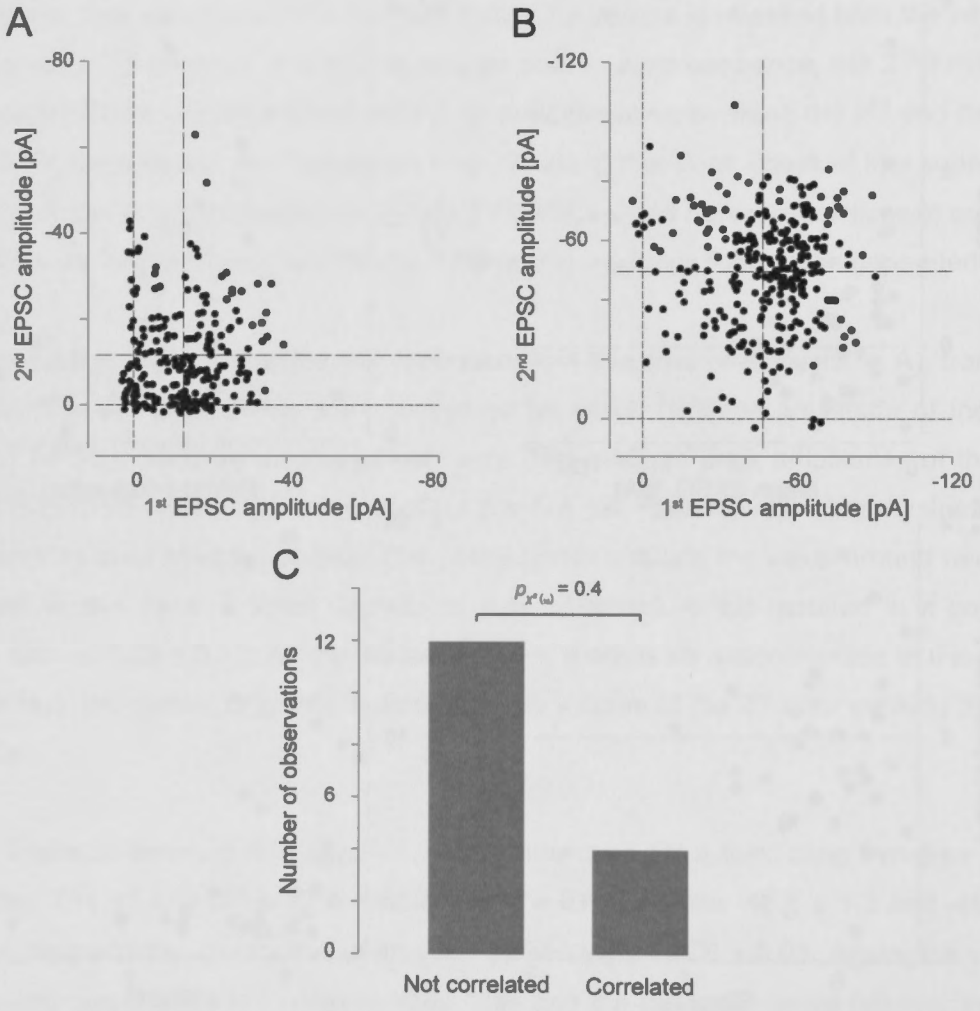

Figure 3.3.9. Release-independence of subsequent EPSCs. A) 1st and 2nd EPSCs are plotted against each other in the case of a synapse with paired-pulse depression. The dashed lines indicate the average values and the line around zero. B) Similar plot as in A) but in this case for a synapse showing facilitation. C) Summary plot of the data set of 16 stationary EPSCs showing the number of EPSCs, which did not show a correlation and the ones that showed one. On the basis of a χ^2 test, the number of correlated EPSCs is not significant.

3.3.2. Changes of EPSCs caused by NA

In this section, I directly tested the hypothesis that NA increases the peak EPSC amplitude consistent with the findings in part I of this thesis. Recording conditions and set-up are identical to the previous section including 300 trials at 0.25 Hz under stationary conditions, both before and after the application of NA. Out of a data set of 14 experiments, I could recover 7 experiments, which fulfilled the criteria of stationarity and quality. The biggest challenge was to maintain stable recording conditions for over an hour. In the cases not accounted for below, I typically observed the same depression as described in 3.3.1.1.

3.3.2.1. Depression of EPSCs caused by NA

In figure 3.3.10A, the peak EPSC amplitudes are plotted during control conditions; i.e. before NA was applied at time zero and a waiting period of 5 minutes after the superfusion of 10 µM NA was commenced. This ensured that the NA concentration in the bath and perfusion system had equilibrated. During the control conditions and based on a *t*-test at the beginning and end of the recordig period, the EPSC was found not to change significantly (p_{pt} = 0.42). The average peak EPSC amplitude was -47.2 ± 1.2 pA (Fig. 3.3.10B). After application of NA, the average amplitude of the EPSC depressed by 71 ± 5% to -13.7 ± 0.9 pA (Fig. 3.3.10C) but remained stationary during this time of recording. The time courses of the average EPSCs before (B) and after NA (C) are illustrated and compared in D, where the depressed amplitude was scaled for the amplitude before NA. Consistent with Part I of this thesis, I did not observe any significant changes in both the rise time and half-width of this EPSC.

In all seven stable recordings, all EPSC amplitudes were much smaller after the application of NA (Fig. 3.3.10E). The average peak EPSCs amplitudes decreased from -23.8 ± 5.7 pA to -8.1 ± 2.1 pA; i.e. by 66 ± 23% (p_{pt} = 0.01, Fig. 3.3.10F). The rise times and half-widths during the control period were 1.3 ± 0.1 and 3.9 ± 0.2 ms, respectively, and after application of NA, neither EPSC rise times nor half-widths changed (1.5 ± 0.1 and 4.1 ± 0.5 ms, respectively; p_{pt} = 0.4).

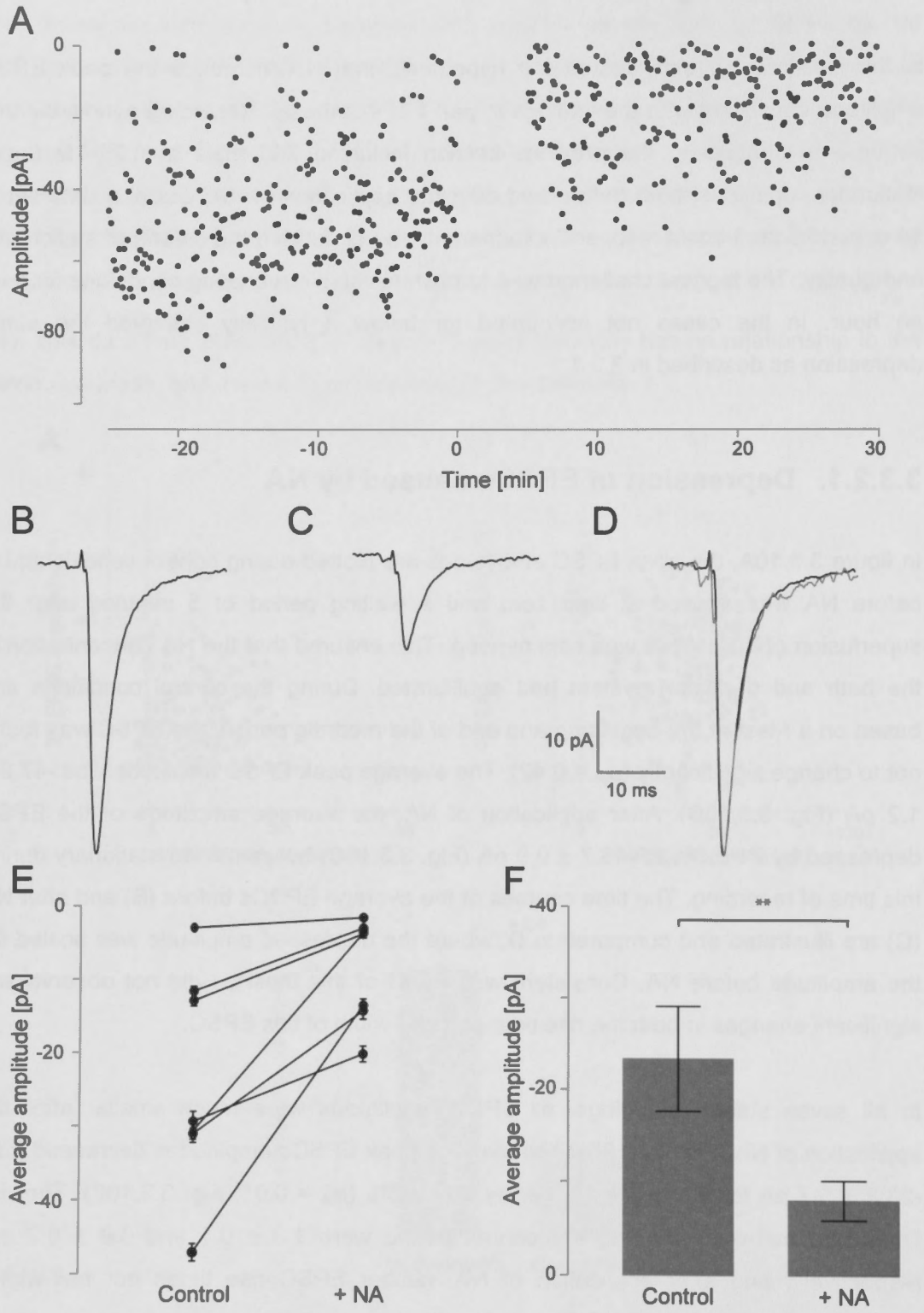

Figure 3.3.10. EPSCs before and after exposure to 10 µM NA. A) Time course of the peak EPSC amplitudes during the entire experiment. Superfusion of NA was started at time zero and maintained at a constant rate during the remainder of the experiment. The time course of the average EPSCs evoked B) during control conditions and C) after addition of NA. D) The normalised time course of the EPSC in NA (grey line) superimposed on that in control conditions (black line). E) Summary plot of all seven experiments with the extent of depression indicated for each experiment. F) Corresponding bar graph comparing the average peak EPSC amplitudes before and addition of NA. The double starred brackets indicate significance at $p_{pt} < 0.01$.

3.3.2.2. Paired-pulse ratio is not altered after NA exposure

To rule out that NA changed the shape of the action potential I checked if there were changes to the action potential amplitudes and half-widths caused by NA in this data set when two stimuli were applied at an interval of 50 ms (n = 7). I plotted the amplitudes and half-widths of the 2nd versus that of the 1st action potential. This is shown in figures 3.3.11A and B respectively. NA did not change either the amplitude of the action potential or its half-width (p_{pt} of 0.48 and 0.40, respectively). When these data points were included with the ones shown in figures 3.3.12A and B, no differences could be identified. I, therefore, conclude from this type of data that there is no or a minimal effect on the presynaptic action potential.

Utilising this paired-pulse paradigm, I also analysed the changes in the parameters of the EPSCs before and after application of NA for the example illustrated in the previous figure. The average time courses of the action potentials and EPSCs are given in figure 3.3.12. In A), the time courses are illustrated for the control period. In this case, the paired-pulse ratio was 1.10 ± 0.04. After superfusion with NA (B), a significant depression of both EPSCs was visible. The depression of the 2nd EPSC was 72.4 ± 4.2%. The time courses are overlayed in C) and peak-scaled in D). In this example where there was a slight facilitation to start with and after NA, there was a minimal (0.90 ± 0.10) and insignificant change in paired-pulse ratio (p_{pt} = 0.07).

For this type of data, I checked if there were systematic changes in the properties of the EPSCs. The relevant figures are 3.3.11C–E (filled circles during control and open circles in NA). There were no significant and systematic changes in either the latencies, rise times or half-widths of either the 2nd or 1st EPSCs (p_{pt} = 0.93, 0.58 and 0.49, respectively). When these data points were compared with the ones shown in figures 3.3.4A–C, no differences could be identified. Consistent with previous findings in this thesis, NA has no or minimal effects on the EPSCs in a paired-pulse protocol.

For all experiments after NA superfusion, I consistently observed a depression in both the EPSC amplitudes as shown in figure 3.3.11F. On average, the peak amplitudes of the 2nd EPSCs depressed from -23.2 ± 6.5 to -8.4 ± 0.1 pA, which corresponds to an average decrease of 64 ± 18% (p_{pt} = 0.03). Under these conditions, the average paired-pulse ratio did not significantly change (0.90 ± 0.08 to 1.09 ± 0.10; p_{pt} = 0.1, respectively).

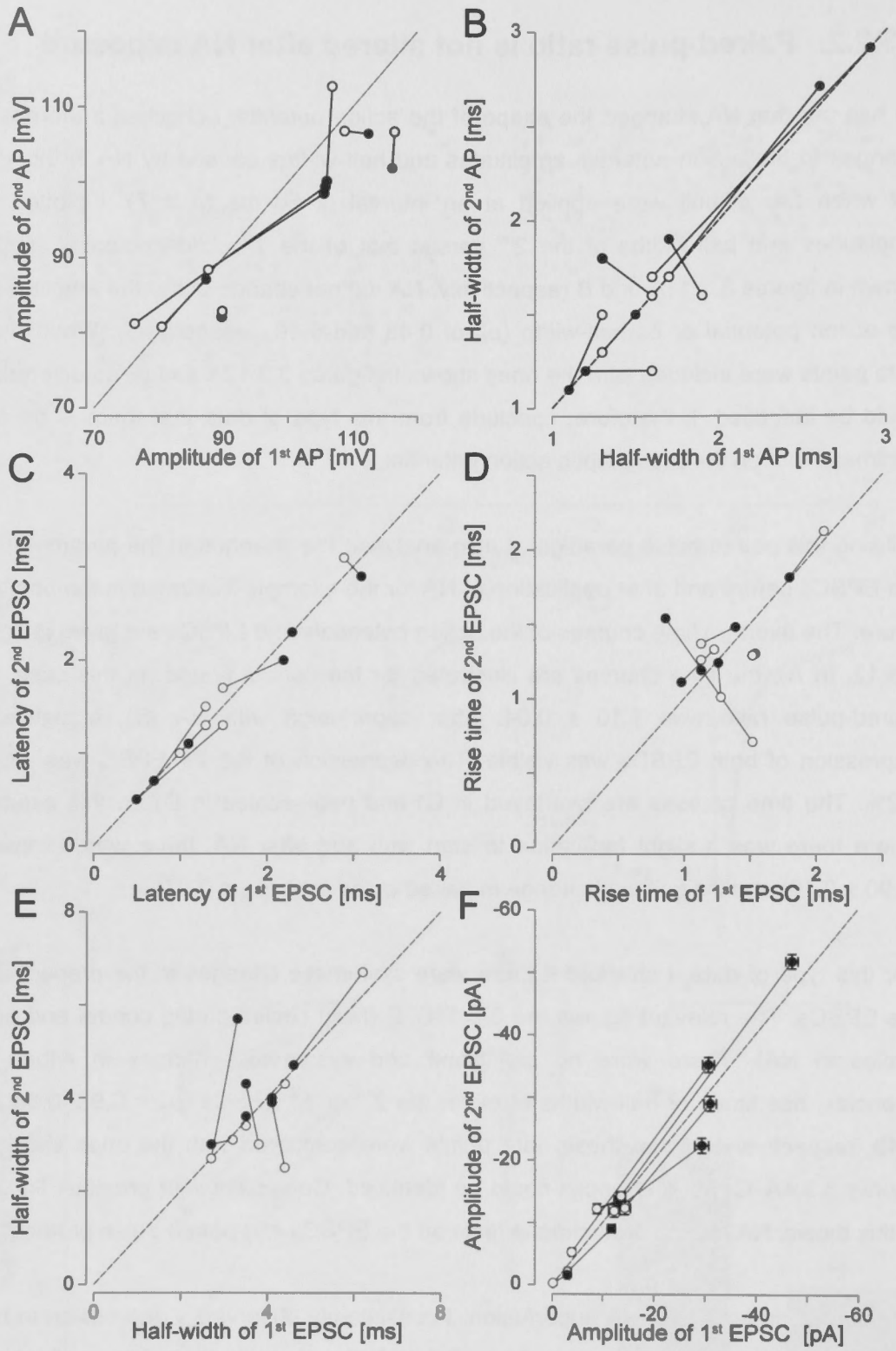

Figure 3.3.11. Comparison of some properties of the action potentials and EPSCs. Plot of A) amplitudes and B) half-widths of 2nd *vs.* 1st action potential before (filled circles) and after application of NA (open circles). In C – E, the latencies, rise times and half-widths before and after NA are plotted of the 2nd versus the 1st EPSCs, respectively. Dashed line indicates equality of both parameters. In F), the amplitudes of the 2nd and the 1st EPSCs are given for the control period (filled circles) and after NA (open circles). Error bars mark the values of the respective standard error of the mean (SEM).

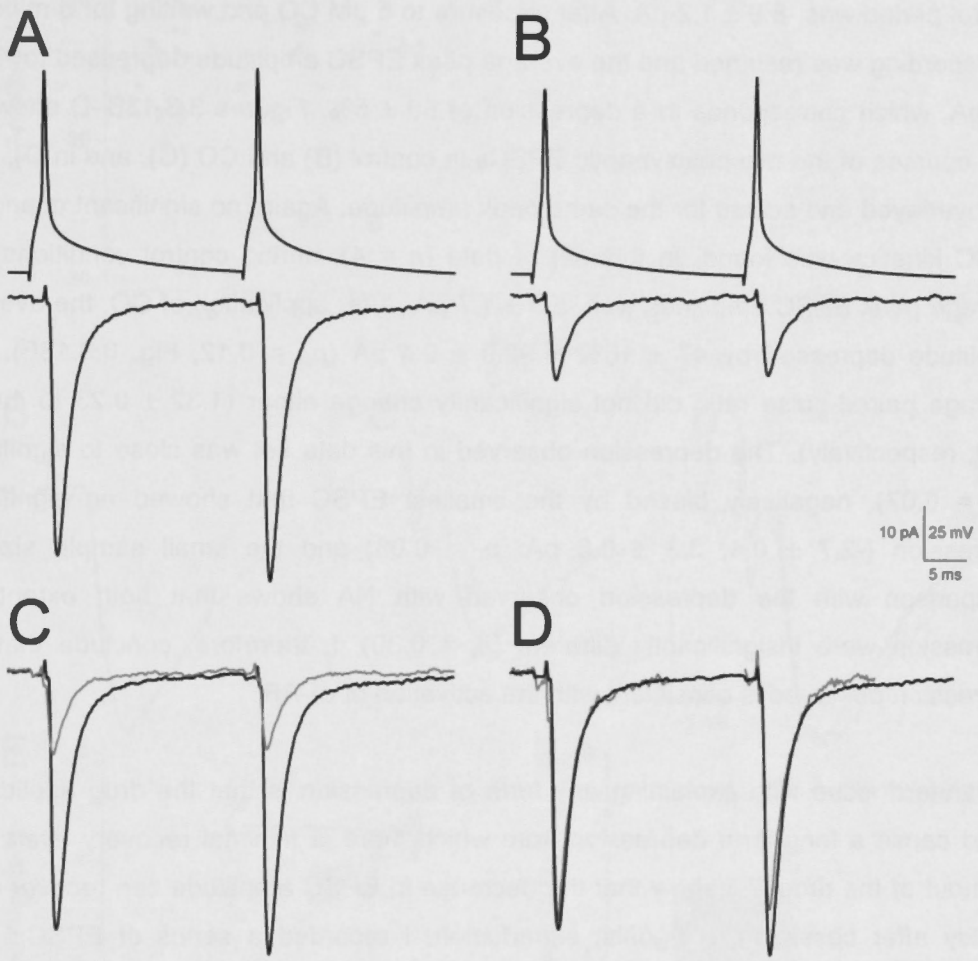

Figure 3.3.12. Paired-pulse stimulation before and after application of NA. The average action potentials and EPSCs during A) control condition and B) after application of NA are illustrated. In C), the two EPSC time courses are overlaid and in D) peak-scaled for the respective average EPSC during control condition (black line) and after application of NA (grey line).

3.3.2.3. α_1-AR activation depresses the EPSCs

To further corroborate that the response from NA is caused by α_1-AR activation, I applied the specific α_1-AR agonist cirazoline (CO, 5 µM) using the same paired-pulse paradigm as before. The 1st EPSC amplitudes over the 55 minutes of a single experiment are shown in figure 3.3.13A. The average peak EPSC amplitude during the control period was -8.9 ± 1.2 pA. After exposure to 5 µM CO and waiting for 5 minutes, the recording was resumed and the average peak EPSC amplitude depressed to -3.8 ± 0.7 pA, which corresponds to a depression of 60 ± 5%. Figures 3.3.13B–D show the time courses of the two postsynaptic EPSCs in control (B) and CO (C), and in D), both are overlayed and scaled for the same peak amplitude. Again, no significant change in EPSC kinetics was found. In this set of data (n = 4), during control conditions, the average peak EPSC amplitude was -5.5 ± 1.7 pA. After application of CO, the average amplitude depressed by 47 ± 16% to -2.9 ± 0.4 pA (p_{pt} = 0.12, Fig. 3.3.13F). The average paired-pulse ratio did not significantly change either (1.32 ± 0.23 to 1.06 ± 0.20, respectively). The depression observed in this data set was close to significant (p_{pt} = 0.07), negatively biased by the smallest EPSC that showed no significant depression (-2.7 ± 0.4, 3.3 ± 0.8 pA; p_t = 0.08) and the small sample size. A comparison with the depression observed with NA shows that both extents of depression were insignificantly different (p_t = 0.30). I, therefore, conclude that the depression observed is consistent with the activation of α_1-AR.

A standard issue with explaining any form of depression is that the drug application could cause a long-term depression from which there is minimal recovery even after washout of the drug. To show that the decrease in EPSC amplitude can recover quite quickly after cessation of agonist superfusion, I recorded a series of EPSCs after application of CO followed by the washout for at least 15 minutes. Such an experiment is shown in figure 3.3.14. During control conditions, the average peak amplitude was -8.7 ± 1.2 pA. After application of CO, the EPSC depressed to -2.3 ± 0.2 pA, i.e. by 73 ± 7%. After washout of CO and resumption of recordings after 5 minutes, the average amplitude of the first EPSC returned to -5.7 ± 1.3 pA (p_t = 0.15). This data suggests that the depression observed can be washed out and that the effect is not long-lasting, i.e. the depression can be relieved in less than 5 minutes.

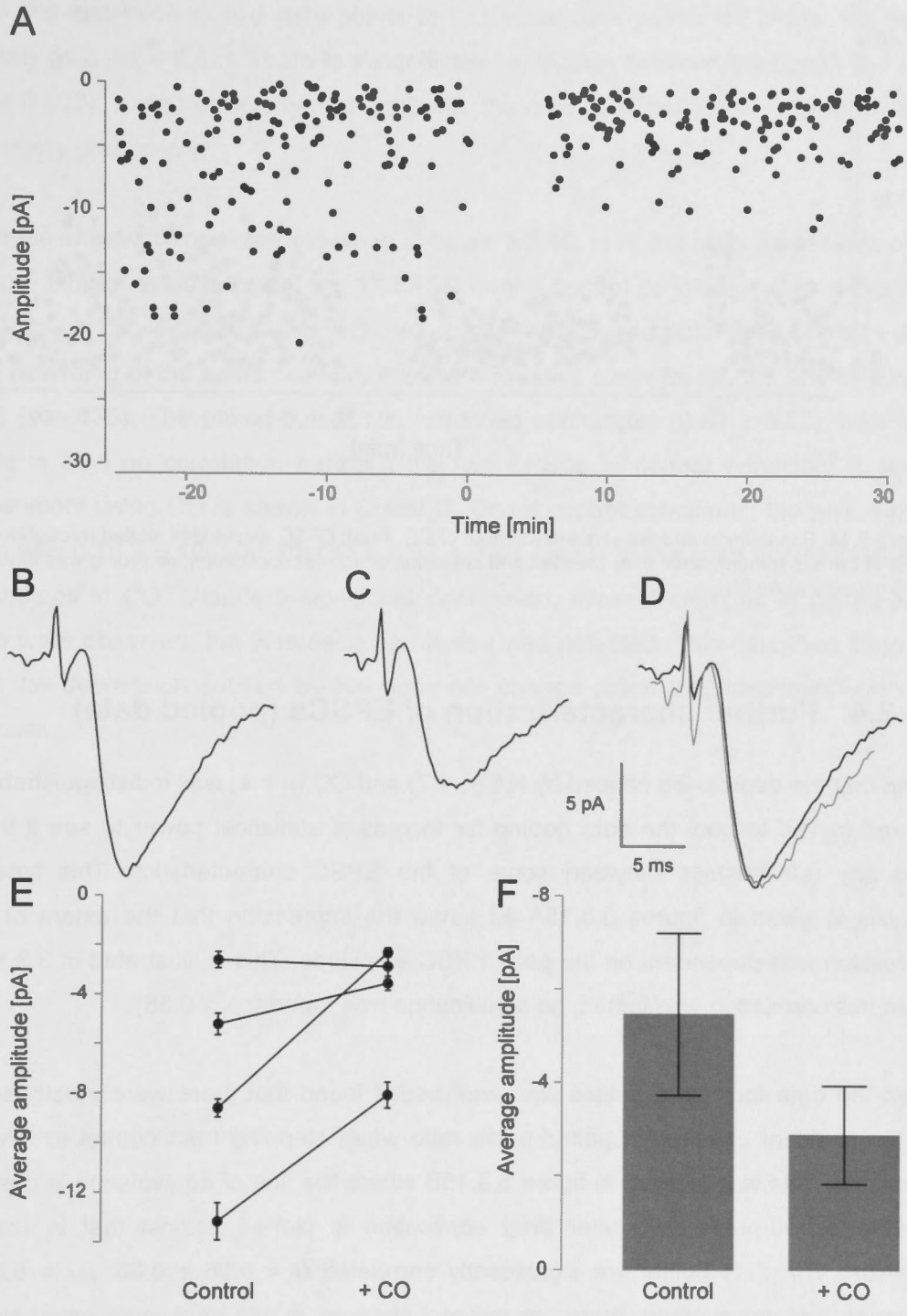

Figure 3.3.13. Peak EPSC amplitudes before and after application of 5 μM CO. A) Peak amplitudes plotted throughout a single experiment. Perfusion of CO was started at time zero and maintained at a constant rate. Recording was resumed after a break for 5 minutes. Time courses of EPSCs evoked B) during control conditions and C) after the application of CO. D) The normalised amplitude of the average EPSC after the application of CO (grey line) superimposed on that during control conditions (black line). E) Summary plot of all four experiments indicating the average amplitudes before and after agonist application with the lines following the values for each experiment. F) Pooled data of all 4 experiments comparing the average EPSC amplitudes before and after application of CO. The extent of depression was close to being significant in this small sample.

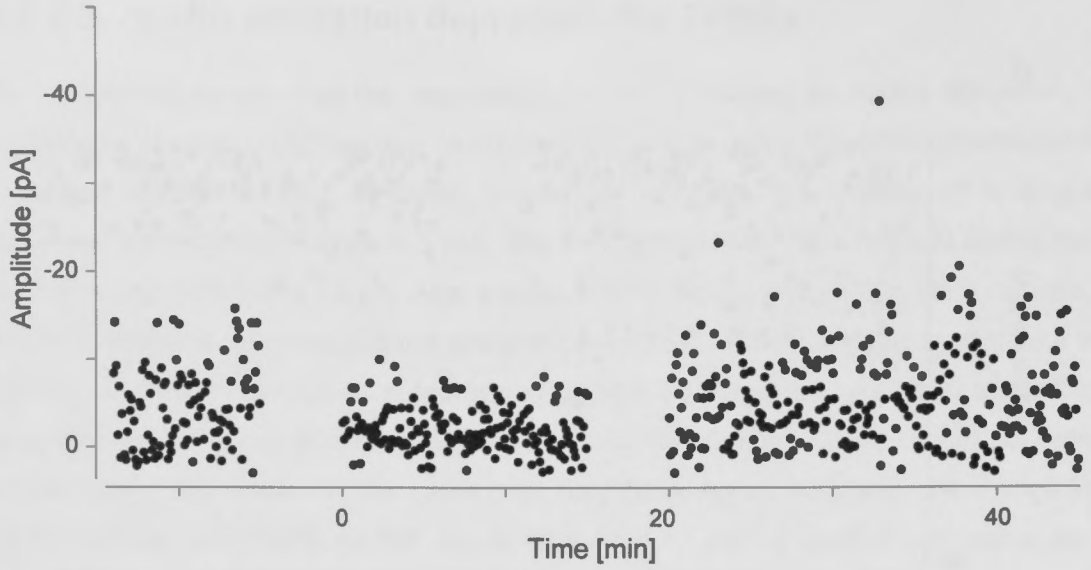

Figure 3.3.14. Exposure to and subsequent washout of CO. Peak EPSC amplitudes plotted throughout the course of the experiment. Both, after the start and cessation of agonist application, recording was resumed after 5 minutes of waiting.

3.3.2.4. Further characterization of EPSCs (pooled data)

Given that the depression caused by NA (n = 7) and CO (n = 4) was indistinguishable, I allowed myself to pool the data hoping for increased statistical power to see if there were any relationships between some of the EPSC characteristics. This type of analysis is given in figures 3.3.15A–E. I had the impression that the extent of the depression was dependent on the peak EPSC amplitude. This is illustrated in 3.3.15A. When this correlation was tested, no significance was found (p_{Pr} = 0.38).

When the data for paired pulses was analysed, I found that there were mostly small and insignificant changes in paired-pulse ratio when stepping from control to NA/CO conditions. This is illustrated in figure 3.3.15B where the line of equivalence is dashed and the paired-pulse ratio after drug application is plotted against that in control condition. The data points are significantly correlated (r = 0.96 ± 0.08; p_{Pr} = 0.005) indicating that, on average, there are minimal changes in this ratio when either NA or CO was applied, despite a considerable depression. Testing if this relationship was significantly different from the line of equality provided p_{ANCOVA} = 0.47, indicating that it is not different. In figure 3.3.15C, the relative change in average EPSC amplitude is plotted against the paired pulse ratio to see if the change was dependent on the probability during control conditions. This was not the case. Nor was there any change in the normalised paired-pulse ratio and the normalised EPSC amplitude (3.3.15D). In

E), the normalised CV^{-2} is plotted against the normalised average EPSC amplitude. With the exception of two data points in CO, most data points fall below the line of identity ($p_{ANCOVA} < 0.02$). There is a significant correlation between the points ($r = 0.80$; $p_{Pr} = 0.003$). Based on this type of analysis, the change in the EPSC is considered to be mostly presynaptic.

Release-independence was assessed in figure 3.3.16. In A, the peak amplitudes of the 2nd are plotted against that of the 1st EPSC during control conditions. In this example, the data set consisted of 219 EPSCs, which showed a paired pulse ratio of 0.82 ± 0.10. The recording of the same cell after exposure to NA is given for the 2nd and 1st EPSCs in B ($n = 135$). The paired-pulse ratio remained unchanged (0.83 ± 0.20). Like in A, there is also no correlation between the two EPSCs in neither condition. A similar experiment using CO is shown in C and D. Under control conditions, the paired-pulse ratio was 0.70 ± 0.10, and after CO, 0.92 ± 0.20. Like with the case in NA, in all such recordings in CO, despite a significant depression, minimal changes in paired-pulse ratio were observed, but in none, a correlation was detected. This data then suggests that the depression caused by NA does not change much the release-independent process.

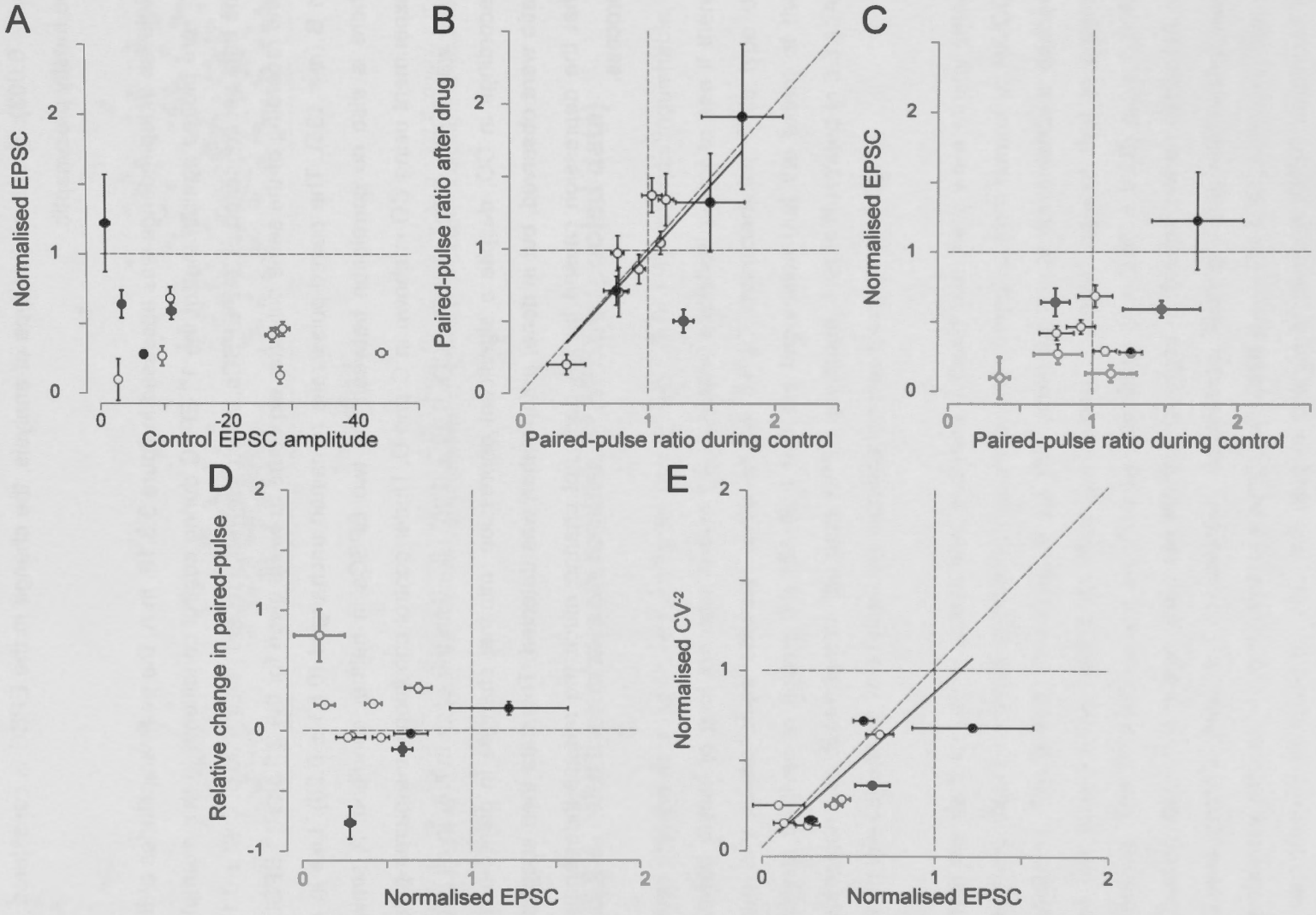
A
Normalised EPSC
2
1
0
0
-20
-40
Control EPSC amplitude
B
Paired-pulse ratio after drug
2
1
0
0
1
2
Paired-pulse ratio during control
C
Normalised EPSC
2
1
0
0
1
2
Paired-pulse ratio during control
D
Relative change in paired-pulse
2
1
0
-1
0
1
2
Normalised EPSC
E
Normalised CV-2
2
1
0
0
1
2
Normalised EPSC

Figure 3.3.15. Characteristic changes to EPSCs after drug application. A) Changes in peak amplitude of the 1st EPSC after application of NA (open circles) or CO (filled circles). Horizontal dashed line represents the normalised value of 1. B) Comparison of changes in paired pulse caused by application of NA or CO to the paired-pulse ratio during control condition. A solid line, fixed to the centre of the origin, was fitted to the data. Dashed line indicates equality of both parameters. C) Comparison of the depression caused by NA to the paired-pulse ratio during control condition. D) Comparison of the amount of depression to the 1st EPSC amplitude. E) Comparison of the CV^{-2} after application of NA.

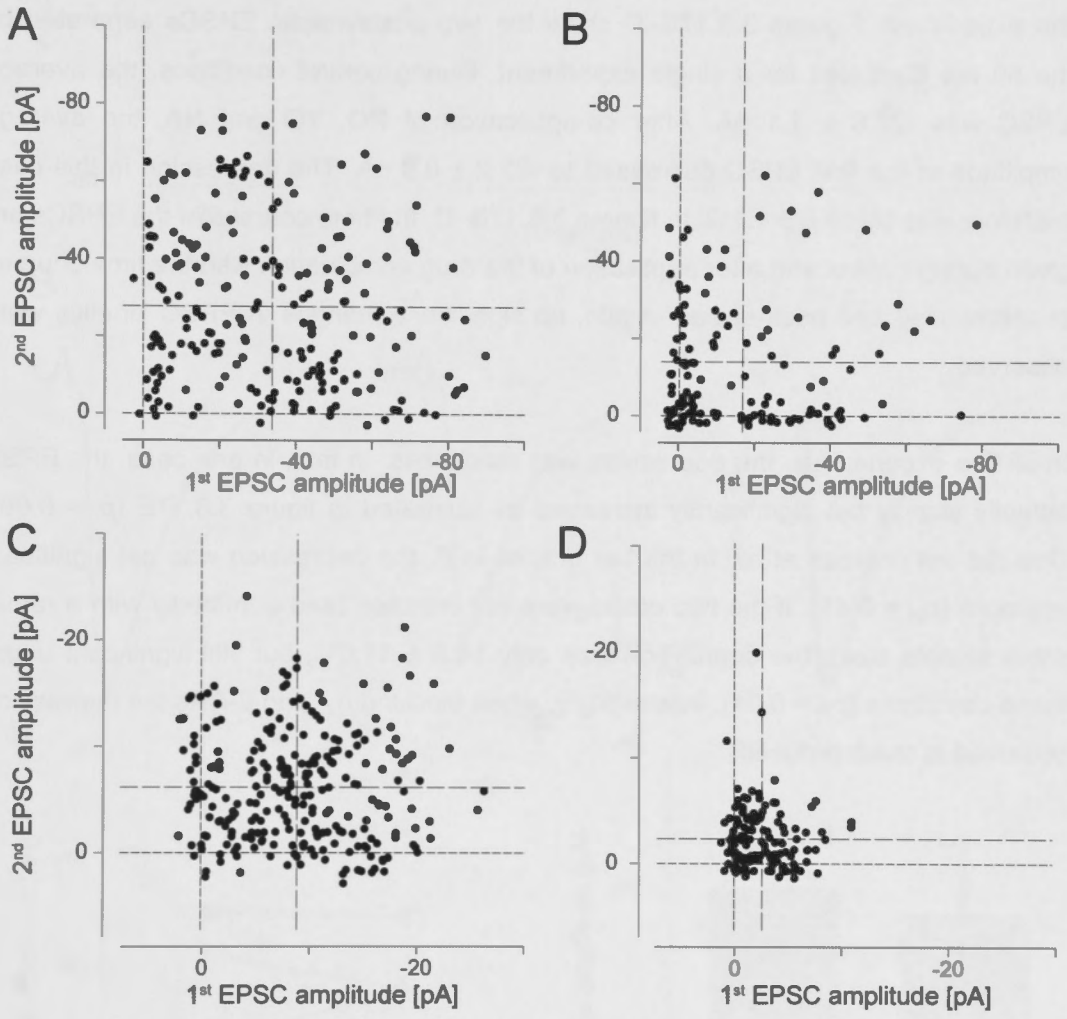

Figure 3.3.16. Examples of release-independence in NA and CO. 2nd EPSCs are plotted against 1st during control conditions as in A) and B) after application of 10 µM NA. The horizontal and dashed lines around zero indicate the failure range and the other set marks the average amplitude of the respective EPSC. A similar case is illustrated during control (C) and after superfusion with 5 µM CO (D).

3.3.2.5. Simultaneous block of α_2- and β-ARs

In an attempt to further narrow down that NA effectively predominantly activates α_1-ARs in this case, both the α_2-ARs (yohimbine, 1 µM) and β-ARs (propranolol, 1 µM) were blocked while the α_1-ARs were activated by 10 µM NA. After a control period, this combination of pharmacological compounds was superfused for five minutes before resuming the recording of another 300 EPSCs. The outcomes of such an experiment is given in figure 3.3.17A in which again the peak EPSC amplitudes are given throughout the experiment. Figures 3.3.17B–D show the two postsynaptic EPSCs separated by the 50 ms illustrated for a single experiment. During control conditions, the average EPSC was -27.6 ± 1.1 pA. After co-application of PO, YO and NA, the average amplitude of the first EPSC decreased to -22.2 ± 0.9 pA. The depression in this case therefore was by 19.6 ± 1.1%. In figures 3.3.17B–D, the time courses of the EPSCs are given during control and after application of the drug combination with the time courses superimposed and peak-scaled. Again, no significant changes in EPSC kinetics were observed.

In all five experiments, the depression was much less. In fact, in one case, the EPSC actually slightly but significantly increased as illustrated in figure 3.3.17E (p_t = 0.05). One did not depress at all. In the bar graphs in F, the depression was not significant anymore (p_{pt} = 0.41). If the two cases were not included (and admittedly with a rather small sample size), the depression was only 18.5 ± 11.6%, but still significant under these conditions (p_{pt} = 0.01), Interestingly, when blocking α_2- and β-ARs the depression observed is much reduced.

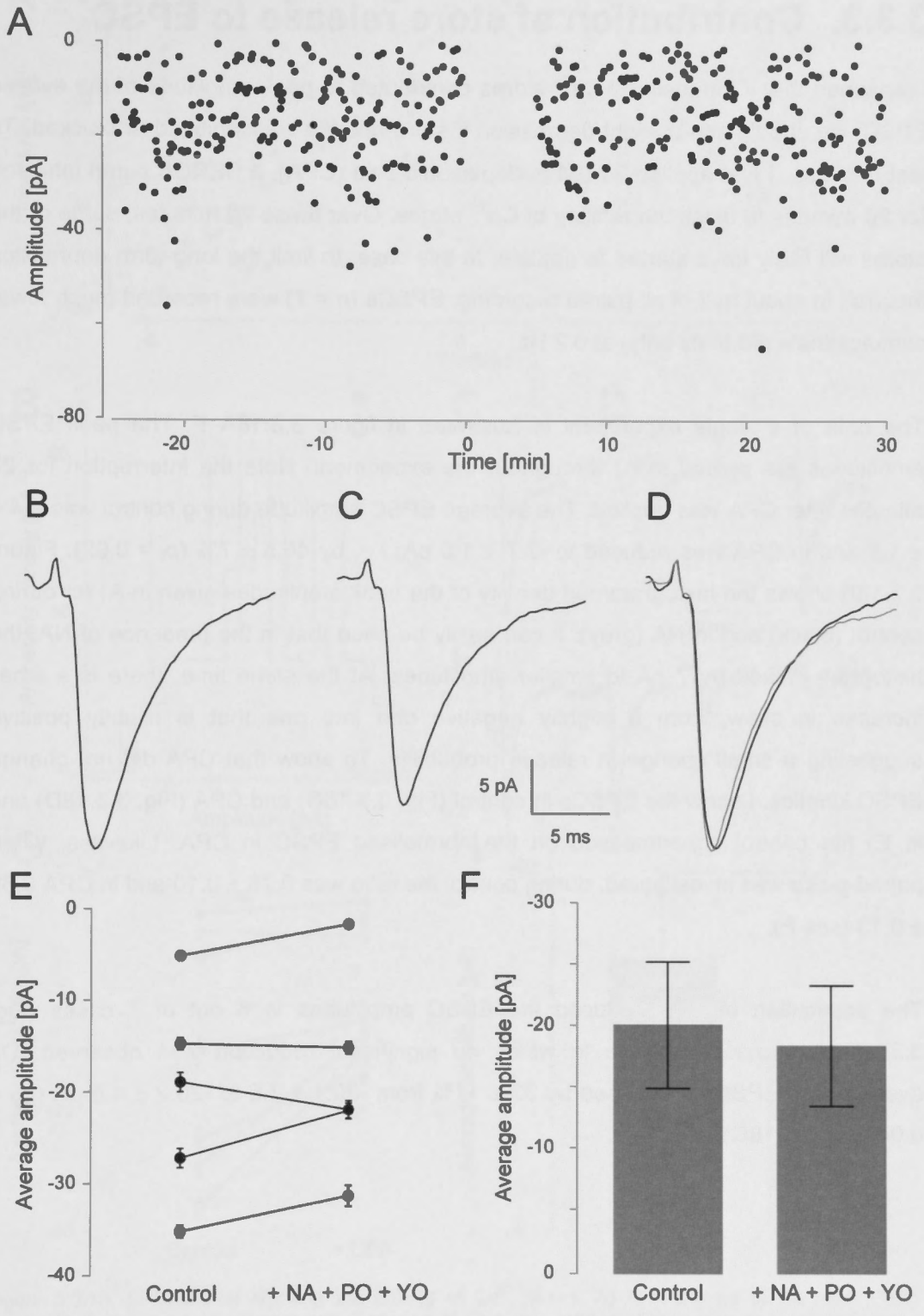

Figure 3.3.17. EPSC before and after exposure to PO, YO and NA. A) Peak EPSC amplitudes are plotted throughout the entire experiment. Perfusion of PO, YO, NA and were started at time zero and maintained at a constant rate the recording resumed after 5 minutes of wash-in. Time course of the average EPSCs evoked B) before and C) after perfusion of PO, YO and NA. D) Normalised amplitude of the EPSC time course after (grey) superimposed on that during control conditions (black). E) Summary plot of all five experiments with the extent of the plasticity indicated for each experiment. F) Corresponding bar graph comparing the peak EPSC amplitudes before and after. The changes were insignificant.

3.3.3. Contribution of store release to EPSC

I reasoned that if intracellular Ca^{2+} stores contributed to peak amplitude of the evoked EPSC, we should see a slight depression if store release was inhibited or blocked. To test this idea, I first applied 20 µM cyclopiazonic acid (CPA), a SERCA pump inhibitor, for 20 minutes to block the refilling of Ca^{2+} stores. Over these 20 minutes, some of the stores will likely have started to deplete. In this case, to limit the long-term depression incurred in about half of all paired recording, EPSCs (n = 7) were recorded much fewer stimulus trials (60 trials only) at 0.2 Hz.

The data of a single experiment is illustrated in figure 3.3.18A–F. The peak EPSC amplitudes are plotted in A) throughout the experiment. Note the interruption for 20 minutes after CPA was applied. The average EPSC amplitude during control was -14.4 ± 1.1 and in CPA was reduced to -7.7 ± 1.0 pA; i.e. by 46.5 ± 7% (p_t = 0.02). Figure 3.3.18B shows the histogrammed density of the peak amplitudes given in A) for during control (black) and in NA (grey). It can easily be seen that in the presence of NA, the histogram shifted by 7 pA to smaller amplitudes. At the same time, there is a small increase in skew, from a slightly negative one into one that is slightly positive suggesting a small change in release probability. To show that CPA did not change EPSC kinetics, I show the EPSCs in control (Fig. 3.3.18C) and CPA (Fig. 3.3.18D) and in E) the control superimposed on the normalised EPSC in CPA. Likewise, when paired-pulse was investigated, during control the ratio was 0.78 ± 0.10 and in CPA 0.66 ± 0.13 (see F).

The application of CPA reduced the EPSC amplitudes in 6 out of 7 cases (Fig. 3.3.18F); there is one case in which no significant reduction was observed. On average, the EPSCs decreased by 33 ± 11% from -30.1 ± 7.6 to -20.2 ± 4.5 pA (p_{pt} = 0.04, Fig. 3.3.18G).

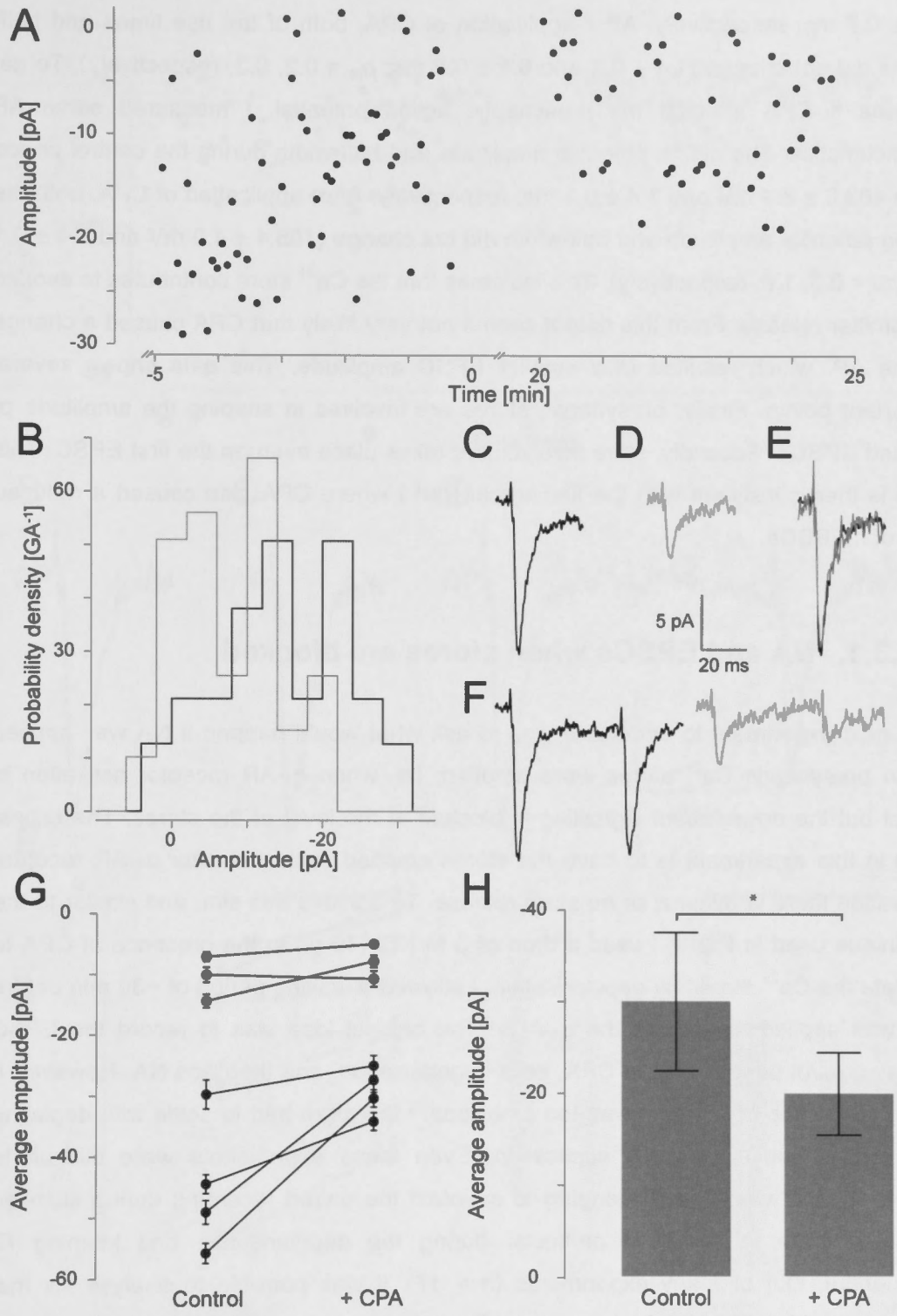

Figure 3.3.18. EPSCs after blocking the refilling of Ca^{2+} stores. A) Time course of the peak EPSC amplitude during the entire experiment. Perfusion of CPA was started at time zero and maintained at a constant rate throughout. B) Histograms of EPSCs before (black bar) and after (grey bar) application of CPA. Average EPSC evoked C) during control conditions (black line) and D) after application of CPA (grey line). E) The normalised amplitude of the average EPSC in CPA (grey line) superimposed on that in control conditions (black line). F) Two EPSCs evoked during control conditions (black line) and after application of CPA (grey line). G) Summary plot of all seven experiments with the depression indicated for each experiment. H) Corresponding bar graph comparing the average EPSC amplitudes before and after application of CPA. Single starred brackets indicate significant change ($p_{pt} < 0.05$).

The rise times and half-widths of the 1st EPSCs in the control period were 1.3 ± 0.1 and 5.4 ± 0.7 ms, respectively. After application of CPA, both of the rise times and half-widths did not change (1.4 ± 0.1 and 6.1 ± 0.8 ms; p_{pt} = 0.2, 0.3, respectively). To get an idea if CPA affected the presynaptic action potential, I measured some AP characteristics. The action potential amplitude and half-width during the control period were 103.6 ± 3.4 mV and 1.4 ± 0.1 ms, respectively. After application of CPA, both the action potential amplitude and half-width did not change (105.4 ± 4.0 mV and 1.4 ± 0.1 ms; p_{pt} = 0.3, 1.0, respectively). This indicates that the Ca^{2+} store contributes to evoked transmitter release. From this data it seems not very likely that CPA caused a change in the AP, which resulted in a smaller EPSC amplitude. This data shows several important points. Firstly, presynaptic stores are involved in shaping the amplitude of evoked EPSCs. Secondly, store involvement takes place even on the first EPSC. This data is then consistent with the findings in Part I where CPA also caused a reduced rate of mEPSCs.

3.3.3.1. NA and EPSCs when stores are blocked

The next experiment to undertake was to ask what would happen if NA was applied when presynaptic Ca^{2+} stores were emptied; i.e. when α_1-AR receptor activation is intact but the downstream signalling is blocked at the level of the stores. The critical step in this experiment is to have the stores emptied such that after α_1-AR receptor activation there is minimal or no store release. To achieve this aim, and similar to the technique used in Part I, I used a drop of 3 M KCl (40 µl) in the presence of CPA to deplete the Ca^{2+} stores by depolarisation. I allowed a waiting period of ~30 min before NA was applied to activate the α_1-ARs. The original idea was to record the EPSC during control period, then in CPA, do a depolarisation, and then add NA. However, it proved that this experiment was too ambitious. I therefore had to settle with depleting stores and subsequent NA application. Even these experiments were difficult to perform, as it was very challenging to maintain the paired recording during such an extended time (> 1 h), in particular during the depolarisation and keeping R_s throughout. Out of many experiments (n = 17), it was possible to analyse six that fulfilled the criteria of stationarity and quality.

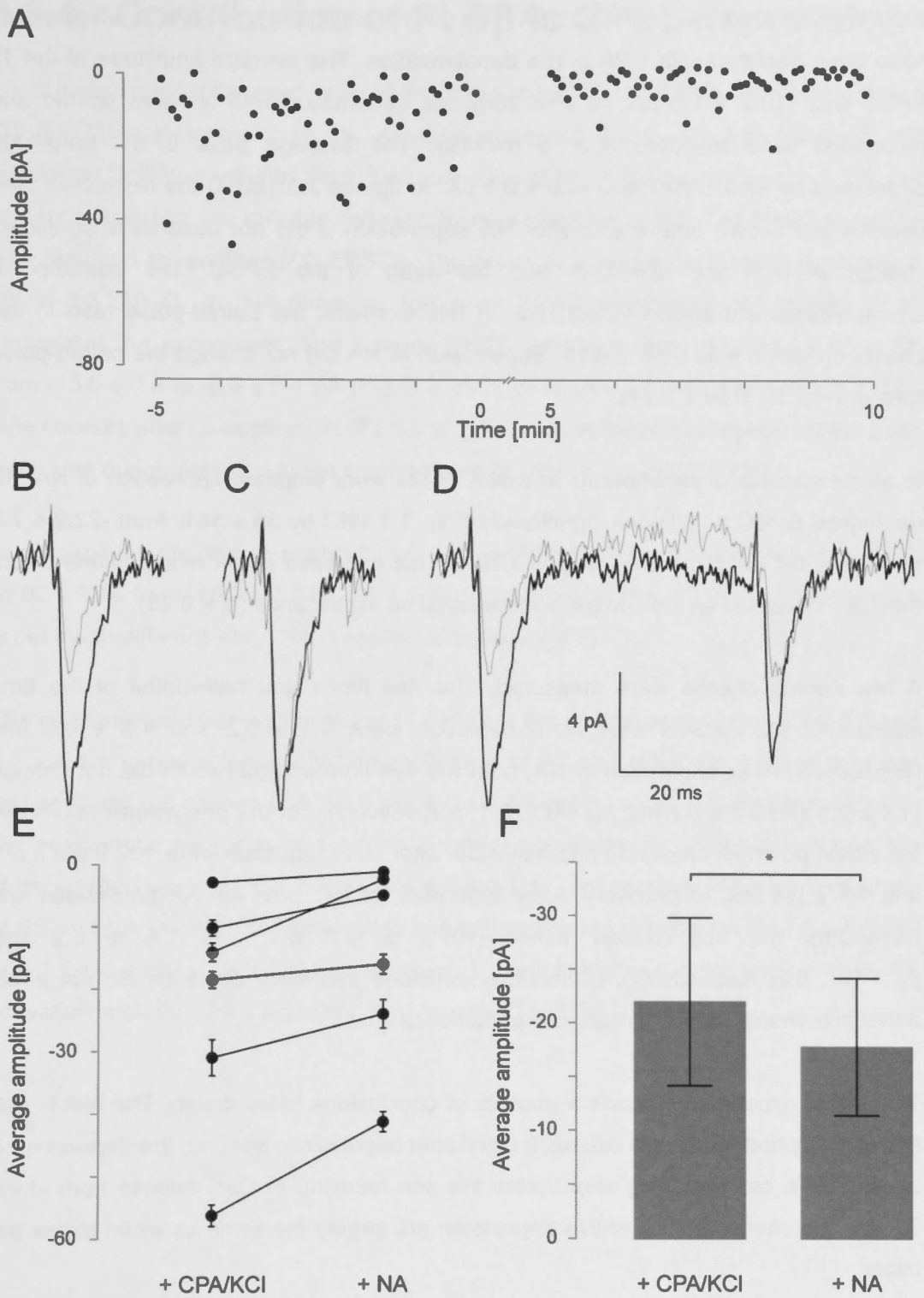

Figure 3.3.19. Characteristics of EPSCs after store depletion and subsequent exposure to NA. A) Peak EPSC amplitudes plotted during the course of a single experiment. Superfusion with NA was started at time zero and maintained at a constant rate thereafter. B) EPSC time course after store depletion (black line) and subsequent superfusion with NA (grey line). C) The normalised amplitude of the average EPSC in NA (grey line) superimposed on that in control conditions (black line). D) Two EPSCs evoked after store depletion (black line) and subsequent application of NA (grey line). E) Summary plot of all six experiments with the extent of depression indicated for each individual experiment. F) Corresponding bar graph comparing the peak EPSC amplitudes before and after application of NA. The starred bracket indicates a significant depression.

In a single experiment, the peak EPSC amplitudes over the course of such an experiment is shown in figure 3.3.19A. The control condition is the one in which stores have been depleted with CPA and a depolarisation. The average amplitude of the 1st EPSC was -10.2 ± 1.3 pA. At time zero, the superfusion with NA was started and recordings were resumed after 5 minutes. The average peak EPSC amplitude depressed by 52.0 ± 10.7% to -4.9 ± 0.8 pA. In figures 3.3.19B–D the respective time courses are shown before and after NA superfusion. I did not observe a significant change in both the rise time and half-width of the EPSC. The paired-pulse characteristics are shown in 3.3.19D. In this example, the paired-pulse ratio in the control condition was 0.66 ± 0.14. Superfusion of NA did not change the paired-pulse ratio (p_{pt} = 0.15, 0.84 ± 0.27).

In all six successful experiments in which stores were emptied, application of NA still depressed EPSC amplitudes significantly (Fig. 3.3.19E) by 33 ± 18% from -22.2 ± 7.8 to -14.9 ± 6.4 pA (p_{pt} = 0.02, Fig. 3.3.19F). This decrease is not much different from that with stores full as the comparison revealed no significance (p_t = 0.20).

A few control checks were measured. The rise times and half-widths of the time courses of the EPSCs after store depletion were 1.2 ± 0.2 and 4.5 ± 0.5 ms, respectively. After application of NA, both the rise time and half-width did not change (1.4 ± 0.1 and 5.5 ± 0.7 ms; p_{pt} = 0.2, 0.1, respectively). For the presynaptic neurones, the action potential amplitude and half-width after store depletion were 102.9 ± 3.9 mV and 1.4 ± 0.1 ms, respectively. After application of NA, both the AP amplitudes and half-widths did not change either (107.9 ± 5.7 mV and 1.6 ± 0.2 ms; p_{pt} = 0.1, 0.2, respectively). I, therefore, conclude that store depletion did not affect either presynaptic or postsynaptic characteristics much.

This set of experiments allows a number of conclusions to be drawn. The first is that NA with emptied stores still causes a significant depression. Second, the depression is caused by a cell signalling step before the one resulting in Ca^{2+} release from store. Thirdly, the characteristics of this depression are largely the same as when stores are intact.

3.3.4. Contribution of PLCβ to EPSC depression

I next investigated if the production of IP_3 from the hydrolysis of PIP_2 via phospholipase Cβ (PLCβ) was involved in the depression caused by α_1-AR activation. 30 μM edelfosine (ES) was used to block the production of IP_3. After a control period, ES was first superfused for two minutes, followed by co-application of NA. The EPSC recording was resumed for another 300 EPSCs. The result of a single experiment is shown in figure 3.3.20A–D. In this example, the peak EPSC amplitudes are plotted in A) throughout the experiment. The average EPSC amplitude was reduced by 38 ± 3% from -13.0 ± 0.8 to -8.0 ± 0.4 pA (Fig. 3.3.20C). In figures 3.3.20D, the average EPSC time courses after co-application of ES and NA were overlayed and scaled for the peak amplitude during control. I found no significant change in the EPSC kinetics.

In six experiments, the co-application of ES and NA decreased the EPSC amplitudes by 65 ± 23% from -16.1 ± 3.0 to -5.6 ± 1.7 pA (p_{pt} = 0.004; Fig. 3.3.20F). This decrease is not much different when NA is applied alone (p_{pt} = 0.6).

The rise times and half-widths of the 1st EPSC in the control period were 2.2 ± 0.5 and 6.1 ± 1.4 ms, respectively. After co-application of ES and NA, both the rise time and half-width did not change (2.4 ± 0.5 and 6.0 ± 1.34 ms; p_{pt} = 0.5, 0.5, respectively). For the presynaptic neurones, the action potential amplitude and half-width during the control period were 110.8 ± 2.3 mV and 1.4 ± 0.1 ms, respectively. After co-application of ES and NA, both the AP amplitudes and half-widths did not change (114.0 ± 5.1 mV and 1.7 ± 0.3 ms; p_{pt} = 0.3, 0.2, respectively). I conclude that the depression by α_1-AR activation is caused by a signalling step proximal to PLCβ activation.

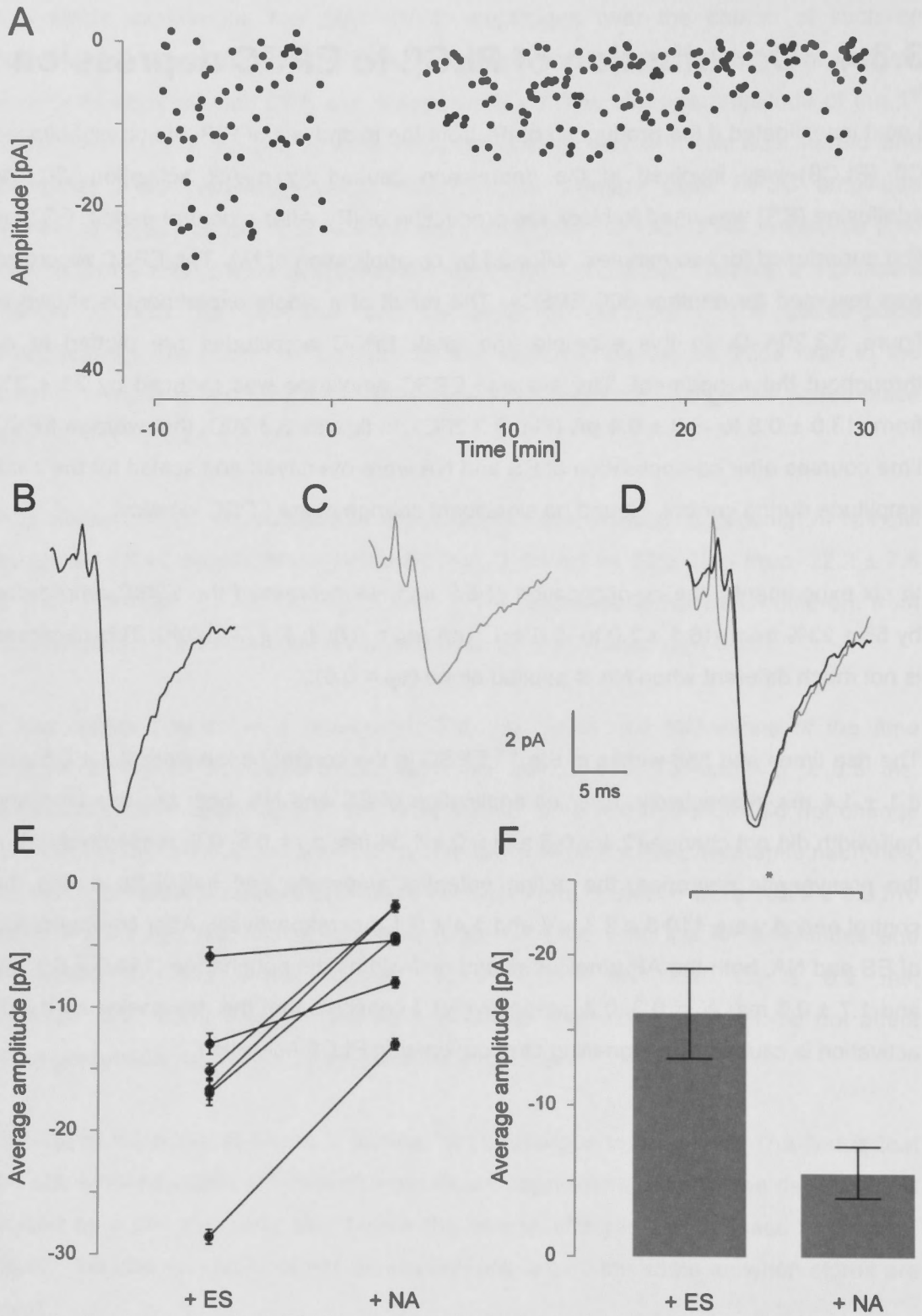

Figure 3.3.20. Characteristics of EPSCs after inhibiting PLCβ and subsequent exposure to NA. A) Peak EPSC amplitudes plotted during the course of a single experiment. Superfusion with NA was started at time zero and maintained at a constant rate thereafter. B) EPSC time course after inhibiting PLCβ (black line) and C) subsequent superfusion with NA (grey line). D) The normalised amplitude of the average EPSC in NA (grey line) superimposed on that in control conditions (black line). E) Summary plot of all six experiments with the extent of depression indicated for each individual experiment. F) Corresponding bar graph comparing the peak EPSC amplitudes before and after application of NA. The starred bracket indicates a significant depression.

3.3.4.1. Control experiment for ES

Because the addition of edelfosine did not change the depression, it could be argued that this drug did not work as predicted. To check that PLCβ was indeed blocked by ES, spontaneous EPSCs (sEPSC) were recorded and compared before and after co-application of ES and NA. The result of a single experiment is shown in figures 3.3.21A–E. In this example, co-application of ES and NA did not change sEPSC frequency (51 ± 1 *vs.* 53 ± 1 Hz) and amplitude. The average amplitudes of the mEPSC before (black line), after co-application of ES and NA (grey line) were normalised to the amplitude of the control and truncated at 50% of the decay phase, shown in figure 2.3.21E. I observed no significant change in the mEPSC kinetics after co-application of ES and NA.

In four experiments, co-application of ES and NA did not change the average sEPSC frequency (54 ± 3 *vs.* 49 ± 7; p_t = 0.29; Fig. 3.3.21F) and amplitude (-13.5 ± 1.0 *vs.* -8.7 ± 1.8 pA; p_t = 0.5; Fig. 3.3.21G), suggesting that ES fully blocked PLCβ.

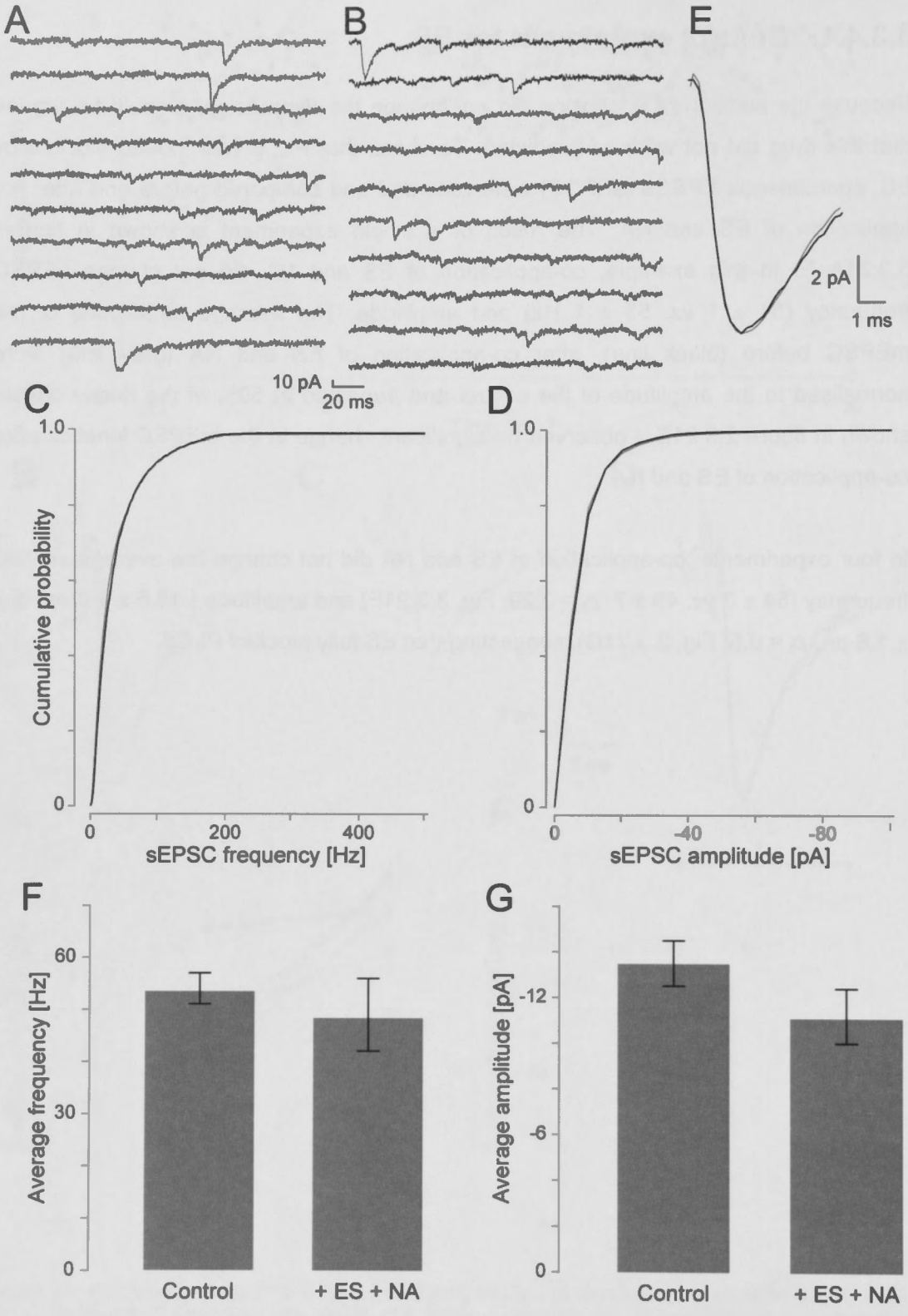

Figure 3.3.21. ES abolished the increase in sEPSC frequency caused by NA. A) Recording sequences taken before and B) after the co-application of ES and NA. C) cPDF of instantaneous sEPSC frequencies and D) amplitudes before (black line) and after co-application of ES with NA (grey line). Co-application of ES and NA did not increase sEPSC frequency or amplitude. E) Normalised amplitude of average sEPSC time course before (black line) and after the co-application of ES with NA (grey line). F) The average instantaneous sEPSC frequencies and G) amplitudes after before and after co-application of ES with NA.

3.3.5. Speed-up from depression by NA

As NA depresses the peak EPSC amplitudes without much altering other release characteristics, I wondered if it would alter the recovery from depression when EPSCs were evoked by multiple action potentials. To test this idea in a next set of experiments I applied 20 action potentials at a rate of 50 Hz to establish a steady-state depression. Thereafter, with an interval of 500 ms, I evoked an action potential to check the recovery from this depression and characterize R_{50}; i.e. the rate of recovery at 50 Hz. These stimulus sequences were repeated every 25 s.

Such an experiment is illustrated in figure 3.3.22. During control conditions (A), the 1st EPSC had an average peak amplitude of -33.0 ± 5.4 pA and the 2nd -20.8 ± 3.4 pA. It showed paired-pulse depression of 0.63 ± 0.23. It can be seen that in this sequence of stimuli a steady-state EPSC is reached of -2.9 ± 0.7 pA. When the recovery stimulus was evoked, the peak amplitude was -23.2 ± 3.9 pA. From this data, R_{50} at 500 ms can be determined. In this case, it was 0.33 ± 0.22. After addition of 10 µM NA to the superfusate (B), the 1st EPSC depressed by 56.4 ± 12.4% to -14.4 ± 2.1 pA. The extent of depression is consistent with that observed earlier. In this experiment, however, the 2nd EPSC was slightly bigger than the 1st, indicating that a small amount of facilitation may be uncovered with NA (1.02 ± 0.3). This change was not significant (p_{pt} = 0.15). The overall depression reached a steady state of -1.8 ± 1.3 pA. Surprisingly, the recovery EPSC was much larger than the 1st EPSC (-18.4 ± 1.8 and 14.4 ± 2.1 pA). R_{50} was calculated as -0.36 ± 0.13. This data indicates that a significant facilitatory component was now present, which was not there during control conditions.

In three out of four experiments, the recovery pulse was bigger than the first EPSC (Fig 3.3.22C). This is illustrated in figure 3.3.22D, where the data for all four paired experiments is indicated by lines. In E), I asked the question if the setting of the synapse influenced the R_{50} value, i.e. determined how much the recovery from depression could be accelerated. I found no correlation. In F) the pooled values for the R_{50} are given for the two conditions. During control conditions, R_{50} was 0.21 ± 0.05 but in the presence of NA was -0.48 ± 0.03. I found no significant change when both the R_{50} were compared (p_t = 0.06).

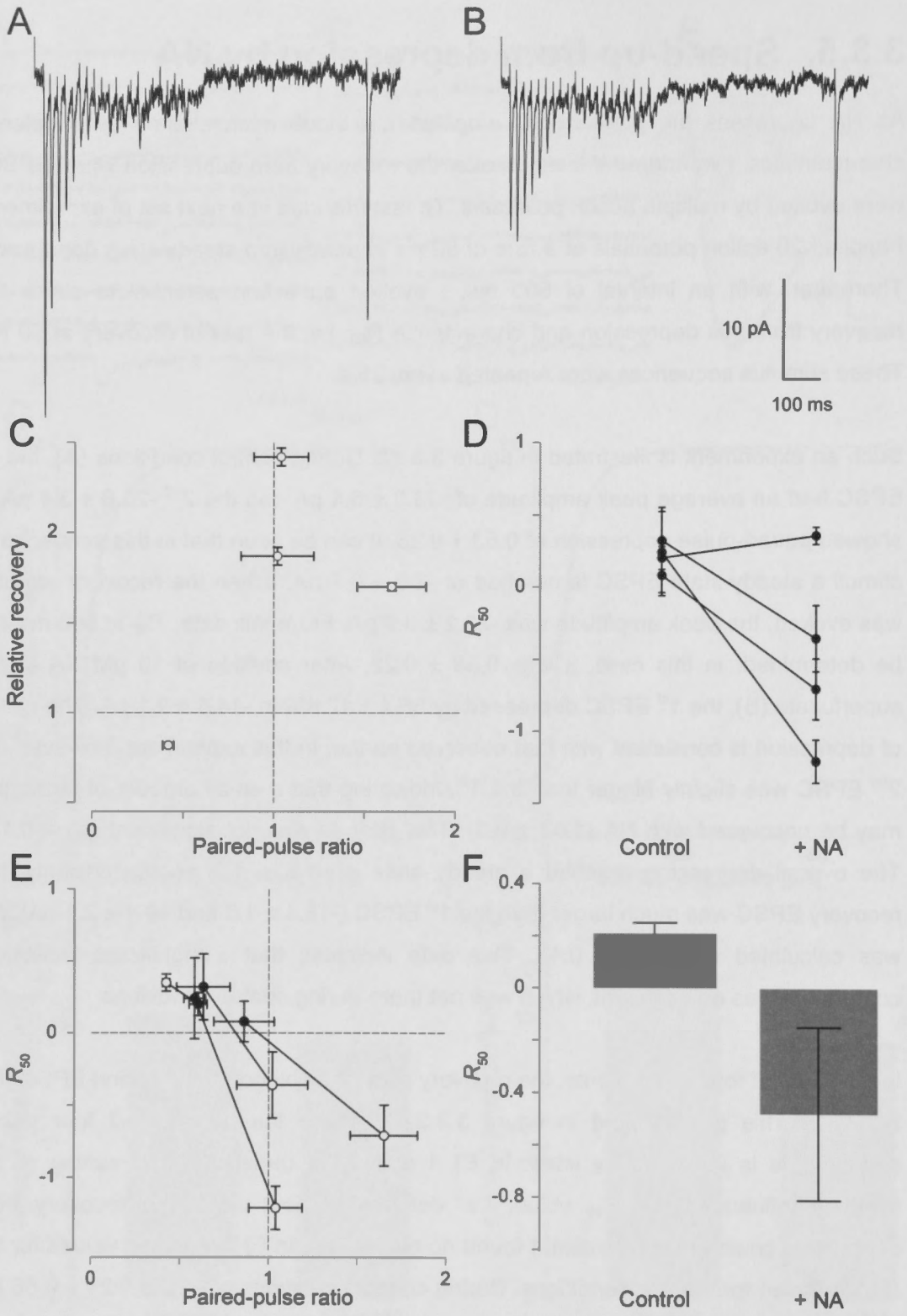

Figure 3.3.22. EPSCs evoked during a burst of 20 APs at 50 Hz together with a recovery AP at 500 ms. A) Average overall EPSC time course of 20 trials before and B) after the application of NA. Note that over the time course of the EPSC at 50 Hz, there is a net inward current remaining from stimulus to stimulus. C) Comparison of relative recovery caused by application of NA to the paired-pulse ratio during control condition. In D) the individual R_{50} values are given for each experiment before and after NA. The lines indicate the paired experiments. E) Comparison of changes in the R_{50} values caused by application of NA to the paired-pulse ratio after application of NA. In F), the average values are given during control and after NA. The starred bracket indicates $p_{pt} < 0.05$.

From these experiments, a number of conclusions can be made. Firstly, NA not only depresses the EPSCs at these synapses, but the recovery from depression is much larger than the 1st response after waiting for 25 s. Secondly, this means that there is a time dependent facilitatory process at work which within 25 s has subsided again.

3.4. Discussion

In Part II of the thesis, I investigated the effect of NA on evoked transmitter release in pairs of identified layer II pyramidal neurones. In obtaining these recordings, I also recorded baseline data characterising release characteristics of the synapses in this layer. I, therefore, split the following discussion into two parts, firstly into the characterisation of basic transmission and secondly into how NA changes the release dynamics at these nerve terminals.

3.4.1. Transmitter release in pyramidal cell pairs

In this study, the synaptic responses were recorded in voltage-clamp as currents. The reason to do so was to have improved signal-to-noise ratio compared to when recording in current-clamp (for arguments see Cowan & Stricker, 2004). I am very aware that the EPSCs suffer from poor space clamp and two correlations in the data show that voltage-clamp is poor. Firstly, if the clamp were perfect, then I should not have been able to demonstrate a tight correlation between EPSC half-width and rise-time as the latter would have been more or less constant at all synapses. Secondly, the negative correlation between EPSC latency and amplitude may also point into a similar direction as the latency is not only due to the delay caused between presynaptic activation and postsynaptic current, but also due to the rising phase of the postsynaptic EPSC. Above all, the observed correlation, while significant, has a small slope. As it has been demonstrated that EPSCs suffering from poor space clamp have a faster rising phase (Spruston *et al.*, 1993), it is not surprising that larger EPSCs may have shorter latencies.

This is the first study to publish a large set of EPSCs between pairs in layer II of somatosensory cortex. I found that of 40 stable recordings, the average EPSC amplitude was -27.7 ± 2.4 pA with an average CV of 0.67 ± 0.37. This value is

comparable to the values published by Feldmeyer *et al.* (2006) in the same layer where they found an average EPSC (n = 7) of -58 ± 35 pA. From the remainder of the data, the CV was estimated to be 0.33 ± 0.18. The EPSCs in my data set show a much larger CV (p_t = 0.014). The only noticeable difference was the age of the rats, with my rats on average being 3 days younger than theirs. I don't think that this difference may be able to account for the difference in the CV. As their data set was quite small, they may have had a biased sample.

My data set is also not different in regard to the average paired-pulse ratio. In my data set, the average was 0.95 ± 0.16 and in Feldmeyer *et al.* (2006) it was 0.73 ± 0.23 (n = 5). However, I have been able to account not only for "depressors" (n = 22), but also for "facilitators" (n = 18). From my set I conclude that the average paired-pulse plasticity is small and variable.

A surprising finding in this data set was that the synaptic characteristics were quite different to the ones reported by Cowan & Stricker (2004) and Fuhrmann *et al.* (2004) for layer IV and V, respectively. Whilst in these studies, there were significant correlations found between paired-pulse ratio and between skew and CV^{-2} and skew of the EPSCs, there were no such relationships uncovered for synapses in layer II. The only and again differing linear correlation was between CV^{-2} and the mean EPSC (Figure 3.3.8B). To explain this relationship on the basis of a binomial process, it becomes evident that the common shared parameter between the two measures is the number of release sites (n), suggesting that larger EPSCs are the result of releasing from more sites with minimal impact by the probability at these sites.

Utilising, therefore, the slope of this relationship (-0.165 ± 0.016), the question can be asked by how much must the postsynaptic current increase to cause a shift by one unit of CV^{-2}. This increase then corresponds to the average quantal size. When I did that, I obtained a value of -6.0 ± 0.6 pA. This average quantal size is drawn from the population of all EPSCs. Its size when compared to values found for layer IV (Cowan & Stricker, 2004) is about double the size (-2.8 ± 0.7 pA; n = 19; p_t = 0.05). This value is consistent with values derived from individual EPSC fluctuations from pairs in layer II based on density estimation (Li, Choy & Stricker; to appear elsewhere). If the average EPSC amplitude is now divided by this quantal size, the average quantal content becomes 4.6 ± 0.6 for these synapses. This value is not significantly different from the value obtained for pairs in layer IV (3.3 ± 1.6; n = 19; p_t = 0.2).

Interpretations of changes in paired-pulse plasticity typically rely on release-dependence of subsequent EPSCs; i.e. there is an anticorrelation between the 2nd and 1st EPSCs for a particular recording such that a release causing a large EPSC is followed by a large depression and *vice versa*. Such relationships, both significant and insignificant, were certainly found in neurones both in layers IV and V (Cowan & Stricker, 2004; Fuhrmann *et al.*, 2004). When this type of analysis was done on a subset of 16 EPSCs in this Part II, I found that in only one case such an anticorrelation was established. Specifically, there was a correlation in four out of twelve cases, but none of them was consistent with release-dependence. Again in contrast to findings in layer IV and V neurones, where the extent of release-dependence was correlated with release probability, there is no such relationship at synapses in layer II. They all depress and facilitate in a release-independent fashion questioning the value of the paired-pulse measure in making predictions about the dynamics of depression and facilitation.

In summary, the synapses between pairs of pyramidal cells in layer II have an efficacy that is largely dominated by the number of release sites, but not by the release probability. On average, the paired-pulse plasticity can either be facilitation or depression; in both cases the average plasticity is typically quite small. This paired-pulse plasticity is mostly dominated by release-independent factors, the nature of which remains unclear.

3.4.2. NA depresses evoked EPSCs

The results for the evoked transmitter release came as a surprise as these were different to the findings for spontaneous release. Given that the rate of mEPSC was increased after NA application, I would have expected that evoked transmitter release would show an increased peak EPSC amplitude in line with the Ca^{2+} release from stores. However, I observed a depression of 66 ± 23% (n = 7) caused by NA and a significant speed-up of the recovery from depression, in fact, so much that the recovery pulse in most recordings became larger than the initial EPSC.

At this stage, it is important to stress that the data gained in my experiments was from the recordings of connected pairs of excitatory pyramidal neurones. As a single cell was stimulated by current injection and as such, the stimulus was limited to the cell under investigation, it is highly unlikely that activity within the network could have been generated to the extent that other presynaptic factors may have to be considered. In

particular, it is important to note that no extracellular stimulus electrodes were used which could have resulted in stimulating axon collaterals from other neuromodulatory systems, including NA itself. My experimental design is quite different to many studies that have looked at noradrenergic modulation in various cortical tissues and therefore provides "clean" data for subsequent interpretation.

3.4.2.1. Noradrenergic modulation of EPSCs

A depression caused by NA has been reported since early investigations into transmitter release in the central nervous system when the read-out was largely restricted to spontaneous action potential firing of individual cells (Krnjevic & Phillis, 1963; Phillis *et al.*, 1968; Lake *et al.*, 1972; Segal & Bloom, 1974). For example, Mynlieff and Dunwiddle (1988) in the rat hippocampus described that NA depressed the amplitude of the population spike by 14 ± 5.1% (n = 19). However, in my data set, I have not been able to find much evidence for postsynaptic modulation. In fact, neither action potential nor EPSC properties changed significantly when switching to a superfusate containing 10 µM NA. When looking at R_{in}, I did not find any significant changes either. I am not claiming that such alterations of postsynaptic membrane properties do not exist, as I only looked at a very limited number of parameters, but I am confident that NA has insignificant effects on the EPSC kinetics as consistently shown with both adrenergic agonists and antagonists and in both Part I and here in Part II as well.

The first people to notice that there may be a presynaptic action of NA were Mody *et al.* (1983), who showed that when NA was applied to slices of rat hippocampus, the field EPSP in CA1 depressed by about 50%. This line of investigation was later extended by Scanziani *et al.* (1993), who in organotypic slice cultures of hippocampus reported that application of 5 µM NA decreased the EPSP amplitude by 43 ± 12% (n = 12) and who identified the receptor mediating this response as belonging to the group of α_1-ARs. Their extent of depression was not different to the one I observed in barrel cortex (p_t = 0.24). At the same time, these authors reported that upon NA application, they did not observe any change in miniature EPSPs. Similar in the extent of depression but dissimilar in regard to the transducing receptor, Delaney *et al.* (2007) observed a 63.2 ± 4.7% reduction in EPSP amplitude mediated after α_2-AR activation when stimulating the parabrachial nucleus in the central amygdala of the rat (p_t = 0.48).

A similar decrease has also been reported for IPSPs by Madison & Nicoll (1988) and Langmoen *et al.* (1981) in hippocampus. The extent of this depression is indistinguishable from the one I have reported for EPSCs for the former case (p_t = 0.32; no numbers given for the latter). However, the nature of the receptor mediating this depression remained unclear in these studies. Given that Madison & Nicoll (1988) also saw a large increase in spontaneous IPSPs during NA superfusion, it is tempting to assume that the action of NA in this brain area may be caused by α_1-ARs.

Given these independent reports, it looks as if the depression caused by NA is similar at excitatory and inhibitory synapses, but also when different α-ARs are activated. This begs the question if there are common underlying mechanisms at work (see below.)

3.4.2.2. Depression is caused by α_1-ARs

My data clearly shows that this depression remains the same when cirazoline as agonist was used. As this drug is also an antagonist at α_2-ARs, this data implicitly rules α_2-ARs out. Unfortunately, the alternative experiment in which receptors other α_1-ARs were blocked with yohimbine and propranolol did not support the conclusion above as the observed depression was much smaller. I am unclear why this may have occurred. A possible explanation may be that when three drugs were applied simultaneously and at similar concentrations (NA, YO and PO), unexpected interactions may have arisen. I have not investigated this discrepancy any further.

The onset of the depression is quite fast; in fact, it is not possible with the superfusion system that I employed to document the speed of onset. Likewise, when the agonist is washed-out, the EPSCs return to their previous amplitude within a few minutes. These details may well set boundaries for timing of the molecular mechanisms involved.

3.4.2.3. Extent of depression and presynaptic parameters

A surprise for me was that, on average, only small changes in the paired-pulse ratio from control condition to one with NA in the superfusate were uncovered. I expected that for a depression of 66 ± 23% that a considerable change would appear. This could indicate that not the Ca^{2+} influx and with it the probability at the synapses is altered by NA, but rather release sites become functionally silent (see below). This view is consistent with the CV^{-2} analysis in Figure 3.3.15E, in which most points after NA fall

right below the line of identity, classically interpreted as indicating a presynaptic form of depression. It is also consistent with the data shown in Figure 3.3.16 where most EPSCs showed release-independent depression before and after NA.

3.4.2.4. Stores contribute to each EPSC

If stores contribute to increase mEPSC frequency, then their contribution should result in a larger amplitude of the EPSC. I did the converse experiment and observed that when store release was reduced after blocking the SERCA pump with 20 µM CPA, the EPSC decreased in amplitude by 33 ± 11% while minimally affecting the paired-pulse ratio. This store contribution is similar to the one observed in layer V pyramidal cells (Cowan & Stricker, 2007, unpublished). This observation is, therefore, consistent with the findings in Part I of this thesis.

It is perhaps surprising to realise that store release contributes even to the first EPSC as a typical conception of store release maintains that it may elevate Ca^{2+} quite slowly and as a consequence, "priming" is required to see its full effect. My findings are consistent with experiments at the NMJ (Narita *et al.*, 2000) and at the inhibitory synapse between basket cell and Purkinje neurone in cerebellum (Galante & Marty, 2003). When ryanodine receptors on Ca^{2+} stores were blocked, even the first EPPs and IPSCs, respectively, became much smaller. There are several factors that may render store release fast. Firstly, the depolarisation of the nerve terminal by the action potential primes store release as the voltage-change favours opening of IP_3 receptors and ryanodine receptors. Secondly, Ca^{2+} entry could cause CICR, particularly of the ryanodine receptors but also prime IP_3 receptors for subsequent release. Thirdly, as presynaptic Ca^{2+} stores are quite close to the release machinery (Westrum & Gray, 1986; Hartter *et al.*, 1987), the time for diffusion of Ca^{2+} is very fast, i.e. a few tens of µs. Experimentally, it is just about impossible to distinguish such a contribution on the rising phase of an EPSC.

Unfortunately, it has not been possible to separate the increased store release in NA from the depression. As a consequence, it remains unclear if NA due to increased store release makes the EPSC a bit larger as I have not been able to block this depression without also affecting store release.

3.4.2.5. Depression is independent of Ca^{2+} stores

When stores were actively depleted with CPA and a concomitant potassium depolarisation, upon superfusion with NA, the EPSCs still depressed; in fact, the extent of depression whilst appearing slightly smaller was indistinguishable from when NA was applied in the absence of CPA (p_t = 0.22). It may be that if I had a larger sample, the depression observed under this condition may be slightly smaller pointing to the possibility that store release caused by NA could make the EPSC larger. These results raise at least three different points to make here: Firstly, store release is not much involved in shaping the extent of this depression. Secondly, it suggests that this form of depression is, therefore, unlikely to be dependent on presynaptic calcium in the nerve terminal. And thirdly, this data points towards that the α_1-AR signalling cascade downstream of IP_3 production is unlikely involved, as its production would have caused store release. This latter point leads to the next consideration about the molecular events involved in causing this depression (see below).

3.4.2.6. Depression is also independent of PLCβ

When PLCβ was blocked with 30 µM edelfosine, the full extent of depression was still observable, indicating that the molecular downstream of PIP_2 hydrolysis were not involved either. An objection to the conclusion may be that edelfosine did not block PLCβ as suggested. To rule this possibility out, I checked if when PLCβ was blocked, the concomitant increase in spontaneous release was blocked in the presence of NA. This indeed was the case and as a consequence rules this alternative out.

As PLCβ is activated by hydrolysed G protein subunits, this set of experiments suggests that the depression is caused by a step proximal to PLCβ activation. This rules the possibility out that PIP_2 depletion in the membrane as a consequence of receptor activation results in reduced calcium influx. Such a mechanism has been identified as a major cause of voltage-dependent calcium current rundown in several systems ($Ca_V2.1$, P/Q-type, for review see Delmas & Brown, 2005). It is unlikely that in my case PIP_2 depletion after NA exposure reduced subsequent calcium entry. Even as PIP_2 depletion can inhibit the calcium currents by up to 33 – 66% (Suh *et al.*, 2010), this would be sufficient to cause a depression of 66% as observed. Assuming a calcium cooperativity of 4 (Dodge & Rahamimoff, 1967), a reduction by 10% would

have been enough. This consideration, therefore, does not rule this possibility out. However, it renders this scenario very unlikely.

As a consequence, knowing that α_1-AR receptor activation is required, this leaves the potential that either a direct and so far unknown signalling pathway causes the depression or that it is one of the hydrolysed products, either G_α or $G_{\beta\gamma}$ that ultimately causes the depression.

3.4.2.7. Recovery from depression is accelerated

An unexpected finding was that the recovery rate from depression at 500 ms was much accelerated; in fact so much that the size of the recovery EPSC was larger than the first EPSC at the beginning of the stimulus protocol. In this limited data set, however, there was a single case out of four, which did not demonstrate these characteristics. The recovery after NA in this case was slower as judged by the slightly increased R_{50}. I have no explanation to offer for this case except to say that perhaps, because only 20 stimulus sequences were evoked during control and after NA application, that the EPSC may have undergone some long-term depression as indicated in the early parts of the Results section. It may be that this long-term depression seen in about 50% of all EPSCs could have changed the response properties at this synapse.

This experiment allows drawing the following conclusions. Firstly, acceleration of the recovery rate appears quite fast during the stimulus sequence because its magnitude is considerable after 500 ms after the last EPSC, for which no facilitatory component could be identified. I am not saying that at this stage there was no facilitation, but rather that the rate of depression is matched by facilitation. Secondly, the facilitation lasts much longer than 500 ms, quite different to forms of short-term facilitation that have been described for many synapses (Eccles *et al.*, 1941; Zucker & Regehr, 2002). It is also unlikely that this form of facilitation is caused by post-tetanic potentiation, as this typically lasts for minutes in contrast to the less than 20 s in this case. It may be caused by augmentation as the number of stimuli consisted of 20 action potentials. At synapses in cortex, Fuhrmann *et al.* (2004) reported that the time constant of recovery from augmentation in layer V pyramidal neurones was 11 ± 5 s. However, for 100 action potentials, the augmentation was around 60%. For 20 as in this case, a smaller amount would therefore be expected. However, in at least two experiments the increase was by more than 80%. Therefore, I think that augmentation is an unlikely candidate for this facilitation. Given that the speed-up in recovery from depression at

layer V synapses was shown to depend on calcium, I am tempted to think that this increase is also caused by Ca^{2+} and notably by store release. A conception how this could occur at a molecular level is given below.

3.4.2.8. Molecular mechanisms causing this depression

Realising that firstly, α_1-ARs are required to be activated, secondly, that neither IP_3 production nor PLCβ activation are required for depression, I am left with a potential molecular mechanisms very early in the α_1-AR signalling cascade. These include firstly, the hydrolysis of the receptor adaptor protein, in this case the G_q protein, and secondly the downstream effects of this hydrolysis, namely, G_α and $G_{\beta\gamma}$ production..

Downstream of G protein hydrolysis is the production of G_α and $G_{\beta\gamma}$. It is typically the former of the two, which has shown strong signalling abilities in neurones. However, it has been shown that $G_{\beta\gamma}$ can also modulate high-voltage activated calcium channels (group of Ca_V2; Tedford & Zamponi, 2006). Furthermore, the sites of direct interaction between $G_{\beta\gamma}$ have been identified to be on the I-II linker region and on the N-terminus of the calcium channel subunit. This interaction, in addition, is modulated by PKC, which can phosphorylate T422 on the I-II linker region and, in doing, that inhibits binding of the $G_{\beta\gamma}$ to this site (for review see Tedford & Zamponi, 2006). This idea is consistent with what Scanziani *et al.* (1993) reported when activating PKC using staurosporine and observing that the EPSPs (in their case) became larger. However, given that presynaptic calcium may not be involved, I think that the modulation of calcium channels by $G_{\beta\gamma}$ is unlikely.

$G_{\beta\gamma}$ has been shown to directly interact with the release machinery (Blackmer *et al.*, 2001; Blackmer *et al.*, 2005; Gerachshenko *et al.*, 2005; Yoon *et al.*, 2007). In a set of beautiful experiments, Blackmer *et al.* (2001) showed that $G_{\beta\gamma}$ depresses transmitter release directly without requiring to inhibit calcium entry into the nerve terminals. In fact, Gerachshenko *et al.* (2005) identified that $G_{\beta\gamma}$ interferes with the Ca^{2+}-dependent binding of synaptotagmin to the SNARE complex in lamprey spinal cord. The extent of the depression observed was similar to the one seen in our system (see their Figure 8).

In addition, the binding of $G_{\beta\gamma}$ to the synaptotagmin/SNARE complex is sensitive to calcium such that when calcium in the terminal is increased, the $G_{\beta\gamma}$ binding is reduced

resulting in more transmitter release. Such a mechanism provides the best explanation for the speed-up in recovery observed where in 3 out of 4 cases the recovery pulse after 500 ms was significantly larger than the first pulse during the sequence of action potentials. The sequence of events is best described as follows during this type of experiment: NA activates α_1-ARs causing the production of $G_{\beta\gamma}$ which then prevents the binding between synaptotagmin and the SNARE complex resulting in the depression observed. After considerable build-up of terminal calcium from stores and VDCCs after 20 action potentials, the calcium is increased by such an amount that the $G_{\beta\gamma}$ inhibition is relieved and as a consequence, the recovery EPSC is now larger than the first in the stimulus series. At an interval of 25 s, most if not all the calcium will have cleared from the terminals and as a consequence, $G_{\beta\gamma}$ rebinds to maintain the depression observed in NA. If this scheme is correct, there are a number of predictions for future experiments: Firstly, if store release is blocked (either via IP_3 receptor block, or SERCA pump inhibition), this change in dynamics should disappear and the recovery EPSC should remain largely at the same amplitude. Secondly, increased extracellular calcium should counter the depression observed (as in Figure 8 in Yoon *et al.*, 2007). Thirdly, blocking the calcium clearance from the terminal by inhibiting the Na^+/Ca^{2+}-exchanger should retain this "facilitatory" component for much longer.

I prefer this mechanism over the other possibilities above as it is further supported by the fact that the nature of the receptor causing the depression does not matter much. I draw this conclusion from the fact that even when α_2-ARs are stimulated, the extent of depression is the same (Delaney *et al.*, 2007). Also when 5-HT_1 receptors were stimulated (Yoon *et al.*, 2007), the depression is of the same magnitude. Further, when group I metabotropic glutamate receptors were stimulated, the depression was indistinguishable (Cowan *et al.*, unpublished). In addition, a similar decrease in IPSP amplitude was also reported for hippocampal inhibitory synapses (Doze *et al.*, 1991). This raises the important point that the type of the G protein hydrolysed is of secondary importance; what matters is the availability of $G_{\beta\gamma}$ which causes a powerful depression independent of the receptor stimulated. Further, this data suggests that upon receptor activation a sufficient amount of $G_{\beta\gamma}$ is produced to saturate most of its binding sites.

This last point raises an important point, namely if $G_{\beta\gamma}$ is available in the cytosol of the nerve terminal without receptor activation. Indeed, activators of G-protein signalling (AGS) have been found to cause G protein signalling without receptor activation (for review see Blumer *et al.*, 2007). At this stage, not much is known about their distribution in the brain. However, one study found that AGS1 was expressed in neurites of embryonic hippocampal cells (Sachdev *et al.*, 2007). It is therefore likely

that such proteins are around in neocortex as well. In fact, AGS1 is markedly expressed in neocortex and upregulated within 3 hours, after a single dose of amphetamine, the AR agonist implicated in drug abuse (Schwendt & McGinty, 2010). There is a line of thought that these AGS proteins may play a very important role in fine-tuning transmitter release and in particular, in determining levels of addiction.

The scenario described here also suggests that even though some vesicles, i.e. the ones responsible for spontaneous release, are allowed to fuse more easily as a consequence of NA, others are not, i.e. the ones involved in evoked transmitter release. This suggests that there may be differential effects onto at least two different vesicle populations or molecular mechanisms resulting in transmitter release.

3.4.2.9. Functional consequences

In excitatory circuits in cortex, NA will on one side increase background synaptic activity by increasing mEPSCs, but on the other, depress evoked synaptic EPSCs considerably. There are several consequences given that the dynamics of these synapses are altered. Firstly, given that the depression by both EPSPs and IPSPs is about the same, I doubt that there is a massive switch in the balance between excitation and inhibition. Secondly, however, given that both mEPSCs as well as mIPSPs are increased, the background conductance of the cell may well be altered and as a consequence larger synaptic inputs are required to drive cells above threshold. This is consistent with all early data using iontophoresis in both hippocampus and cortex (Segal, 1982; Devilbiss & Waterhouse, 2000). Thirdly, given that synaptic dynamics are accelerated after NA superfusion, I expect that sensory input from the periphery and other locally generated activity relayed via action potential series may become much larger over time, as the $G_{\beta\gamma}$ inhibition is relieved both via calcium influx and store release. This could ultimately give rise to sensory overflow as reported by patients suffering from psychotic episodes. In fact, it is worth mentioning here that most antipsychotic drugs have, among others, powerful anti-adrenergic actions.

3.5. Conclusion

In conclusion, I have successfully documented the release characteristics of excitatory synapses between pyramidal neurones of layer II of the barrel cortex. In cell pairs (n = 101) the postsynaptic neurone revealed an average EPSC amplitude of -31.4 ± 3.6 pA. I found that 60.4% of the EPSC amplitudes in layer II pyramidal neurones of the barrel cortex depress without the presence of neuromodulators. From the remainder of the cell population for which the EPSC amplitudes do not depress over the time of recording, the coefficient of variation (CV) of all EPSC amplitudes were 0.6 ± 0.1. A significant correlation between the CV^{-2} and EPSC was observed. From these values, the quantal current of the population is estimated to be -6.0 ± 0.6 pA. The correlation between the CV^{-2} and EPSC also indicates that at these synapses, the EPSC amplitude is dominated by the number of release sites. This characteristic is different from cells in layer IV and V, in which the EPSC size is governed by the release probability. There was little paired-pulse plasticity in the cell population in layer II.

I next looked into how NA changes the release dynamics at the nerve terminals. Application of NA depressed evoked EPSC amplitude by 66 ± 23% (n = 7) via the α_1-ARs. When presynaptic Ca^{2+} stores were emptied, application of NA still depressed EPSC amplitudes significantly by 33 ± 18%. This indicates that activation of the α_1-ARs is independent of Ca^{2+} stores. In addition, when PLCβ was blocked with edelfosine, despite blocking the increase caused by NA in spontaneous release, the depression still remained. Both observations indicate that NA signalling caused the depression of the EPSC at a step very early in the signalling cascade.

Finally, I checked if NA altered the recovery from depression after a train of action potentials at a rate of 50 Hz. In most cases, the recovery EPSC was much larger than the average 1st EPSCs. A potential mechanism may be that activation of α_1-ARs by NA causes the production of $G_{\beta\gamma}$, which prevents the binding between synaptotagmin and the SNARE complex, resulting in a much depressed EPSC amplitude. The build-up of Ca^{2+} in the nerve terminals during a train of twenty action potentials starts competing with the inhibition caused by $G_{\beta\gamma}$ and subsequently produces a recovery EPSC that is larger than the first EPSC in the series. As Ca^{2+} is cleared from the presynaptic terminal, $G_{\beta\gamma}$ re-binds to the SNARE complex and causes a much smaller first EPSC.

A summary cartoon including this potential mechanism is given in figure 3.5.1.

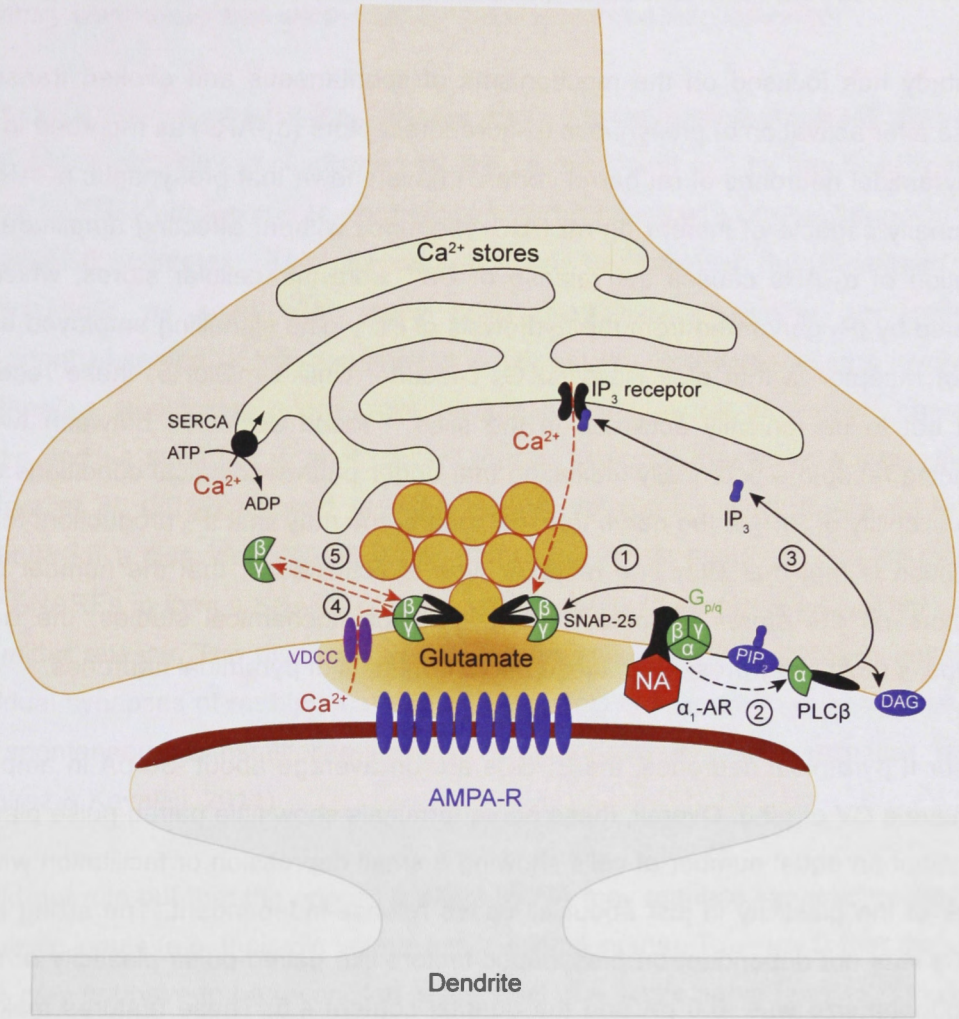

Figure 3.5.1. Cartoon illustrating the potential mechanism in a presynaptic nerve terminal synapsing onto a postsynaptic spine. After activation by its physiological agonist (NA), the α_1-AR caused the hydrolysis of of the receptor-bound G protein into the G_α and $G_{\beta\gamma}$. The latter immediately binds to SNAP-25 (①) inhibiting the interaction between synaptotagmin and the SNARE complex and causing the depression observed. The former activates PLCβ to hydrolyse membrane resident PIP_2 into IP_3 and DAG (②). The latter has no direct effect on transmitter release while the former is capable to cause activation of IP_3 receptors on the Ca^{2+} stores (③). The results from this study suggest that Ca^{2+} mobilisation from presynaptic stores increases the evoked release of glutamate at these neocortical synapses. During sustained activity by many action potentials, the elevation of Ca^{2+} from VDCCs and Ca^{2+} stores in the nerve terminal outcompetes the binding of the $G_{\beta\gamma}$ subunit to the SNARE complex, relieving the inhibition caused by $G_{\beta\gamma}$ binding (④), which upon Ca^{2+} clearance reverts back to the initial state (⑤).

4. Conclusion

The study has focused on the mechanisms of spontaneous and evoked transmitter release after activation of presynaptic α_1-adrenoreceptors (α_1-ARs) as recorded in layer II/III pyramidal neurones of rat barrel cortex. I have shown that presynaptic α_1-ARs are functionally capable of increasing mEPSC frequency without affecting amplitude. The activation of α_1-ARs causes the release of Ca^{2+} from intracellular stores, which are activated by IP_3 generated from the hydrolysis of PIP_2. The signalling employed by this type of receptor is that of a classical G_q cascade. Unlike mGluR5, these receptors seem not to be tonically activated in the slice. I found occlusion between two IP_3 producing receptors potentially indicating that under pharmacological conditions either the availability of PIP_2 in the nerve terminal membrane may limit IP_3 production, that IP_3 production is maximal after one receptor type is activated or that the number of IP_3 receptors on the stores is limited. From immunohistochemical studies, the α_{1B}-AR subtype is most likely present on these nerve terminals of pyramidal neurones.

In layer II pyramidal neurones, the EPSCs are on average about -30 pA in amplitude and have a CV of ~0.6. Overall, these nerve terminals show little paired-pulse plasticity with about an equal number of cells showing a small depression or facilitation with the nature of the plasticity in just about all cases release-independent. The sizing of the EPSCs was not dependent on presynaptic factors like paired-pulse plasticity or skew. The quantal size was -6.0 pA and the quantal content 4.5. These features make the synapses in layer II very different to those found in layer IV or V. It may indicate that the synapses in this layer serve to contribute an "average" contribution to the EPSC that is determined largely by the number of release sites, reminiscent of an "average synaptic weight synapse" used in computational neuroscience.

Noradrenaline, whilst increasing mEPSC rate, significantly depressed evoked transmitter release by about 66%. This depression was caused by α_1-AR activation but did not involve Ca^{2+} release from presynaptic stores indicating that the molecular event leading to this depression was before α_1-AR mediated store release. Consistent with this conclusion, when store release was blocked the EPSCs became smaller by about 30%, even the first one, indicating that store release augments the EPSC amplitude. Upon testing synaptic dynamics using 20 action potentials at 50 Hz, recovery from depression was much accelerated; in fact so much that the recovery EPSC at 500 ms

was abut 20% larger than that 1st EPSC in the stimulus sequence indicating that a facilitatory component was uncovered by the number of action potentials.

As an explanation, I propose that the data about the depression of the EPSCs caused by NA can most likely be explained by the production of $G_{\beta\gamma}$ by the α_1-ARs and its binding to SNAP-25 leading to an inhibition of the interaction of snaptotagmin-1 with the SNARE complex. This depression can be relieved by increased Ca^{2+} concentrations as seen after many action potentials explaining the facilitatory component observed. If this explanation is correct, the molecular events involved in spontaneous transmitter release are distinct to those seen in evoked transmitter release and as such NA is an excellent tool to separate these two effects. Indeed, Ramirez *et al.* (2012) showed that the protein Vps10p-tail-interactor-1a (vti1a) can substitute for a classical SNARE (likely SNAP-25) and in doing so, can interact with other SNAREs to form a SNARE complex which results in spontaneous but not evoked transmitter release. The evidence was based on simultaneous multicolour imaging at individual synapses of rat hippocampal cultures. This is in line with recent observation that spontaneous transmitter release is distinct from evoked transmitter release (Ramirez & Kavalali, 2011).

I could not rule out that the opposing effect by NA may regulate synaptic transmission at specific inputs (e.g. thalamic *versus* associational inputs). The idea is that the effects of NA may not have to be reconciled at the level of a single nerve terminal. However, I think that this is an unlikely explanation for the following reasons. Firstly, layer II cells receive most synaptic input from other layer II cells; in addition also from layer IV (Hersch & White, 1982) and V (Herkenham, 1980). Secondly, a similar decrease in EPSC amplitude was also observed both in excitatory cells both in layers V and IV when DHPG was superfused (Anna Cowan, personal communication).

4.1. Stores in synaptic transmission

Ca^{2+} stores have the potential to affect the synaptic transmission of neurones. Simkus and Stricker (2002a) have reported that in layer II/III neurones of rat barrel cortex, the release of Ca^{2+} from presynaptic stores via activation of either the RyR or the IP_3R can increase mEPSC frequency. The Ca^{2+} stores in the barrel cortex are most likely the smooth endoplasmic reticulum because mitochondria have a slower turnover rate of

Ca^{2+} and the majority of intracellular Ca^{2+} is amassed in non-mitochondrial compartments (Rubiales de Barioglio & Orrego, 1982).

I found that there was a background IP_3 production. This observation is in accordance with the observation by Simkus and Stricker (2002a), where they also reported a drop in mEPSC frequency in the presence of 14 μM 2-APB. This tonic activation of IP_3R and putatively also RyR influences the Ca^{2+} homeostasis in these nerve terminals.

There are a few diseases associated with dysregulation of Ca^{2+} homeostasis. The major example is Alzheimer's disease (AD). AD is characterized by deposition of oligomeric amyloid β-peptides, synaptic loss and ultimately neuronal death (De Strooper *et al.*, 1999). These effects correlate with the development of presenile dementia.

There is some evidence to suggest the involvement of RyR and IP_3R in the pathogenesis of AD. Presenilins, which are localised to the ER have been shown to upregulate the function of IP_3Rs (Cheung *et al.*, 2008), SERCA pump (Green *et al.*, 2008) and RyRs (Zhang *et al.*, 2009). Mutations in the presenilin-1 (PS1) gene can lead to a rapid progressing, early onset form of AD, while mutations in the presenilin-2 (PS2) gene can lead to the late onset of AD (for review see Mattson *et al.*, 1998). Chan *et al.* (2000) reported that the mutated PS1 protein greatly enhances RyR expression in the hippocampus. Pack-Chung *et al.* (2000) showed that the C-terminal endoproteolytic fragment of the PS2 protein interacts with sorcin, an EF hand Ca^{2+} binding protein that modulates the RyR. Both the PS1 and PS2 can potentially cause an elevation of intracellular Ca^{2+}, which can increase the proteolytic processing of β-secretase, which is crucial in forming β-amyloid. Thus, a detailed investigation of the role of Ca^{2+} release from intracellular Ca^{2+} stores might provide fruitful insights into the pathophysiology of AD.

4.2. α_1-AR in pathophysiology

The Ca^{2+} release from stores is important in setting the excitability of layer II/III neurones of the barrel cortex. I have shown that activation of the α_1-ARs by NA causes Ca^{2+} release from presynaptic stores. Whist innervation of noradrenergic neurones comes directly from the *locus coeruleus* (Simpson *et al.*, 2006), the loss of noradrenergic innervations could affect the excitability of the neurones in layer II/III.

Rett syndrome is a neurodevelopmental disorder caused by loss of function mutation in the X-linked gene encoding the methyl-CpG-binding protein-2 (MeCP2) (Amir *et al.*, 1999), resulting in derangements in cognition (for review see Weaving *et al.*, 2005). In a mouse model of Rett syndrome, the loss of MeCP2 causes a series of changes in the properties of cells in the *locus coeruleus* (Taneja *et al.*, 2009). The neurones of MeCP null mutant mice exhibit electrical hyperexcitability, are morphologically smaller in size and express a smaller amount of tyrosine hydroxylase, which is a NA-synthesizing enzyme. Layer 5 pyramidal neurones in somatosensory cortex in these MeCP2 mutant mice showed a marked decrease in average mEPSC amplitude compared to wild type mice, from 15.9 ± 0.6 to 13.5 ± 0.5 pA (Dani *et al.*, 2005).

NA is also well known for its importance in attention and vigilance (Clark *et al.*, 1987). In fact, selective noradrenaline reuptake inhibitors (NRIs) are a popular class of antidepressants and effective treatments for depression are those that promote adrenergic activity (for review see Hájos *et al.*, 2004). NRI could be used as a stimulant to treat attention-deficit hyperactivity disorders (ADHD) or major depressive disorders (MDD). Although the mechanisms underlying the effectiveness of NRIs in treating depression is still unclear, my study, which illustrates that spontaneous release is increased and that the ability of NA to depress the EPSCs and increase their recovery after a burst of action potentials, might shed some light as to the underlying mechanisms. A decrease in NA uptake by NRIs, which leads to an increase in adrenergic activity, could increase activities of brain areas involved in mood regulation and sensory perception. The understanding of the noradrenergic effect may help to explain some of the behavioural actions of psychostimulant drugs such as cocaine and amphetamine.

5. References

Abdul-Ghani MA, Valiante TA, Carlen PL & Pennefather PS. (1996). Metabotropic glutamate receptors coupled to IP_3 production mediate inhibition of IAHP in rat dentate granule neurons. *J Neurophysiol* **76,** 2691-2700.

Abraham WC & Huggett A. (1997). Induction and reversal of long-term potentiation by repeated high-frequency stimulation in rat hippocampal slices. *Hippocampus* **7,** 137-145.

Adler EM, Augustine GJ, Duffy SN & Charlton MP. (1991). Alien intracellular calcium chelators attenuate neurotransmitter release at the squid giant synapse. *J Neurosci* **11,** 1496-1507.

Aghajanian GK & Marek GJ. (1999). Serotonin, via $5\text{-}HT_{2A}$ receptors, increases EPSCs in layer V pyramidal cells of prefrontal cortex by an asynchronous mode of glutamate release. *Brain Res* **825,** 161-171.

Aihara Y, Inoue T, Tashiro T, Okamoto K, Komiya Y & Mikoshiba K. (2001). Movement of endoplasmic reticulum in the living axon is distinct from other membranous vesicles in its rate, form, and sensitivity to microtubule inhibitors. *J Neurosci Res* **65,** 236-246.

Akert K, Moor H, Pfenninger K & Sandri C. (1969). Contributions of new impregnation methods and freeze etching to the problems of synaptic fine structure. *Prog Brain Res* **31,** 223-240.

Allen C & Stevens CF. (1994). An evaluation of causes for unreliability of synaptic transmission. *Proc Natl Acad Sci U S A* **91,** 10380-10383.

Allen RD, Metuzals J, Tasaki I, Brady ST & Gilbert SP. (1982). Fast axonal transport in squid giant axon. *Science* **218,** 1127-1129.

Almers W. (1990). Exocytosis. *Annu Rev Physiol* **52,** 607-624.

Alonso GL, Bazerque PM, Arrigo DM & Tumilasci OR. (1971). Adenosine triphosphate--dependent calcium uptake by rat submaxillary gland microsomes. *J Gen Physiol* **58,** 340-350.

Alvarez de Toledo G, Fernandez-Chacon R & Fernandez JM. (1993). Release of secretory products during transient vesicle fusion. *Nature* **363,** 554-558.

Amir RE, Van den Veyver IB, Wan M, Tran CQ, Francke U & Zoghbi HY. (1999). Rett syndrome is caused by mutations in X-linked MECP2, encoding methyl-CpG-binding protein 2. *Nat Genet* **23,** 185-188.

An SJ, Grabner CP & Zenisek D. (2010). Real-time visualization of complexin during single exocytic events. *Nat Neurosci* **13,** 577-583.

Arriza JL, Eliasof S, Kavanaugh MP & Amara SG. (1997). Excitatory amino acid transporter 5, a retinal glutamate transporter coupled to a chloride conductance. *Proc Natl Acad Sci U S A* **94,** 4155-4160.

Aston-Jones G & Bloom FE. (1981). Norepinephrine-containing locus coeruleus neurons in behaving rats exhibit pronounced responses to non-noxious environmental stimuli. *J Neurosci* **1,** 887-900.

Aston-Jones G & Cohen JD. (2005). Adaptive gain and the role of the locus coeruleus-norepinephrine system in optimal performance. *J Comp Neurol* **493,** 99-110.

Aston-Jones G, Rajkowski J, Kubiak P & Alexinsky T. (1994). Locus coeruleus neurons in monkey are selectively activated by attended cues in a vigilance task. *J Neurosci* **14,** 4467-4480.

Attwell D & Gibb A. (2005). Neuroenergetics and the kinetic design of excitatory synapses. *Nature reviews* **6,** 841-849.

Augustin H, Grosjean Y, Chen K, Sheng Q & Featherstone DE. (2007). Nonvesicular release of glutamate by glial xCT transporters suppresses glutamate receptor clustering in vivo. *J Neurosci* **27,** 111-123.

Augustine GJ, Charlton MP & Smith SJ. (1985). Calcium entry and transmitter release at voltage-clamped nerve terminals of squid. *J Physiol* **367,** 163-181.

Axelrod J, Weil-Malherbe H & Tomchick R. (1959). The physiological disposition of H^3-epinephrine and its metabolite metanephrine. *J Pharmacol Exp Ther* **127,** 251-256.

Babcock DF, Herrington J, Goodwin PC, Park YB & Hille B. (1997). Mitochondrial participation in the intracellular Ca^{2+} network. *J Cell Biol* **136,** 833-844.

Bacic F, McCarron RM, Uematsu S & Spatz M. (1992). Adrenergic receptors coupled to adenylate cyclase in human cerebromicrovascular endothelium. *Metab Brain Dis* **7,** 125-137.

Bading H, Hardingham GE, Johnson CM & Chawla S. (1997). Gene regulation by nuclear and cytoplasmic calcium signals. *Biochem Biophys Res Commun* **236,** 541-543.

Bai J, Earles CA, Lewis JL & Chapman ER. (2000). Membrane-embedded synaptotagmin penetrates cis or trans target membranes and clusters via a novel mechanism. *J Biol Chem* **275,** 25427-25435.

Bai J, Wang CT, Richards DA, Jackson MB & Chapman ER. (2004). Fusion pore dynamics are regulated by synaptotagmin·t-SNARE interactions. *Neuron* **41,** 929-942.

Barrionuevo G & Brown TH. (1983). Associative long-term potentiation in hippocampal slices. *Proc Natl Acad Sci U S A* **80,** 7347-7351.

Barry PH. (1994). JPCalc, a software package for calculating liquid junction potential corrections in patch-clamp, intracellular, epithelial and bilayer measurements and for correcting junction potential measurements. *J Neurosci Methods* **51,** 107-116.

Baryshnikov SG, Rogachevskaja OA & Kolesnikov SS. (2003). Calcium signaling mediated by P2Y receptors in mouse taste cells. *J Neurophysiol* **90,** 3283-3294.

Bayazitov IT, Richardson RJ, Fricke RG & Zakharenko SS. (2007). Slow presynaptic and fast postsynaptic components of compound long-term potentiation. *J Neurosci* **27,** 11510-11521.

Bekkers JM & Stevens CF. (1990). Presynaptic mechanism for long-term potentiation in the hippocampus. *Nature* **346,** 724-729.

Bellingham MC & Walmsley B. (1999). A novel presynaptic inhibitory mechanism underlies paired pulse depression at a fast central synapse. *Neuron* **23,** 159-170.

Bellocchio EE, Reimer RJ, Fremeau RT, Jr. & Edwards RH. (2000). Uptake of glutamate into synaptic vesicles by an inorganic phosphate transporter. *Science* **289,** 957-960.

Belousov AB, Godfraind JM & Krnjevic K. (1995). Internal Ca^{2+} stores involved in anoxic responses of rat hippocampal neurons. *J Physiol* **486 (Pt 3),** 547-556.

Ben-Chaim Y, Chanda B, Dascal N, Bezanilla F, Parnas I & Parnas H. (2006). Movement of 'gating charge' is coupled to ligand binding in a G-protein-coupled receptor. *Nature* **444,** 106-109.

Bender KJ, Allen CB, Bender VA & Feldman DE. (2006). Synaptic basis for whisker deprivation-induced synaptic depression in rat somatosensory cortex. *J Neurosci* **26,** 4155-4165.

Bennett HS. (1941). Cytological manifestation of secretion in the adrenal medulla of the cat. *Am J Anat* **69**.

Bentivoglio M. (1998). 1898: the Golgi apparatus emerges from nerve cells. *Trends Neurosci* **21,** 195-200.

Benveniste M & Mayer ML. (1991). Kinetic analysis of antagonist action at N-methyl-D-aspartic acid receptors. Two binding sites each for glutamate and glycine. *Biophys J* **59,** 560-573.

Berger M, Gray JA & Roth BL. (2009). The expanded biology of serotonin. *Annu Rev Med* **60,** 355-366.

Berridge CW & Foote SL. (1991). Effects of locus coeruleus activation on electroencephalographic activity in neocortex and hippocampus. *J Neurosci* **11,** 3135-3145.

Berridge MJ. (1983). Rapid accumulation of inositol trisphosphate reveals that agonists hydrolyse polyphosphoinositides instead of phosphatidylinositol. *Biochem J* **212,** 849-858.

Betz A, Okamoto M, Benseler F & Brose N. (1997). Direct interaction of the rat *unc-13* homologue Munc13-1 with the N terminus of syntaxin. *J Biol Chem* **272,** 2520-2526.

Betz WJ. (1970). Depression of transmitter release at the neuromuscular junction of the frog. *J Physiol* **206,** 629-644.

Betz WJ, Bewick GS & Ridge RM. (1992). Intracellular movements of fluorescently labeled synaptic vesicles in frog motor nerve terminals during nerve stimulation. *Neuron* **9,** 805-813.

Bhalla A, Chicka MC, Tucker WC & Chapman ER. (2006). Ca^{2+}-synaptotagmin directly regulates t-SNARE function during reconstituted membrane fusion. *Nat Struct Mol Biol* **13,** 323-330.

Bi GQ & Poo MM. (1998). Synaptic modifications in cultured hippocampal neurons: dependence on spike timing, synaptic strength, and postsynaptic cell type. *J Neurosci* **18,** 10464-10472.

Binah O, Dolnikov K, Sadan O, Shilkrut M, Zeevi-Levin N, Amit M, Danon A & Itskovitz-Eldor J. (2007). Functional and developmental properties of human embryonic stem cells-derived cardiomyocytes. *J Electrocardiol* **40,** S192-196.

Birman S, Israël M, Lesbats B & Morel N. (1986). Solubilization and partial purification of a presynaptic membrane protein ensuring calcium-dependent acetylcholine release from proteoliposomes. *J Neurochem* **47,** 433-444.

Blackmer T, Larsen EC, Bartleson C, Kowalchyk JA, Yoon EJ, Preininger AM, Alford S, Hamm HE & Martin TF. (2005). G protein βγ directly regulates SNARE protein fusion machinery for secretory granule exocytosis. *Nat Neurosci* **8,** 421-425.

Blackmer T, Larsen EC, Takahashi M, Martin TF, Alford S & Hamm HE. (2001). G protein βγ subunit-mediated presynaptic inhibition: regulation of exocytotic fusion downstream of Ca^{2+} entry. *Science* **292,** 293-297.

Blanchard H, Grochulski P, Li Y, Arthur JS, Davies PL, Elce JS & Cygler M. (1997). Structure of a calpain Ca^{2+}-binding domain reveals a novel EF-hand and Ca^{2+}-induced conformational changes. *Nat Struct Biol* **4,** 532-538.

Blaustein MP, Ratzlaff RW, Kendrick NC & Schweitzer ES. (1978). Calcium buffering in presynaptic nerve terminals. I. Evidence for involvement of a nonmitochondrial ATP-dependent sequestration mechanism. *J Gen Physiol* **72,** 15-41.

Blight AR & Precht W. (1982a). Miniature endplate potentials related to neuronal injury. *Brain Res* **238,** 233-238.

Blight AR & Precht W. (1982b). Miniature synaptic potentials absent from motoneurons of intact spinal cord. *Brain Res* **238,** 228-232.

Bliss TV & Collingridge GL. (1993). A synaptic model of memory: long-term potentiation in the hippocampus. *Nature* **361,** 31-39.

Bliss TV & Lømo T. (1973). Long-lasting potentiation of synaptic transmission in the dentate area of the anaesthetized rabbit following stimulation of the perforant path. *J Physiol* **232,** 331-356.

Bloedel J, Gage PW, Llinás R & Quastel DM. (1966). Transmitter release at the squid giant synapse in the presence of tetrodotoxin. *Nature* **212,** 49-50.

Blumer JB, Smrcka AV & Lanier SM. (2007). Mechanistic pathways and biological roles for receptor-independent activators of G-protein signaling. *Pharmacol & Ther* **113,** 488-506.

Bockaert J, Tassin JP, Thierry AM, Glowinski J & Premont J. (1977). Characteristics of dopamine and β-adrenergic sensitive adenylate cyclases in the frontal cerebral cortex of the rat. Comparative effects of neuroleptics on frontal cortex and striatal dopamine sensitive adenylate cyclases. *Brain Res* **122,** 71-86.

Bollmann JH, Sakmann B & Borst JG. (2000). Calcium sensitivity of glutamate release in a calyx-type terminal. *Science* **289,** 953-957.

Bona M, Antalík M, Gažová Z, Kuchár A, Dadák V & Podhradský D. (1993). Interaction of carbonyl cyanide 3-chlorophenylhydrazone with cytochrome c oxidase. *Gen Physiol Biophys* **12,** 533-542.

Bosanac I, Alattia JR, Mal TK, Chan J, Talarico S, Tong FK, Tong KI, Yoshikawa F, Furuichi T, Iwai M, Michikawa T, Mikoshiba K & Ikura M. (2002). Structure of the inositol 1,4,5-trisphosphate receptor binding core in complex with its ligand. *Nature* **420,** 696-700.

Bouevitch O, Lewis A, Pinevsky I, Wuskell JP & Loew LM. (1993). Probing membrane potential with nonlinear optics. *Biophys J* **65,** 672-679.

Boutjdir M, Restivo M, Wei Y & el-Sherif N. (1992). α_1- and β-adrenergic interactions on L-type calcium current in cardiac myocytes. *Pflügers Arch* **421,** 397-399.

Boyajian CL, Loughlin SE & Leslie FM. (1987). Anatomical evidence for *Alpha*-2 adrenoceptor heterogeneity: differential autoradiographic distributions of [^{3}H]rauwolscine and [^{3}H]idazoxan in rat brain. *J Pharmacol Exp Ther* **241,** 1079-1091.

Boyd IA & Martin AR. (1955). The quantal composition of the mammalian end-plate potential. *J Physiol* **129,** 14-15P.

Boyd IA & Martin AR. (1956). Spontaneous subthreshold activity at mammalian neural muscular junctions. *J Physiol* **132,** 61-73.

Brillantes AB, Ondrias K, Scott A, Kobrinsky E, Ondriasova E, Moschella MC, Jayaraman T, Landers M, Ehrlich BE & Marks AR. (1994). Stabilization of calcium release channel (ryanodine receptor) function by FK506-binding protein. *Cell* **77,** 513-523.

Brini M & Carafoli E. (2009). Calcium pumps in health and disease. *Physiol Rev* **89,** 1341-1378.

Brochier G, Israël M & Lesbats B. (1993). Immunolabelling of the presynaptic membrane of Torpedo electric organ nerve terminals with an antiserum towards the acetylcholine releasing protein mediatophore. *Biol Cell* **78,** 145-154.

Brock LG, Coombs JS & Eccles JC. (1952). The recording of potentials from motoneurones with an intracellular electrode. *J Physiol* **117,** 431-460.

Brody DL & Yue DT. (2000). Release-independent short-term synaptic depression in cultured hippocampal neurons. *J Neurosci* **20,** 2480-2494.

Brown JT, Weatherall KL, Corria LR, Chater TE, Isaac JT & Marrion NV. (2010). Vesicular release of glutamate utilizes the proton gradient between the vesicle and synaptic cleft. *Frontiers in Synaptic Neuroscience* **2,** 1-13.

Bucurenciu I, Kulik A, Schwaller B, Frotscher M & Jonas P. (2008). Nanodomain coupling between Ca^{2+} channels and Ca^{2+} sensors promotes fast and efficient transmitter release at a cortical GABAergic synapse. *Neuron* **57,** 536-545.

Buntinas L, Gunter KK, Sparagna GC & Gunter TE. (2001). The rapid mode of calcium uptake into heart mitochondria (RaM): comparison to RaM in liver mitochondria. *Biochim Biophys Acta* **1504,** 248-261.

Burger PM, Mehl E, Cameron PL, Maycox PR, Baumert M, Lottspeich F, De Camilli P & Jahn R. (1989). Synaptic vesicles immunoisolated from rat cerebral cortex contain high levels of glutamate. *Neuron* **3,** 715-720.

Burke RE, Rudomin P & Zajac FE, 3rd. (1970). Catch property in single mammalian motor units. *Science* **168,** 122-124.

Buxton IL & Brunton LL. (1985). Action of the cardiac α_1-adrenergic receptor. Activation of cyclic AMP degradation. *J Biol Chem* **260,** 6733-6737.

Bylund DB, Eikenberg DC, Hieble JP, Langer SZ, Lefkowitz RJ, Minneman KP, Molinoff PB, Ruffolo RR, Jr. & Trendelenburg U. (1994). International Union of Pharmacology nomenclature of adrenoceptors. *Pharmacol Rev* **46,** 121-136.

Cambridge D, Davey MJ & Massingham R. (1977). Prazosin, a selective antagonist of post-synaptic α-adrenoceptors [proceedings]. *Br J Pharmacol* **59,** 514P-515P.

Cammack JN, Rakhilin SV & Schwartz EA. (1994). A GABA transporter operates asymmetrically and with variable stoichiometry. *Neuron* **13,** 949-960.

Cammer W. (1990). Glutamine synthetase in the central nervous system is not confined to astrocytes. *J Neuroimmunol* **26,** 173-178.

Campbell KP, Knudson CM, Imagawa T, Leung AT, Sutko JL, Kahl SD, Raab CR & Madson L. (1987). Identification and characterization of the high affinity [^{3}H]ryanodine receptor of the junctional sarcoplasmic reticulum Ca^{2+} release channel. *J Biol Chem* **262,** 6460-6463.

Carafoli E, Tiozzo R, Lugli G, Crovetti F & Kratzing C. (1974). The release of calcium from heart mitochondria by sodium. *Journal of molecular and cellular cardiology* **6,** 361-371.

Carlson GC, Slawecki ML, Lancaster E & Keller A. (1997). Distribution and activation of intracellular Ca^{2+} stores in cultured olfactory bulb neurons. *J Neurophysiol* **78,** 2176-2185.

Carter AG & Regehr WG. (2002). Quantal events shape cerebellar interneuron firing. *Nat Neurosci* **5,** 1309-1318.

Cartmell J & Schoepp DD. (2000). Regulation of neurotransmitter release by metabotropic glutamate receptors. *J Neurochem* **75,** 889-907.

Casale TB, Wescott S, Rodbard D & Kaliner M. (1985). Characterization of histamine H-1 receptors on human mononuclear cells. *Int J Immunopharmacol* **7,** 639-645.

Cash R, Raisman R, Lanfumey L, Ploska A & Agid Y. (1986). Cellular localization of adrenergic receptors in rat and human brain. *Brain Res* **370,** 127-135.

Castellucci V & Kandel ER. (1976). Presynaptic facilitation as a mechanism for behavioral sensitization in Aplysia. *Science* **194,** 1176-1178.

Cataldo AM & Broadwell RD. (1984). Cytochemical staining of the endoplasmic reticulum and glycogen in mouse anterior pituitary cells. *J Histochem Cytochem* **32,** 1285-1294.

Catterall WA. (1999). Interactions of presynaptic Ca^{2+} channels and snare proteins in neurotransmitter release. *Ann N Y Acad Sci* **868,** 144-159.

Ceccarelli B & Hurlbut WP. (1980). Ca^{2+}-dependent recycling of synaptic vesicles at the frog neuromuscular junction. *J Cell Biol* **87,** 297-303.

Ceccarelli B, Hurlbut WP & Mauro A. (1973). Turnover of transmitter and synaptic vesicles at the frog neuromuscular junction. *J Cell Biol* **57,** 499-524.

Celikel T, Szostak VA & Feldman DE. (2004). Modulation of spike timing by sensory deprivation during induction of cortical map plasticity. *Nat Neurosci* **7,** 534-541.

Chalothorn D, McCune DF, Edelmann SE, Garcia-Cazarin ML, Tsujimoto G & Piascik MT. (2002). Differences in the cellular localization and agonist-mediated internalization properties of the α_1-adrenoceptor subtypes. *Molecular pharmacology* **61,** 1008-1016.

Chan SL, Mayne M, Holden CP, Geiger JD & Mattson MP. (2000). Presenilin-1 mutations increase levels of ryanodine receptors and calcium release in PC12 cells and cortical neurons. *J Biol Chem* **275,** 18195-18200.

Chaudhry FA, Reimer RJ, Bellocchio EE, Danbolt NC, Osen KK, Edwards RH & Storm-Mathisen J. (1998). The vesicular GABA transporter, VGAT, localizes to synaptic vesicles in sets of glycinergic as well as GABAergic neurons. *J Neurosci* **18,** 9733-9750.

Chaudhry FA, Reimer RJ, Krizaj D, Barber D, Storm-Mathisen J, Copenhagen DR & Edwards RH. (1999). Molecular analysis of system N suggests novel physiological roles in nitrogen metabolism and synaptic transmission. *Cell* **99,** 769-780.

Cheetham CE, Hammond MS, Edwards CE & Finnerty GT. (2007). Sensory experience alters cortical connectivity and synaptic function site specifically. *J Neurosci* **27,** 3456-3465.

Chen Q, Li DP & Pan HL. (2006). Presynaptic α_1 adrenergic receptors differentially regulate synaptic glutamate and GABA release to hypothalamic presympathetic neurons. *J Pharmacol Exp Ther* **316,** 733-742.

Cheng H, Lederer WJ & Cannell MB. (1993). Calcium sparks: elementary events underlying excitation-contraction coupling in heart muscle. *Science* **262,** 740-744.

Cheung G, Jupp OJ & Cousin MA. (2010). Activity-dependent bulk endocytosis and clathrin-dependent endocytosis replenish specific synaptic vesicle pools in central nerve terminals. *J Neurosci* **30,** 8151-8161.

Cheung KH, Shineman D, Muller M, Cardenas C, Mei L, Yang J, Tomita T, Iwatsubo T, Lee VM & Foskett JK. (2008). Mechanism of Ca^{2+} disruption in Alzheimer's disease by presenilin regulation of $InsP_3$ receptor channel gating. *Neuron* **58,** 871-883.

Choi S & Kellogg CK. (1992). Norepinephrine utilization in the hypothalamus of the male rat during adolescent development. *Dev Neurosci* **14,** 369-376.

Choi UB, Strop P, Vrljic M, Chu S, Brunger AT & Weninger KR. (2010). Single-molecule FRET-derived model of the synaptotagmin 1-SNARE fusion complex. *Nat Struct Mol Biol* **17,** 318-324.

Chu A, Diaz-Munoz M, Hawkes MJ, Brush K & Hamilton SL. (1990). Ryanodine as a probe for the functional state of the skeletal muscle sarcoplasmic reticulum calcium release channel. *Molecular pharmacology* **37,** 735-741.

Chueh SH & Gill DL. (1986). Inositol 1,4,5-trisphosphate and guanine nucleotides activate calcium release from endoplasmic reticulum via distinct mechanisms. *J Biol Chem* **261,** 13883-13886.

Clapham DE. (2007). Calcium signaling. *Cell* **131,** 1047-1058.

Clark CR, Geffen GM & Geffen LB. (1987). Catecholamines and attention. I: Animal and clinical studies. *Neurosci Biobehav Rev* **11,** 341-352.

Cleary L, Murad K, Bexis S & Docherty JR. (2005). The α_{1D}-adrenoceptor antagonist BMY 7378 is also an α_{2C}-adrenoceptor antagonist. *Auton Autacoid Pharmacol* **25,** 135-141.

Clemente F & Meldolesi J. (1975). Calcium and pancreatic secretion. I. Subcellular distribution of calcium and magnesium in the exocrine pancreas of the guinea pig. *J Cell Biol* **65,** 88-102.

Clements J. (1991). Quantal synaptic transmission? *Nature* **353,** 396.

Clements JD & Bekkers JM. (1997). Detection of spontaneous synaptic events with an optimally scaled template. *Biophys J* **73,** 220-229.

Clements JD, Lester RA, Tong G, Jahr CE & Westbrook GL. (1992). The time course of glutamate in the synaptic cleft. *Science* **258,** 1498-1501.

Clements JR, Magnusson KR & Beitz AJ. (1990). Ultrastructural description of glutamate-, aspartate-, taurine-, and glycine-like immunoreactive terminals from five rat brain regions. *J Electron Microsc Tech* **15,** 49-66.

Coffee CJ & Bradshaw RA. (1973). Carp muscle calcium-binding protein. I. Characterization of the tryptic peptides and the complete amino acid sequence of component B. *J Biol Chem* **248,** 3305-3312.

Cohen I, Kita H & Van Der Kloot W. (1974). The stochastic properties of spontaneous quantal release of transmitter at the frog neuromuscular junction. *J Physiol* **236,** 341-361.

Collingridge GL, Peineau S, Howland JG & Wang YT. (2010). Long-term depression in the CNS. *Nature reviews* **11,** 459-473.

Colquhoun D, Jonas P & Sakmann B. (1992). Action of brief pulses of glutamate on AMPA/kainate receptors in patches from different neurones of rat hippocampal slices. *The Journal of physiology* **458,** 261-287.

Conn PJ & Pin JP. (1997). Pharmacology and functions of metabotropic glutamate receptors. *Annu Rev Pharmacol Toxicol* **37,** 205-237.

Connors BW, Benardo LS & Prince DA. (1983). Coupling between neurons of the developing rat neocortex. *J Neurosci* **3,** 773-782.

Cordeiro JM, Goncalves PP & Dunant Y. (2010). Synaptic vesicles control the time-course of neurotransmitter secretion via a Ca^{2+}/H^{+} antiport. *J Physiol.*

Couteaux R & Pécot-Dechavassine M. (1970). Synaptic vesicles and pouches at the level of "active zones" of the neuromuscular junction. *C R Acad Sci Hebd Seances Acad Sci D* **271,** 2346-2349.

Cowan AI & Stricker C. (2004). Functional connectivity in layer IV local excitatory circuits of rat somatosensory cortex. *J Neurophysiol* **92,** 2137-2150.

Cowan AI, Stricker C, Reece LJ & Redman SJ. (1998). Long-term plasticity at excitatory synapses on aspinous interneurons in area CA1 lacks synaptic specificity. *J Neurophysiol* **79,** 13-20.

Creutz CE, Pazoles CJ & Pollard HB. (1978). Identification and purification of an adrenal medullary protein (synexin) that causes calcium-dependent aggregation of isolated chromaffin granules. *J Biol Chem* **253,** 2858-2866.

Crompton M, Capano M & Carafoli E. (1976). The sodium-induced efflux of calcium from heart mithchondria. A possible mechanism for the regulation of mitochondrial calcium. *Eur J Biochem* **69,** 453-462.

Crompton M, Moser R, Ludi H & Carafoli E. (1978). The interrelations between the transport of sodium and calcium in mitochondria of various mammalian tissues. *Eur J Biochem* **82,** 25-31.

Cuadras J & Marti A. (1992). Granule containing cells in the crayfish third abdominal ganglion. *Comp Biochem Physiol Comp Physiol* **101,** 453-457.

Curtis DR & Eccles JC. (1960). Synaptic action during and after repetitive stimulation. *J Physiol* **150,** 374-398.

Curtis DR, Phillis JW & Watkins JC. (1959). Chemical excitation of spinal neurones. *Nature* **183,** 611-612.

Cutler DJ, Morris R, Sheridhar V, Wattam TA, Holmes S, Patel S, Arch JR, Wilson S, Buckingham RE, Evans ML, Leslie RA & Williams G. (1999). Differential distribution of orexin-A and orexin-B immunoreactivity in the rat brain and spinal cord. *Peptides* **20,** 1455-1470.

Dale H. (1934). Chemical Transmission of the Effects of Nerve Impulses. *Br Med J* **1,** 835-841.

Dani VS, Chang Q, Maffei A, Turrigiano GG, Jaenisch R & Nelson SB. (2005). Reduced cortical activity due to a shift in the balance between excitation and inhibition in a mouse model of Rett syndrome. *Proc Natl Acad Sci U S A* **102,** 12560-12565.

Dash MB, Douglas CL, Vyazovskiy VV, Cirelli C & Tononi G. (2009). Long-term homeostasis of extracellular glutamate in the rat cerebral cortex across sleep and waking states. *J Neurosci* **29,** 620-629.

Datyner NB & Gage PW. (1980). Phasic secretion of acetylcholine at a mammalian neuromuscular junction. *J Physiol* **303,** 299-314.

Davies SN, Lester RA, Reymann KG & Collingridge GL. (1989). Temporally distinct pre- and post-synaptic mechanisms maintain long-term potentiation. *Nature* **338,** 500-503.

Davis AF, Bai J, Fasshauer D, Wolowick MJ, Lewis JL & Chapman ER. (1999). Kinetics of synaptotagmin responses to Ca^{2+} and assembly with the core SNARE complex onto membranes. *Neuron* **24,** 363-376.

Davletov BA & Südhof TC. (1993). A single C_2 domain from synaptotagmin I is sufficient for high affinity Ca^{2+}/phospholipid binding. *J Biol Chem* **268,** 26386-26390.

De Backer MD, Gommeren W, Moereels H, Nobels G, Van Gompel P, Leysen JE & Luyten WH. (1993). Genomic cloning, heterologous expression and pharmacological characterization of a human histamine H1 receptor. *Biochem Biophys Res Commun* **197,** 1601-1608.

De Crescenzo V, ZhuGe R, Velazquez-Marrero C, Lifshitz LM, Custer E, Carmichael J, Lai FA, Tuft RA, Fogarty KE, Lemos JR & Walsh JV, Jr. (2004). Ca^{2+} syntillas, miniature Ca^{2+} release events in terminals of hypothalamic neurons, are increased in frequency by depolarization in the absence of Ca^{2+} influx. *J Neurosci* **24,** 1226-1235.

De Harven E & Coërs C. (1959). Electron microscope study of the human neuromuscular junction. *J Biophys Biochem Cytol* **6,** 7-10.

De Lecea L, Kilduff TS, Peyron C, Gao X, Foye PE, Danielson PE, Fukuhara C, Battenberg EL, Gautvik VT, Bartlett FS, 2nd, Frankel WN, van den Pol AN, Bloom FE, Gautvik KM & Sutcliffe JG. (1998). The hypocretins: hypothalamus-specific peptides with neuroexcitatory activity. *Proc Natl Acad Sci U S A* **95,** 322-327.

De Strooper B, Annaert W, Cupers P, Saftig P, Craessaerts K, Mumm JS, Schroeter EH, Schrijvers V, Wolfe MS, Ray WJ, Goate A & Kopan R. (1999). A presenilin-1-dependent gamma-secretase-like protease mediates release of Notch intracellular domain. *Nature* **398,** 518-522.

Deken SL, Beckman ML, Boos L & Quick MW. (2000). Transport rates of GABA transporters: regulation by the N-terminal domain and syntaxin 1A. *Nat Neurosci* **3,** 998-1003.

Del Castillo J & Engbaek L. (1954). The nature of the neuromuscular block produced by magnesium. *J Physiol* **124,** 370-384.

Del Castillo J & Katz B. (1954). Quantal components of the end-plate potential. *J Physiol* **124,** 560-573.

Delaney AJ, Crane JW & Sah P. (2007). Noradrenaline modulates transmission at a central synapse by a presynaptic mechanism. *Neuron* **56,** 880-892.

Delaney KR, Zucker RS & Tank DW. (1989). Calcium in motor nerve terminals associated with posttetanic potentiation. *J Neurosci* **9,** 3558-3567.

Delbarre F, Laoussadi S, Amor B & Kahan A. (1981). Hydroxyapatite microcrystals in synovial mitochondria in human and experimental rheumatism. *Comptes rendus des seances de l'Academie des sciences* **293,** 567-574.

Delmas P & Brown DA. (2005). Pathways modulating neural KCNQ/M (Kv7) potassium channels. *Nature reviews* **6,** 850-862.

Desai NS, Cudmore RH, Nelson SB & Turrigiano GG. (2002). Critical periods for experience-dependent synaptic scaling in visual cortex. *Nat Neurosci* **5,** 783-789.

Devilbiss DM & Waterhouse BD. (2000). Norepinephrine exhibits two distinct profiles of action on sensory cortical neuron responses to excitatory synaptic stimuli. *Synapse* **37,** 273-282.

Di Giovanni J, Boudkkazi S, Mochida S, Bialowas A, Samari N, Lèvêque C, Youssouf F, Brechet A, Iborra C, Maulet Y, Moutot N, Debanne D, Seagar M & El Far O. (2010). V-ATPase membrane sector associates with synaptobrevin to modulate neurotransmitter release. *Neuron* **67,** 268-279.

Diamond JS & Jahr CE. (1995). Asynchronous release of synaptic vesicles determines the time course of the AMPA receptor-mediated EPSC. *Neuron* **15,** 1097-1107.

DiAntonio A & Schwarz TL. (1994). The effect on synaptic physiology of synaptotagmin mutations in Drosophila. *Neuron* **12,** 909-920.

Diaz-Munoz M, Hamilton SL, Kaetzel MA, Hazarika P & Dedman JR. (1990). Modulation of Ca^{2+} release channel activity from sarcoplasmic reticulum by annexin VI (67-kDa calcimedin). *J Biol Chem* **265,** 15894-15899.

Disbrow JK, Gershten MJ & Ruth JA. (1982). Uptake of L-[^{3}H] glutamic acid by crude and purified synaptic vesicles from rat brain. *Biochem Biophys Res Commun* **108,** 1221-1227.

Dismukes RK & Mulder AH. (1976). Cyclic AMP and α-receptor-mediated modulation of noradrenaling release from rat brain slices. *Eur J Pharmacol* **39,** 383-388.

Dittman JS & Regehr WG. (1998). Calcium dependence and recovery kinetics of presynaptic depression at the climbing fiber to Purkinje cell synapse. *J Neurosci* **18,** 6147-6162.

Dodge FA, Jr. & Rahamimoff R. (1967). Co-operative action of calcium ions in transmitter release at the neuromuscular junction. *J Physiol* **193,** 419-432.

Douglas RJ & Martin KA. (2004). Neuronal circuits of the neocortex. *Annu Rev Neurosci* **27,** 419-451.

Douglas WW & Paton WD. (1954). The mechanisms of motor end-plate depolarization due to a cholinesterase-inhibiting drug. *J Physiol* **124,** 325-344.

Dowal L, Provitera P & Scarlata S. (2006). Stable association between $G\alpha_q$ and phospholipase $C\beta_1$ in living cells. *J Biol Chem* **281,** 23999-24014.

Doze VA, Cohen GA & Madison DV. (1991). Synaptic localization of adrenergic disinhibition in the rat hippocampus. *Neuron* **6,** 889-900.

Duchen MR. (1992). Ca^{2+}-dependent changes in the mitochondrial energetics in single dissociated mouse sensory neurons. *Biochem J* **283 (Pt 1),** 41-50.

Dudek SM & Bear MF. (1992). Homosynaptic long-term depression in area CA1 of hippocampus and effects of N-methyl-D-aspartate receptor blockade. *Proc Natl Acad Sci U S A* **89,** 4363-4367.

Dudel J. (1977). Voltage dependence of amplitude and time course of inhibitory synaptic current in crayfish muscle. *Pflügers Arch* **371,** 167-174.

Dudel J, Parnas I & Parnas H. (1983). Neurotransmitter release and its facilitation in crayfish muscle. VI. Release determined by both, intracellular calcium concentration and depolarization of the nerve terminal. *Pflügers Arch* **399,** 1-10.

Dunham ET & Glynn IM. (1961). Adenosinetriphosphatase activity and the active movements of alkali metal ions. *J Physiol* **156,** 274-293.

Earles CA, Bai J, Wang P & Chapman ER. (2001). The tandem C2 domains of synaptotagmin contain redundant Ca^{2+} binding sites that cooperate to engage t-SNAREs and trigger exocytosis. *J Cell Biol* **154,** 1117-1123.

Eccles JC, Katz B & S.W. K. (1941). Nature of the "endplate potential" in curarized muscle. *J Neurophysiol* **4,** 362-387.

Eccles JC & McGeer PL. (1979). Ionotropic and metabotropic neurotransmission. *Trends Neurosci* **2,** 39-40.

Eccles JC & O'Connor WJ. (1939). Responses which nerve impulses evoke in mammalian striated muscles. *J Physiol* **97,** 44-102.

Edwards FA, Konnerth A & Sakmann B. (1990). Quantal analysis of inhibitory synaptic transmission in the dentate gyrus of rat hippocampal slices: a patch-clamp study. *J Physiol* **430,** 213-249.

Engelman HS & MacDermott AB. (2004). Presynaptic ionotropic receptors and control of transmitter release. *Nature reviews* **5,** 135-145.

Engert F & Bonhoeffer T. (1997). Synapse specificity of long-term potentiation breaks down at short distances. *Nature* **388,** 279-284.

Enyedi A, Flura M, Sarkadi B, Gardos G & Carafoli E. (1987). The maximal velocity and the calcium affinity of the red cell calcium pump may be regulated independently. *J Biol Chem* **262,** 6425-6430.

Fadel J & Deutch AY. (2002). Anatomical substrates of orexin-dopamine interactions: lateral hypothalamic projections to the ventral tegmental area. *Neurosci* **111,** 379-387.

Fairman WA, Vandenberg RJ, Arriza JL, Kavanaugh MP & Amara SG. (1995). An excitatory amino-acid transporter with properties of a ligand-gated chloride channel. *Nature* **375,** 599-603.

Falkenburger BH, Jensen JB & Hille B. (2010). Kinetics of PIP_2 metabolism and KCNQ2/3 channel regulation studied with a voltage-sensitive phosphatase in living cells. *J Gen Physiol* **135,** 99-114.

Fatt P & Katz B. (1950). Some observations on biological noise. *Nature* **166,** 597-598.

Fatt P & Katz B. (1951). An analysis of the end-plate potential recorded with an intracellular electrode. *J Physiol* **115,** 320-370.

Fatt P & Katz B. (1952). Spontaneous subthreshold activity at motor nerve endings. *J Physiol* **117,** 109-128.

Feldmeyer D, Lübke J & Sakmann B. (2006). Efficacy and connectivity of intracolumnar pairs of layer 2/3 pyramidal cells in the barrel cortex of juvenile rats. *J Physiol* **575,** 583-602.

Felten DL, Hallman H & Jonsson G. (1982). Evidence for a neurotropic role of noradrenaline neurons in the postnatal development of rat cerebral cortex. *J Neurocytol* **11,** 119-135.

Fesce R, Grohovaz F, Valtorta F & Meldolesi J. (1994). Neurotransmitter release: fusion or 'kiss-and-run'? *Trends Cell Biol* **4,** 1-4.

Finch EA, Turner TJ & Goldin SM. (1991). Calcium as a coagonist of inositol 1,4,5-trisphosphate-induced calcium release. *Science* **252,** 443-446.

Finch L & Hicks PE. (1977). Involvement of hypothalamic histamine-receptors in the central cardiovascular actions of histamine. *Neuropharmac* **16,** 211-218.

Finley MF, Patel SM, Madison DV & Scheller RH. (2002). The core membrane fusion complex governs the probability of synaptic vesicle fusion but not transmitter release kinetics. *J Neurosci* **22,** 1266-1272.

Fischer von Mollard G, Stahl B, Khokhlatchev A, Südhof TC & Jahn R. (1994). Rab3C is a synaptic vesicle protein that dissociates from synaptic vesicles after stimulation of exocytosis. *J Biol Chem* **269,** 10971-10974.

Fitzjohn SM, Palmer MJ, May JE, Neeson A, Morris SA & Collingridge GL. (2001). A characterisation of long-term depression induced by metabotropic glutamate receptor activation in the rat hippocampus in vitro. *J Physiol* **537,** 421-430.

Florey E & Kriebel ME. (1988). Reversible effect of depolarization by K-propionate on sub-miniature endplate potential to bell-miniature endplate potential ratios, on miniature endplate potential frequencies and amplitudes, and on synaptic vesicle diameters and densities in frog neuromuscular junctions. *Neurosci* **27,** 1055-1072.

Florin-Lechner SM, Druhan JP, Aston-Jones G & Valentino RJ. (1996). Enhanced norepinephrine release in prefrontal cortex with burst stimulation of the locus coeruleus. *Brain Res* **742,** 89-97.

Fontana G, Rogowski RS & Blaustein MP. (1995). Kinetic properties of the sodium-calcium exchanger in rat brain synaptosomes. *J Physiol* **485 (Pt 2),** 349-364.

Ford AP, Williams TJ, Blue DR & Clarke DE. (1994). α_1-adrenoceptor classification: sharpening Occam's razor. *Trends Pharmacol Sci* **15,** 167-170.

Forsythe ID, Tsujimoto T, Barnes-Davies M, Cuttle MF & Takahashi T. (1998). Inactivation of presynaptic calcium current contributes to synaptic depression at a fast central synapse. *Neuron* **20,** 797-807.

Fort P, Khateb A, Pegna A, Mühlethaler M & Jones BE. (1995). Noradrenergic modulation of cholinergic nucleus basalis neurons demonstrated by in vitro pharmacological and immunohistochemical evidence in the guinea-pig brain. *Eur J Neurosci* **7,** 1502-1511.

Foster M. (1897). *A Textbook of Physiology*. MacMillan and Co. Limited.

Fredj NB & Burrone J. (2009). A resting pool of vesicles is responsible for spontaneous vesicle fusion at the synapse. *Nat Neurosci* **12,** 751-758.

Fremeau RT, Jr., Burman J, Qureshi T, Tran CH, Proctor J, Johnson J, Zhang H, Sulzer D, Copenhagen DR, Storm-Mathisen J, Reimer RJ, Chaudhry FA & Edwards RH. (2002). The identification of vesicular glutamate transporter 3 suggests novel modes of signaling by glutamate. *Proc Natl Acad Sci U S A* **99,** 14488-14493.

Fremeau RT, Jr., Troyer MD, Pahner I, Nygaard GO, Tran CH, Reimer RJ, Bellocchio EE, Fortin D, Storm-Mathisen J & Edwards RH. (2001). The expression of vesicular glutamate transporters defines two classes of excitatory synapse. *Neuron* **31,** 247-260.

Friedman LF, Zeitzer JM, Lin L, Hoff D, Mignot E, Peskind ER & Yesavage JA. (2007). In Alzheimer disease, increased wake fragmentation found in those with lower hypocretin-1. *Neurol* **68,** 793-794.

Fuente PG, Savineau JP & Marthan R. (1995). Control of pulmonary vascular smooth muscle tone by sarcoplasmic reticulum Ca^{2+} pump blockers: thapsigargin and cyclopiazonic acid. *Pflügers Arch* **429,** 617-624.

Fuhrmann G, Cowan A, Segev I, Tsodyks M & Stricker C. (2004). Multiple mechanisms govern the dynamics of depression at neocortical synapses of young rats. *J Physiol* **557,** 415-438.

Fujiwara N, Higashi H, Shimoji K & Yoshimura M. (1987). Effects of hypoxia on rat hippocampal neurones in vitro. *J Physiol* **384,** 131-151.

Fujiyama F, Furuta T & Kaneko T. (2001). Immunocytochemical localization of candidates for vesicular glutamate transporters in the rat cerebral cortex. *J Comp Neurol* **435,** 379-387.

Fuldner HH & Stadler H. (1982). ^{31}P-NMR analysis of synaptic vesicles. Status of ATP and internal pH. *Eur J Biochem* **121,** 519-524.

Full SJ, Deinzer ML, Ho PS & Greenwood JA. (2007). Phosphoinositide binding regulates α-actinin CH2 domain structure: analysis by hydrogen/deuterium exchange mass spectrometry. *Protein Sci* **16,** 2597-2604.

Furshpan EJ & Potter DD. (1959). Transmission at the giant motor synapses of the crayfish. *J Physiol* **145,** 289-325.

Gafni J, Munsch JA, Lam TH, Catlin MC, Costa LG, Molinski TF & Pessah IN. (1997). Xestospongins: potent membrane permeable blockers of the inositol 1,4,5-trisphosphate receptor. *Neuron* **19,** 723-733.

Galante M & Marty A. (2003). Presynaptic ryanodine-sensitive calcium stores contribute to evoked neurotransmitter release at the basket cell-Purkinje cell synapse. *J Neurosci* **23,** 11229-11234.

Garaschuk O, Yaari Y & Konnerth A. (1997). Release and sequestration of calcium by ryanodine-sensitive stores in rat hippocampal neurones. *J Physiol* **502 (Pt 1),** 13-30.

Gatto C & Milanick MA. (1993). Inhibition of the red blood cell calcium pump by eosin and other fluorescein analogues. *Am J Physiol* **264,** C1577-1586.

Geisow MJ, Walker JH, Boustead C & Taylor W. (1987). Annexins--new family of Ca^{2+}-regulated-phospholipid binding protein. *Bioscience reports* **7,** 289-298.

Georgiev P, Garcia-Murillas I, Ulahannan D, Hardie RC & Raghu P. (2005). Functional INAD complexes are required to mediate degeneration in photoreceptors of the *Drosophila rdgA* mutant. *J Cell Sci* **118,** 1373-1384.

Geppert M, Goda Y, Hammer RE, Li C, Rosahl TW, Stevens CF & Südhof TC. (1994). Synaptotagmin I: a major Ca^{2+} sensor for transmitter release at a central synapse. *Cell* **79,** 717-727.

Gerachshenko T, Blackmer T, Yoon EJ, Bartleson C, Hamm HE & Alford S. (2005). Gβγ acts at the C terminus of SNAP-25 to mediate presynaptic inhibition. *Nat Neurosci* **8,** 597-605.

Gerke V & Moss SE. (2002). Annexins: from structure to function. *Physiol Rev* **82,** 331-371.

Glazewski S & Fox K. (1996). Time course of experience-dependent synaptic potentiation and depression in barrel cortex of adolescent rats. *J Neurophysiol* **75,** 1714-1729.

Goda Y & Stevens CF. (1998). Readily releasable pool size changes associated with long term depression. *Proc Natl Acad Sci U S A* **95,** 1283-1288.

Goetz AS, King HK, Ward SD, True TA, Rimele TJ & Saussy DL, Jr. (1995). BMY 7378 is a selective antagonist of the D subtype of α_1-adrenoceptors. *Eur J Pharmacol* **272,** R5-6.

Golding NL, Staff NP & Spruston N. (2002). Dendritic spikes as a mechanism for cooperative long-term potentiation. *Nature* **418,** 326-331.

Goldstein LS & Yang Z. (2000). Microtubule-based transport systems in neurons: the roles of kinesins and dyneins. *Annu Rev Neurosci* **23,** 39-71.

Gonçalves PP, Meireles SM, Gravato C & Vale MG. (1998). Ca^{2+}-H^+ antiport activity in synaptic vesicles isolated from sheep brain cortex. *Neurosci Lett* **247,** 87-90.

Gonçalves PP, Meireles SM, Neves P & Vale MG. (1999). Synaptic vesicle Ca^{2+}/H^{+} antiport: dependence on the proton electrochemical gradient. *Brain Res Mol Brain Res* **71,** 178-184.

Gonçalves PP, Meireles SM, Neves P & Vale MG. (2000). Distinction between Ca^{2+} pump and Ca^{2+}/H^{+} antiport activities in synaptic vesicles of sheep brain cortex. *Neurochem Int* **37,** 387-396.

González JC, Albinana E, Baldelli P, Garcia AG & Hernandez-Guijo JM. (2011). Presynaptic muscarinic receptor subtypes involved in the enhancement of spontaneous GABAergic postsynaptic currents in hippocampal neurons. *The European journal of neuroscience* **33,** 69-81.

Goodhardt M, Ferry N, Geynet P & Hanoune J. (1982). Hepatic α_1-adrenergic receptors show agonist-specific regulation by guanine nucleotides. Loss of nucleotide effect after adrenalectomy. *J Biol Chem* **257,** 11577-11583.

Gordon GR & Bains JS. (2003). Priming of excitatory synapses by α_1 adrenoceptor-mediated inhibition of group III metabotropic glutamate receptors. *J Neurosci* **23,** 6223-6231.

Gordon GR & Bains JS. (2005). Noradrenaline triggers multivesicular release at glutamatergic synapses in the hypothalamus. *J Neurosci* **25,** 11385-11395.

Görlach A, Klappa P & Kietzmann T. (2006). The endoplasmic reticulum: folding, calcium homeostasis, signaling, and redox control. *Antioxid Redox Signal* **8,** 1391-1418.

Gottlieb JP & Keller A. (1997). Intrinsic circuitry and physiological properties of pyramidal neurons in rat barrel cortex. *Exp Brain Res* **115,** 47-60.

Grafstein B & Forman DS. (1980). Intracellular transport in neurons. *Physiol Rev* **60,** 1167-1283.

Granseth B, Odermatt B, Royle SJ & Lagnado L. (2006). Clathrin-mediated endocytosis is the dominant mechanism of vesicle retrieval at hippocampal synapses. *Neuron* **51,** 773-786.

Gras C, Herzog E, Bellenchi GC, Bernard V, Ravassard P, Pohl M, Gasnier B, Giros B & El Mestikawy S. (2002). A third vesicular glutamate transporter expressed by cholinergic and serotoninergic neurons. *J Neurosci* **22,** 5442-5451.

Gray EG. (1959). Axo-somatic and axo-dendritic synapses of the cerebral cortex: an electron microscope study. *J Anat* **93,** 420-433.

Grayson TH, Ellis JM, Chen S, Graham RM, Brown RD & Hill CE. (1998). Immunohistochemical localisation of α_{1B}-adrenergic receptors in the rat iris. *Cell Tissue Res* **293,** 435-444.

Graziadei I, Zernig G, Boer R & Glossman H. (1989). Stereoselective binding of niguldipine enantiomers to α_{1A}-adrenoceptors labeled with [^{3}H]5-methyl-urapidil. *Eur J Pharmacol* **172,** 329-337.

Green KN, Demuro A, Akbari Y, Hitt BD, Smith IF, Parker I & LaFerla FM. (2008). SERCA pump activity is physiologically regulated by presenilin and regulates amyloid beta production. *J Cell Biol* **181,** 1107-1116.

Grillner P, Bonci A, Svensson TH, Bernardi G & Mercuri NB. (1999). Presynaptic muscarinic (M3) receptors reduce excitatory transmission in dopamine neurons of the rat mesencephalon. *Neurosci* **91,** 557-565.

Gunter TE & Gunter KK. (2001). Uptake of calcium by mitochondria: transport and possible function. *IUBMB life* **52,** 197-204.

Haiech J, Derancourt J, Pechère JF & Demaille JG. (1979). Magnesium and calcium binding to parvalbumins: evidence for differences between parvalbumins and an explanation of their relaxing function. *Biochem* **18,** 2752-2758.

Hajnóczky G, Lin C & Thomas AP. (1994). Luminal communication between intracellular calcium stores modulated by GTP and the cytoskeleton. *J Biol Chem* **269,** 10280-10287.

Hájos M, Fleishaker JC, Filipiak-Reisner JK, Brown MT & Wong EH. (2004). The selective norepinephrine reuptake inhibitor antidepressant reboxetine: pharmacological and clinical profile. *CNS Drug Rev* **10,** 23-44.

Hamada S, Senzaki K, Hamaguchi-Hamada K, Tabuchi K, Yamamoto H, Yamamoto T, Yoshikawa S, Okano H & Okado N. (1998). Localization of 5-HT2A receptor in rat cerebral cortex and olfactory system revealed by immunohistochemistry using two antibodies raised in rabbit and chicken. *Brain Res Mol Brain Res* **54,** 199-211.

Hamberger A & Nyström B. (1984). Extra- and intracellular amino acids in the hippocampus during development of hepatic encephalopathy. *Neurochem Res* **9,** 1181-1192.

Hamberger AC, Chiang GH, Nylen ES, Scheff SW & Cotman CW. (1979). Glutamate as a CNS transmitter. I. Evaluation of glucose and glutamine as precursors for the synthesis of preferentially released glutamate. *Brain Res* **168,** 513-530.

Han C, Abel PW & Minneman KP. (1987). α_1-adrenoceptor subtypes linked to different mechanisms for increasing intracellular Ca^{2+} in smooth muscle. *Nature* **329,** 333-335.

Hanson PI, Roth R, Morisaki H, Jahn R & Heuser JE. (1997). Structure and conformational changes in NSF and its membrane receptor complexes visualized by quick-freeze/deep-etch electron microscopy. *Cell* **90,** 523-535.

Hardie RC, Gu Y, Martin F, Sweeney ST & Raghu P. (2004). *In vivo* light-induced and basal phospholipase C activity in *Drosophila* photoreceptors measured with genetically targeted phosphatidylinositol 4,5-bisphosphate-sensitive ion channels (Kir2.1). *J Biol Chem* **279,** 47773-47782.

Hardingham NR & Larkman AU. (1998). Rapid report: the reliability of excitatory synaptic transmission in slices of rat visual cortex in vitro is temperature dependent. *J Physiol* **507 (Pt 1),** 249-256.

Harik SI, LaManna JC, Light AI & Rosenthal M. (1979). Cerebral norepinephrine: influence on cortical oxidative metabolism in situ. *Science* **206,** 69-71.

Harris EW & Cotman CW. (1986). Long-term potentiation of guinea pig mossy fiber responses is not blocked by N-methyl D-aspartate antagonists. *Neurosci Lett* **70,** 132-137.

Harris KM & Stevens JK. (1988). Dendritic spines of rat cerebellar Purkinje cells: serial electron microscopy with reference to their biophysical characteristics. *J Neurosci* **8,** 4455-4469.

Hartter DE, Burton PR & Laveri LA. (1987). Distribution and calcium-sequestering ability of smooth endoplasmic reticulum in olfactory axon terminals of frog brain. *Neurosci* **23,** 371-386.

Hasegawa Y, Hida T & Arai R. (1999). Noradrenaline-degrading activity of monoamine oxidase is localized in noradrenergic neurons of the locus coeruleus of the rat. *Neurosci Lett* **264,** 61-64.

Hashimotodani Y, Ohno-Shosaku T, Tsubokawa H, Ogata H, Emoto K, Maejima T, Araishi K, Shin HS & Kano M. (2005). Phospholipase Cβ serves as a coincidence detector through its Ca^{2+} dependency for triggering retrograde endocannabinoid signal. *Neuron* **45,** 257-268.

Hasuo H, Matsuoka T & Akasu T. (2002). Activation of presynaptic 5-hydroxytryptamine 2A receptors facilitates excitatory synaptic transmission via protein kinase C in the dorsolateral septal nucleus. *J Neurosci* **22,** 7509-7517.

Hatt H & Smith DO. (1976). Synaptic depression related to presynaptic axon conduction block. *J Physiol* **259,** 367-393.

Haworth RA & Hunter DR. (1979). The Ca^{2+}-induced membrane transition in mitochondria. II. Nature of the Ca^{2+} trigger site. *Arch Biochem Biophys* **195,** 460-467.

Hayar A & Guyenet PG. (1999). α_2-adrenoceptor-mediated presynaptic inhibition in bulbospinal neurons of rostral ventrolateral medulla. *Am J Physiol* **277,** H1069-1080.

He L, Xue L, Xu J, McNeil BD, Bai L, Melicoff E, Adachi R & Wu LG. (2009). Compound vesicle fusion increases quantal size and potentiates synaptic transmission. *Nature* **459,** 93-97.

He Y, Janssen WG, Rothstein JD & Morrison JH. (2000). Differential synaptic localization of the glutamate transporter EAAC1 and glutamate receptor subunit GluR2 in the rat hippocampus. *J Comp Neurol* **418,** 255-269.

Hebb DO. (1949). *The Organization of Behavior: A Neuropsychological Theory*. Wiley, New York.

Heidelberger R, Heinemann C, Neher E & Matthews G. (1994). Calcium dependence of the rate of exocytosis in a synaptic terminal. *Nature* **371,** 513-515.

Hendrickson WA & Karle J. (1973). Carp muscle calcium-binding protein. 3. Phase refinement using the tangent formula. *J Biol Chem* **248,** 3327-3334.

Herbette L, DeFoor P, Fleischer S, Pascolini D, Scarpa A & Blasie JK. (1985). The separate profile structures of the functional calcium pump protein and the phospholipid bilayer within isolated sarcoplasmic reticulum membranes determined by X-ray and neutron diffraction. *Biochim Biophys Acta* **817,** 103-122.

Herkenham M. (1980). Laminar organization of thalamic projections to the rat neocortex. *Science* **207,** 532-535.

Hersch SM & White EL. (1982). A quantitative study of the thalamocortical and other synapses in layer IV of pyramidal cells projecting from mouse SmI cortex to the caudate-putamen nucleus. *The Journal of comparative neurology* **211,** 217-225.

Heuser JE & Reese TS. (1981). Structural changes after transmitter release at the frog neuromuscular junction. *J Cell Biol* **88,** 564-580.

Hilgemann DW, Nicoll DA & Philipson KD. (1991). Charge movement during Na^+ translocation by native and cloned cardiac Na^+/Ca^{2+} exchanger. *Nature* **352,** 715-718.

Hirasawa A, Sugawara T, Awaji T, Tsumaya K, Ito H & Tsujimoto G. (1997). Subtype-specific differences in subcellular localization of α_1-adrenoceptors: chlorethylclonidine preferentially alkylates the accessible cell surface α_1-adrenoceptors irrespective of the subtype. *Molecular pharmacology* **52,** 764-770.

Hirschi KD, Zhen RG, Cunningham KW, Rea PA & Fink GR. (1996). CAX1, an H^+/Ca^{2+} antiporter from *Arabidopsis*. *Proc Natl Acad Sci U S A* **93,** 8782-8786.

Hirst GD, Bramich NJ, Teramoto N, Suzuki H & Edwards FR. (2002). Regenerative component of slow waves in the guinea-pig gastric antrum involves a delayed increase in $[Ca^{2+}]_i$ and Cl^- channels. *J Physiol* **540,** 907-919.

Ho N, Liauw JA, Blaeser F, Wei F, Hanissian S, Muglia LM, Wozniak DF, Nardi A, Arvin KL, Holtzman DM, Linden DJ, Zhuo M, Muglia LJ & Chatila TA. (2000). Impaired synaptic plasticity and cAMP response element-binding protein activation in Ca^{2+}/calmodulin-dependent protein kinase type IV/Gr-deficient mice. *J Neurosci* **20,** 6459-6472.

Hochner B, Parnas H & Parnas I. (1991). Effects of intra-axonal injection of Ca^{2+} buffers on evoked release and on facilitation in the crayfish neuromuscular junction. *Neurosci Lett* **125,** 215-218.

Hoffmann C, Moro S, Nicholas RA, Harden TK & Jacobson KA. (1999). The role of amino acids in extracellular loops of the human P2Y1 receptor in surface expression and activation processes. *J Biol Chem* **274,** 14639-14647.

Holford HHG. (1984). Drug concentration, binding and effect *in vivo*. *Pharmaceutical research* **1**.

Holzapfel CW. (1968). The isolation and structure of cyclopiazonic acid, a toxic metabolite of *Penicillium cyclopium* Westling. *Tetrahedron* **24,** 2101-2119.

Horie K, Obika K, Foglar R & Tsujimoto G. (1995). Selectivity of the imidazoline α-adrenoceptor agonists (oxymetazoline and cirazoline) for human cloned α_1-adrenoceptor subtypes. *Br J Pharmacol* **116,** 1611-1618.

Horinouchi T, Miyake Y, Nishiya T, Nishimoto A, Yorozu S, Jinno A, Kajita E & Miwa S. (2007). Characterization of noradrenaline-induced increases in intracellular Ca^{2+} levels in Chinese hamster ovary cells stably expressing human α_{1A}-adrenoceptor. *J Pharmacol Sci* **105,** 103-111.

Hornung R, Presek P & Glossmann H. (1979). Alpha adrenoceptors in rat brain: direct identification with prazosin. *Naunyn Schmiedebergs Arch Pharmacol* **308,** 223-230.

Horowitz LF, Hirdes W, Suh BC, Hilgemann DW, Mackie K & Hille B. (2005). Phospholipase C in living cells: activation, inhibition, Ca^{2+} requirement, and regulation of M current. *J Gen Physiol* **126,** 243-262.

Horvath TL, Peyron C, Diano S, Ivanov A, Aston-Jones G, Kilduff TS & van Den Pol AN. (1999). Hypocretin (orexin) activation and synaptic innervation of the locus coeruleus noradrenergic system. *J Comp Neurol* **415,** 145-159.

Houeland G, Nakhost A, Sossin WS & Castellucci VF. (2007). PKC modulation of transmitter release by SNAP-25 at sensory-to-motor synapses in *Aplysia*. *J Neurophysiol* **97,** 134-143.

Hu HZ, Gu Q, Wang C, Colton CK, Tang J, Kinoshita-Kawada M, Lee LY, Wood JD & Zhu MX. (2004). 2-aminoethoxydiphenyl borate is a common activator of TRPV1, TRPV2, and TRPV3. *J Biol Chem* **279,** 35741-35748.

Hunter DR & Haworth RA. (1979). The Ca^{2+}-induced membrane transition in mitochondria. III. Transitional Ca^{2+} release. *Arch Biochem Biophys* **195,** 468-477.

Iino M. (1990). Biphasic Ca^{2+} dependence of inositol 1,4,5-trisphosphate-induced Ca release in smooth muscle cells of the guinea pig taenia caeci. *J Gen Physiol* **95,** 1103-1122.

Imagawa T, Smith JS, Coronado R & Campbell KP. (1987). Purified ryanodine receptor from skeletal muscle sarcoplasmic reticulum is the Ca^{2+}-permeable pore of the calcium release channel. *J Biol Chem* **262,** 16636-16643.

Imanishi T, Yamanaka H, Rhee JS & Akaike N. (1996). Interaction between the intracellular Ca^{2+} stores in rat dissociated hippocampal neurones. *NeuroReport* **7,** 1421-1426.

Inesi G, Cantilina T, Yu X, Nikic D, Sagara Y & Kirtley ME. (1992). Long-range intramolecular linked functions in activation and inhibition of SERCA ATPases. *Ann N Y Acad Sci* **671,** 32-47; discussion 48.

Isaac JT, Nicoll RA & Malenka RC. (1995). Evidence for silent synapses: implications for the expression of LTP. *Neuron* **15,** 427-434.

Ishii T, Lemas MV & Takeyasu K. (1994). Na^+-, ouabain-, Ca^{2+}-, and thapsigargin-sensitive ATPase activity expressed in chimeras between the calcium and the sodium pump α subunits. *Proc Natl Acad Sci U S A* **91,** 6103-6107.

Ishikawa T, Sahara Y & Takahashi T. (2002). A single packet of transmitter does not saturate postsynaptic glutamate receptors. *Neuron* **34,** 613-621.

Israël M & Lesbats B. (1981). Continuous determination by a chemiluminescent method of acetylcholine release and compartmentation in Torpedo electric organ synaptosomes. *J Neurochem* **37,** 1475-1483.

Israël M, Meunier FM, Morel N & Lesbats B. (1987). Calcium-induced desensitization of acetylcholine release from synaptosomes or proteoliposomes equipped with mediatophore, a presynaptic membrane protein. *J Neurochem* **49,** 975-982.

Israël M, Morel N, Lesbats B, Birman S & Manaranche R. (1986). Purification of a presynaptic membrane protein that mediates a calcium-dependent translocation of acetylcholine. *Proc Natl Acad Sci U S A* **83,** 9226-9230.

Iwamoto T, Watano T & Shigekawa M. (1996). A novel isothiourea derivative selectively inhibits the reverse mode of Na^+/Ca^{2+} exchange in cells expressing NCX1. *J Biol Chem* **271,** 22391-22397.

Jack JJ, Redman SJ & Wong K. (1981). The components of synaptic potentials evoked in cat spinal motoneurones by impulses in single group Ia afferents. *J Physiol* **321,** 65-96.

Jackson MB & Redman SJ. (2003). Calcium dynamics, buffering, and buffer saturation in the boutons of dentate granule-cell axons in the hilus. *J Neurosci* **23,** 1612-1621.

Jafri MS, Moore KA, Taylor GE & Weinreich D. (1997). Histamine H_1 receptor activation blocks two classes of potassium current, $I_{K(rest)}$ and I_{AHP}, to excite ferret vagal afferents. *J Physiol* **503 (Pt 3),** 533-546.

Jahn R, Lang T & Südhof TC. (2003). Membrane fusion. *Cell* **112,** 519-533.

Jakab RL & Goldman-Rakic PS. (1998). 5-Hydroxytryptamine2A serotonin receptors in the primate cerebral cortex: possible site of action of hallucinogenic and antipsychotic drugs in pyramidal cell apical dendrites. *Proc Natl Acad Sci U S A* **95,** 735-740.

James P, Maeda M, Fischer R, Verma AK, Krebs J, Penniston JT & Carafoli E. (1988). Identification and primary structure of a calmodulin binding domain of the Ca^{2+} pump of human erythrocytes. *J Biol Chem* **263,** 2905-2910.

Janetzko A, Zimmermann H & Volknandt W. (1989). Intraneuronal distribution of a synaptic vesicle membrane protein: antibody binding sites at axonal membrane compartments and trans-Golgi network and accumulation at nodes of Ranvier. *Neurosci* **32,** 65-77.

Janmey PA, Iida K, Yin HL & Stossel TP. (1987). Polyphosphoinositide micelles and polyphosphoinositide-containing vesicles dissociate endogenous gelsolin-actin complexes and promote actin assembly from the fast-growing end of actin filaments blocked by gelsolin. *J Biol Chem* **262,** 12228-12236.

Jarsky T, Tian M & Singer JH. (2010). Nanodomain control of exocytosis is responsible for the signaling capability of a retinal ribbon synapse. *J Neurosci* **30,** 11885-11895.

Jaskolski F, Mulle C & Manzoni OJ. (2005). An automated method to quantify and visualize colocalized fluorescent signals. *J Neurosci Methods* **146,** 42-49.

Jenkinson DH. (1957). The nature of the antagonism between calcium and magnesium ions at the neuromuscular junction. *J Physiol* **138,** 434-444.

Jensen BC, Swigart PM & Simpson PC. (2009). Ten commercial antibodies for alpha-1-adrenergic receptor subtypes are nonspecific. *Naunyn Schmiedebergs Arch Pharmacol* **379,** 409-412.

Ji XH, Cao XH, Zhang CL, Feng ZJ, Zhang XH, Ma L & Li BM. (2008). Pre- and postsynaptic β-adrenergic activation enhances excitatory synaptic transmission in layer V/VI pyramidal neurons of the medial prefrontal cortex of rats. *Cereb Cortex* **18,** 1506-1520.

Jonas P, Bischofberger J & Sandkuhler J. (1998). Corelease of two fast neurotransmitters at a central synapse. *Science* **281,** 419-424.

Jones LM, Cockcroft S & Michell RH. (1979). Stimulation of phosphatidylinositol turnover in various tissues by cholinergic and adrenergic agonists, by histamine and by caerulein. *Biochem J* **182,** 669-676.

Jones LS, Gauger LL & Davis JN. (1985). Anatomy of brain alpha$_1$-adrenergic receptors: in vitro autoradiography with [^{125}I]-heat. *J Comp Neurol* **231,** 190-208.

Jouvet M, Albarede JL, Lubin S & Meyrignac C. (1991). Noradrenaline and cerebral aging. *Encephale* **17,** 187-195.

Julius D, Huang KN, Livelli TJ, Axel R & Jessell TM. (1990). The 5HT2 receptor defines a family of structurally distinct but functionally conserved serotonin receptors. *Proc Natl Acad Sci U S A* **87,** 928-932.

Kamiya H & Zucker RS. (1994). Residual Ca^{2+} and short-term synaptic plasticity. *Nature* **371,** 603-606.

Kamo N, Muratsugu M, Hongoh R & Kobatake Y. (1979). Membrane potential of mitochondria measured with an electrode sensitive to tetraphenyl phosphonium and relationship between proton electrochemical potential and phosphorylation potential in steady state. *The Journal of membrane biology* **49,** 105-121.

Kampa BM, Letzkus JJ & Stuart GJ. (2006). Cortical feed-forward networks for binding different streams of sensory information. *Nat Neurosci* **9,** 1472-1473.

Kanai Y & Hediger MA. (1992). Primary structure and functional characterization of a high-affinity glutamate transporter. *Nature* **360,** 467-471.

Kang TM & Hilgemann DW. (2004). Multiple transport modes of the cardiac Na^+/Ca^{2+} exchanger. *Nature* **427,** 544-548.

Katchman AN & Hershkowitz N. (1993). Early anoxia-induced vesicular glutamate release results from mobilization of calcium from intracellular stores. *J Neurophysiol* **70,** 1-7.

Katz B. (1962). The Croonian lecture: The transmission of impulses from nerve to muscle and the subcellular unit of synaptic action. *Proc Roy Soc B* **155,** 455-477.

Katz B. (1996). Neural transmitter release: from quantal secretion to exocytosis and beyond. The Fenn Lecture. *J Neurocytol* **25,** 677-686.

Katz B & Miledi R. (1965). The effect of calcium on acetylcholine release from motor nerve terminals. *Proceedings of the Royal Society of London Series B, Containing papers of a Biological character* **161,** 496-503.

Katz B & Miledi R. (1967a). Ionic requirements of synaptic transmitter release. *Nature* **215,** 651.

Katz B & Miledi R. (1967b). Tetrodotoxin and neuromuscular transmission. *Proceedings of the Royal Society of London Series B, Containing papers of a Biological character* **167,** 8-22.

Katz B & Miledi R. (1968). The role of calcium in neuromuscular facilitation. *J Physiol* **195,** 481-492.

Katz B & Miledi R. (1977). Transmitter leakage from motor nerve endings. *Proceedings of the Royal Society of London Series B, Containing papers of a Biological character* **196,** 59-72.

Kawaguchi Y & Shindou T. (1998). Noradrenergic excitation and inhibition of GABAergic cell types in rat frontal cortex. *J Neurosci* **18,** 6963-6976.

Kee Y & Scheller RH. (1996). Localization of synaptotagmin-binding domains on syntaxin. *J Neurosci* **16,** 1975-1981.

Kendall DA & Hill SJ. (1988). Adenosine inhibition of histamine-stimulated inositol phospholipid hydrolysis in mouse cerebral cortex. *J Neurochem* **50,** 497-502.

Khanin R, Parnas H & Segel L. (1994). Diffusion cannot govern the discharge of neurotransmitter in fast synapses. *Biophys J* **67,** 966-972.

Khodakhah K & Armstrong CM. (1997). Induction of long-term depression and rebound potentiation by inositol trisphosphate in cerebellar Purkinje neurons. *Proc Natl Acad Sci U S A* **94,** 14009-14014.

Kim T, Gondre-Lewis MC, Arnaoutova I & Loh YP. (2006). Dense-core secretory granule biogenesis. *Physiology (Bethesda)* **21,** 124-133.

Kiselar JG, Janmey PA, Almo SC & Chance MR. (2003). Visualizing the Ca^{2+}-dependent activation of gelsolin by using synchrotron footprinting. *Proc Natl Acad Sci U S A* **100,** 3942-3947.

Knoll VM & Ruska E. (1932). Das elektronenmikroskop. *Z Physik A, Hadrons and nuclei* **78,** 318-339.

Knowles MK, Barg S, Wan L, Midorikawa M, Chen X & Almers W. (2010). Single secretory granules of live cells recruit syntaxin-1 and synaptosomal associated protein 25 (SNAP-25) in large copy numbers. *Proc Natl Acad Sci U S A* **107,** 20810-20815.

Kobayashi M, Sasabe T, Shiohama Y & Koshikawa N. (2008). Activation of α_1-adrenoceptors increases firing frequency through protein kinase C in pyramidal neurons of rat visual cortex. *Neurosci Lett* **430,** 175-180.

Koenig JH & Ikeda K. (1996). Synaptic vesicles have two distinct recycling pathways. *J Cell Biol* **135,** 797-808.

Koester HJ & Johnston D. (2005). Target cell-dependent normalization of transmitter release at neocortical synapses. *Science* **308,** 863-866.

Koh DS, Burnashev N & Jonas P. (1995). Block of native Ca^{2+}-permeable AMPA receptors in rat brain by intracellular polyamines generates double rectification. *J Physiol* **486 (Pt 2),** 305-312.

Kölliker A. (1853). *Manual of Human Histology. (Translated by G. Busk and T. Huxley)*. London: Sydenham Society.

Kombian SB, Hirasawa M, Mouginot D, Chen X & Pittman QJ. (2000). Short-term potentiation of miniature excitatory synaptic currents causes excitation of supraoptic neurons. *J Neurophysiol* **83,** 2542-2553.

Korn H & Faber DS. (1991). Quantal analysis and synaptic efficacy in the CNS. *Trends Neurosci* **14,** 439-445.

Krasne FB & Stirling CA. (1972). Synapses of crayfish abdominal ganglia with special attention to afferent and efferent connections of the lateral giant fibers. *Z Zellforsch Mikrosk Anat* **127,** 526-544.

Kraushaar U & Jonas P. (2000). Efficacy and stability of quantal GABA release at a hippocampal interneuron-principal neuron synapse. *J Neurosci* **20,** 5594-5607.

Kretsinger RH & Nockolds CE. (1973). Carp muscle calcium-binding protein. II. Structure determination and general description. *J Biol Chem* **248,** 3313-3326.

Kriebel ME, Llados F & Matteson DR. (1976). Spontaneous subminature end-plate potentials in mouse diaphragm muscle: evidence for synchronous release. *J Physiol* **262,** 553-581.

Krnjevic K & Phillis JW. (1963). Actions of certain amines on cerebral cortical neurones. *Br J Pharmacol Chemother* **20,** 471-490.

Krupp JJ, Vissel B, Heinemann SF & Westbrook GL. (1998). N-terminal domains in the NR2 subunit control desensitization of NMDA receptors. *Neuron* **20,** 317-327.

Kuffler SW & Yoshikami D. (1975). The number of transmitter molecules in a quantum: an estimate from iontophoretic application of acetylcholine at the neuromuscular synapse. *J Physiol* **251,** 465-482.

Kukkonen JP & Åkerman KE. (2001). Orexin receptors couple to Ca^{2+} channels different from store-operated Ca^{2+} channels. *NeuroReport* **12,** 2017-2020.

Kuno M. (1964). Quantal Components of Excitatory Synaptic Potentials in Spinal Motoneurones. *J Physiol* **175,** 81-99.

Kupchik YM, Barchad-Avitzur O, Wess J, Ben-Chaim Y, Parnas I & Parnas H. (2011). A novel fast mechanism for GPCR-mediated signal transduction-control of neurotransmitter release. *J Cell Biol* **192,** 137-151.

Kwiatkowski DJ. (1999). Functions of gelsolin: motility, signaling, apoptosis, cancer. *Curr Opin Cell Biol* **11,** 103-108.

Lacy D. (1957). The Golgi apparatus in neurons and epithelial cells of the common limpet Patella vulgata. *J Biophys Biochem Cytol* **3,** 779-796.

Lake N, Jordan LM & Phillis JW. (1972). Mechanism of noradrenaline action in cat cerebral cortex. *Nat New Biol* **240,** 249-250.

Lalo U, Voitenko N & Kostyuk P. (1998). Iono- and metabotropically induced purinergic calcium signalling in rat neocortical neurons. *Brain Res* **799,** 285-291.

Landò L & Zucker RS. (1994). Ca^{2+} cooperativity in neurosecretion measured using photolabile Ca^{2+} chelators. *J Neurophysiol* **72,** 825-830.

Langmoen IA, Segal M & Andersen P. (1981). Mechanisms of norepinephrine actions on hippocampal pyramidal cells in vitro. *Brain Res* **208,** 349-362.

Lanini L, Bachs O & Carafoli E. (1992). The calcium pump of the liver nuclear membrane is identical to that of endoplasmic reticulum. *J Biol Chem* **267,** 11548-11552.

Larkman A, Stratford K & Jack J. (1991). Quantal analysis of excitatory synaptic action and depression in hippocampal slices. *Nature* **350,** 344-347.

LaVoie MJ, Fraering PC, Ostaszewski BL, Ye W, Kimberly WT, Wolfe MS & Selkoe DJ. (2003). Assembly of the gamma-secretase complex involves early formation of an intermediate subcomplex of Aph-1 and nicastrin. *J Biol Chem* **278,** 37213-37222.

Le Rouzic M, Angel I, Schoemaker H, Allen J, Arbilla S & Langer SZ. (1995). Binding of [^{3}H]cirazoline to an imidazoline site in rat brain and kidney membranes. *Eur J Pharmacol* **278,** 261-264.

Lee HK, Barbarosie M, Kameyama K, Bear MF & Huganir RL. (2000a). Regulation of distinct AMPA receptor phosphorylation sites during bidirectional synaptic plasticity. *Nature* **405,** 955-959.

Lee SC, Cruikshank SJ & Connors BW. (2010). Electrical and chemical synapses between relay neurons in developing thalamus. *J Physiol* **588,** 2403-2415.

Lee SH, Rosenmund C, Schwaller B & Neher E. (2000b). Differences in Ca^{2+} buffering properties between excitatory and inhibitory hippocampal neurons from the rat. *J Physiol* **525 Pt 2,** 405-418.

Leeb-Lundberg LM, Cotecchia S, DeBlasi A, Caron MG & Lefkowitz RJ. (1987). Regulation of adrenergic receptor function by phosphorylation. I. Agonist-promoted desensitization and phosphorylation of α_1-adrenergic receptors coupled to inositol phospholipid metabolism in DDT_1 MF-2 smooth muscle cells. *J Biol Chem* **262,** 3098-3105.

Lehninger AL, Vercesi A & Bababunmi EA. (1978). Regulation of Ca^{2+} release from mitochondria by the oxidation-reduction state of pyridine nucleotides. *Proc Natl Acad Sci U S A* **75,** 1690-1694.

Leuner B & Shors TJ. (2004). New spines, new memories. *Mol Neurobiol* **29,** 117-130.

Leurs R, Smit MJ, Tensen CP, Ter Laak AM & Timmerman H. (1994). Site-directed mutagenesis of the histamine H1-receptor reveals a selective interaction of asparagine207 with subclasses of H1-receptor agonists. *Biochem Biophys Res Commun* **201,** 295-301.

Levey AI, Kitt CA, Simonds WF, Price DL & Brann MR. (1991). Identification and localization of muscarinic acetylcholine receptor proteins in brain with subtype-specific antibodies. *J Neurosci* **11,** 3218-3226.

Levin BE. (1977). Axonal transport of [3H]fucosyl glycoproteins in noradrenergic neurons in the rat brain. *Brain Res* **130,** 421-432.

Levy WB & Steward O. (1983). Temporal contiguity requirements for long-term associative potentiation/depression in the hippocampus. *Neurosci* **8,** 791-797.

Lewit-Bentley A & Réty S. (2000). EF-hand calcium-binding proteins. *Curr Opin Struct Biol* **10,** 637-643.

Li C, Ullrich B, Zhang JZ, Anderson RG, Brose N & Südhof TC. (1995a). Ca^{2+}-dependent and -independent activities of neural and non-neural synaptotagmins. *Nature* **375,** 594-599.

Li J, Ma J & Potter H. (1995b). Identification and expression analysis of a potential familial Alzheimer disease gene on chromosome 1 related to AD3. *Proc Natl Acad Sci U S A* **92,** 12180-12184.

Li PP, Sibony D & Warsh JJ. (1988). Pharmacologic characterization of cirazoline-activated inositol phospholipid hydrolysis in rat brain cortical slices. *Can J Physiol Pharmacol* **66,** 1460-1463.

Li YF & Shi ST. (2009). Age-dependent differential crosstalk between α_1-adrenergic and angiotensin receptors. *The Canadian journal of cardiology* **25,** 481-485.

Liang J, Takeuchi H, Doi Y, Kawanokuchi J, Sonobe Y, Jin S, Yawata I, Li H, Yasuoka S, Mizuno T & Suzumura A. (2008). Excitatory amino acid transporter expression by astrocytes is neuroprotective against microglial excitotoxicity. *Brain Res* **1210,** 11-19.

Lidov HG, Grzanna R & Molliver ME. (1980). The serotonin innervation of the cerebral cortex in the rat-an immunohistochemical analysis. *Neurosci* **5,** 207-227.

Liley AW & North KA. (1953). An electrical investigation of effects of repetitive stimulation on mammalian neuromuscular junction. *J Neurophysiol* **16,** 509-527.

Lin KM, Mejillano M & Yin HL. (2000). Ca^{2+} regulation of gelsolin by its C-terminal tail. *J Biol Chem* **275,** 27746-27752.

Lin P, Le-Niculescu H, Hofmeister R, McCaffery JM, Jin M, Hennemann H, McQuistan T, De Vries L & Farquhar MG. (1998). The mammalian calcium-binding protein, nucleobindin (CALNUC), is a Golgi resident protein. *J Cell Biol* **141,** 1515-1527.

Littleton JT, Stern M, Schulze K, Perin M & Bellen HJ. (1993). Mutational analysis of Drosophila synaptotagmin demonstrates its essential role in Ca^{2+}-activated neurotransmitter release. *Cell* **74,** 1125-1134.

Llano I, Gonzalez J, Caputo C, Lai FA, Blayney LM, Tan YP & Marty A. (2000). Presynaptic calcium stores underlie large-amplitude miniature IPSCs and spontaneous calcium transients. *Nat Neurosci* **3,** 1256-1265.

Llinás R, Steinberg IZ & Walton K. (1981). Relationship between presynaptic calcium current and postsynaptic potential in squid giant synapse. *Biophys J* **33,** 323-351.

Llinás R, Sugimori M & Silver RB. (1992). Presynaptic calcium concentration microdomains and transmitter release. *J Physiol Paris* **86,** 135-138.

Llinás RR. (1982). Calcium in synaptic transmission. *Sci Am* **247,** 56-65.

Lomasney JW, Cotecchia S, Lefkowitz RJ & Caron MG. (1991). Molecular biology of α-adrenergic receptors: implications for receptor classification and for structure-function relationships. *Biochim Biophys Acta* **1095,** 127-139.

Longsworth LG. (1953). Diffusion measurements, at 25°C, of aqueous solutions of amino acids, peptides and sugars. *J Am Chem Soc* **75,** 5705-5709.

López de Jesús M, Zalduegui A, Ruiz de Azúa I, Callado LF, Meana JJ & Sallés J. (2006). Levels of G-protein $\alpha_{q/11}$ subunits and of phospholipase C-$\beta_{(1-4)}$, -γ, and -δ_1 isoforms in postmortem human brain caudate and cortical membranes: potential functional implications. *Neurochem Int* **49,** 72-79.

Lopez I, Giner D, Ruiz-Nuno A, Fuentealba J, Viniegra S, Garcia AG, Davletov B & Gutierrez LM. (2007). Tight coupling of the t-SNARE and calcium channel microdomains in adrenomedullary slices and not in cultured chromaffin cells. *Cell Calcium* **41,** 547-558.

Lovinger DM & Choi S. (1995). Activation of adenosine A1 receptors initiates short-term synaptic depression in rat striatum. *Neurosci Lett* **199,** 9-12.

Lujan R, Roberts JD, Shigemoto R, Ohishi H & Somogyi P. (1997). Differential plasma membrane distribution of metabotropic glutamate receptors mGluR1α, mGluR2 and mGluR5, relative to neurotransmitter release sites. *J Chem Neuroanat* **13,** 219-241.

Lund PE, Shariatmadari R, Uustare A, Detheux M, Parmentier M, Kukkonen JP & Åkerman KE. (2000). The orexin OX_1 receptor activates a novel Ca^{2+} influx pathway necessary for coupling to phospholipase C. *J Biol Chem* **275,** 30806-30812.

Lynch G, Larson J, Kelso S, Barrionuevo G & Schottler F. (1983). Intracellular injections of EGTA block induction of hippocampal long-term potentiation. *Nature* **305,** 719-721.

Lytton J & Nigam SK. (1992). Intracellular calcium: molecules and pools. *Curr Opin Cell Biol* **4,** 220-226.

Lytton J, Westlin M & Hanley MR. (1991). Thapsigargin inhibits the sarcoplasmic or endoplasmic reticulum Ca-ATPase family of calcium pumps. *J Biol Chem* **266,** 17067-17071.

Maccaferri G, Janigro D, Lazzari A & DiFrancesco D. (1994). Cesium prevents maintenance of long-term depression in rat hippocampal CA1 neurons. *NeuroReport* **5,** 1813-1816.

Madison DV & Nicoll RA. (1988). Norepinephrine decreases synaptic inhibition in the rat hippocampus. *Brain Res* **442,** 131-138.

Magee JC & Cook EP. (2000). Somatic EPSP amplitude is independent of synapse location in hippocampal pyramidal neurons. *Nat Neurosci* **3,** 895-903.

Magee JC & Johnston D. (1997). A synaptically controlled, associative signal for Hebbian plasticity in hippocampal neurons. *Science* **275,** 209-213.

Magleby KL & Pallotta BS. (1981). A study of desensitization of acetylcholine receptors using nerve-released transmitter in the frog. *J Physiol* **316,** 225-250.

Magleby KL & Terrar DA. (1975). Factors affecting the time course of decay of end-plate currents: a possible cooperative action of acetylcholine on receptors at the frog neuromuscular junction. *J Physiol* **244,** 467-495.

Malinow R & Tsien RW. (1990). Presynaptic enhancement shown by whole-cell recordings of long-term potentiation in hippocampal slices. *Nature* **346,** 177-180.

Mallart A & Brigant JL. (1982). Electrical activity at motor nerve terminals of the mouse. *J Physiol (Paris)* **78,** 407-411.

Malomouzh AI, Mukhtarov MR, Nikolsky EE, Vyskočil F, Lieberman EM & Urazaev AK. (2003). Glutamate regulation of non-quantal release of acetylcholine in the rat neuromuscular junction. *J Neurochem* **85,** 206-213.

Malomouzh AI, Nikolsky EE, Lieberman EM, Sherman JA, Lubischer JL, Grossfeld RM & Urazaev A. (2005). Effect of N-acetylaspartylglutamate (NAAG) on non-quantal and spontaneous quantal release of acetylcholine at the neuromuscular synapse of rat. *J Neurochem* **94,** 257-267.

Manahan-Vaughan D, Kulla A & Frey JU. (2000). Requirement of translation but not transcription for the maintenance of long-term depression in the CA1 region of freely moving rats. *J Neurosci* **20,** 8572-8576.

Marek GJ & Aghajanian GK. (1996). α_{1B}-adrenoceptor-mediated excitation of piriform cortical interneurons. *Eur J Pharmacol* **305,** 95-100.

Marek GJ & Aghajanian GK. (1999). 5-HT_{2A} receptor or α_1-adrenoceptor activation induces excitatory postsynaptic currents in layer V pyramidal cells of the medial prefrontal cortex. *Eur J Pharmacol* **367,** 197-206.

Markram H, Lubke J, Frotscher M & Sakmann B. (1997). Regulation of synaptic efficacy by coincidence of postsynaptic APs and EPSPs. *Science* **275,** 213-215.

Martí D, Miquel R, Ziani K, Gisbert R, Ivorra MD, Anselmi E, Moreno L, Villagrasa V, Barettino D & D'Ocon P. (2005). Correlation between mRNA levels and functional role of α_1-adrenoceptor subtypes in arteries: evidence of α_{1L} as a functional isoform of the α_{1A}-adrenoceptor. *Am J Physiol Heart Circ Physiol* **289,** H1923-1932.

Martin AR & Pilar G. (1963). Dual Mode of Synaptic Transmission in the Avian Ciliary Ganglion. *J Physiol* **168,** 443-463.

Martin AR & Pilar G. (1964). Presynaptic and post-synaptic events during post-tetanic potentiation and facilitation in the avian ciliary ganglion. *J Physiol* **175,** 17-30.

Martinez-Hernandez A, Bell KP & Norenberg MD. (1977). Glutamine synthetase: glial localization in brain. *Science* **195,** 1356-1358.

Maruyama T, Kanaji T, Nakade S, Kanno T & Mikoshiba K. (1997). 2APB, 2-aminoethoxydiphenyl borate, a membrane-penetrable modulator of Ins(1,4,5)P_3-induced Ca^{2+} release. *J Biochem* **122,** 498-505.

Mathe JM, Nomikos GG, Hildebrand BE, Hertel P & Svensson TH. (1996). Prazosin inhibits MK-801-induced hyperlocomotion and dopamine release in the nucleus accumbens. *Eur J Pharmacol* **309,** 1-11.

Matthews G. (1996). Neurotransmitter release. *Annu Rev Neurosci* **19,** 219-233.

Mattson MP, Guo Q, Furukawa K & Pedersen WA. (1998). Presenilins, the endoplasmic reticulum, and neuronal apoptosis in Alzheimer's disease. *J Neurochem* **70,** 1-14.

Maycox PR, Deckwerth T, Hell JW & Jahn R. (1988). Glutamate uptake by brain synaptic vesicles. Energy dependence of transport and functional reconstitution in proteoliposomes. *J Biol Chem* **263,** 15423-15428.

McAllister AK & Stevens CF. (2000). Nonsaturation of AMPA and NMDA receptors at hippocampal synapses. *Proc Natl Acad Sci U S A* **97,** 6173-6178.

McCune DF, Edelmann SE, Olges JR, Post GR, Waldrop BA, Waugh DJ, Perez DM & Piascik MT. (2000). Regulation of the cellular localization and signaling properties of the α_{1B}- and α_{1D}-adrenoceptors by agonists and inverse agonists. *Molecular pharmacology* **57,** 659-666.

McCune SK, Voigt MM & Hill JM. (1993). Expression of multiple alpha adrenergic receptor subtype messenger RNAs in the adult rat brain. *Neurosci* **57,** 143-151.

McKinney RA, Capogna M, Durr R, Gähwiler BH & Thompson SM. (1999). Miniature synaptic events maintain dendritic spines via AMPA receptor activation. *Nat Neurosci* **2,** 44-49.

McMahon HT, Missler M, Li C & Südhof TC. (1995). Complexins: cytosolic proteins that regulate SNAP receptor function. *Cell* **83,** 111-119.

McNaughton BL, Douglas RM & Goddard GV. (1978). Synaptic enhancement in fascia dentata: cooperativity among coactive afferents. *Brain Res* **157,** 277-293.

Meissner G, Darling E & Eveleth J. (1986). Kinetics of rapid Ca^{2+} release by sarcoplasmic reticulum. Effects of Ca^{2+}, Mg^{2+}, and adenine nucleotides. *Biochem* **25,** 236-244.

Mennerick S & Matthews G. (1996). Ultrafast exocytosis elicited by calcium current in synaptic terminals of retinal bipolar neurons. *Neuron* **17,** 1241-1249.

Mennerick S & Zorumski CF. (1995). Paired-pulse modulation of fast excitatory synaptic currents in microcultures of rat hippocampal neurons. *J Physiol* **488 (Pt 1),** 85-101.

Metuzals J, Chang D, Hammar K & Reese TS. (1997). Organization of the cortical endoplasmic reticulum in the squid giant axon. *J Neurocytol* **26,** 529-539.

Meyer RK, Schindler H & Burger MM. (1982). α-Actinin interacts specifically with model membranes containing glycerides and fatty acids. *Proc Natl Acad Sci U S A* **79,** 4280-4284.

Miller TM & Heuser JE. (1984). Endocytosis of synaptic vesicle membrane at the frog neuromuscular junction. *J Cell Biol* **98,** 685-698.

Minelli A, Castaldo P, Gobbi P, Salucci S, Magi S & Amoroso S. (2007). Cellular and subcellular localization of Na^+-Ca^{2+} exchanger protein isoforms, NCX1, NCX2, and NCX3 in cerebral cortex and hippocampus of adult rat. *Cell Calcium* **41,** 221-234.

Minocherhomjee AM, Beauregard G, Potier M & Roufogalis BD. (1983). The molecular weight of the calcium-transport-ATPase of the human red blood cell determined by radiation inactivation. *Biochem Biophys Res Commun* **116,** 895-900.

Misonou H, Menegola M, Buchwalder L, Park EW, Meredith A, Rhodes KJ, Aldrich RW & Trimmer JS. (2006). Immunolocalization of the Ca^{2+}-activated K^+ channel Slo1 in axons and nerve terminals of mammalian brain and cultured neurons. *J Comp Neurol* **496,** 289-302.

Mobley P & Greengard P. (1985). Evidence for widespread effects of noradrenaline on axon terminals in the rat frontal cortex. *Proc Natl Acad Sci U S A* **82,** 945-947.

Modirrousta M, Mainville L & Jones BE. (2004). Gabaergic neurons with α_2-adrenergic receptors in basal forebrain and preoptic area express c-Fos during sleep. *Neurosci* **129,** 803-810.

Mody I, Leung P & Miller JJ. (1983). Role of norepinephrine in seizurelike activity of hippocampal pyramidal cells maintained in vitro: alteration by 6-hydroxydopamine lesions of norepinephrine-containing systems. *Can J Physiol Pharmacol* **61,** 841-846.

Mogami H, Lloyd Mills C & Gallacher DV. (1997). Phospholipase C inhibitor, U73122, releases intracellular Ca^{2+}, potentiates Ins(1,4,5)P_3-mediated Ca^{2+} release and directly activates ion channels in mouse pancreatic acinar cells. *Biochem J* **324 (Pt 2),** 645-651.

Mohrmann R, de Wit H, Verhage M, Neher E & Sorensen JB. (2010). Fast vesicle fusion in living cells requires at least three SNARE complexes. *Science* **330,** 502-505.

Molenaar PC, Oen BS, Polak RL & van der Laaken AL. (1987). Surplus acetylcholine and acetylcholine release in the rat diaphragm. *J Physiol* **385,** 147-167.

Moore DJ, Chambers JK, Wahlin JP, Tan KB, Moore GB, Jenkins O, Emson PC & Murdock PR. (2001). Expression pattern of human P2Y receptor subtypes: a quantitative reverse transcription-polymerase chain reaction study. *Biochim Biophys Acta* **1521,** 107-119.

Moran-Jimenez MJ & Matute C. (2000). Immunohistochemical localization of the $P2Y_1$ purinergic receptor in neurons and glial cells of the central nervous system. *Brain Res Mol Brain Res* **78,** 50-58.

Moriyama Y & Yamamoto A. (1995). Vesicular L-glutamate transporter in microvesicles from bovine pineal glands. Driving force, mechanism of chloride anion activation, and substrate specificity. *J Biol Chem* **270,** 22314-22320.

Mosbacher J, Schoepfer R, Monyer H, Burnashev N, Seeburg PH & Ruppersberg JP. (1994). A molecular determinant for submillisecond desensitization in glutamate receptors. *Science* **266,** 1059-1062.

Moult PR, Gladding CM, Sanderson TM, Fitzjohn SM, Bashir ZI, Molnar E & Collingridge GL. (2006). Tyrosine phosphatases regulate AMPA receptor trafficking during metabotropic glutamate receptor-mediated long-term depression. *J Neurosci* **26,** 2544-2554.

Mulkey RM & Zucker RS. (1992). Posttetanic potentiation at the crayfish neuromuscular junction is dependent on both intracellular calcium and sodium ion accumulation. *J Neurosci* **12,** 4327-4336.

Mulkey RM & Zucker RS. (1993). Calcium released by photolysis of DM-nitrophen triggers transmitter release at the crayfish neuromuscular junction. *J Physiol* **462,** 243-260.

Muller D, Garcia-Segura LM, Parducz A & Dunant Y. (1987). Brief occurrence of a population of presynaptic intramembrane particles coincides with transmission of a nerve impulse. *Proc Natl Acad Sci U S A* **84,** 590-594.

Mynlieff M & Dunwiddie TV. (1988). Noradrenergic depression of synaptic responses in hippocampus of rat: evidence for mediation by alpha$_1$-receptors. *Neuropharmac* **27,** 391-398.

Naito S & Ueda T. (1985). Characterization of glutamate uptake into synaptic vesicles. *J Neurochem* **44,** 99-109.

Nakadate K, Imamura K & Watanabe Y. (2006). Cellular and subcellular localization of alpha-1 adrenoceptors in the rat visual cortex. *Neurosci* **141,** 1783-1792.

Nalepa I, Pintor A, Fortuna S, Vetulani J & Michalek H. (1989). Increased responsiveness of the cerebral cortical phosphatidylinositol system to noradrenaline and carbachol in senescent rats. *Neurosci Lett* **107,** 195-199.

Naraghi M & Neher E. (1997). Linearized buffered Ca^{2+} diffusion in microdomains and its implications for calculation of $[Ca^{2+}]$ at the mouth of a calcium channel. *J Neurosci* **17,** 6961-6973.

Narahashi T, Moore JW & Scott WR. (1964). Tetrodotoxin blockage of sodium conductance increase in lobster giant axons. *J Gen Physiol* **47,** 965-974.

Narita K, Akita T, Hachisuka J, Huang S, Ochi K & Kuba K. (2000). Functional coupling of Ca^{2+} channels to ryanodine receptors at presynaptic terminals. Amplification of exocytosis and plasticity. *The Journal of general physiology* **115,** 519-532.

Neher E. (1998). Usefulness and limitations of linear approximations to the understanding of Ca^{++} signals. *Cell Calcium* **24,** 345-357.

Neher E & Marty A. (1982). Discrete changes of cell membrane capacitance observed under conditions of enhanced secretion in bovine adrenal chromaffin cells. *Proc Natl Acad Sci U S A* **79,** 6712-6716.

Neher E & Zucker RS. (1993). Multiple calcium-dependent processes related to secretion in bovine chromaffin cells. *Neuron* **10,** 21-30.

Nelson MR, Thulin E, Fagan PA, Forsen S & Chazin WJ. (2002). The EF-hand domain: a globally cooperative structural unit. *Protein Sci* **11,** 198-205.

Nelson TJ, Cavallaro S, Yi CL, McPhie D, Schreurs BG, Gusev PA, Favit A, Zohar O, Kim J, Beushausen S, Ascoli G, Olds J, Neve R & Alkon DL. (1996). Calexcitin: a signaling protein that binds calcium and GTP, inhibits potassium channels, and enhances membrane excitability. *Proc Natl Acad Sci U S A* **93,** 13808-13813.

Neveu D & Zucker RS. (1996). Postsynaptic levels of $[Ca^{2+}]_i$ needed to trigger LTD and LTP. *Neuron* **16,** 619-629.

Newton CL, Mignery GA & Südhof TC. (1994). Co-expression in vertebrate tissues and cell lines of multiple inositol 1,4,5-trisphosphate ($InsP_3$) receptors with distinct affinities for $InsP_3$. *J Biol Chem* **269,** 28613-28619.

Nicholls DG & Scott ID. (1980). The regulation of brain mitochondrial calcium-ion transport. The role of ATP in the discrimination between kinetic and membrane-potential-dependent calcium-ion efflux mechanisms. *Biochem J* **186,** 833-839.

Nichols DE & Nichols CD. (2008). Serotonin receptors. *Chem Rev* **108,** 1614-1641.

Nicoll RA & Alger BE. (1981). A simple chamber for recording from submerged brain slices. *J Neurosci Methods* **4,** 153-156.

Nicotera P, Orrenius S, Nilsson T & Berggren PO. (1990). An inositol 1,4,5-trisphosphate-sensitive Ca^{2+} pool in liver nuclei. *Proc Natl Acad Sci U S A* **87,** 6858-6862.

Niggli V & Carafoli E. (1981). Interaction of the purified Ca^{2+}, Mg^{2+}-ATPase from human erythrocytes with phospholipids and calmodulin. *Acta biologica et medica Germanica* **40,** 437-442.

Nishimaru H, Iizuka M, Ozaki S & Kudo N. (1996). Spontaneous motoneuronal activity mediated by glycine and GABA in the spinal cord of rat fetuses in vitro. *J Physiol* **497 (Pt 1),** 131-143.

Nissen R, Hu B & Renaud LP. (1995). Regulation of spontaneous phasic firing of rat supraoptic vasopressin neurones in vivo by glutamate receptors. *J Physiol* **484 (Pt 2),** 415-424.

Niswender CM & Conn PJ. (2010). Metabotropic glutamate receptors: physiology, pharmacology, and disease. *Annu Rev Pharmacol Toxicol* **50,** 295-322.

Norenberg MD & Martinez-Hernandez A. (1979). Fine structural localization of glutamine synthetase in astrocytes of rat brain. *Brain Res* **161,** 303-310.

O'Carroll AM, Bardsley ME & Tipton KF. (1986). The oxidation of adrenaline and noradrenaline by the two forms of monoamine oxidase from human and rat brain. *Neurochem Int* **8,** 493-500.

Obermair GJ, Kaufmann WA, Knaus HG & Flucher BE. (2003). The small conductance Ca^{2+}-activated K^+ channel SK3 is localized in nerve terminals of excitatory synapses of cultured mouse hippocampal neurons. *Eur J Neurosci* **17,** 721-731.

Ohsumi Y & Anraku Y. (1983). Calcium transport driven by a proton motive force in vacuolar membrane vesicles of Saccharomyces cerevisiae. *J Biol Chem* **258,** 5614-5617.

Otani S, Marshall CJ, Tate WP, Goddard GV & Abraham WC. (1989). Maintenance of long-term potentiation in rat dentate gyrus requires protein synthesis but not messenger RNA synthesis immediately post-tetanization. *Neurosci* **28,** 519-526.

Ottersen OP, Storm-Mathisen J, Bramham C, Torp R, Laake J & Gundersen V. (1990). A quantitative electron microscopic immunocytochemical study of the distribution and synaptic handling of glutamate in rat hippocampus. *Prog Brain Res* **83,** 99-114.

Ottersen OP, Zhang N & Walberg F. (1992). Metabolic compartmentation of glutamate and glutamine: morphological evidence obtained by quantitative immunocytochemistry in rat cerebellum. *Neurosci* **46,** 519-534.

Ottosson A, Jansen I & Edvinsson L. (1988). Characterization of histamine receptors in isolated human cerebral arteries. *Br J Pharmacol* **94,** 901-907.

Ouanounou A, Zhang L, Tymianski M, Charlton MP, Wallace MC & Carlen PL. (1996). Accumulation and extrusion of permeant Ca^{2+} chelators in attenuation of synaptic transmission at hippocampal CA1 neurons. *Neurosci* **75,** 99-109.

Pabst S, Margittai M, Vainius D, Langen R, Jahn R & Fasshauer D. (2002). Rapid and selective binding to the synaptic SNARE complex suggests a modulatory role of complexins in neuroexocytosis. *J Biol Chem* **277,** 7838-7848.

Pack-Chung E, Meyers MB, Pettingell WP, Moir RD, Brownawell AM, Cheng I, Tanzi RE & Kim TW. (2000). Presenilin 2 interacts with sorcin, a modulator of the ryanodine receptor. *J Biol Chem* **275,** 14440-14445.

Palay SL. (1956). Synapses in the central nervous system. *J Biophys Biochem Cytol* **2,** 193-202.

Palmada M & Centelles JJ. (1998). Excitatory amino acid neurotransmission. Pathways for metabolism, storage and reuptake of glutamate in brain. *Front Biosci* **3,** d701-718.

Pan YZ, Li DP & Pan HL. (2002). Inhibition of glutamatergic synaptic input to spinal lamina II_o neurons by presynaptic α_2-adrenergic receptors. *J Neurophysiol* **87,** 1938-1947.

Panula P, Yang HY & Costa E. (1984). Histamine-containing neurons in the rat hypothalamus. *Proc Natl Acad Sci U S A* **81,** 2572-2576.

Parker D. (1995). Depression of synaptic connections between identified motor neurons in the locust. *J Neurophysiol* **74,** 529-538.

Parnas H & Parnas I. (2007). The chemical synapse goes electric: Ca^{2+}- and voltage-sensitive GPCRs control neurotransmitter release. *Trends Neurosci* **30,** 54-61.

Parnas I. (1972). Differential block at high frequency of branches of a single axon innervating two muscles. *J Neurophysiol* **35,** 903-914.

Pasternak JR & Woolsey TA. (1975). The number, size and spatial distribution of neurons in lamina IV of the mouse SmI neocortex. *J Comp Neurol* **160,** 291-306.

Pastor C, Badia A & Sabria J. (1996). Possible involvement of α_1-adrenoceptors in the modulation of [^{3}H]noradrenaline release in rat brain cortical and hippocampal synaptosomes. *Neurosci Lett* **216,** 187-190.

Patel S, Morris SA, Adkins CE, O'Beirne G & Taylor CW. (1997). Ca^{2+}-independent inhibition of inositol trisphosphate receptors by calmodulin: redistribution of calmodulin as a possible means of regulating Ca^{2+} mobilization. *Proc Natl Acad Sci U S A* **94,** 11627-11632.

Patkar SA, Rasmussen U & Diamant B. (1979). On the mechanism of histamine release induced by thapsigargin from *Thapsia garganica* L. *Agents and actions* **9,** 53-57.

Peng LA, Schousboe A & Hertz L. (1991). Utilization of alpha-ketoglutarate as a precursor for transmitter glutamate in cultured cerebellar granule cells. *Neurochem Res* **16,** 29-34.

Persechini A, Moncrief ND & Kretsinger RH. (1989). The EF-hand family of calcium-modulated proteins. *Trends Neurosci* **12,** 462-467.

Petersen CC. (2007). The functional organization of the barrel cortex. *Neuron* **56,** 339-355.

Peyron C, Tighe DK, van den Pol AN, de Lecea L, Heller HC, Sutcliffe JG & Kilduff TS. (1998). Neurons containing hypocretin (orexin) project to multiple neuronal systems. *J Neurosci* **18,** 9996-10015.

Phillis JW, Tebecis AK & York DH. (1968). Depression of spinal motoneurones by noradrenaline, 5-hydroxytryptamine and histamine. *Eur J Pharmacol* **4,** 471-475.

Pivovarova NB, Hongpaisan J, Andrews SB & Friel DD. (1999). Depolarization-induced mitochondrial Ca accumulation in sympathetic neurons: spatial and temporal characteristics. *J Neurosci* **19,** 6372-6384.

Podlisny MB, Citron M, Amarante P, Sherrington R, Xia W, Zhang J, Diehl T, Levesque G, Fraser P, Haass C, Koo EH, Seubert P, St George-Hyslop P, Teplow DB & Selkoe DJ. (1997). Presenilin proteins undergo heterogeneous endoproteolysis between Thr291 and Ala299 and occur as stable N- and C-terminal fragments in normal and Alzheimer brain tissue. *Neurobiol Dis* **3,** 325-337.

Porter KR, Claude A & Fullam EF. (1945). A study of tissue culture cells by electron microscopy: methods and perliminary observations. *J Exp Med* **81,** 233-246.

Powis G, Seewald MJ, Gratas C, Melder D, Riebow J & Modest EJ. (1992). Selective inhibition of phosphatidylinositol phospholipase C by cytotoxic ether lipid analogues. *Cancer Res* **52,** 2835-2840.

Pozzan T & Azzone GF. (1976). The coupling of electrical ion fluxes in rat liver mitochondria. *FEBS letters* **71,** 62-66.

Puumala T, Greijus S, Narinen K, Haapalinna A, Riekkinen P, Sr. & Sirviö J. (1998). Stimulation of alpha-1 adrenergic receptors facilitates spatial learning in rats. *Eur Neuropsychopharmacol* **8,** 17-26.

Rainbow TC, Parsons B & Wolfe BB. (1984). Quantitative autoradiography of β_1- and β_2-adrenergic receptors in rat brain. *Proc Natl Acad Sci U S A* **81,** 1585-1589.

Ramirez DM & Kavalali ET. (2011). Differential regulation of spontaneous and evoked neurotransmitter release at central synapses. *Curr Opin Neurobiol* **21,** 275-282.

Ramirez DM, Khvotchev M, Trauterman B & Kavalali ET. (2012). Vti1a identifies a vesicle pool that preferentially recycles at rest and maintains spontaneous neurotransmission. *Neuron* **73,** 121-134.

Ramos BP & Arnsten AF. (2007). Adrenergic pharmacology and cognition: focus on the prefrontal cortex. *Pharmacol & Ther* **113,** 523-536.

Raymond CR. (2008). Different requirements for action potentials in the induction of different forms of long-term potentiation. *J Physiol* **586,** 1859-1865.

Raymond CR & Redman SJ. (2002). Different calcium sources are narrowly tuned to the induction of different forms of LTP. *J Neurophysiol* **88,** 249-255.

Raymond CR, Thompson VL, Tate WP & Abraham WC. (2000). Metabotropic glutamate receptors trigger homosynaptic protein synthesis to prolong long-term potentiation. *J Neurosci* **20,** 969-976.

Redman S. (1990). Quantal analysis of synaptic potentials in neurons of the central nervous system. *Physiol Rev* **70,** 165-198.

Redman SJ. (1973). The attenuation of passively propagating dendritic potentials in a motoneurone cable model. *J Physiol* **234,** 637-664.

Reuter H & Seitz N. (1968). The dependence of calcium efflux from cardiac muscle on temperature and external ion composition. *J Physiol* **195,** 451-470.

Revett SP, King G, Shabanowitz J, Hunt DF, Hartman KL, Laue TM & Nelson DJ. (1997). Characterization of a helix-loop-helix (EF hand) motif of silver hake parvalbumin isoform B. *Protein Sci* **6,** 2397-2408.

Rhee SG, Kim H, Suh PG & Choi WC. (1991). Multiple forms of phosphoinositide-specific phospholipase C and different modes of activation. *Biochem Soc Trans* **19,** 337-341.

Richards DA, Mateos JM, Hugel S, de Paola V, Caroni P, Gahwiler BH & McKinney RA. (2005). Glutamate induces the rapid formation of spine head protrusions in hippocampal slice cultures. *Proc Natl Acad Sci U S A* **102,** 6166-6171.

Richards DA, Rizzoli SO & Betz WJ. (2004). Effects of wortmannin and latrunculin A on slow endocytosis at the frog neuromuscular junction. *J Physiol* **557,** 77-91.

Riveros N, Fiedler J, Lagos N, Muñoz C & Orrego F. (1986). Glutamate in rat brain cortex synaptic vesicles: influence of the vesicle isolation procedure. *Brain Res* **386,** 405-408.

Rizo J & Rosenmund C. (2008). Synaptic vesicle fusion. *Nat Struct Mol Biol* **15,** 665-674.

Rizzoli SO & Betz WJ. (2005). Synaptic vesicle pools. *Nature reviews* **6,** 57-69.

Rizzuto R & Pozzan T. (2006). Microdomains of intracellular Ca^{2+}: molecular determinants and functional consequences. *Physiol Rev* **86,** 369-408.

Roberts WM, Jacobs RA & Hudspeth AJ. (1990). Colocalization of ion channels involved in frequency selectivity and synaptic transmission at presynaptic active zones of hair cells. *J Neurosci* **10,** 3664-3684.

Rodney GG, Moore CP, Williams BY, Zhang JZ, Krol J, Pedersen SE & Hamilton SL. (2001). Calcium binding to calmodulin leads to an N-terminal shift in its binding site on the ryanodine Receptor. *J Biol Chem* **276,** 2069-2074.

Rogawski MA & Aghajanian GK. (1980). Activation of lateral geniculate neurons by norepinephrine: mediation by an α-adrenergic receptor. *Brain Res* **182,** 345-359.

Romano C, Sesma MA, McDonald CT, O'Malley K, Van den Pol AN & Olney JW. (1995). Distribution of metabotropic glutamate receptor mGluR5 immunoreactivity in rat brain. *J Comp Neurol* **355,** 455-469.

Roncarati R, Di Chio M, Sava A, Terstappen GC & Fumagalli G. (2001). Presynaptic localization of the small conductance calcium-activated potassium channel SK3 at the neuromuscular junction. *Neurosci* **104,** 253-262.

Rorabaugh BR, Gaivin RJ, Papay RS, Shi T, Simpson PC & Perez DM. (2005). Both $alpha_{1A}$- and $alpha_{1B}$-adrenergic receptors crosstalk to down regulate β_1-ARs in mouse heart: coupling to differential PTX-sensitive pathways. *Journal of molecular and cellular cardiology* **39,** 777-784.

Roth TF & Porter KR. (1964). Yolk protein uptake in the oocyte of the mosquito *Aedes Aegypti.* L. *J Cell Biol* **20,** 313-332.

Rothman JE & Warren G. (1994). Implications of the SNARE hypothesis for intracellular membrane topology and dynamics. *Curr Biol* **4,** 220-233.

Rousseau E, Smith JS & Meissner G. (1987). Ryanodine modifies conductance and gating behavior of single Ca^{2+} release channel. *Am J Physiol* **253,** C364-368.

Rozov A, Burnashev N, Sakmann B & Neher E. (2001). Transmitter release modulation by intracellular Ca^{2+} buffers in facilitating and depressing nerve terminals of pyramidal cells in layer 2/3 of the rat neocortex indicates a target cell-specific difference in presynaptic calcium dynamics. *J Physiol* **531,** 807-826.

Rubiales de Barioglio S & Orrego F. (1982). A study of calcium compartments in rat brain cortex thin slices: effects of veratridine, lithium and of a mitochondrial uncoupler. *Neurochem Res* **7,** 1427-1435.

Ruffolo RR, Jr. & Waddell JE. (1982). Receptor interactions of imidazolines. IX. Cirazoline is an alpha-1 adrenergic agonist and an alpha-2 adrenergic antagonist. *J Pharmacol Exp Ther* **222,** 29-36.

Ruffolo RR, Jr., Yaden EL & Waddell JE. (1982). Stereochemical requirements of *alpha*-2 adrenergic receptors. *J Pharmacol Exp Ther* **222,** 645-651.

Ruska E. (1986). Ernst Ruska- Nobel Lecture. *Nobelprizeorg.*

Rutherford EC, Pomerleau F, Huettl P, Stromberg I & Gerhardt GA. (2007). Chronic second-by-second measures of L-glutamate in the central nervous system of freely moving rats. *J Neurochem* **102,** 712-722.

Ryan TA & Smith SJ. (1995). Vesicle pool mobilization during action potential firing at hippocampal synapses. *Neuron* **14,** 983-989.

Saavedra JM, Palkovits M, Brownstein MJ & Axelrod J. (1974). Localisation of phenylethanolamine N-methyl transferase in the rat brain nuclei. *Nature* **248,** 695-696.

Sachdev P, Menon S, Kastner DB, Chuang JZ, Yeh TY, Conde C, Caceres A, Sung CH & Sakmar TP. (2007). G protein βγ subunit interaction with the dynein light-chain component Tctex-1 regulates neurite outgrowth. *EMBO J* **26,** 2621-2632.

Sah P. (1992). Role of calcium influx and buffering in the kinetics of Ca^{2+}-activated K^+ current in rat vagal motoneurons. *J Neurophysiol* **68,** 2237-2247.

Sailer CA, Hu H, Kaufmann WA, Trieb M, Schwarzer C, Storm JF & Knaus HG. (2002). Regional differences in distribution and functional expression of small-conductance Ca^{2+}-activated K^+ channels in rat brain. *J Neurosci* **22,** 9698-9707.

Sajikumar S & Frey JU. (2003). Anisomycin inhibits the late maintenance of long-term depression in rat hippocampal slices in vitro. *Neurosci Lett* **338,** 147-150.

Sakaba T & Neher E. (2001). Calmodulin mediates rapid recruitment of fast-releasing synaptic vesicles at a calyx-type synapse. *Neuron* **32,** 1119-1131.

Sakurai T. (2007). The neural circuit of orexin (hypocretin): maintaining sleep and wakefulness. *Nature reviews* **8,** 171-181.

Samso M, Shen X & Allen PD. (2006). Structural characterization of the RyR1-FKBP12 interaction. *J Mol Biol* **356,** 917-927.

Samsó M & Wagenknecht T. (2002). Apocalmodulin and Ca^{2+}-calmodulin bind to neighboring locations on the ryanodine receptor. *J Biol Chem* **277,** 1349-1353.

Sander LE, Lorentz A, Sellge G, Coeffier M, Neipp M, Veres T, Frieling T, Meier PN, Manns MP & Bischoff SC. (2006). Selective expression of histamine receptors H1R, H2R, and H4R, but not H3R, in the human intestinal tract. *Gut* **55,** 498-504.

Sanders-Bush E, Tsutsumi M & Burris KD. (1990). Serotonin receptors and phosphatidylinositol turnover. *Ann N Y Acad Sci* **600,** 224-235; discussion 235-226.

Sankaranarayanan S & Ryan TA. (2000). Real-time measurements of vesicle-SNARE recycling in synapses of the central nervous system. *Nat Cell Biol* **2,** 197-204.

Sans N, Petralia RS, Wang YX, Blahos J, 2nd, Hell JW & Wenthold RJ. (2000). A developmental change in NMDA receptor-associated proteins at hippocampal synapses. *J Neurosci* **20,** 1260-1271.

Santella L & Kyozuka K. (1997). Effects of 1-methyladenine on nuclear Ca^{2+} transients and meiosis resumption in starfish oocytes are mimicked by the nuclear injection of inositol 1,4,5-trisphosphate and cADP-ribose. *Cell Calcium* **22,** 11-20.

Savic N & Sciancalepore M. (1998). Intracellular calcium stores modulate miniature GABA-mediated synaptic currents in neonatal rat hippocampal neurons. *The European journal of neuroscience* **10,** 3379-3386.

Scanziani M, Gähwiler BH & Thompson SM. (1993). Presynaptic inhibition of excitatory synaptic transmission mediated by alpha adrenergic receptors in area CA3 of the rat hippocampus in vitro. *J Neurosci* **13,** 5393-5401.

Schaub JR, Lu X, Doneske B, Shin YK & McNew JA. (2006). Hemifusion arrest by complexin is relieved by Ca^{2+}-synaptotagmin I. *Nat Struct Mol Biol* **13,** 748-750.

Schenck S, Wojcik SM, Brose N & Takamori S. (2009). A chloride conductance in VGLUT1 underlies maximal glutamate loading into synaptic vesicles. *Nat Neurosci* **12,** 156-162.

Schikorski T & Stevens CF. (2001). Morphological correlates of functionally defined synaptic vesicle populations. *Nat Neurosci* **4,** 391-395.

Schliwa M & Woehlke G. (2003). Molecular motors. *Nature* **422,** 759-765.

Schneggenburger R & Neher E. (2000). Intracellular calcium dependence of transmitter release rates at a fast central synapse. *Nature* **406,** 889-893.

Schneider Gasser EM, Straub CJ, Panzanelli P, Weinmann O, Sassoè-Pognetto M & Fritschy JM. (2006). Immunofluorescence in brain sections: simultaneous detection of presynaptic and postsynaptic proteins in identified neurons. *Nat Protoc* **1,** 1887-1897.

Schousboe A, Sarup A, Bak LK, Waagepetersen HS & Larsson OM. (2004). Role of astrocytic transport processes in glutamatergic and GABAergic neurotransmission. *Neurochem Int* **45,** 521-527.

Schulz DJ. (2006). Plasticity and stability in neuronal output via changes in intrinsic excitability: it's what's inside that counts. *J Exp Biol* **209,** 4821-4827.

Schürmann FW, Sanderman R & Sanderman D. (1991). Dense-core vesicles and non-synaptic exocytosis in the central body of the crayfish brain. *Cell Tiss Res* **265,** 493-501.

Schwaller B, Meyer M & Schiffmann S. (2002). 'New' functions for 'old' proteins: the role of the calcium-binding proteins calbindin D-28k, calretinin and parvalbumin, in cerebellar physiology. Studies with knockout mice. *Cerebellum* **1,** 241-258.

Schwendt M & McGinty JF. (2010). Amphetamine up-regulates activator of G-protein signaling 1 mRNA and protein levels in rat frontal cortex: the role of dopamine and glucocorticoid receptors. *Neurosci* **168,** 96-107.

Segal M. (1982). Norepinephrine modulates reactivity of hippocampal cells to chemical stimulation *in vitro*. *Exp Neurol* **77,** 86-93.

Segal M & Bloom FE. (1974). The action of norepinephrine in the rat hippocampus. II. Activation of the input pathway. *Brain Res* **72,** 99-114.

Serrano P, Yao Y & Sacktor TC. (2005). Persistent phosphorylation by protein kinase Mζ maintains late-phase long-term potentiation. *J Neurosci* **25,** 1979-1984.

Sharma MR, Jeyakumar LH, Fleischer S & Wagenknecht T. (2006). Three-dimensional visualization of FKBP12.6 binding to an open conformation of cardiac ryanodine receptor. *Biophys J* **90,** 164-172.

Sharp T, Backus LI, Hjorth S, Bramwell SR & Grahame-Smith DG. (1990). Further investigation of the in vivo pharmacological properties of the putative 5-HT_{1A} antagonist, BMY 7378. *Eur J Pharmacol* **176,** 331-340.

Shen KZ & Johnson SW. (2000). Presynaptic dopamine D2 and muscarine M3 receptors inhibit excitatory and inhibitory transmission to rat subthalamic neurones in vitro. *J Physiol* **525 Pt 2,** 331-341.

Shi J, Townsend M & Constantine-Paton M. (2000). Activity-dependent induction of tonic calcineurin activity mediates a rapid developmental downregulation of NMDA receptor currents. *Neuron* **28,** 103-114.

Shi SH, Hayashi Y, Petralia RS, Zaman SH, Wenthold RJ, Svoboda K & Malinow R. (1999). Rapid spine delivery and redistribution of AMPA receptors after synaptic NMDA receptor activation. *Science* **284,** 1811-1816.

Shimegi S, Ichikawa T, Akasaki T & Sato H. (1999). Temporal characteristics of response integration evoked by multiple whisker stimulations in the barrel cortex of rats. *The Journal of neuroscience : the official journal of the Society for Neuroscience* **19,** 10164-10175.

Shirataki H, Kaibuchi K, Sakoda T, Kishida S, Yamaguchi T, Wada K, Miyazaki M & Takai Y. (1993). Rabphilin-3A, a putative target protein for *smg* p25A/*rab*3A p25 small GTP-binding protein related to synaptotagmin. *Mol Cell Biol* **13,** 2061-2068.

Shull GE & Greeb J. (1988). Molecular cloning of two isoforms of the plasma membrane Ca^{2+}-transporting ATPase from rat brain. Structural and functional domains exhibit similarity to Na^+,K^+- and other cation transport ATPases. *J Biol Chem* **263,** 8646-8657.

Simkus CR & Stricker C. (2002a). The contribution of intracellular calcium stores to mEPSCs recorded in layer II neurones of rat barrel cortex. *J Physiol* **545,** 521-535.

Simkus CR & Stricker C. (2002b). Properties of mEPSCs recorded in layer II neurones of rat barrel cortex. *J Physiol* **545,** 509-520.

Simon J, Webb TE & Barnard EA. (1997). Distribution of [^{35}S]dATPαS binding sites in the adult rat neuraxis. *Neuropharmac* **36,** 1243-1251.

Simon SM & Llinás RR. (1985). Compartmentalization of the submembrane calcium activity during calcium influx and its significance in transmitter release. *Biophys J* **48,** 485-498.

Simpson KL, Altman DW, Wang L, Kirifides ML, Lin RC & Waterhouse BD. (1997). Lateralization and functional organization of the locus coeruleus projection to the trigeminal somatosensory pathway in rat. *J Comp Neurol* **385,** 135-147.

Simpson KL, Waterhouse BD & Lin RC. (2006). Characterization of neurochemically specific projections from the locus coeruleus with respect to somatosensory-related barrels. *The anatomical record* **288,** 166-173.

Smith CB & Betz WJ. (1996). Simultaneous independent measurement of endocytosis and exocytosis. *Nature* **380,** 531-534.

Smith JS, Imagawa T, Ma J, Fill M, Campbell KP & Coronado R. (1988). Purified ryanodine receptor from rabbit skeletal muscle is the calcium-release channel of sarcoplasmic reticulum. *J Gen Physiol* **92,** 1-26.

Snedecor GW & Cochran WG. (1989). *Statistical methods, eighth ed.* Iowa State University Press.

Snyder SH & Supattapone S. (1989). Isolation and functional characterization of an inositol trisphosphate receptor from brain. *Cell Calcium* **10,** 337-342.

Sokolov MV, Rossokhin AV, Behnisch T, Reymann KG & Voronin LL. (1998). Interaction between paired-pulse facilitation and long-term potentiation of minimal excitatory postsynaptic potentials in rat hippocampal slices: a patch-clamp study. *Neurosci* **85,** 1-13.

Solovyova N, Veselovsky N, Toescu EC & Verkhratsky A. (2002). Ca^{2+} dynamics in the lumen of the endoplasmic reticulum in sensory neurons: direct visualization of Ca^{2+}-induced Ca^{2+} release triggered by physiological Ca^{2+} entry. *EMBO J* **21,** 622-630.

Sparagna GC, Gunter KK, Sheu SS & Gunter TE. (1995). Mitochondrial calcium uptake from physiological-type pulses of calcium. A description of the rapid uptake mode. *J Biol Chem* **270,** 27510-27515.

Spasic D, Tolia A, Dillen K, Baert V, De Strooper B, Vrijens S & Annaert W. (2006). Presenilin-1 maintains a nine-transmembrane topology throughout the secretory pathway. *J Biol Chem* **281,** 26569-26577.

Spruston N, Jaffe DB, Williams SH & Johnston D. (1993). Voltage- and space-clamp errors associated with the measurement of electrotonically remote synaptic events. *J Neurophysiol* **70,** 781-802.

Staras K, Branco T, Burden JJ, Pozo K, Darcy K, Marra V, Ratnayaka A & Goda Y. (2010). A vesicle superpool spans multiple presynaptic terminals in hippocampal neurons. *Neuron* **66,** 37-44.

Stauffer TP, Guerini D & Carafoli E. (1995). Tissue distribution of the four gene products of the plasma membrane Ca^{2+} pump. A study using specific antibodies. *J Biol Chem* **270,** 12184-12190.

Stelzner DJ. (1971). The relationship between synaptic vesicles, Golgi apparatus, and smooth endoplasmic reticulum: a developmental study using the zinc iodide-osmium technique. *Z Zellforsch Mikrosk Anat* **120,** 332-345.

Storck T, Schulte S, Hofmann K & Stoffel W. (1992). Structure, expression, and functional analysis of a Na^{+}-dependent glutamate/aspartate transporter from rat brain. *Proc Natl Acad Sci U S A* **89,** 10955-10959.

Strehler EE & Treiman M. (2004). Calcium pumps of plasma membrane and cell interior. *Curr Mol Med* **4,** 323-335.

Stricker C, Field AC & Redman SJ. (1996a). Changes in quantal parameters of EPSCs in rat CA1 neurones in vitro after the induction of long-term potentiation. *J Physiol* **490 (Pt 2),** 443-454.

Stricker C, Field AC & Redman SJ. (1996b). Statistical analysis of amplitude fluctuations in EPSCs evoked in rat CA1 pyramidal neurones in vitro. *J Physiol* **490 (Pt 2),** 419-441.

Stricker C, Grijalvo-perez AM & Cowan AI. (2007). Presynaptic calcium stores determine transmitter release characteristics in neocortex. *SFN abstract 2007.*

Sugimori M, Lang EJ, Silver RB & Llinás R. (1994). High-resolution measurement of the time course of calcium-concentration microdomains at squid presynaptic terminals. *Biol Bull* **187,** 300-303.

Sugita S, Hata Y & Südhof TC. (1996). Distinct Ca^{2+}-dependent properties of the first and second C_2-domains of synaptotagmin I. *J Biol Chem* **271,** 1262-1265.

Suh BC, Leal K & Hille B. (2010). Modulation of high-voltage activated Ca^{2+} channels by membrane phosphatidylinositol 4,5-bisphosphate. *Neuron* **67,** 224-238.

Sullivan JM. (2007). A simple depletion model of the readily releasable pool of synaptic vesicles cannot account for paired-pulse depression. *J Neurophysiol* **97,** 948-950.

Sun J, Pang ZP, Qin D, Fahim AT, Adachi R & Südhof TC. (2007). A dual-Ca^{2+}-sensor model for neurotransmitter release in a central synapse. *Nature* **450,** 676-682.

Sun JY & Wu LG. (2001). Fast kinetics of exocytosis revealed by simultaneous measurements of presynaptic capacitance and postsynaptic currents at a central synapse. *Neuron* **30,** 171-182.

Sun T, Wu XS, Xu J, McNeil BD, Pang ZP, Yang W, Bai L, Qadri S, Molkentin JD, Yue DT & Wu LG. (2010). The role of calcium/calmodulin-activated calcineurin in rapid and slow endocytosis at central synapses. *J Neurosci* **30,** 11838-11847.

Sun XZ, Takahashi S, Cui C, Inoue M & Fukui Y. (2002). Distribution of calbindin-D28K immunoreactive neurons in rat primary motor cortex. *J Med Invest* **49,** 35-39.

Sutton MA, Wall NR, Aakalu GN & Schuman EM. (2004). Regulation of dendritic protein synthesis by miniature synaptic events. *Science* **304,** 1979-1983.

Suzuki S, Osanai M, Murase M, Suzuki N, Ito K, Shirasaki T, Narita K, Ohnuma K, Kuba K & Kijima H. (2000). Ca^{2+} dynamics at the frog motor nerve terminal. *Pflügers Arch* **440,** 351-365.

Szatkowski M, Barbour B & Attwell D. (1990). Non-vesicular release of glutamate from glial cells by reversed electrogenic glutamate uptake. *Nature* **348,** 443-446.

Tabb JS, Kish PE, Van Dyke R & Ueda T. (1992). Glutamate transport into synaptic vesicles. Roles of membrane potential, pH gradient, and intravesicular pH. *J Biol Chem* **267,** 15412-15418.

Takamori S, Rhee JS, Rosenmund C & Jahn R. (2001). Identification of differentiation-associated brain-specific phosphate transporter as a second vesicular glutamate transporter (VGLUT2). *J Neurosci* **21,** RC182.

Takei K, McPherson PS, Schmid SL & De Camilli P. (1995). Tubular membrane invaginations coated by dynamin rings are induced by GTP-γS in nerve terminals. *Nature* **374,** 186-190.

Taneja P, Ogier M, Brooks-Harris G, Schmid DA, Katz DM & Nelson SB. (2009). Pathophysiology of locus ceruleus neurons in a mouse model of Rett syndrome. *J Neurosci* **29,** 12187-12195.

Tang Y & Zucker RS. (1997). Mitochondrial involvement in post-tetanic potentiation of synaptic transmission. *Neuron* **18,** 483-491.

Tao Z, Rosental N, Kanner BI, Gameiro A, Mwaura J & Grewer C. (2010). Mechanism of cation binding to the glutamate transporter EAAC1 probed with mutation of the conserved amino acid residue Thr101. *J Biol Chem* **285,** 17725-17733.

Taylor RS, Jones SM, Dahl RH, Nordeen MH & Howell KE. (1997). Characterization of the Golgi complex cleared of proteins in transit and examination of calcium uptake activities. *Mol Biol Cell* **8,** 1911-1931.

Taylor SJ, Chae HZ, Rhee SG & Exton JH. (1991). Activation of the β1 isozyme of phospholipase C by α subunits of the G_q class of G proteins. *Nature* **350,** 516-518.

Tedford HW & Zamponi GW. (2006). Direct G protein modulation of Ca_v2 calcium channels. *Pharmacol Rev* **58,** 837-862.

Terasaki M, Slater NT, Fein A, Schmidek A & Reese TS. (1994). Continuous network of endoplasmic reticulum in cerebellar Purkinje neurons. *Proc Natl Acad Sci USA* **91,** 7510-7514.

Thayer SA & Miller RJ. (1990). Regulation of the intracellular free calcium concentration in single rat dorsal root ganglion neurones in vitro. *J Physiol* **425,** 85-115.

Thies RE. (1965). Neuromuscular depression and the apparent depletion of transmitter in mammalian muscle. *J Neurophysiol* **28,** 428-442.

Togashi K, Inada H & Tominaga M. (2008). Inhibition of the transient receptor potential cation channel TRPM2 by 2-aminoethoxydiphenyl borate (2-APB). *Br J Pharmacol* **153,** 1324-1330.

Tognarini DP & Moulds RF. (1997). Intracellular Ca^{2+} and contractile responses to alpha 1-adrenoceptor subtype activation in rat aortic vascular smooth muscle. *Eur J Pharmacol* **322,** 31-36.

Togneri J, Cheng YS, Munson M, Hughson FM & Carr CM. (2006). Specific SNARE complex binding mode of the Sec1/Munc-18 protein, Sec1p. *Proc Natl Acad Sci U S A* **103,** 17730-17735.

Tong G & Jahr CE. (1994). Block of glutamate transporters potentiates postsynaptic excitation. *Neuron* **13,** 1195-1203.

Törk I. (1990). Anatomy of the serotonergic system. *Ann N Y Acad Sci* **600,** 9-34; discussion 34-35.

Torres-Escalante JL, Barral JA, Ibarra-Villa MD, Pérez-Burgos A, Góngora-Alfaro JL & Pineda JC. (2004). 5-HT_{1A}, 5-HT_2, and $GABA_B$ receptors interact to modulate neurotransmitter release probability in layer 2/3 somatosensory rat cortex as evaluated by the paired pulse protocol. *J Neurosci Res* **78,** 268-278.

Torri-Tarelli F, Haimann C & Ceccarelli B. (1987). Coated vesicles and pits during enhanced quantal release of acetylcholine at the neuromuscular junction. *J Neurocytol* **16,** 205-214.

Toyoshima C, Nakasako M, Nomura H & Ogawa H. (2000). Crystal structure of the calcium pump of sarcoplasmic reticulum at 2.6 Å resolution. *Nature* **405,** 647-655.

Tremblay JP, Colonnier M & McLennan H. (1979). An electron microscope study of synaptic contacts in the abdominal ganglion of Aplysia californica. *J Comp Neurol* **188,** 367-389.

Trendelenburg U. (1989). The uptake and metabolism of ^{3}H-catecholamines in rat cerebral cortex slices. *Naunyn Schmiedebergs Arch Pharmacol* **339,** 293-297.

Troadec JD, Marien M, Darios F, Hartmann A, Ruberg M, Colpaert F & Michel PP. (2001). Noradrenaline provides long-term protection to dopaminergic neurons by reducing oxidative stress. *J Neurochem* **79,** 200-210.

Tsien RY. (1980). New calcium indicators and buffers with high selectivity against magnesium and protons: design, synthesis, and properties of prototype structures. *Biochem* **19,** 2396-2404.

Tsien RY. (1981). A non-disruptive technique for loading calcium buffers and indicators into cells. *Nature* **290,** 527-528.

Tsuchiya T & Rosen BP. (1976). Calcium transport driven by a proton gradient and inverted membrane vesicles of Escherichia coli. *J Biol Chem* **251,** 962-967.

Tu H, Nelson O, Bezprozvanny A, Wang Z, Lee SF, Hao YH, Serneels L, De Strooper B, Yu G & Bezprozvanny I. (2006). Presenilins form ER Ca^{2+} leak channels, a function disrupted by familial Alzheimer's disease-linked mutations. *Cell* **126,** 981-993.

Tucker T & Fettiplace R. (1995). Confocal imaging of calcium microdomains and calcium extrusion in turtle hair cells. *Neuron* **15,** 1323-1335.

Turner RS & Fuhrman FA. (1947). Modification of the action potential of amphibian nerves by Triturus embryonic toxin. *Am J Physiol* **150,** 325-328.

Tyler WJ & Pozzo-Miller L. (2003). Miniature synaptic transmission and BDNF modulate dendritic spine growth and form in rat CA1 neurones. *J Physiol* **553,** 497-509.

Ueoka-Nakanishi H, Tsuchiya T, Sasaki M, Nakanishi Y, Cunningham KW & Maeshima M. (2000). Functional expression of mung bean Ca^{2+}/H^{+} antiporter in yeast and its intracellular localization in the hypocotyl and tobacco cells. *Eur J Biochem* **267,** 3090-3098.

Urazaev AK, Naumenko NV, Poletayev GI, Nikolsky EE & Vyskočil F. (1997). Acetylcholine and carbachol prevent muscle depolarization in denervated rat diaphragm. *NeuroReport* **8,** 403-406.

Van den Bogaart G, Holt MG, Bunt G, Riedel D, Wouters FS & Jahn R. (2010). One SNARE complex is sufficient for membrane fusion. *Nat Struct Mol Biol* **17,** 358-364.

Varoqueaux F, Sigler A, Rhee JS, Brose N, Enk C, Reim K & Rosenmund C. (2002). Total arrest of spontaneous and evoked synaptic transmission but normal synaptogenesis in the absence of Munc13-mediated vesicle priming. *Proc Natl Acad Sci U S A* **99,** 9037-9042.

Vautrin J, Kriebel ME & Holsapple J. (1992). Further evidence for the dynamic formation of transmitter quanta at the neuromuscular junction. *J Neurosci Res* **32,** 245-254.

Venter JC, Horne P, Eddy B, Greguski R & Fraser CM. (1984). *Alpha*$_1$-adrenergic receptor structure. *Molecular pharmacology* **26,** 196-205.

Voets T, Moser T, Lund PE, Chow RH, Geppert M, Südhof TC & Neher E. (2001). Intracellular calcium dependence of large dense-core vesicle exocytosis in the absence of synaptotagmin I. *Proc Natl Acad Sci U S A* **98,** 11680-11685.

Volpe P & Simon BJ. (1991). The bulk of Ca^{2+} released to the myoplasm is free in the sarcoplasmic reticulum and does not unbind from calsequestrin. *FEBS letters* **278,** 274-278.

Volpicelli LA & Levey AI. (2004). Muscarinic acetylcholine receptor subtypes in cerebral cortex and hippocampus. *Prog Brain Res* **145,** 59-66.

Vyskočil F. (1985). Inhibition of non-quantal acetylcholine leakage by 2(4-phenylpiperidine)cyclohexanol in the mouse diaphragm. *Neurosci Lett* **59,** 277-280.

Vyskočil F & Illés P. (1977). Non-quantal release of transmitter at mouse neuromuscular junction and its dependence on the activity of Na^{+}-K^{+} ATP-ase. *Pflügers Arch* **370,** 295-297.

Waldeyer-Hartz HWGv. (1891). Ueber einige neuere Forschungen im Gebiete der Anatomie des Centralnervensystems. *Dtsch Med Wochenschr* **17,** 1213-1218, 1244-1246, 1267-1269, 1287-1289, 1331-1332, 1352-1356.

Wanaverbecq N, Marsh SJ, Al-Qatari M & Brown DA. (2003). The plasma membrane calcium-ATPase as a major mechanism for intracellular calcium regulation in neurones from the rat superior cervical ganglion. *J Physiol* **550,** 83-101.

Wang C & Zucker RS. (1998). Regulation of synaptic vesicle recycling by calcium and serotonin. *Neuron* **21,** 155-167.

Wang LY & Kaczmarek LK. (1998). High-frequency firing helps replenish the readily releasable pool of synaptic vesicles. *Nature* **394,** 384-388.

Wang S, Trumble WR, Liao H, Wesson CR, Dunker AK & Kang CH. (1998). Crystal structure of calsequestrin from rabbit skeletal muscle sarcoplasmic reticulum. *Nat Struct Biol* **5,** 476-483.

Wang SS & Thompson SH. (1995). Local positive feedback by calcium in the propagation of intracellular calcium waves. *Biophys J* **69,** 1683-1697.

Watanabe H, Hochi T, Mizukawa K & Otsuka N. (1986). Electron microscopic study of mossy fiber endings in the hippocampal formation of rats after picrotoxin administration. *Neurosci Res* **3,** 237-241.

Watanabe T, Taguchi Y, Shiosaka S, Tanaka J, Kubota H, Terano Y, Tohyama M & Wada H. (1984). Distribution of the histaminergic neuron system in the central nervous system of rats; a fluorescent immunohistochemical analysis with histidine decarboxylase as a marker. *Brain Res* **295,** 13-25.

Waterhouse BD, Moises HC, Yeh HH & Woodward DJ. (1982). Norepinephrine enhancement of inhibitory synaptic mechanisms in cerebellum and cerebral cortex: mediation by beta adrenergic receptors. *J Pharmacol Exp Ther* **221,** 495-506.

Waterhouse BD & Woodward DJ. (1980). Interaction of norepinephrine with cerebrocortical activity evoked by stimulation of somatosensory afferent pathways in the rat. *Exp Neurol* **67,** 11-34.

Watras J, Bezprozvanny I & Ehrlich BE. (1991). Inositol 1,4,5-trisphosphate-gated channels in cerebellum: presence of multiple conductance states. *J Neurosci* **11,** 3239-3245.

Weaving LS, Ellaway CJ, Gecz J & Christodoulou J. (2005). Rett syndrome: clinical review and genetic update. *J Med Genet* **42,** 1-7.

Weber A & Herz R. (1968). The relationship between caffeine contracture of intact muscle and the effect of caffeine on reticulum. *J Gen Physiol* **52,** 750-759.

Weiger T, Stevens DR, Wunder L & Haas HL. (1997). Histamine H1 receptors in C6 glial cells are coupled to calcium-dependent potassium channels via release of calcium from internal stores. *Naunyn Schmiedebergs Arch Pharmacol* **355,** 559-565.

Weil-Malherbe H, Axelrod J & Tomchick R. (1959). Blood-brain barrier for adrenaline. *Science* **129,** 1226-1227.

Welker C & Woolsey TA. (1974). Structure of layer IV in the somatosensory neocortex of the rat: description and comparison with the mouse. *J Comp Neurol* **158,** 437-453.

Werman R. (1966). Criteria for identification of a central nervous system transmitter. *Comp Biochem Physiol* **18,** 745-766.

Werth JL & Thayer SA. (1994). Mitochondria buffer physiological calcium loads in cultured rat dorsal root ganglion neurons. *J Neurosci* **14,** 348-356.

Westrum LE & Gray EG. (1986). New observations on the substructure of the active zone of brain synapses and motor endplates. *Proceedings of the Royal Society of London Series B, Containing papers of a Biological character Royal Society* **229,** 29-38.

Whirby LG, Axelrod J & Weil-Malherbe H. (1961). The fate of H^3-norepinephrine in aminals. *J Pharmacol Exp Ther* **132,** 193-201.

Wickelgren WO, Leonard JP, Grimes MJ & Clark RD. (1985). Ultrastructural correlates of transmitter release in presynaptic areas of lamprey reticulospinal axons. *J Neurosci* **5,** 1188-1201.

Williams SR & Stuart GJ. (2002). Dependence of EPSP efficacy on synapse location in neocortical pyramidal neurons. *Science* **295,** 1907-1910.

Willins DL, Deutch AY & Roth BL. (1997). Serotonin 5-HT_{2A} receptors are expressed on pyramidal cells and interneurons in the rat cortex. *Synapse* **27,** 79-82.

Wilson VG, Grohmann M & Trendelenburg U. (1988). The uptake and O-methylation of ^{3}H-(±)-isoprenaline in rat cerebral cortex slices. *Naunyn Schmiedebergs Arch Pharmacol* **337,** 397-405.

Wolburg H, Beer A & Finger W. (1990). Quantal secretion and loss of vesicles induced by veratridine at the crayfish neuromuscular junction. *Neurosci Lett* **115,** 7-12.

Woolsey TA & Van der Loos H. (1970). The structural organization of layer IV in the somatosensory region (SI) of mouse cerebral cortex. The description of a cortical field composed of discrete cytoarchitectonic units. *Brain Res* **17,** 205-242.

Wu D, Jiang H, Katz A & Simon MI. (1993). Identification of critical regions on phospholipase C-β1 required for activation by G-proteins. *J Biol Chem* **268,** 3704-3709.

Wu Y, Wang W, Diez-Sampedro A & Richerson GB. (2007). Nonvesicular inhibitory neurotransmission via reversal of the GABA transporter GAT-1. *Neuron* **56,** 851-865.

Xia JX, Fan SY, Yan J, Chen F, Li Y, Yu ZP & Hu ZA. (2009). Orexin A-induced extracellular calcium influx in prefrontal cortex neurons involves L-type calcium channels. *J Physiol Biochem* **65,** 125-136.

Xu J & Wu LG. (2005). The decrease in the presynaptic calcium current is a major cause of short-term depression at a calyx-type synapse. *Neuron* **46,** 633-645.

Xu-Friedman MA & Regehr WG. (2004). Structural contributions to short-term synaptic plasticity. *Physiol Rev* **84,** 69-85.

Yamada KA & Tang CM. (1993). Benzothiadiazides inhibit rapid glutamate receptor desensitization and enhance glutamatergic synaptic currents. *J Neurosci* **13,** 3904-3915.

Yamasaki M, Hashimoto K & Kano M. (2006). Miniature synaptic events elicited by presynaptic Ca^{2+} rise are selectively suppressed by cannabinoid receptor activation in cerebellar Purkinje cells. *J Neurosci* **26,** 86-95.

Yamashita T, Ishikawa T & Takahashi T. (2003). Developmental increase in vesicular glutamate content does not cause saturation of AMPA receptors at the calyx of Held synapse. *J Neurosci* **23,** 3633-3638.

Yin HL & Stossel TP. (1979). Control of cytoplasmic actin gel-sol transformation by gelsolin, a calcium-dependent regulatory protein. *Nature* **281,** 583-586.

Yoon EJ, Gerachshenko T, Spiegelberg BD, Alford S & Hamm HE. (2007). Gβγ interferes with Ca^{2+}-dependent binding of synaptotagmin to the soluble *N*-ethylmaleimide-sensitive factor attachment protein receptor (SNARE) complex. *Molecular pharmacology* **72,** 1210-1219.

Yu R & Hinkle PM. (2000). Rapid turnover of calcium in the endoplasmic reticulum during signaling. Studies with cameleon calcium indicators. *J Biol Chem* **275,** 23648-23653.

Yuste R & Denk W. (1995). Dendritic spines as basic functional units of neuronal integration. *Nature* **375,** 682-684.

Zemlan FP, Zieleniewski-Murphy A, Maureen Murphy R & Behbehani MM. (1990). BMY 7378: Partial agonist at spinal cord 5-HT_{1A} receptors. *Neurochem Int* **16,** 515-522.

Zeng H, Chattarji S, Barbarosie M, Rondi-Reig L, Philpot BD, Miyakawa T, Bear MF & Tonegawa S. (2001). Forebrain-specific calcineurin knockout selectively impairs bidirectional synaptic plasticity and working/episodic-like memory. *Cell* **107,** 617-629.

Zerangue N & Kavanaugh MP. (1996). Flux coupling in a neuronal glutamate transporter. *Nature* **383,** 634-637.

Zhang C, Wu B, Beglopoulos V, Wines-Samuelson M, Zhang D, Dragatsis I, Südhof TC & Shen J. (2009). Presenilins are essential for regulating neurotransmitter release. *Nature* **460,** 632-636.

Zhang Z, Nguyen KT, Barrett EF & David G. (2010). Vesicular ATPase inserted into the plasma membrane of motor terminals by exocytosis alkalinizes cytosolic pH and facilitates endocytosis. *Neuron* **68,** 1097-1108.

Zholos AV, Fenech CJ, Prestwich SA & Bolton TB. (2000). Membrane currents in cultured human intestinal smooth muscle cells. *J Physiol* **528,** 521-537.

Zhu Y, Xu J & Heinemann SF. (2009). Two pathways of synaptic vesicle retrieval revealed by single-vesicle imaging. *Neuron* **61,** 397-411.

Zucchi R & Ronca-Testoni S. (1997). The sarcoplasmic reticulum Ca^{2+} channel/ryanodine receptor: modulation by endogenous effectors, drugs and disease states. *Pharmacol Rev* **49,** 1-51.

Zucker RS & Regehr WG. (2002). Short-term synaptic plasticity. *Annu Rev Physiol* **64,** 355-405.

6. Appendix

6.1. Detecting and analyzing mEPSC

This guide provides a step-by-step description of how the detection of mEPSC is done. A continuous recording which is stored in a binary 16 bit format requires to be first converted into an IGOR binary wave which contains 32 bit floating point numbers and which can be read by Axograph X. A function in IGOR was created to do this conversion and save the converted wave on disk. This file is then imported into Axograph X and the entire wave is displayed on the screen (Fig. 6.1).

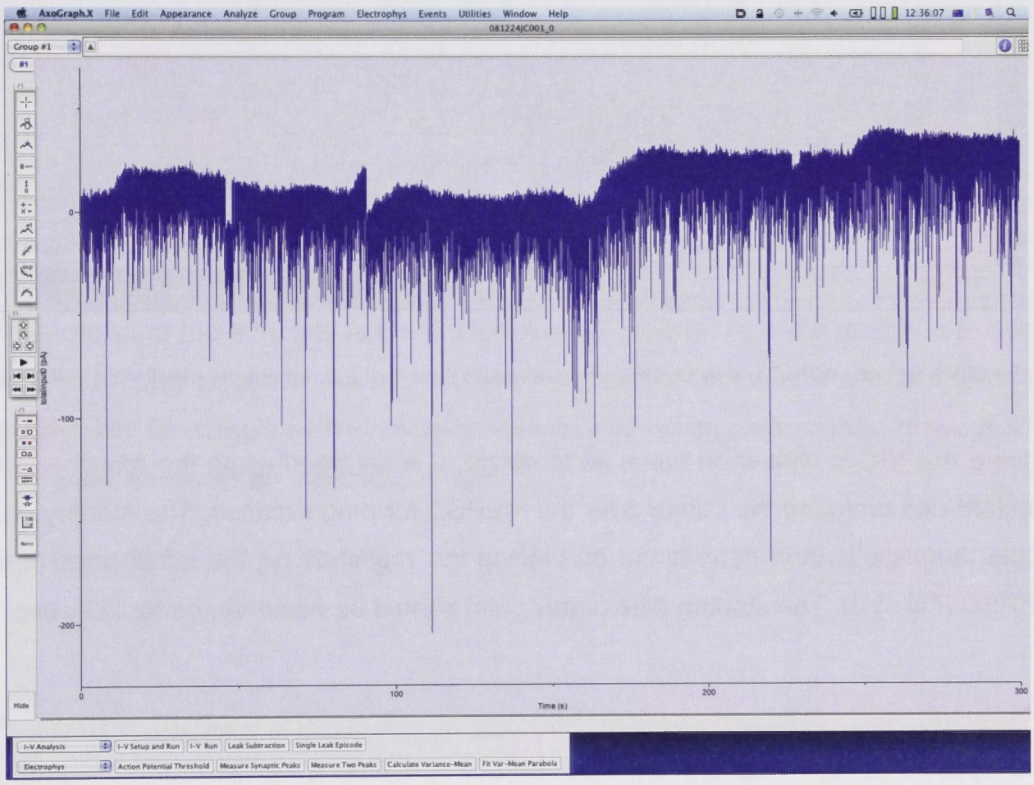

Figure 6.1. Overview of a continuous recording lasting 5 minutes in Axograph X. Note the many mEPSCs indicated by inward currents from a baseline around zero pA. It can easily be seen that the range of mEPSC peak amplitudes is between a few to maximally about 200 pA.

The recordings are inspected using the movement icons (bottom left) to find a representative mEPSC, which can serve as template. This mEPSC template (Fig. 6.2) is chosen based on a few criteria. Firstly, the mEPSC needs to be free from collisions of other mEPSCs during the rising or decay phase. Secondly, the amplitude of the template should be as large as possible (typically >100 pA) to obtain a smooth curve in

which the recording noise in regard to the peak amplitude is relatively small. Third, the rise time of the template should be fast (<1 ms) while the decay time should be 5–10 ms.

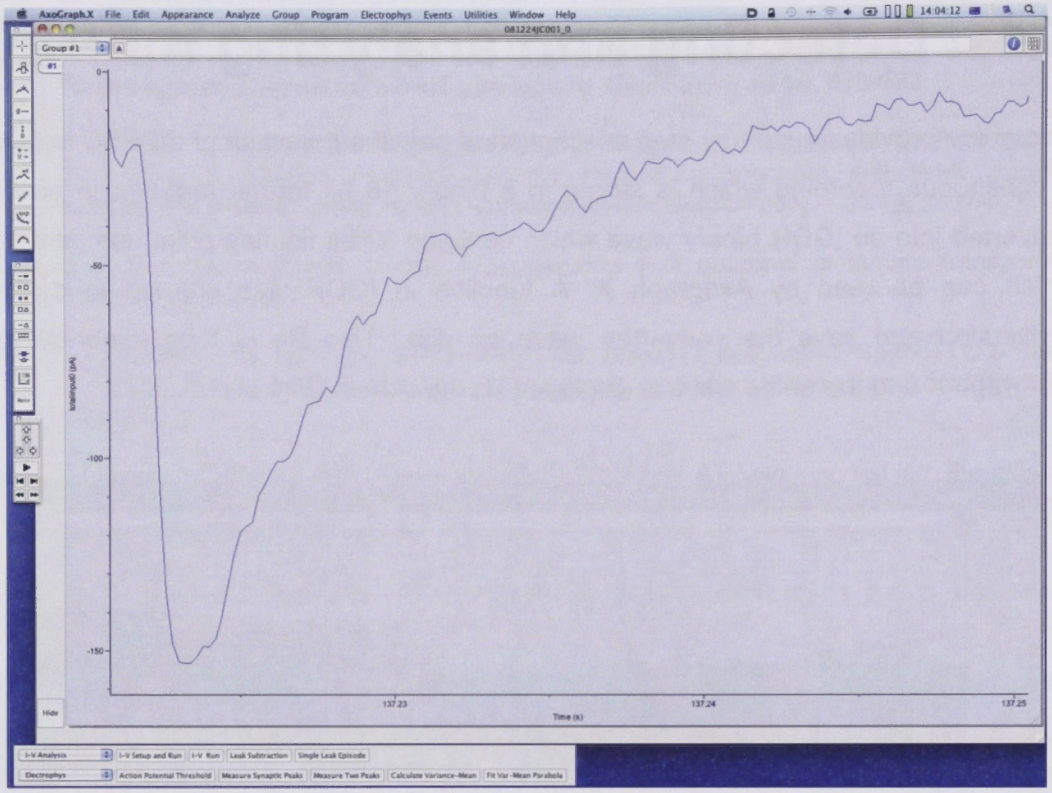

Figure 6.2. A typical mEPSC well suited to form a template that fits the three criteria mentioned in the text.

Once a mEPSC is chosen to serve as template, it is enlarged using the crosshair icon (top left) and dragging the cursor over the mEPSC for magnification. The starting point of the template is then determined by placing the crosshair on the initial point of the mEPSC (Fig. 6.3). The starting time of this point should be documented for later use.

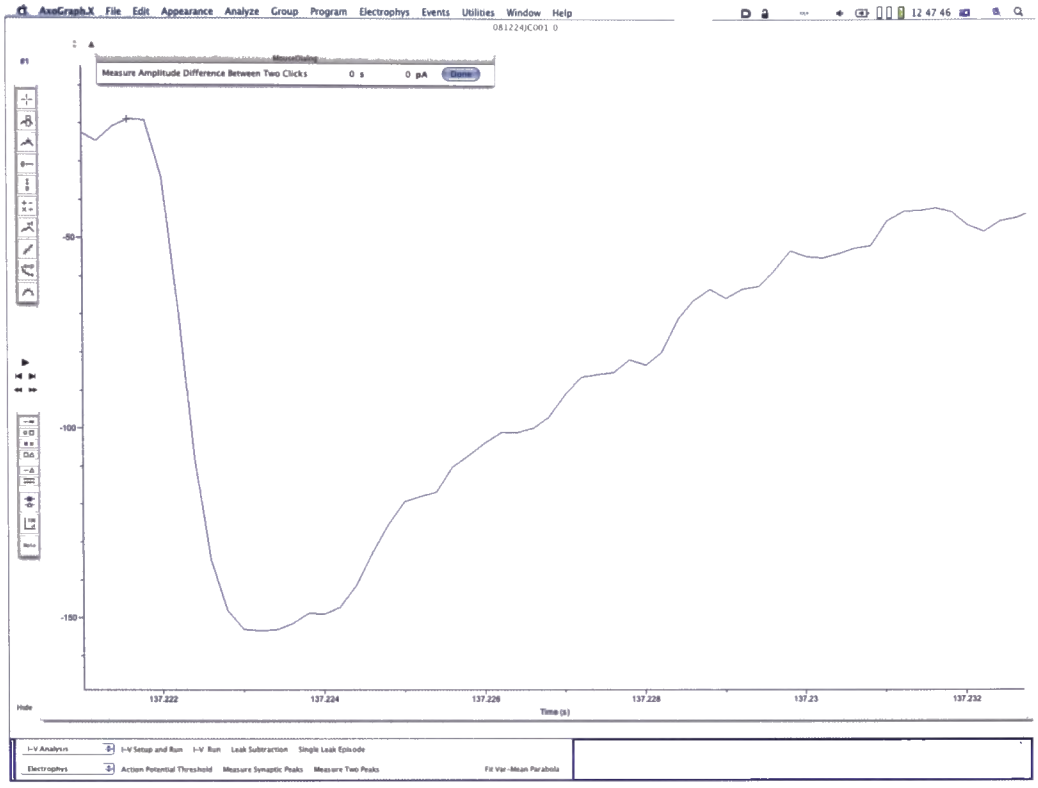

Figure 6.3. Determining the starting point of the template.

The endpoint of the template is then determined (Fig. 6.4). To allow mEPSCs to occur during the decay phase of the mEPSC, only part of the decay time of the mEPSC is included with the template. The value is typically that which corresponds to about 50% of the peak amplitude on the decay phase.

Figure 6.4. Determination of the template endpoint.

The next step serves to define the template function by choosing the "Define Template Function" option from the "Events" menu item. The "From graph" option is selected in the mask shown to allow a recorded mEPSC to be used as template rather than a mathematical function. For this to be effective, the starting point of the template must be entered into the location selector mask (Fig. 6.5).

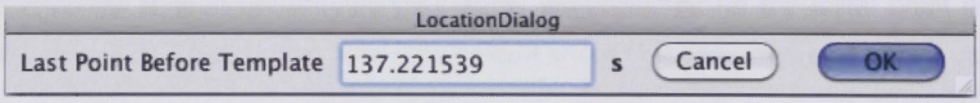

Figure 6.5. The starting point of the template can be entered using the location selector window.

This will prompt a subsequent mask, which asks for information about the template baseline and length (Fig. 6.6). The template baseline (generally 0.1 ms; i.e. very short so as to allow for colliding mEPSCs in the decay phase of another mEPSC) and the length of the template as calculated as the difference between the end and starting points are entered.

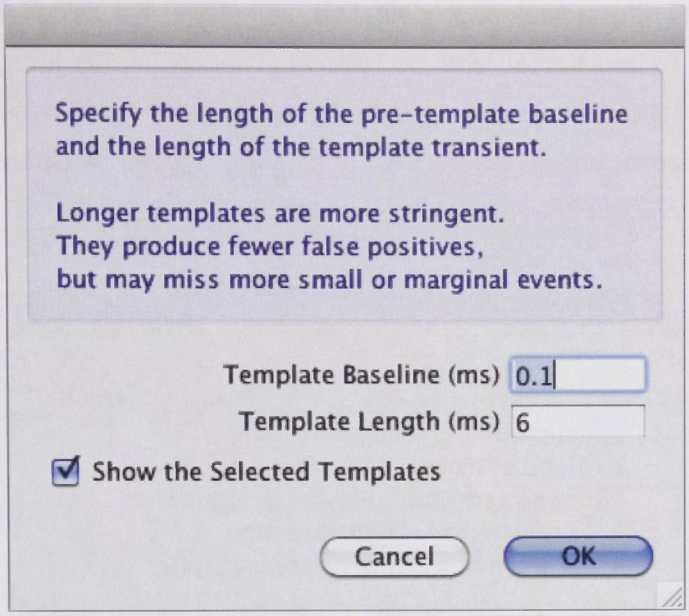

Figure 6.6. The values of the length of the baseline and the template length are entered in the mask shown.

If "Display the Template Function" is selected, a window appears, which shows the chosen template (Fig. 6.7).

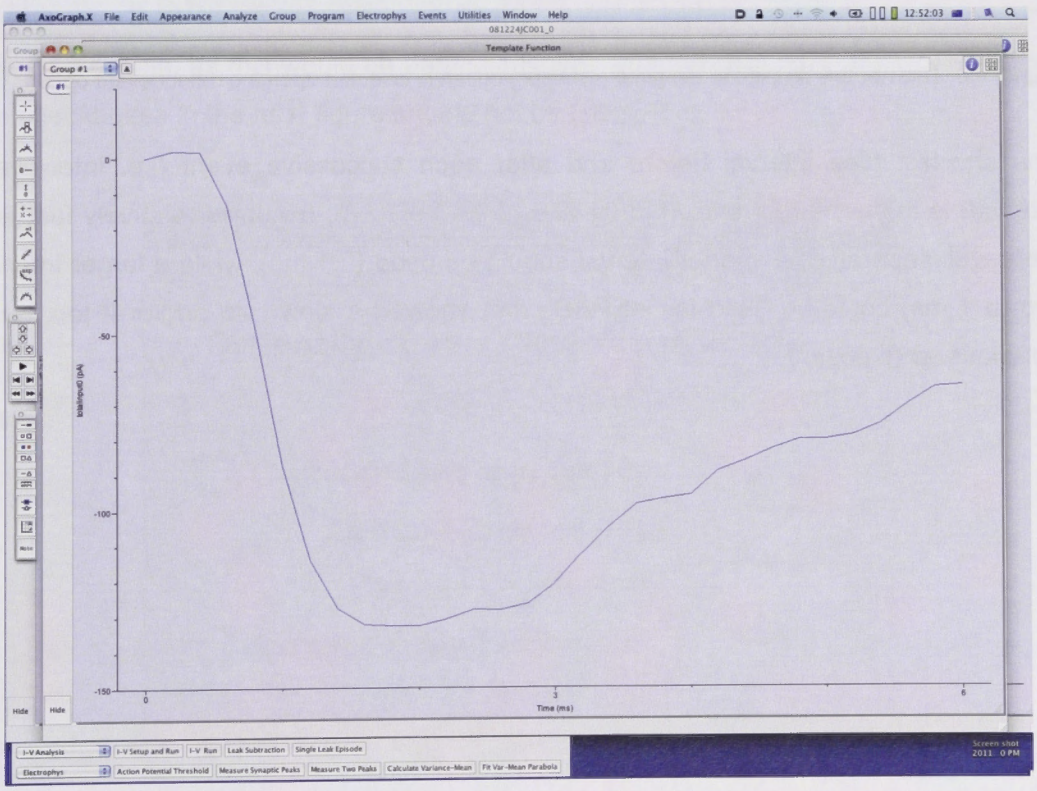

Figure 6.7. Display of the template chosen.

In order to start the actual mini detection algorithm, the window displaying the recording needs to be selected and the template window kept in the background. The "Detect events" option is selected from the "Events" menu item. At this stage, various detection techniques are available. For this study, "Variable Amplitude Template (synaptic)" was selected from the mask (Fig. 6.8).

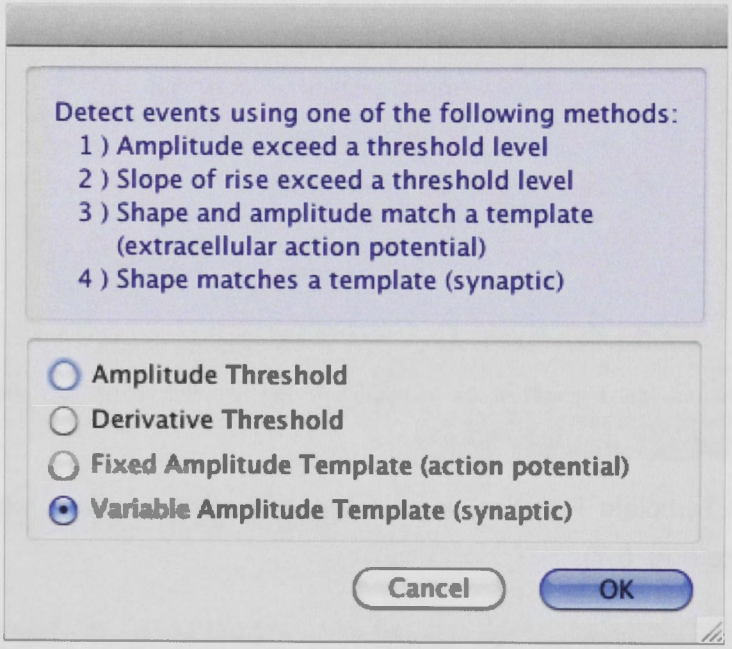

Figure 6.8. The variable amplitude template (synaptic) option is selected upon the detect event option.

The shortest time interval before and after each successive event (i.e. inter-event interval) is then entered, shown in fig. 6.9. If the mEPSCs occurred relatively fast and were well separated, a shorter interval should be used (0.1 ms), while a larger interval (up to 1 ms) could be used for mEPSCs that showed a slow rate and/or if too many collisions were observed.

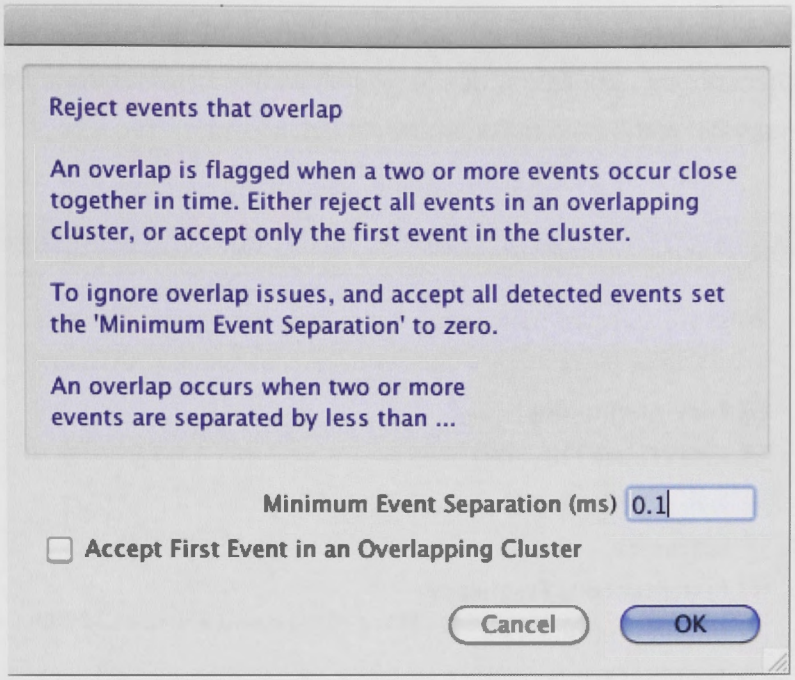

Figure 6.9. A value of 0.1 ms is chosen before and after a mEPSC.

To obtain the average of all mEPSCs detected during the recording, the checkbox "captured detected events" and "baseline captured events" are ticked. The displayed events can then be averaged. In most instances, it is not desirable to display the detected events, as this would be particularly time and memory consuming. Therefore, the checkboxes in the next figure should not be ticked (Fig. 6.10).

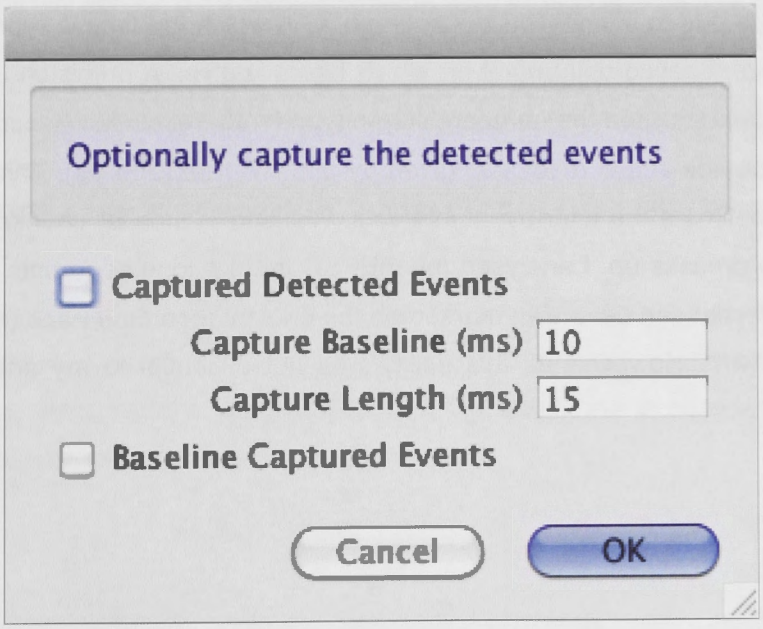

Figure 6.10. No actions are required if the detected events are not displayed in Axograph X.

The algorithm has the ability to return many parameters associated with the detection of the mEPSCs. In this study, the parameters required for further analysis are shown with ticked checkboxes (amplitude, rise-time, half width, instantaneous frequency and inter-event intervals) in the next mask, shown in figure 6.11.

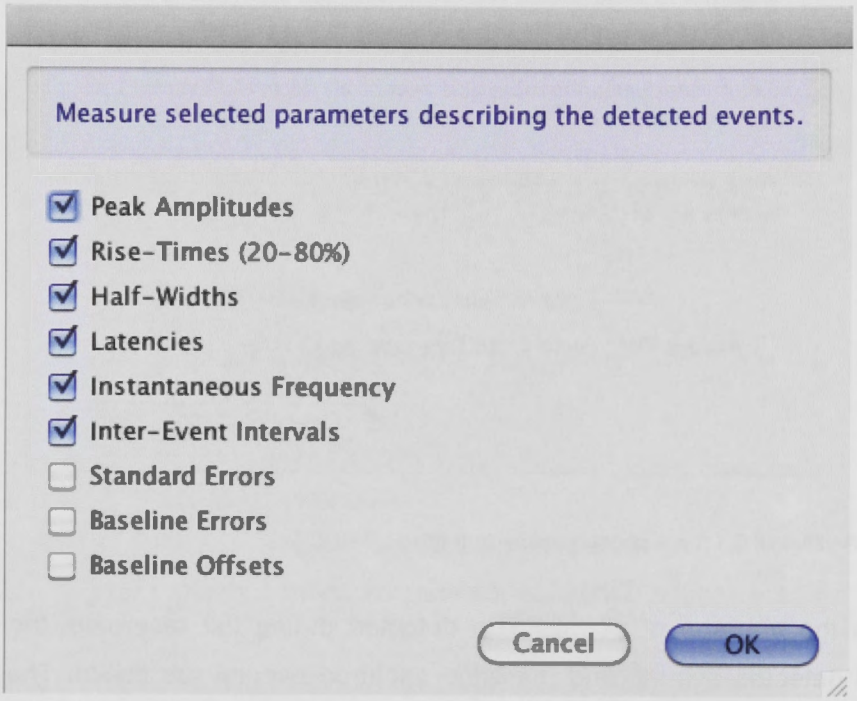

Figure 6.11. The check-boxes for amplitudes, rise-times, half-widths, latencies, instantaneous frequencies and inter-event intervals are checked for export for further analysis.

For recordings lasting longer than 100 s, the analysis should be performed in segments of 99 s. This is due to a limitation in Axograph X, in which the time is represented as a single precision floating-point number, which typically gives a precision up to 6 digits. As a consequence, when the numbers step beyond 100, resolution becomes limited to 1 ms far below the actual resolution given by the A/D rate (200 µs). This reduces the precision to estimate the inter-event intervals. Working in smaller chunks also speeds the detection process up. I analysed my mEPSC in 30 s long segments (fig. 12). The mEPSCs detected can be shown marked on the original recording trace (red and green dots; not shown). However, as this ability was not essential to my analysis, I have omitted it.

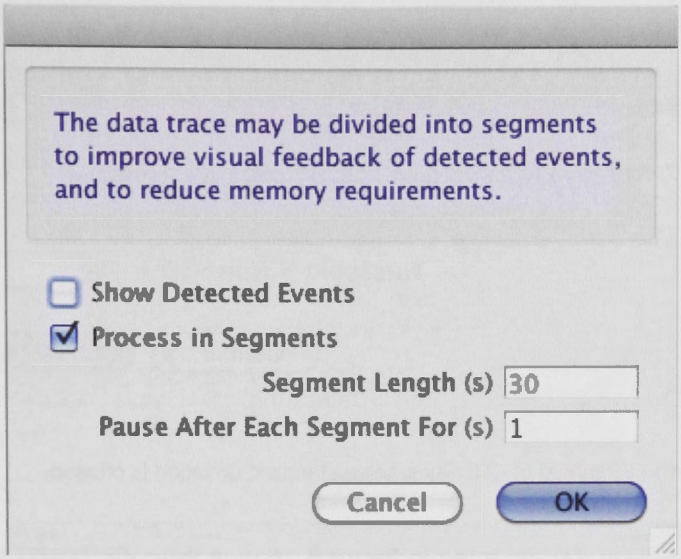

Figure 6.12. The mEPSC recordings were processed in segments of 30 s to save time.

The point, from which the overall latencies are calculated, is defined (Fig. 6.13).

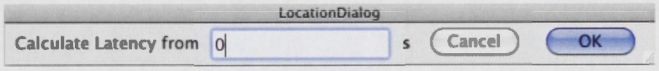

Figure 6.13. The starting point of the mEPSC recording is entered at the location in time selector.

This point in time generally coincides with the start of the recording. The interval of the recording to be analysed for mEPSC is defined in the range selector mask. As my recordings typically last for 5 minutes, that value is entered (Fig. 6.14).

Figure 6.14. The time window during which mEPSCs are to be detected is entered in the range selector.

A detection "threshold" of -2.5 times the noise standard deviation is then entered in the subsequent mask (Fig. 6.15). From experience, this value produces an optimal detection only, when used in combination with the amplitude thresholding technique described below.

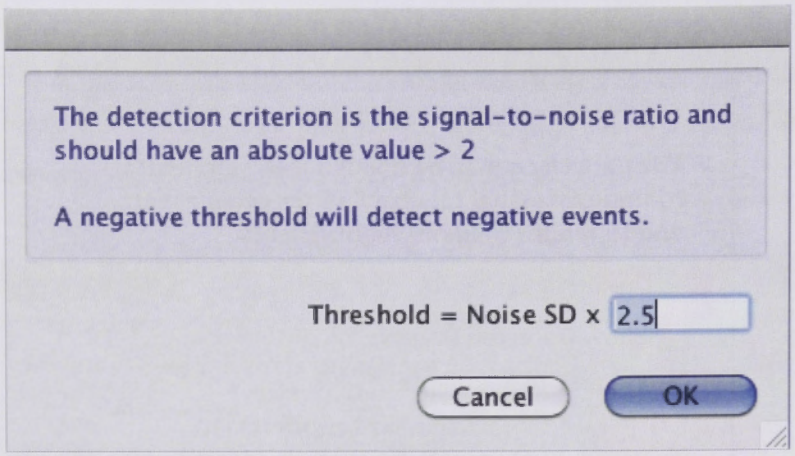

Figure 6.15. A detection threshold of -2.5 times noise standard devation is chosen.

A graph of each parameter selected in figure 6.16 was then displayed.

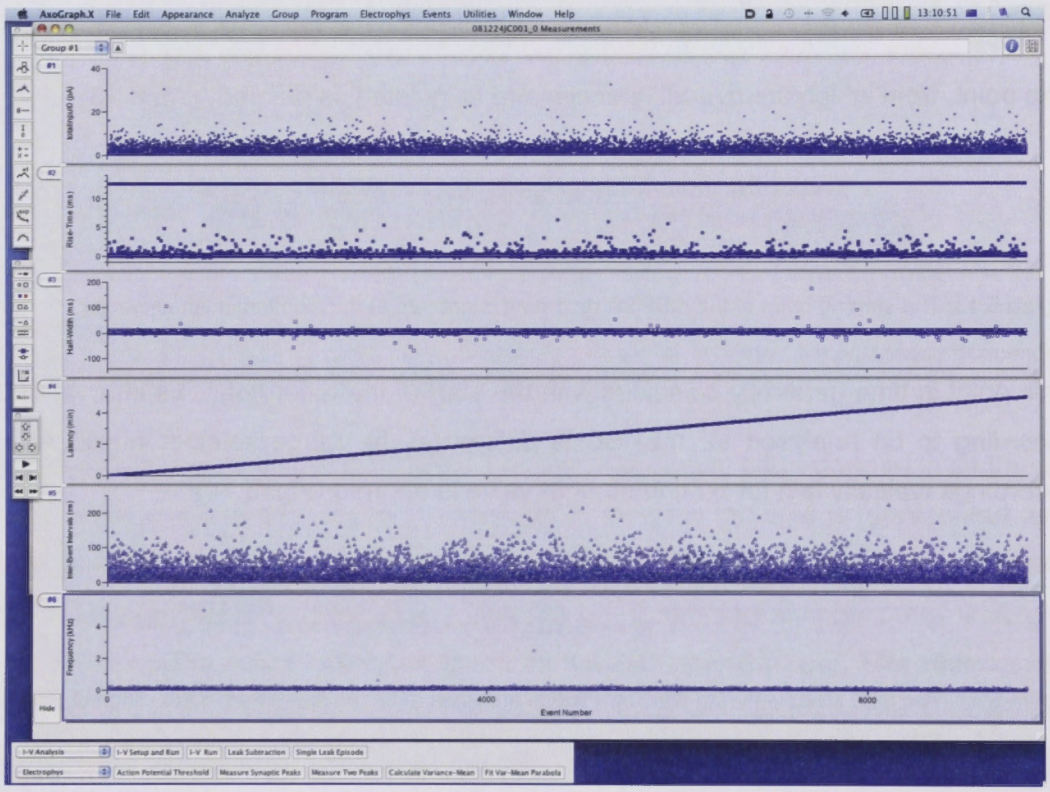

Figure 6.16. Parameters displayed in Axograph X at the end of the analysis. This data is then saved for further analysis using IGOR.

The data is then exported in delimited text format, and loaded using an IGOR stationary for the subsequent analysis.

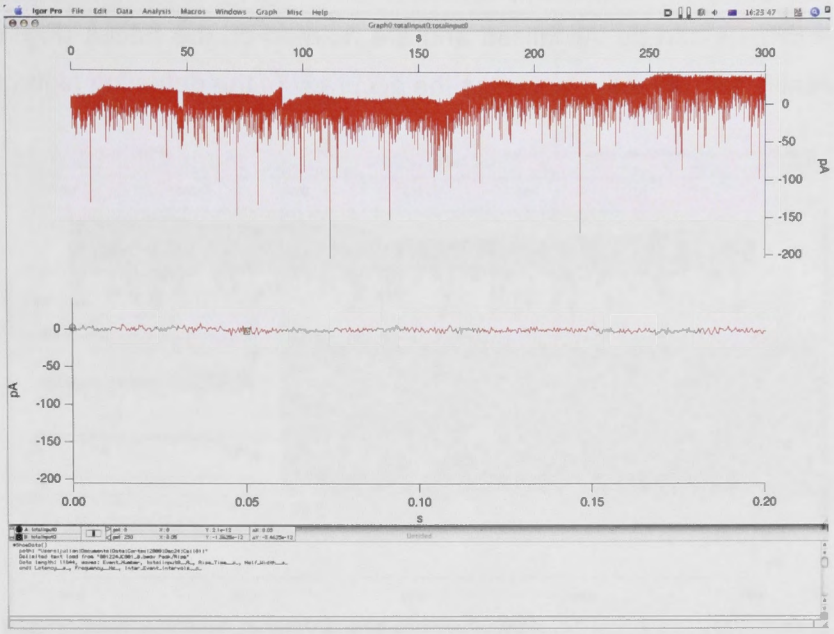

Figure 6.17. A loaded experiment in IGOR.

The IGOR stationary loads the raw data file together with the data obtained by Axograph X and displays it on two scales (Fig. 6.17). On the top trace is the entirety of the recording and on the bottom a section, here the first 200 ms of recording. It allows displaying individual sections of the recording and identifying periods without mEPSCs. Two cursors are placed onto the graph line. In a first step, the cursors should be placed bracketing an interval with no apparent mEPSC. The interval should be at least 50 ms long, which would correspond to about 250 data points. This interval serves to estimate the standard deviation of the noise used for thresholding the mEPSC amplitudes. The standard deviation is calculated for the interval chosen.

A function is then used to eliminate mEPSCs with amplitudes ≤ 2.5 times the standard deviation of the measured noise during the setting of the cursors above. In general, this value is in the range of about 6 ± 1 pA (Fig. 6.18).

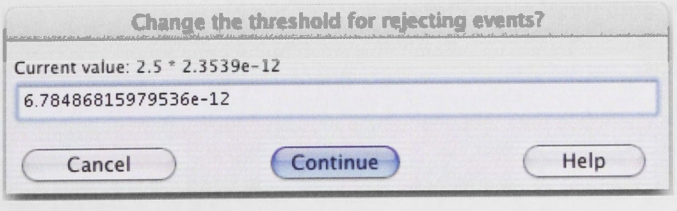

Figure 6.18. Noise value calculated for elimination of the mEPSCs with ≤ 2.5 times the standard deviation of the noise. This value can be overwritten if required.

After eliminating mEPSCs with amplitudes too small to be discerned from noise, the remaining mEPSCs can be visualised and are marked on the traces (Fig. 6.19). This serves to identify and objectively assess the accuracy of the detection algorithm.

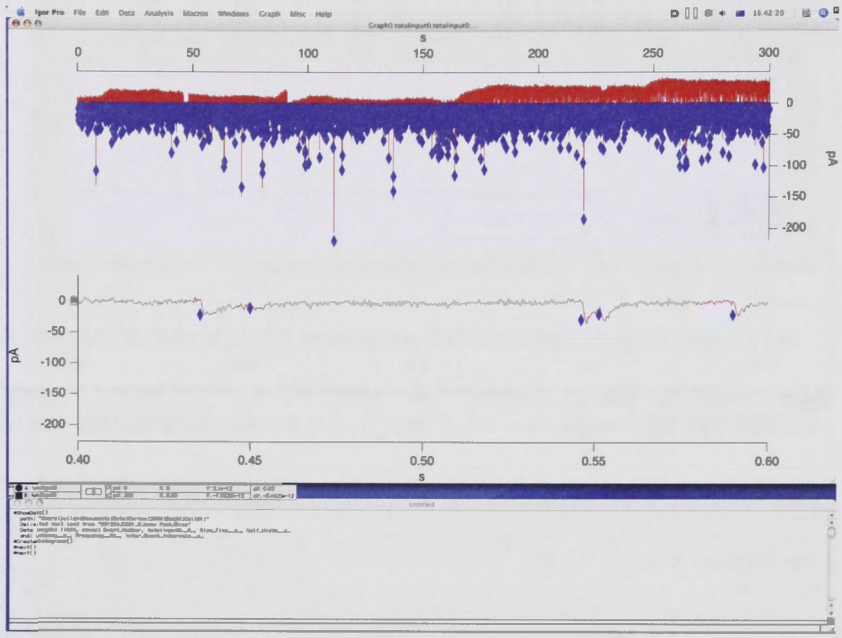

Figure 6.19. The position of the detected mEPSC is displayed in blue diamonds.

If the detection was not satisfactory, the level of the amplitude threshold is altered by reassessing the noise standard deviation. If this alteration did not improve the detection, the whole procedure is redone using a new template.

If the detection was in good agreement with the one done by visual identification, i.e. <15% false positives and negatives as judged by eye, various graphs, including probability density functions (PDFs) and cumulative probability density functions (cPDFs) of the data could were generated and the inter-event intervals and instantaneous frequencies were recalculated. This analysis served to characterise the experimental conditions, typically between a control and a period exposed to a pharmacological intervention. Statistical tests between the different cPDFs were then done to check for statistical significance.

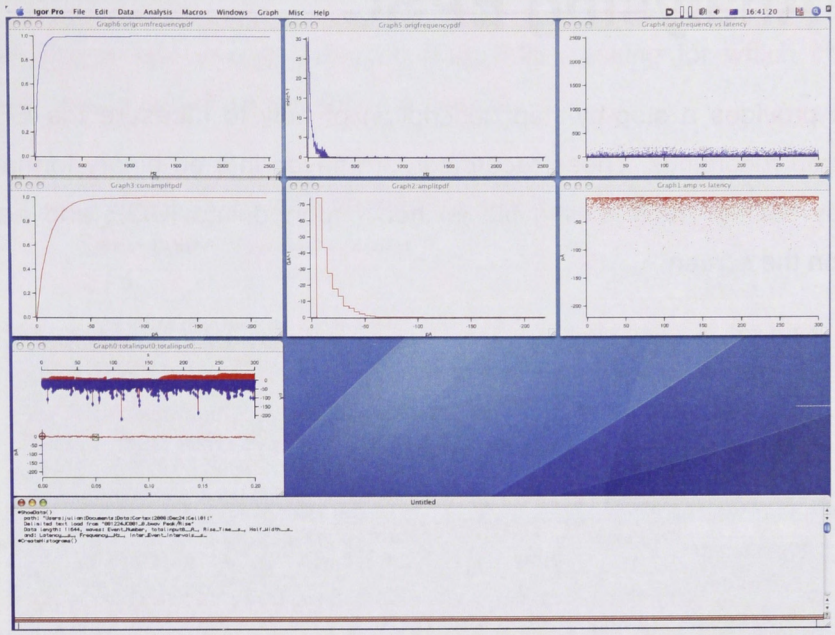

Figure 6.20. Generation of the cPDFs.

6.2. Analysing EPSC

This guide provides a step-by-step description of how to measure the EPSCs from voltage-clamp recordings. These recordings are saved into an binary format, which is readable by IGOR. The resulting file is then imported into IGOR and each trial is displayed on the screen.

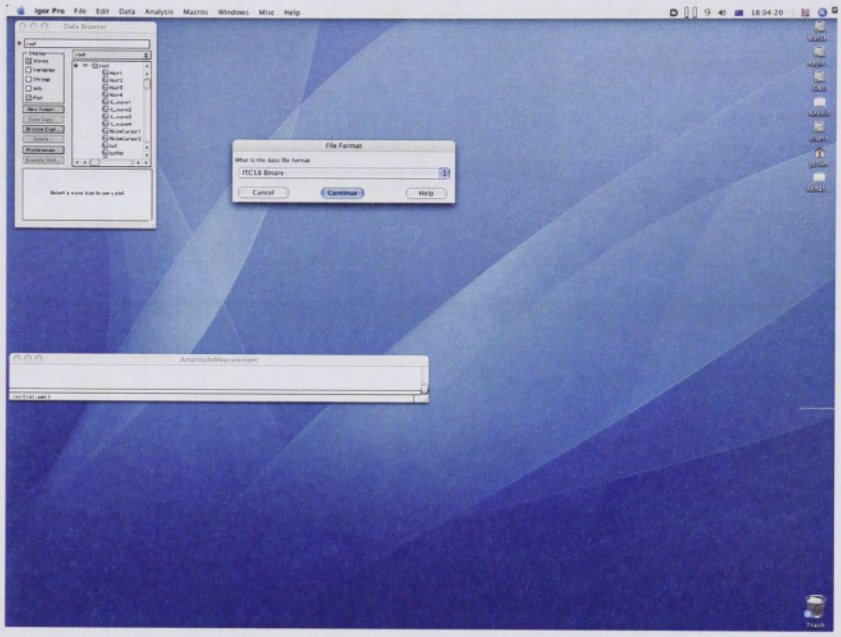

Figure 6.21. Entry to the amplitude measurement stationary in IGOR.

"ITC Binary" is chosen as format. The stimulus parameters used during the recordings are entered in the subsequent window (Fig. 6.22). For paired-pulse recordings, the stimulus time for the first and second pulses are set at 20 ms and 70 ms, respectively (in my case). The stimulus frequency was 0.2 Hz. The action potentials are displayed with each sweep to make sure that on each trial an action potential was generated.

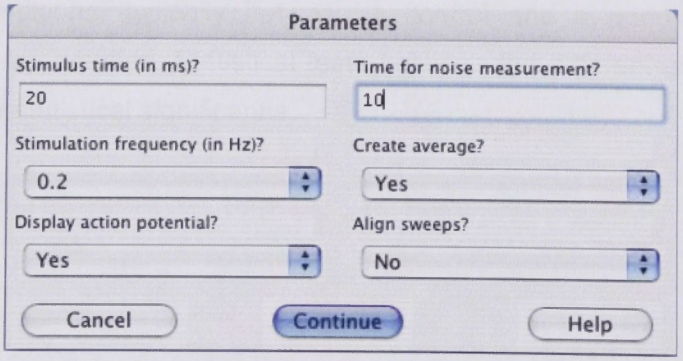

Figure 6.22. An example of how the parameter entry mask is set for the type of recording that I did.

Upon continuing, a text box is displayed (Fig. 6.23), asking for which channel the EPSC was on and on which on the action potential.

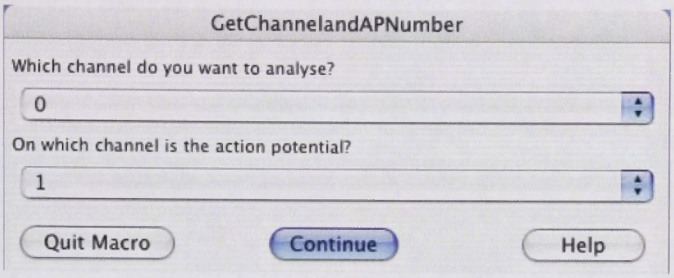

Figure 6.23. A mask to select the channel for analysis. In this case, the channel with the EPSC is channel 0, which was in voltage-clamp. The action potential was recorded in channel 1.

After selecting the appropriate channel for subsequent analysis, the EPSCs are displayed in a new window (Fig. 6.24). A new mask appears asking if artefact subtraction is wanted. In most cases, this artefact subtraction can be ignored.

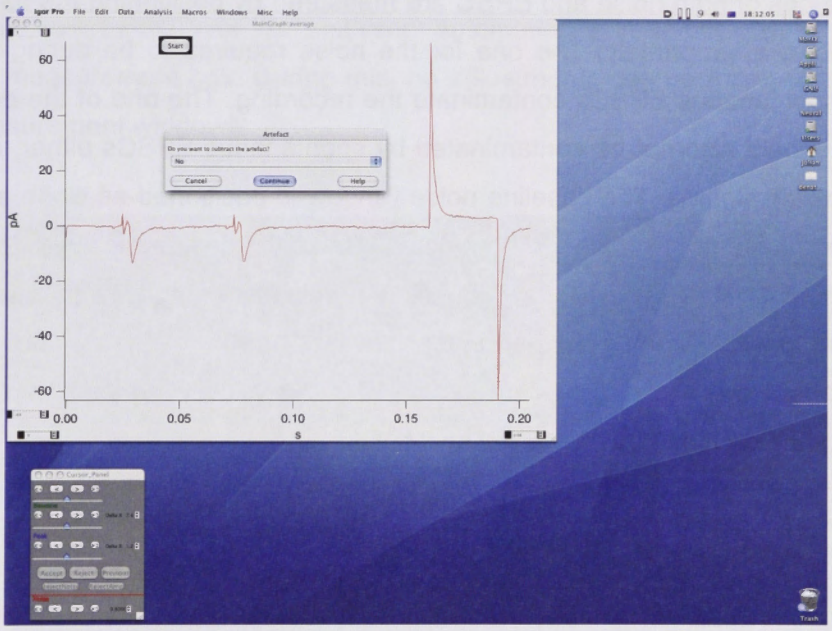

Figure 6.24. Subtraction of the artefact mask with none selected.

The mean EPSC will be displayed with the action potential. The values for the measurements of the baseline and peak windows are proposed by cursor positions. The EPSC amplitude is calculated as the difference of the average during the baseline (yellow) and the average peak window (blue).

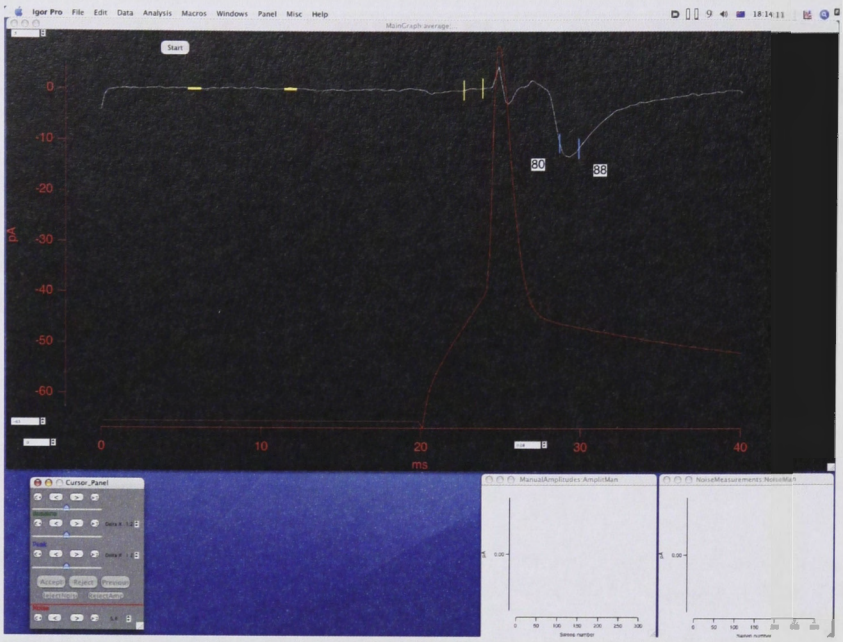

Figure 6.25. The average EPSC aligned with the action potential showing the time windows for measurement of the baseline and peak of the EPSC.

The amplitudes of both noise and EPSC are measured by positioning the baseline and peak windows appropriately. The one for the noise requires to be during an epoch, which no spontaneous EPSCs contaminate the recording. The one of the peak EPSC amplitude should also not be contaminated by spontaneous EPSCs either, nor should the baseline be sloping. The baseline noise window is positioned as close as possible to the rising phase of the EPSC without being affected by the capacitive artefact of the action potential. The peak window should straddle symmetrically the peak of the EPSCs and its width should not be longer than that at 90% of the peak of the EPSC (typically about 0.8 - 1.2 ms). The "program" automatically updates the amplitude histogram after each sweep during the analysis.

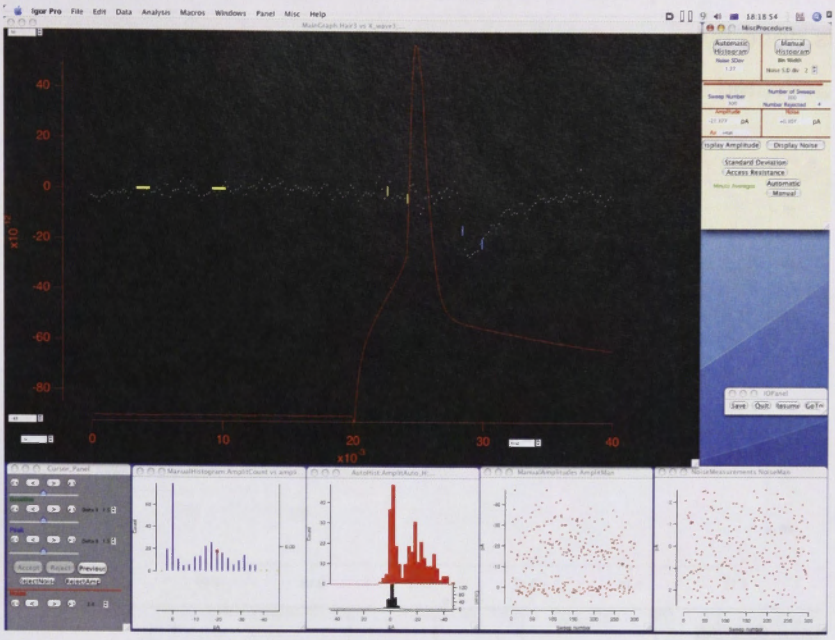

Figure 6.26. A manually analysed experiment with 300 EPSCs. The peak amplitudes of both noise and EPSCs are displayed in scatter plots (bottom right) and as histograms (bottom left).

Alternatively, an EPSC can be analysed automatically in IGOR, by selecting the automatic measurement box. During this, no adjustments can be made for positioning of the measurement windows.

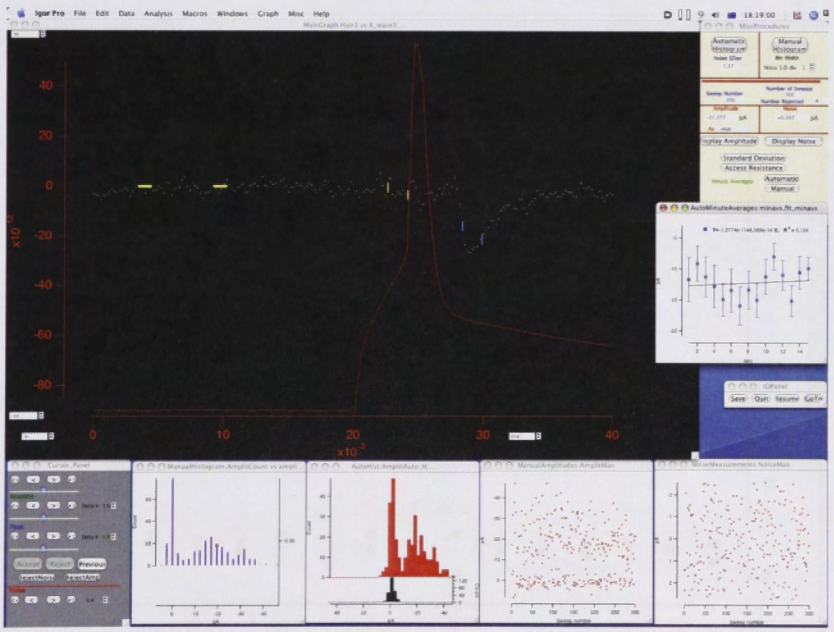

Figure 6.27. Display of the same experiment as above, but automatically measured.

The last part of the analysis is to check that the recordings of EPSCs are stable over time. This is done by measuring the R_s at the end of each of the EPSC sweep. The R_s function is activated by clicking the "access resistance" tab.

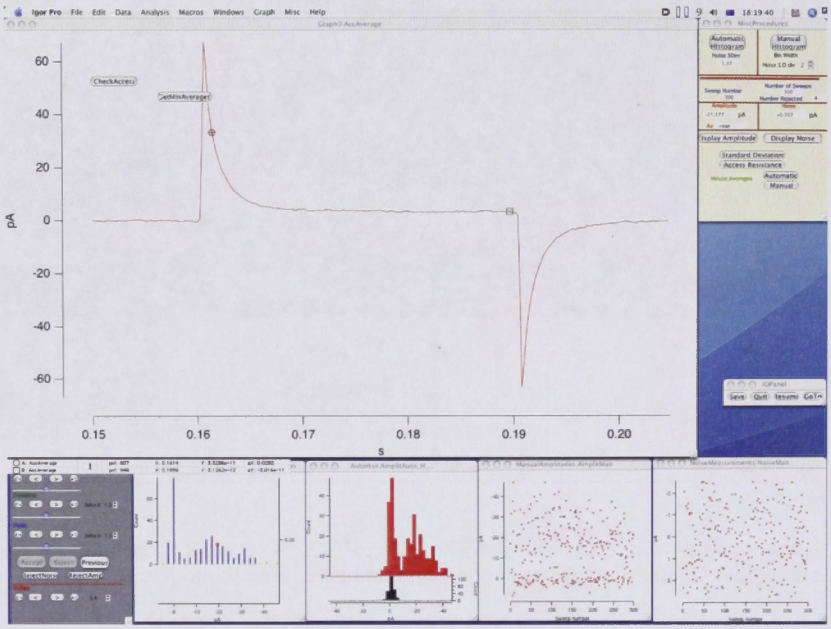

Figure 6.28. How the series resistance (R_s) and input resistance (R_{in}) are measured on the current transient caused by a 0.5 mV voltage step.

To get the value of R_s and R_{in}, the "get min average" box is selected.

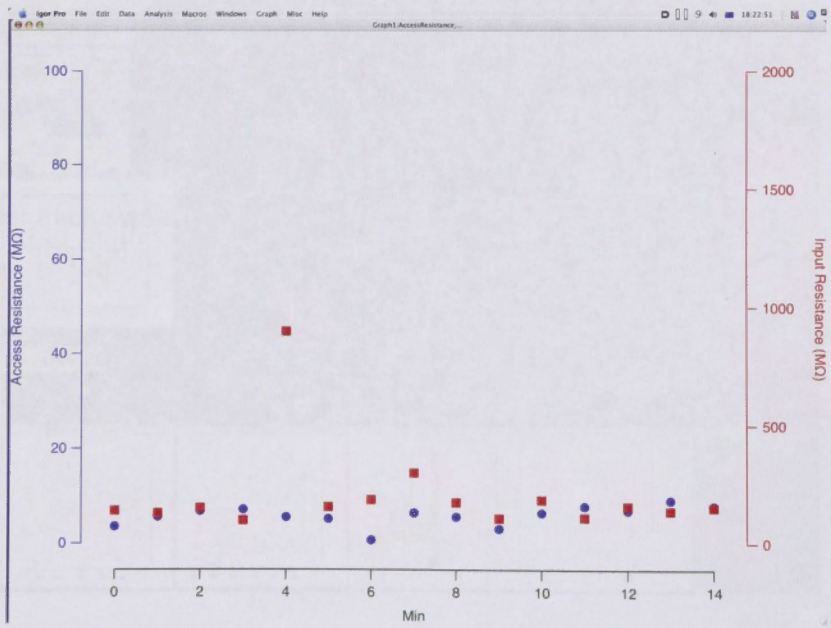

Figure 6.29. Display of R_s (blue) and R_{in} (red) over the time of the experiment.